Optimal Integration of Post-Combustion CO_2 Capture Process with Natural Gas Fired Combined Cycle Power Plants

Fatemeh Rezazadeh

Submitted in accordance with the requirements for the degree of Doctor of Philosophy

The University of Leeds

School of Chemical and Process Engineering

September 2016

The candidate confirms that the work submitted is his own and that appropriate credit has been given where reference has been made to the work of others.

ACKNOWLEDGEMENT

I would like to express my special appreciation and thanks to my supervisor Professor William Gale, you have been a great mentor for me. This research benefited greatly from your guidance, support, and encouragement. I would like to thank Dr Kevin Hughes and Professor Mohamed Pourkashanian from the University of Sheffield for their valuable guidance and constant help. I would also like to express my sincere gratitude and thanks to Professor Gary Rochelle from the University of Texas at Austin who was indeed more than a supervisor to me. Dr Rochelle, this project benefited tremendously from your insight and professionalism as well as your commitment to excellence and attention to details.

I would like to thank my research mates Darshan Sachde and Yu-Jeng Lin from the University of Texas at Austin for their collaboration and their effort in providing me with helpful solutions. I would also like to thank Dr Muhammad Akram from the University of Sheffield for providing me with experimental results from the UKCCSRC/PACT pilot plant studies which enables me to verify the models developed in this thesis. I would also like to express my gratitude to all the staff in the Energy Building at the University of Leeds, particularly, Mr David Hynes, for their constant help, support and information.

I would express my warmest gratitude to my family in Iran, my parents and my brother, whom are always present, supportive and motivating. Finally, I would like to thank Mehdi for his unconditional love and encouragement. He walked this challenging path with me and raised me in the moments of fall. Thank you for your patience and support and coming this far with me.

PUBLICATIONS

Peer-reviewed journal papers:

1. Rezazadeh F., Gale W.F., Hughes K.J., Pourkashanian M. Performance viability of a natural gas fired combined cycle power plant integrated with post-combustion CO_2 capture at part-load and temporary non-capture operations, *International Journal of Greenhouse Gas Control,* 2015 (39), pp 397-406.
2. Rezazadeh F., Gale W.F., Lin Y.J., Rochelle G.T. Energy Performance of Advanced Reboiled and Flash Stripper Configurations for CO_2 Capture Using Monoethanolamine, *Industrial & Engineering Chemistry Research,* 2016, 55 (16), pp 4622-4631
3. Rezazadeh F., Gale W.F., Akram M., Hughes K.J., Pourkashanian M. Performance evaluation and optimisation of post combustion CO_2 capture processes for natural gas applications at pilot scale via a verified rate-based model, *International Journal of Greenhouse Gas Control,* 2016 (53), pp 243-253.
4. Rezazadeh F., Gale W.F., Rochelle G.T., Sachde D. Effectiveness of Absorber Intercooling for CO_2 Absorption from natural gas fired flue gases using monoethanolamine solvent, Submitted to the International Journal of Greenhouse Gas Control on July 2016.

ABSTRACT

Post combustion CO_2 capture (PCC) has been considered as one of the near term solutions to significantly reduce CO_2 emissions associated with fossil fuels combustions. To accelerate the PCC incorporation into the energy market, various political, legal, economic and technical challenges and uncertainties should be successfully tackled. In relation to such, this thesis investigates methods to offer optimal incorporation of post-combustion CO_2 capture process into natural gas fired combined cycle (NGCC) power plants.

The objectives of this thesis is to develop and use thermodynamic models to study various process configurations, evaluate and quantify their benefits in terms of energy requirements on the performance of the integrated PCC-NGCC power plants. A detailed rate-based model of CO_2 absorption/stripping process using 30 wt. % monoethanolamine (MEA) as solvent was developed in Aspen Plus® RateSep™. The developed rate-based model was successfully validated in pilot scale using experimental data obtained from two pilot plants: (1) the UKCCSRC/PACT CO_2 capture pilot plant, and (2) the pilot plant at the Laboratory of Engineering Thermodynamics in TU Kaiserslautern. The application and effectiveness of four alternative process configurations were studied: two absorber intercooling processes, i.e. “in-and-out” intercooling and “recycled intercooling”, and two stripper configurations: “advanced reboiled” stripper and “advanced flash” stripper.

In addition, optimal incorporation of a large-scale PCC plant, including the CO_2 compression unit, into a commercial-scale NGCC plant with a nominal power output of 650 MW_e was investigated. The performance viability of the integrated NGCC-PCC plant was assessed at power plant full-load and part-load operations, to study the feasibility of the PCC operation at power plants full-load and part-loads, and recognise key performance parameters require careful consideration for a stable and efficient operation of the integrated plant at variable loads. In addition, the performance of the NGCC, especially the low pressure steam turbine, at various loads at times the power plant was integrated with the capture plant, and at times

the CO_2 capture plant was offline were investigated, and issues require careful considerations when operating the power plant in case of non-capture operation were addressed.

This research also studied the relationship between the cost of CO_2 capture and the flue gas CO_2 concentration ranging from 4 to 14 %. For each case, the specific regeneration and cooling duties and total capital expenditure (CAPEX) and operational expenditures (OPEX) were calculated and compared. Accordingly, the total annual cost of each plant (TOTEX) was determined using the respective CAPEX and OPEX with taking into account an investment period of 20 years and an interest rate of 10 %. Finally, for each case the cost of CO_2 captured was estimated and compared.

TABLE OF CONTENTS

LIST OF FIGURES

LIST OF TABLES

(This Page is Blank)

(This Page is Blank)

Chapter 1

Introduction & Research Objectives

This chapter provides an introduction to the research work presented in this thesis. It starts with an overview and background of the global CO_2 emissions from fossil fuel combustion and its future prospect. Three main technology options for CO_2 capture and storage are introduced and their current development stages in terms of commercialisation are evaluated. Amine based post combustion CO_2 capture is an important technological option for CO_2 capture from power plant flue gases. The research challenges, the objectives and scope of this research are outlined.

1.1. Global Energy Demand and Future Outlook

For all energy conversion systems, the primary goal is to provide energy services that facilitate productivity and enhance quality of life (1). Therefore, a reliable, affordable, secured, and sustained source of energy is a vital aspect to future prosperity.

The need for and use of energy resources continue to rise to meet requirements of the growing world population and expanding economies (2). *The International Energy Outlook* projects that between 2010 to 2040 world energy consumption will increase by 56% (3). In other words, total global energy use increases from 553 Exa-joules (EJ) in 2010 to 665 EJ in 2020 and to 865 EJ in 2040 (3). Figure 1-1 shows the chronological and projected trend of energy consumption from 1990 to 2040. As it is obvious in Figure 1-1, most of the growth in energy consumption occurs outside the Organization for Economic Cooperation and Development (OECD) region, known as non-OECD countries, where the demand for energy is driven by strong, long-term economic growth. Energy consumption in non-OECD countries grows by 90%, whereas in OECD countries, the growth is 17% (3).

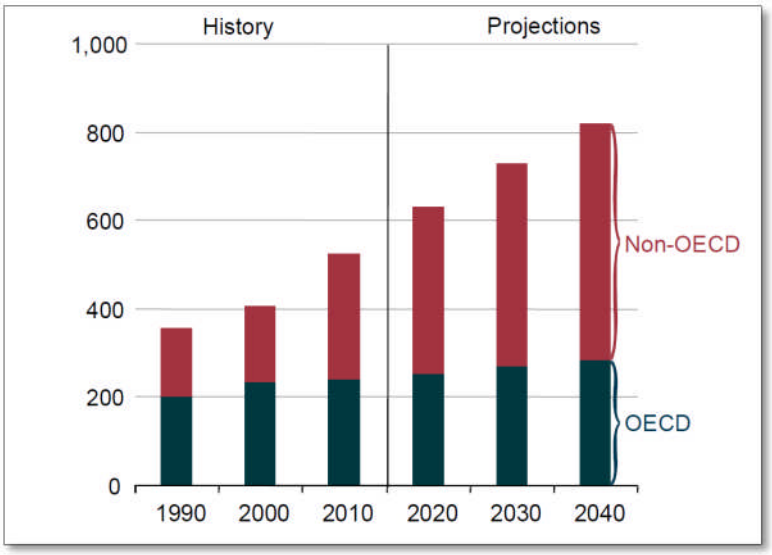

Figure 1-1: World energy consumption trend from 1990 to 2040 in terms of Exa-joule (3)

To date, renewable energy and nuclear power are the world's fastest-growing energy resources with an average growth rate of 2.5% per year (2,3). However, not all energy resources are suitable for base-load electricity generation. Renewable energy such as solar and wind are too intermittent and unpredictable to provide base-load electricity. Despite the fact that nuclear power plants are able to provide base-load electricity, being in a post-Fukushima world leads governments to be more cautious with their plans to expand their nuclear capacity (2). These facts and growing concerns about energy security leave natural gas and coal as the two main resources that could play significant roles in the near to mid-term future of electricity generation. These two fuels have long been reliable resources for base-load electricity generation and are expected to remain to supply approximately 80% of world energy demand through 2040 with natural gas being the fastest-growing fossil fuel (2).

In 2005, the total share of fossil fuels excluding biomass, reached 81% with oil being the main constituent (35%), followed by coal (25%) and natural gas (21%) (4). Although oil and liquid fuels in general hold the largest portion in energy supply, it is forecast that their share will decline from 35% in 2005 to 28% in 2040 (3). This is mainly due to their abatement in

the electricity generation and building sectors. Figure 1-2 shows the chronological and projected consumption trend of all energy sources over the time from 1990 to 2040 (3).

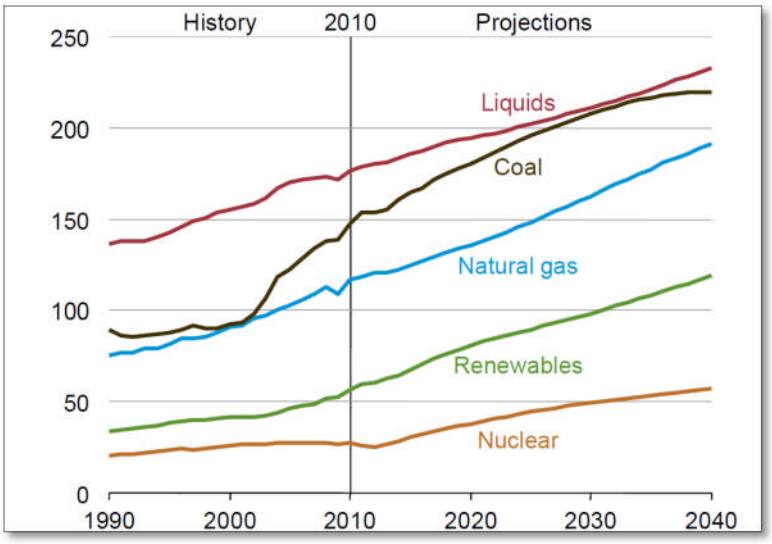

Figure 1-2: World energy consumption trend based on fuel type in terms of Quadrillion BTU (3)

According to the *International Energy Outlook 2013* published data (3), global consumption of natural gas is projected to increase by 1.7% per year on average, from 320 billion cubic meters in 2010 to 375 billion cubic meters in 2020 and 525 billion cubic meters in 2040. The increase in natural gas resources, especially because of shale gas extraction, and technological advances in drilling and extraction have contributed to this growth. Another positive outcome of the outlined factors is the price of natural gas has remained below the oil price, which consequently supports the projected global increase in natural gas consumption.

Both electricity generation and industrial sectors will be the main consumers of natural gas by 2040 (2-4). These two sectors account for 77% of the total increase in global natural gas consumption by 2040. It is projected that from 2010 to 2040, global consumption of natural gas for electricity generation will increase by nearly 80% (3). Figure 1-3 displays the projected global natural gas consumption based on end-user sectors.

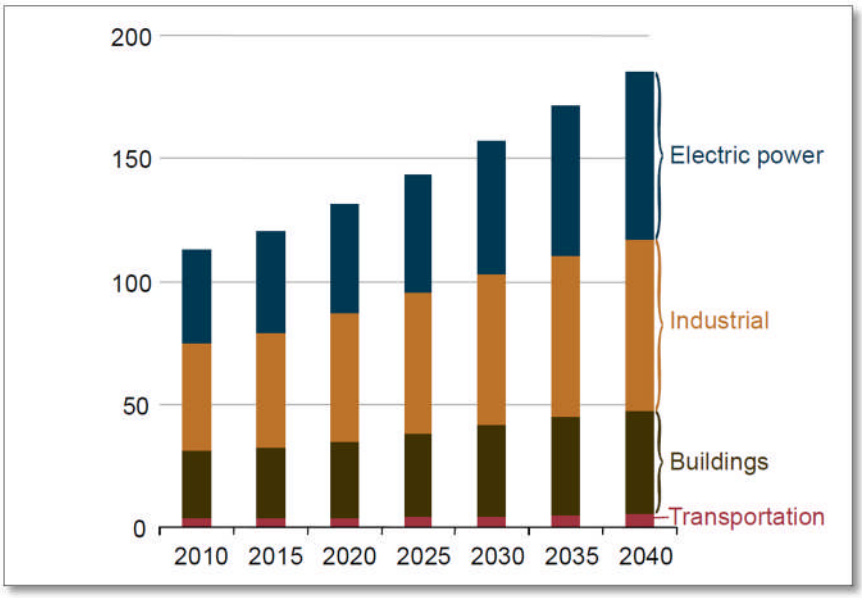

Figure 1-3: Projected natural gas consumption by end-use sector in terms of trillion cubic feet (3)

Coal, on the other hand, continues to play an important role in the world energy market, especially in China and India. On average, coal global consumption is projected to increase by 1.3% per year from 2010 to 2040. In general, coal and oil account for an equal share of global energy consumption of nearly 29% in 2030. After 2030, due to a projected reduction in China's use of coal in its industrial sector, the global share of coal consumption will decline to 27% in 2040, compared to 28% of oil share at the same time (2-4).

1.1.1. Fossil Fuels and Electricity Generation

In 2004, over 40% of total primary energy resources, equivalent of 17,408 TWh, were used to generate electricity. Since 1995, electricity generation has shown a steady average growth of 2.8% per year, and on average a growth rate of 2.5~3.1% per year is expected until 2030 (3,5-6).

To date, coal owns the largest share of global electricity generation. However, its share will decline from 40% in 2010 to 36% in 2040 whereas the share generated from natural gas will increase. For natural gas, the trend will be from 22% in 2010 to 24% in 2040 (3,6). Figure 1-

4 shows the projected trend of global electricity generation by energy resource type from 2010 to 2040.

By 2030, the demand for coal is expected to be more than doubled (2). At the same time, as per the *International Energy Agency* estimation, nearly 4500 GW of new power plants will be required with half of it in developing countries (3). Besides, since 1980, natural gas electricity generation has been growing rapidly because of its innate superiorities to other fossil fuel in terms of fuel efficiency, environmental benefits, operating flexibility, investment costs and short lead time (2).

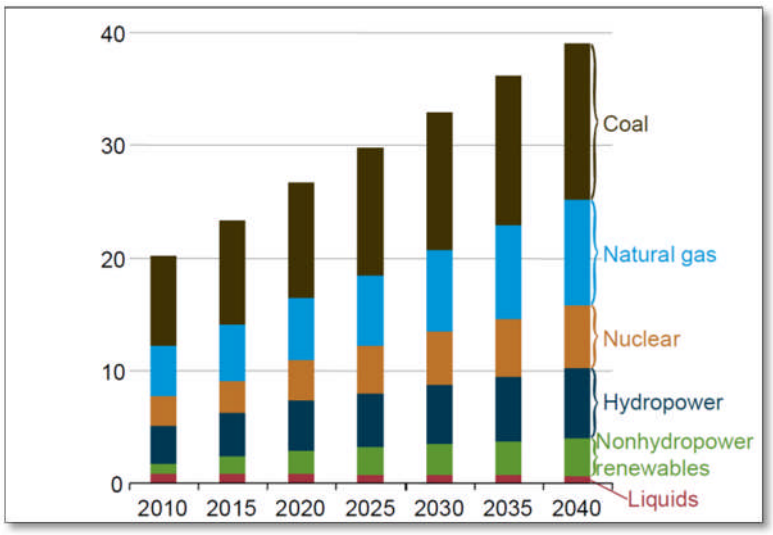

Figure 1-4: Projected global electricity generation in terms of Trillion kWh (3)

Natural gas combined cycle power generation could prevail over any other type of fossil-fuel power generation especially when the fuel cost is relatively low (2). Figure 1-5 shows the average efficiency of electricity generation from fossil fuels (7). From an environmental perspective, among fossil energy resources, excluding nuclear energy, natural gas has the least emission rate per unit of energy consumed and is therefore favoured in mitigation strategies.

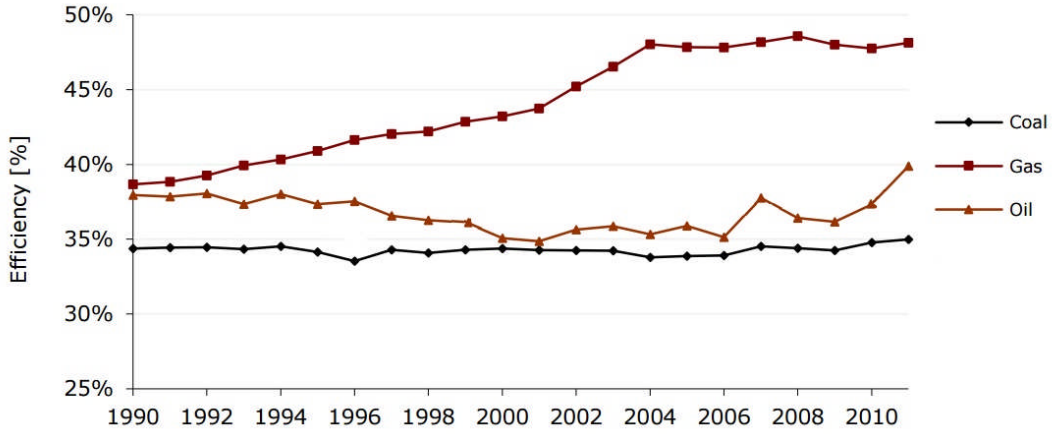

Figure 1-5: Efficiency of electricity production from fossil fuels (7)

1.1.2. Fossil Fuels and Emissions

Fossil fuels emissions account for nearly 85% of the annual anthropogenic CO_2 emission (8). In the context of climate change, it is important to distinguish between coal and natural gas with respect to their CO_2 emission rates. Regardless of type and resource location, the carbon content of coal is greater than that in natural gas; therefore it emits more CO_2 when it burns. For power plants, CO_2 emissions from natural gas are roughly 40-65% lower than that of coal (9-11). Combined cycle natural gas fired power plants have lower CO_2 emissions than simple cycle plants due to their higher efficiency.

Reduction of CO_2 emissions requires fundamental changes in the way electricity is generated. These changes include developing CO_2-free sustainable energy sources (such as renewables), switching to less carbon-intensive fuels (such as natural gas or biomass), and in general being more efficient. However, as discussed earlier, fossil fuels are expected to widely play a dominant role in the future of electricity generation, therefore, something must be done to reduce or moderate the growth of their CO_2 emission. Hence, a switchover from their traditional use to a greater uptake of advanced near zero emission technologies, such as carbon capture and storage (CCS) will be inevitable.

Aligned with this urgency, traditional electricity generation by coal power plants is expected to be eventually displaced with more advanced and highly efficient technologies such as natural gas fired power plants equipped with CCS in order to reduce the growth of CO_2 emissions (2,3,11).

1.2. Carbon Capture and Storage

In short, carbon capture and storage is the only pathway that can let the world continue to enjoy the benefits of using fossil fuels while significantly reducing the emissions associated with them. In other words, CCS is a bridging strategy to buy time for alternative energy resources to fossil energy to be developed (12).

1.2.1. What is Carbon Capture and Storage?

Carbon capture and storage, abbreviated as CCS, is a permanent or long-term isolation of the CO_2 associated with the combustion of fossil fuels, and storage of it deep in suitable geological reservoirs. Also, the captured CO_2 can be used in other processes such as enhanced oil recovery (EOR), food and chemical process industries.

Considering the magnitude of CO_2 emissions from power generation and industrial sectors, CCS is expected to play an important role. In the BLUE Map scenario proposed by the *International Energy Agency*, it is projected that by the year 2050, a 50% reduction in CO_2 emissions is to be achieved by the options illustrated in Figure 1-6, of which, CCS technology is targeted to contribute 19% (13). This estimation is based on a least cost basis. To achieve this goal it is necessary to construct 3400 fossil fuelled power plants worldwide with over 2000 of these being built in developing countries. This is an optimistic estimation and existing constraints on public finances in many countries may result in either delay or cancellation of a number of major projects and as a result the share of CCS be impacted (28).

Furthermore, for the power generation sector, the BLUE Map scenario anticipates that the retrofit of existing power plants with CCS will be the key contributor in reducing CO_2

emissions before 2030 (13). This highlights the importance of foreseeing the essential provisions necessary for future implementation of CCS technologies for new fossil fuel power plants to be built within the next 10 to 20 years.

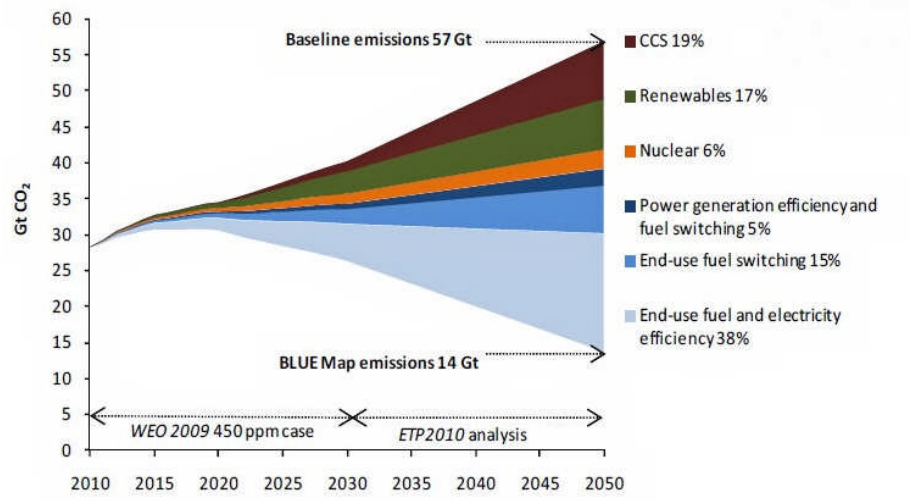

Figure 1-6: Key technologies for reducing CO_2 emissions under the BLUE Map Scenario (13)

1.2.2. Carbon Capture and Storage Technology Routes

There are three different technology routes to capture CO_2, namely pre-combustion CO_2 capture, post-combustion CO_2 capture, and oxy-fuel combustion. Oxy-fuel combustion is a general term used for technologies where nitrogen (N_2) is excluded from the combustion process (14-15). In the following paragraphs, each technology is briefly described, and Figure 1-7 illustrates the basic principle of incorporating these CO_2 capture techniques to power plants (15).

As mentioned earlier, CCS technologies typically involve three stages: capture, transport and storage of CO_2. After capture, the compressed CO_2 will be normally transported by pipeline or ship to storage locations. The topics of transport and storage stages will not be discussed in this thesis.

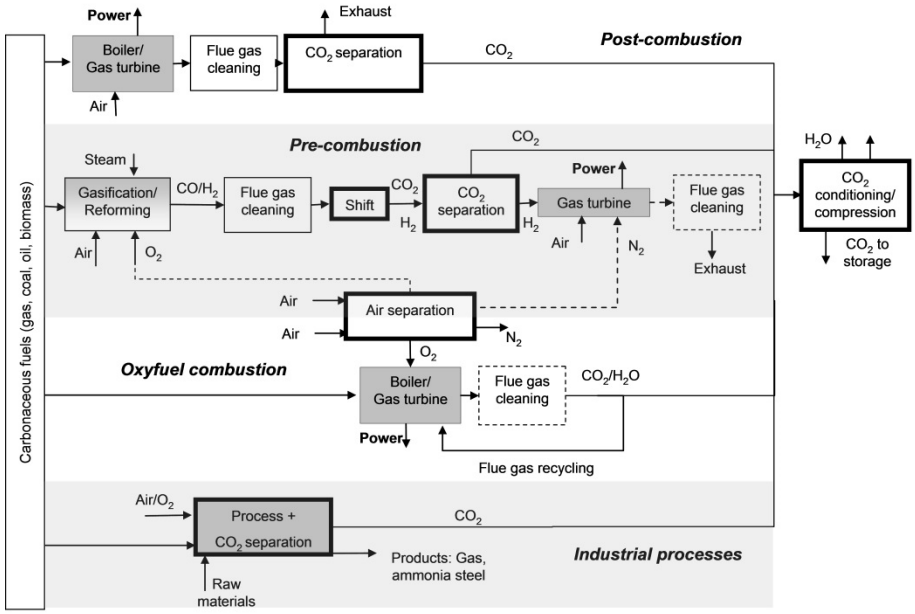

Figure 1-7: The three main processes to capture CO_2 from power plants (15)

1.2.2.1. Pre-Combustion CO_2 Capture

Pre-combustion CO_2 capture is employed in combination with an integrated gasification combined cycle (IGCC) plant. As the name implies, the CO_2 is captured prior to combustion. This technology is well suited for gas fired combined cycle power plants. In this process, the fuel reacts with steam or a steam/oxygen mixture to produce a mixture rich in hydrogen (H_2) and CO_2. For non-gaseous fuels, the H_2/CO_2 gas stream must be cleaned to remove species such as ammonia or sulphur due to either environmental restrictions or that they pose a threat to the plant operation (17). Usually, the CO_2 removal is performed by means of physical or mixed-solvent-based systems, although membrane-based separation is a potential option. The captured CO_2 is then dried, compressed and stored, whilst the rich H_2 stream passes through a gas turbine (or fuel cell, potentially) to generate electricity (16). Pre-combustion capture can achieve nominally 90% capture of CO_2.

1.2.2.2. Post-Combustion CO_2 Capture

In this method, the CO_2 is captured from the power plant exhaust gas (also called flue gas) by using a solvent. The commercially available technology mainly uses an aqueous amine-

based solution, e.g. 30 wt. % monoethanolamine (MEA), as solvent, which reacts with the CO_2 of the exhaust gas coming from the power generating plant and is then regenerated at a higher temperature in a stripper, releasing the captured CO_2 as a pure gas stream suitable for compression and storage (15).

For amine-based solvents, the exhaust gas must be pre-treated and cooled before entering into the absorption section of the capture plant. Pre-treatment is to minimise acidic gas concentrations (such as NO_2 and/or SO_2) in the exhaust gas in order to prevent their irreversible reaction with solvents (18). Afterward, the exhaust gas enters to the absorption section where it directly contacts with the solvent and reacts with it. The CO_2-rich solvent is then transferred to a regenerating unit where it is heated to drive off the CO_2. Next, the lean (CO_2 free) solvent recirculates to the absorber. The heat required for solvent regeneration is high and has a significant impact on the overall thermal efficiency of the power generating plant. The most efficient way to provide the heat required for solvent regeneration is by extracting a portion of low pressure (LP) steam prior to the LP steam turbine (19-20). Similar to pre-combustion CO_2 capture, this technology also can achieve nominally 90% capture of CO_2.

1.2.2.3. Oxy-Fuel Combustion

Oxy-fuel combustion refers to a power plant where the fuel (coal or natural gas) burns with nearly pure oxygen, rather than air, and results in an exhaust stream containing primarily CO_2. The required oxygen is normally obtained from an air separation unit (ASU). In this process, a great portion of the exhaust gas in recycled to feed in the combustion process. The leaving exhaust gas consists of mainly CO_2 and water with a trace of SO_2 and NO_x. The formation of NO_x is very low in oxy-fuel consumption since there is a negligible amount of nitrogen in the oxidant, and it thus forms only from the nitrogen in the fuel. The CO_2-rich exhaust gas is compressed and chilled to separate out oxygen, nitrogen and other impurities, and then sent for storage (14-16). The capture efficiency of Oxy-fuel combustion is extremely high and it can achieve more than 90% capture of CO_2.

1.2.3. CCS Technologies Evaluation

While there are a number of possible techniques to capture CO_2 from fossil power plants, some of them are still in the development stage. The merits and challenges of all these technologies need to be evaluated and compared before selecting the best route to incorporate in a power plant. The advantage of one route over another can be related to the level of maturity, technology availability, the possibility to retrofit to existing power plants, the operational experience and repetition in large and commercial scales, and finally the time required for the implementation. Currently, the only immediately feasible CO_2 capture route for power plants appear to be post combustion CO_2 carbon capture based on chemical absorption.

Selecting the most suitable route for CO_2 capture also depends on the characteristics of the CO_2-rich streams which mainly depend on the type of power plant. In fact, the pressure and the CO_2 content in the gas stream are important parameters in choosing the most appropriate technology for CO_2 removal. Table 1-1 shows the classification of CO_2 capture routes based on CO_2-rich gas streams.

Table 1-1: CO_2 capture technology and CO_2 contents (21)

Technology Route	CO_2-rich Gas stream	Gas pressure (kPa)	CO_2 content (%)
Pre-combustion capture	CO_2/H_2 (shift syngas)	1000-8000	20-40
Post-combustion capture	CO_2/N_2 (exhaust gas)	~ 100	3-15
Oxy-fuel combustion	CO_2/O_2 (exhaust gas)	~ 100	75-95

In the near-term future, it is likely that oxy-fuel combustion will be incorporated to a power boiler with an integrated steam cycle. In such cases, some pilot and demonstration plants for detailed testing of the system operability, and realizing the issues associated with its start-ups and shut downs have to be commissioned (22).

If oxy-fuel combustion is going to be incorporated in gas turbines, the design of gas turbine burners needs to be entirely revised in order to accommodate stoichiometric combustion

(22). Existing gas turbines with to-date design cannot be used for the purpose of stoichiometric combustion where pure oxygen supplied from an air separation unit with more than 97 % purity would be used as an oxidising agent. Such gas turbines, are not a matter of modifying existing equipment, but rather a complete new design to withstand extremely high flame and the turbine inlet temperatures (22). There are various ideas about recycling a portion of the exhaust gas in order to maintain turbine inlet temperatures within an acceptable level. In this case, first it is necessary to demonstrate and evaluate the technical and operational feasibility of gas turbines capable operating with CO_2 as the main working fluid (22). If such gas turbines could be developed in a foreseeable future, this technology will be attractive because of its simplicity. However, the likelihood of such events is unclear.

For pre-combustion capture, each component can be individually regarded as a proven technology. However, one may argue the maturity of hydrogen combustion (or hydrogen-rich fuel) in gas turbines. Gasification systems represent an attractive option for coal power plants since they make it possible to obtain syngas and electricity from coal. However, the capital costs of the required equipment are relatively high. Although, there are currently few IGCC pilot plants under operation, due to the complexity of the operation, the availability of such systems is yet to be guaranteed.

On the other hand, the incorporation of pre-combustion capture to natural gas combined cycle power plants is not a mature technology. The main scope for further developments is related to gas turbines with low NO_X burners utilising fuels containing more than 50% vol. hydrogen.

For coal to be integrated in a combined cycle power plant, it is necessary to be first gasified, while this is not the case for natural gas. Producing hydrogen from natural gas leads to a loss of nearly 20-25% of the fuel heating value, whilst this loss could be eliminated by burning natural gas in a gas turbine combined cycle power plant. Therefore, gasification of natural gas for the purpose of CO_2 capture will appear to be associated with an even higher energy penalty (heat loss for gasification and IGCC associated efficiency penalty). This is why

gasification of coal to generate electricity is a more feasible option. However, full-scale implementation of IGCC plants with coal incorporated with CO_2 capture is only expected in mid to long term timeframes.

Chemical absorption systems, on the contrary, are the best near term option for CO_2 capture from power plants. Incorporating post-combustion CO_2 capture into power plants involves relatively minor modifications in gas turbines and steam turbine cycles. From availability and operability viewpoints, commercial operations of such systems are successfully available, albeit at a smaller scale than required for power plants (23,24). Efficiency wise, applying the current state-of-art absorption-based CO_2 capture process will bring about an 8-12 %-point reduction in the overall power plant net efficiency (9).

In short, post-combustion CO_2 capture is the leading candidate for gas fired power plants. Neither pre-combustion nor oxy-fuel combustion captures are currently suitable for gas power plants. Hence, in this thesis, the main focus is dedicated on the incorporation of post-combustion capture (PCC) into natural gas combined cycle power plants.

1.2.4. Current Status of Post-Combustion CO_2 Capture

Post-combustion capture based on chemical absorption is the most promising state-of-art technology for CO_2 capture, with monoethanolamine (MEA) being the most widely used solvent. This technology is already commercialised is various industries (25). Since the 1930s, it is utilised in food industries to capture CO_2 from ammonia plants (23). There are also successful experiences and a good reputation of this technique in other industrial applications such as enhancing oil recovery (EOR) and upgrading natural gas (26).

To date, MEA is the most preferred solvent for power plant applications because of its relatively high absorption capacity, fast reaction kinetics, and high CO_2 removal efficiencies (14). Furthermore, it can be used with exhaust gases with low CO_2 concentrations (25). The latter characteristic of MEA makes it the preferred candidate for natural gas combined cycle power plants where the CO_2 concentration in the exhaust gases are considerably lower than

that in the flue gas of a typical coal power plant. For MEA based post combustion CO_2 capture, solvent regeneration is the main energy consumer of the plant. the main focus of many research studies related to the incorporation of MEA base post combustion CO_2 capture into power plants are currently focusing on innovative methods for efficient integrations, e.g. flexible operation, and/or reduced energy requirement for solvent regenerations, such as developing new solvents with lower energy requirement for regeneration, lower temperature of regeneration, or introducing alternative configurations to offer better energy balance. Furthermore, an optimum utilisation of heat from the power cycle will lead to lesser steam extraction and consequently lesser energy penalty (26).

1.3. Thesis Objectives

As discussed in the previous sections, post combustion CO_2 capture technology is one of the most preferred options for CO_2 abatement from power plant exhaust gases despite the fact that its commercial-scale implementation is yet to be realised. To accelerate the PCC penetration into the energy market, various political, legal, economic and technical challenges and uncertainties should be successfully tackled. In this regard, this thesis attempts to address two key technical questions:

a. How to minimise the negative impact of PCC operations on the performance of the power plants in terms of energy consumption and flexibility of operation?

b. What are the methods/modifications to be implemented into the current state-of-art PCC process to improve its performance?

This thesis focuses on the particular case of incorporating MEA based post combustion CO_2 capture process (PCC) into a large-scale natural gas fired combined cycle (NGCC) power plant, and accomplishes the following objectives:

1. Validate the PCC model developed in Aspen Plus® V.8.4 with data from two different pilot plants,

2. Propose optimum operating conditions for different packing materials for a standard PCC process,
3. Evaluate the performance viability of integrated PCC-NGCC at power plant part load operations, and non-capture operations,
4. Propose and quantify the performance of innovative stripper configurations in terms of total energy requirements for a range of lean solvent CO_2 loading,
5. Propose and quantity the performance of incorporating simple and advanced absorber intercooling in terms of CO_2 absorption capacity and total energy requirement for a range of lean solvent CO_2 loading,
6. Technical and economical evaluation of various exhaust gas CO_2 concentrations on the PCC plant overall cost.

Objective 1 is satisfied by developing a CO_2 capture process in Aspen Plus® V.8.4 and analysing its results with data from two pilot plants: The UK Carbon Capture and Storage Research Centre/Pilot Scale Advanced Capture Technology (UKCCSRC/PACT) CO_2 capture plant located at Sheffield, UK, and the MEA-based pilot plant at the University of Kaiserslautern, located in Kaiserslautern, Germany.

Objective 2 is satisfied by assessing and evaluating the effect of various performance parameters on the plant energy requirement based on the analysis of the results from objective 1 for the UKCCSRC/PACT pilot plant.

Objective 3 is satisfied by simulating a large-scale PCC with CO_2 compression unit and NGCC integrated plant in Aspen Plus® V.8.4 and evaluating the PCC plant and CO_2 compression unit performance in terms of energy requirement at various power plant loads varying from 100 % gas turbine (GT) load down to 60 % GT load. In addition, the variation of the efficiency penalty with GT load is quantified.

Objective 4 is satisfied with simulating two advanced stripper configurations: advanced reboiled and advanced flash stripper and quantifying the benefits of using these two

alternative stripper configurations on the PCC plant energy requirements for a range of lean solvent CO_2 loading.

Objective 5 is satisfying by evaluating the use of two absorber intercooling systems: simple (in-and-out) intercooling, and advanced (recycled) intercooling. The benefits of using absorber intercooling in terms of CO_2 absorption capacity, absorber packing requirement, and the PCC plant overall energy requirements are evaluated.

Objective 6 is satisfied by techno-economic evolution of three large-scale PCC processes designed for three different exhaust gases: exhaust gases of a large scale NGCC plant, exhaust gases of a large-scale NGCC with exhaust gas recirculation (EGR) cycle, exhaust gases of a large scale coal power plant.

1.4. Thesis Outline

This thesis comprises ten chapters, including this chapter. Chapter 2 presents a critical review of previous research conducted on the performance evaluation of post combustion CO_2 capture and its incorporation into large-scale natural gas fired combined cycle power plants with especial focus on performance challenges, energy requirements, and operational impacts of such integration on the performance and flexibility of power plants. Chapter 3 presents the chemistry and kinetics of CO_2 reaction with monoethanolamine (MEA) and the theory of the thermodynamics of the CO_2-H_2O-MEA system. Chapter 4 provides the details of the CO_2 capture model development in Aspen Plus® V.8.4 and its validation using two different pilot plant data. Chapter 5 summarises the investigation on finding optimum operating condition for a MEA based CO_2 capture plant using two different packing materials using the validated model developed in Chapter 4. Chapter 6 presents the optimal design of a large-scale CO_2 capture process for the application of natural gas fired combined cycle power plant. This chapter also presents the effect of power plant load variations on the CO_2 capture plant performance. Chapter 7 presents the benefits of using alternative stripper configurations on the CO_2 capture plant energy performance. Chapter 8 presents the benefits

of using two absorber intercooling systems on the CO_2 absorption capacity and the plant overall energy requirement. Chapter 9 summarises the techno-economic evaluation of three different exhaust gas CO_2 concentrations, and finally chapter 10 presents the summary of the outcomes of this research as well as recommendations for future work.

1.5. List of References

(1) Hall, C.; Tharakan, P.; Hallock, J.; Cleveland, C.; Jefferson, J. Hydrocarbons and the evolution of human culture. *Nature* 2004 (426) 318-322,

(2) Metz, B.; Davidson, O.; Bosch, P.; Dave, R.; Meyer L. *Climate change 2007 Mitigation*. Report of the Intergovernmental Panel on Climate Change, Cambridge University Press, NY 10013-2473, USA

(3) U.S. Energy Information Administration. *International Energy Outlook 2013 - With Projections to 2040*. DOE/EIA-0484 2013.

(4) *BP Statistical Review of World Energy*. BP Inc. London, 2005.

(5) *World energy outlook 2006. International Energy Agency*, OECD Publication Service, Paris, 2006

(6) *Energy demand in the world in 2004: A global energy data base including OECD data*. Enerta, Grenoble, France, 2004.

(7) U.S. Energy Information Administration. *Annual Energy Outlook 2013*. DOE/EIA-0483, April 2013.

(8) Unander, E. *From oil crisis to climate challenge - understanding CO_2 emission trends in IEA countries*. International Energy Agency, OECD Publication Service, Paris, 2010.

(9) Metz, B.; Davidson, O.; Coninck, H.; Loos, M.; Meyer, L. *IPCC Special Report on Carbon Dioxide Capture and Storage*. Intergovernmental Panel on Climate Change, Cambridge University Press, NY 10013-2473, USA, 2005

(10) *The Future of Coal*.Intergovernmental Panel on Climate Change, Working Group III. 2007.

(11) *Assumptions to the Annual Energy Outlook 2008*. Massachusetts Institute of Technology. 2008.

(12) Herzog, H.; Meldon, J.; Hatton, A. *Task Force Report - Advanced Post-Combustion CO_2 Capture*. Clean Air Task Force, UK. April 2009.

(13) Houssin, D.; *Prospects for power generation from coal to 2050*. International Energy Agnency, November 2013

(14) Folger, P. *Carbon Capture: A Technology Assessment*. Congressional Research Service, November 2013.

(15) Clarke, D. *CO_2 Capture and Storage, VGB Report on the State of Art*. VBG PowerTEch Service GMBH, August 2004.

(16) Tanaka, N. *CO_2 capture and Storage – A key carbon abatement option*. International Energy Agency, France, 2008.

(17) EU Legislation. *Carbon Capture Technology and Carbon Capture Ready Criteria*. UK TWG 18 Submission for Combustion Sector. 2012.

(18) Chapel, D.; Mariz, C.; Ernest J. *Recovery of CO_2 from flue gases: commercial trends*. Proceedings of Canadian Society of Chemical Engineers, Annual Meeting, Saskatoon, Saskatchewan, Canada, 1999.

(19) Gibbins, J.; Crane, R.I. Scope for reductions in the cost of CO_2 capture using flue gas scrubbing with amine solvents. Proceedings of the Institution of Mechanical Engineers, Part A. *Journal of Power and Energy* 2004 (218) 231-239.

(20) Gibbins, J.; Crane, R.; Lambropoulos, D. Maximising the effectiveness of post-combustion CO_2 capture systems. Proceedings of the 7th International Conference on Greenhouse Gas Control Technologies. *Fuel* 2007 (86) 2109–2123.

(21) Abu-Zahra, M. R. M.; Schneiders, L. H. J.; Niederer, J. P. M.; Feron, P. H. M.; Versteeg, G. F. CO_2 capture from power plants. Part I. A parametric study of the technical performance based on monoethanolamine. *International Journal of Greenhouse Gas Control* 2007 (1) 37–46.

(22) Bolland, O.; Undrum, H. A novel methodology for comparing CO_2 capture options for natural gas-fired combined cycle plants. *Advances in Environmental Research* 2003 (7) 901–911.

(23) Herzog, H.; Meldon, J.; Hatton, A. *Advanced Post-Combustion CO_2 Capture*. MIT Energy Initiative, 2009.

(24) Steeneveldt, R.; Berger, B. CO_2 capture and storage - Closing the knowing-doing gap. *Chemical Engineering Research & Design* **2006** (84) 739-763.

(25) Kohl, A. L.; Nielsen, R. B. *Gas Purification 5th edition*. Gulf Publishing Co., Houston, USA, 1997.

(26) Rao, A.; Rubin, E. A technical, economic, and environmental assessment of amine based CO_2 capture technology for power plant greenhouse gas control. *Environmental Science Technologies* 2002 (36) 4467-4475.

(27) Davidson, R. *Post combustion carbon capture from coal fired plants - solvent scrubbing*. Report CCC/125. London, UK. IEA Clean Coal Centre, 2007.

(28) Department of Energy and Climate change, *"CCS Roadmap", supporting deployment of carbon capture and storage in the UK*, April 2012.

Chapter 2

Literature Review

CO_2 capture and storage (CCS) technologies claim to be a long-term solution to reduce CO_2 emissions of power generating plants. The widespread implementation of CCS greatly depends on their ability to cope with complex power generation processes and meet the flexibility required by electricity consumers. Along with pulverized coal (PC) power plants, natural gas combined cycle power plant is a predominant option for both base-load electricity generation in addition to their inherent use for peak-load generation. As appears on the global energy agenda, the most near-term solution to abate CO_2 from fossil power plants is post-combustion capture via chemical absorption. This chapter provides a literature review focusing on key features and challenges of incorporating post-combustion CO_2 capture in natural gas combined cycle power plants.

2.1. Areas of Challenge

CO_2 capture based on chemical absorption/desorption using aqueous solution of amines as solvent is one of the post-combustion methods for CO_2 capture that can be incorporated into new gas fired power plants or retrofired as a tail end solution to an existing one. This process has been widely used in petrochemical processes as natural gas sweetening and ammonia production plants (1-3). One of the advantages of this process is its ability to capture CO_2 from exhaust gases with low CO_2 concentrations and partial pressures (4,5). This feature is highly in favour of natural gas fired power plants where the exhaust gas CO_2 concentrations are normally as low as 3-5 %.

Figure 2-1 shows a standard flow diagram of this process. Typically, the process consists of two columns: the absorber and desorber (stripper) columns. In the absorber column the CO_2

is absorbed by the solvent via fast reversible reactions, and in the stripper column the CO_2-rich solvent is regenerated and recycled back to the absorber to continue CO_2 absorption. Usually a cross heat exchanger is used to heat up the CO_2-rich solvent prior entering the absorber column using the heat available in the lean solvent exiting the stripper column. Details of this process are described in Section 3.1. of Chapter 3. Typical targeted CO_2 removal rate for CCS applications is around 90 % whilst with well-designed absorber columns, CO_2 removal rates ranging from 70 % to 99 % are achievable (6).

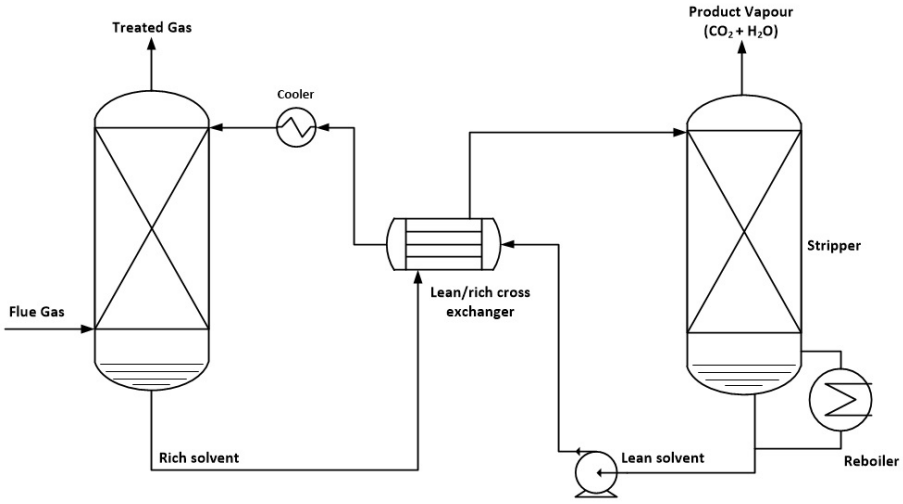

Figure 2-1. the process flow diagram of standard CO_2 capture by absorption/desorption

CO_2 capture based on chemical absorption/desorption processes on its own presents a number of technical and operational challenges beyond the scale-up if incorporated into large scale natural gas fired power plants. Despite the fact that petrochemical industries have been enjoying the deployment of this technology for decades; their integration into a power plant is associated with considerable challenges. The first and foremost challenge is the high amount of energy required by this process. In principle, the required energy is provided by the power plant in forms of steam and electricity. A large amount of steam is needed for the solvent regeneration process and is consumed at the reboiler, whilst the electricity is for blowers, pumps and the compressor. Meeting these requirements leads to nearly 30 % reduction in the net power output, 80 % increase in levelised cost of electricity, and thus a 7-10 %-point efficiency (energy) penalty (7-9).

The energy required for solvent regeneration depends on various factors such as CO_2 concentration in the exhaust gas, capture rate, solvent type and its regeneration temperature. In addition, the energy required for compression depends on regeneration thermodynamic conditions, i.e. temperature and pressure, as a higher regeneration pressure will lead to a higher pressure at the top of the stripper and consequently less compression energy required. To have an optimum integration of post combustion CO_2 capture process with power plant with high capture efficiency and minimal efficiency penalty, technical challenges and key aspects need to be simultaneously looked at. Furthermore, this combination are expected to integrate into the electricity generation mix, thus besides having high overall efficiency, the requirements of that electricity generation mix should be met.

For this technology to be commercially and economically viable, its current high capital and operating costs should be reduced. However, cost reductions must be done without compromising the performance of the process. This is the target of many research studies have been conducted around this topic. This can be achieved by choosing a competitive solvent in terms of rate of reaction and energy for regeneration, and using novel process configurations. In this regard, process modelling and simulation is a very useful tool to find promising alternatives.

2.1.1. Energy for Solvent Regeneration

With regard to the CO_2 capture process based on chemical absorption/desorption, it has been reported based on a number of studies that operating costs are more important than capital costs; and, in terms of operating costs, the energy required for solvent regeneration is the major consumer, followed by the energy required for CO_2 compression (10). On average, two thirds of the total efficiency penalty due to the use of post combustion CO_2 capture process in a power plant is because of reduced gross power output of the turbine generators and the remaining third is due to auxiliary energy requirements (11).

As mentioned earlier, CO_2 capture is based on a reversible reaction between the CO_2 and solvent. Regeneration heat depends on the heat capacity of the solvent, its CO_2 adsorption

heat, and the latent heat of vaporisation of volatile components in the solvent (12). In general, the total regeneration heat required in a CO_2 capture process can be determined by:

$$Q_{REG} = Q_{DES} + Q_{VAP} + Q_{SEN} \quad (2\text{-}1)$$

Where, Q_{REG} stands for total regeneration heat, Q_{DES} is the heat for CO_2 desorption, Q_{VAP} is the latent heat of vaporization of volatile components in solvent, and Q_{SEN} is the sensible heat required to increase the temperature of the solvent to the regeneration temperature. The sensible heat is calculated by:

$$Q_{SEN} = C_p \times \Delta T \quad (2\text{-}2)$$

Where, C_P is the heat capacity of the solvent and ΔT is temperature difference between the regeneration temperature and that of the CO_2-rich solvent entering the stripper. According to a study, for a CO_2 capture process using monoethanolamine (MEA) as solvent, almost half of the regeneration heat, e.g. 51 %, is consumed as the heat of desorption, followed by 26 % for generating stripping steam and, 23 % as sensible heat to heat up the solvent (13). These data imply reducing the sensible heat using different kind of heat integration is one of the effective ways to reduce the regeneration energy requirements. Figure 2-2 illustrates the breakdown of energy required in a typical MEA CO_2 capture plant with 85 % CO_2 capture rate from coal fired flue gases (13).

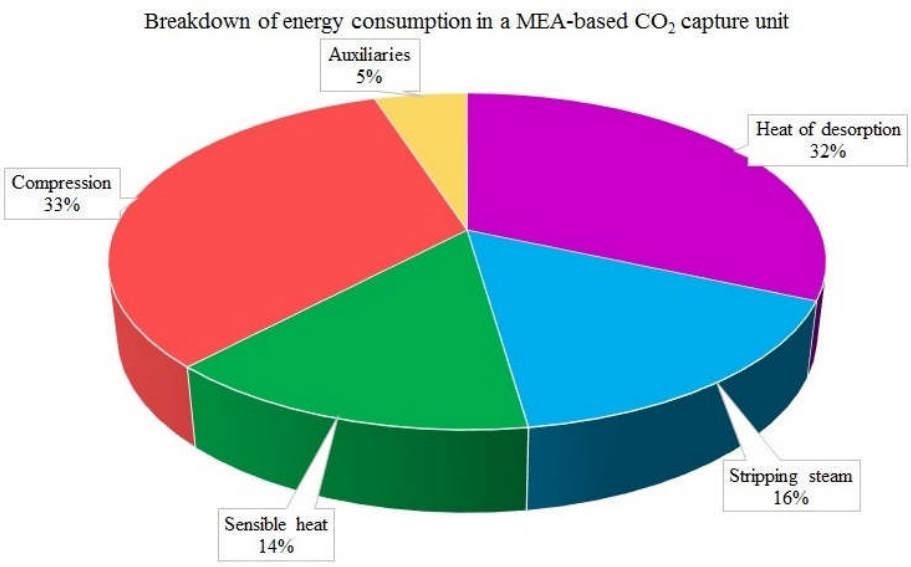

Figure 2-2. Breakdown of energy consumption in a MEA-based CO_2 capture unit (top), breakdown of regeneration energy in a MEA based CO_2 capture unit (bottom) (13)

Solvent heat capacity is a thermodynamic characteristic and for a given solvent this value is constant. The temperature of CO_2-rich solvent prior to entering the stripper could be increased by utilising heat from waste heat available in the process, such as hot lean solvent leaving the stripper column, heat available in the flue gas coming from the power plant, and/or by means of an electrical heater. One experimental study reported that utilizing heat from flue gases contributes about 20-25 % of the total energy required for regeneration. However, reducing the sensible heat means larger equipment (i.e. heat exchanger) and therefore it is associated with a trade-off with increased capital cost (14).

2.1.2. Solvent for CO_2 Capture Process

It is shown in the literature there is a linear relationship between the steam requirement for solvent regeneration and the efficiency penalty (8,15-17). According to Goto *et al*. (17), the estimated gradient is around 2 %, i.e. if the energy required for solvent regeneration reduces by 1 GJ per tonne of captured CO_2, the overall efficiency will improve by 2 %. Hence, using a chemical solvent having lesser regeneration energy would be highly advantageous.

Another important factor is related to the thermodynamic condition of regeneration. Temperature and pressure of regeneration are innate characteristics of the solvent (18). Regeneration at higher pressure will decrease the compression energy at the cost of excess steam energy provided for the reboiler. For MEA solvent, the ideal regeneration pressure is around 180 kPa based on the solvent thermal degradation limitations. This is discussed in detail in Section 5.4.3 of Chapter 5.

The industrial state-of-art solvent for CO_2 capture processes is an aqueous solution of 30 wt. % MEA. MEA is an economic solvent compared to other amines with a relatively fast rate of reaction with CO_2. However, practical problems with this solvent includes its relatively high energy requirement for regeneration, along with its susceptibility to degradation and propensity to cause corrosion. Alternative solvents have been proposed. An ideal solvent must require lower energy for regeneration with equivalent or better mass transfer rates with CO_2, and less degradation and corrosion risks than MEA (19). Kansai electric Power Inc. and Mitsubishi Heavy Industries (20,21) have developed two aqueous solvents (KS-1 and KS-2) which have lower regeneration heat. The performance of KS-1 was tested in a pilot plant, and the operating data confirmed the regeneration energy is almost 20 % lesser than that of MEA solvents. The regeneration energy of KS-2 is also lower than that of MEA though slightly higher than that of KS-1. In addition, it has been reported that KS-1 has a lower regeneration temperature of 110°C. It is likely however, that the KS series solvents have higher initial costs than MEA.

Gibbins and Crane (22) studied application of KS-2 solvent in a coal power plant. Their calculations showed that KS-2 consumes almost 30 % less steam than MEA solvent. The efficiency penalty and net power output when using KS-2 as solvent were estimated to be improved respectively by 5.2 %-points and 7 % than those for MEA solvent. Interestingly, the study reported that the excess levelised cost of energy for KS-2 solvent was nearly 9 % lower than that for MEA solvent.

Ammann and Bouallou (18) assessed the performance of different aqueous solvents: containing MEA, methyldiethanolamine (MDEA) and a blend of MDEA and triethylene-tetramine (TETA) in both natural gas and coal power plants. Their results showed the new solvent based on the blend of MDEA and TETA represents the best solvent with least efficiency penalty. Solvents based on MDEA, although requiring lower energy for regeneration, are less reactive with CO_2 than MEA-based solvents, and thus the size of the installation (absorber column) will be bigger, implying higher capital cost.

As a primary amine, MEA has high absorption capacity and excellent reactivity (23). Despite secondary and tertiary amines (e.g. TETA) possessing higher absorption capacity and less energy requirement for regeneration, compared to MEA, they have a slower rate of reaction with CO_2 (23). For post-combustion CO_2 capture, the amine solvents should have high CO_2 absorption capacity, fast CO_2 absorption/desorption rate, high heat of CO_2 absorption, low degradation, and low volatility (24). MEA is the solvent used for the studies conducted in this thesis, as this is the anticipated solvent to be used in the first generation of commercial CO_2 capture processes (25).

2.1.3. CO_2 Capture Rate

CO_2 capture rate or CO_2 removal rate is an important parameter for incorporating a CO_2 capture process into a power plant, as it directly affects the efficiency penalty and net power output. Higher CO_2 capture rate is associated with higher efficiency penalty and therefore more loss in the net power output. This is due to the fact that more energy is required at the reboiler for solvent regeneration in addition to higher solvent recirculation rate to provide the required driving force for CO_2 absorption (26).

From an environmental point of view, it is beneficial to have a higher removal rate as it leads to more CO_2 abatement (15). CO_2 capture rate is not a fixed term and could be varied. A typical 90 % capture rate is expected from post combustion CO_2 capture applications for fossil power plants. However, for power plants with low base-load efficiency or high electricity demand, it is worthwhile to adjust the capture rate to offer the best possible

electricity generation profile. The U.S. National Energy Technology Laboratory (15) conducted a study to evaluate the feasibility of varying the capture rates (30, 50, 70 and 90 %) and showed reducing the capture rate will improve the overall thermal efficiency and hence the plant output. This variation is shown in Figure 2-3.

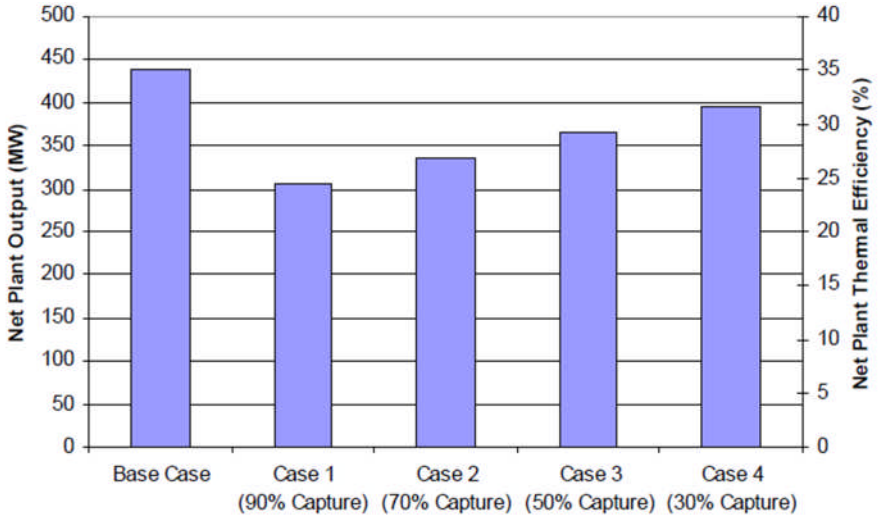

Figure 2-3. Variation of the CO_2 capture rate and its effect on the power plant efficiency and output

Sanpasertparnich *et al.* (27) showed that the relationship between CO_2 removal rate and steam flow requirement is exponential. For instance, increasing the capture rate by 10 %, from 70 % to 80 %, the steam flow rate will increase by about 2.6 %, whilst increasing the capture rate from 80 % to 90 % increases the steam flow extraction by about 6.7 %. Their evaluation concluded, regardless of extraction location, CO_2 removal rate ranging from 60 % to 85 % will offer relatively low efficiency penalty per tonne of CO_2 capture.

Reducing capture rate during peak electricity demand facilitates power plant operators in terms of better electricity selling price and security of supply at the cost of reduced CO_2 capture. Thus, this parameter must be optimised on a project-specific basis according to power plant type, expected power plant partial operation, the pattern of electricity demand, and load variations, CO_2 emission penalty cost, and electricity selling price. A 90 % CO_2 removal rate is considered in the studies conducted in this thesis.

2.2. Novel & Modified Process Configurations

Many studies are being conducted to find alternative processes or strategies to improve efficiency of CO_2 capture based on chemical absorption/desorption processes. For instance, various alternative process configurations have been proposed to reduce operational costs in these processes (28-38). There are different approaches to conserve energy in absorption/desorption processes, such as reducing the total heating or cooling loads, improving temperature levels of provided coolants or heat sources, or a combination of both (39). One practical method to reduce the energy requirements of such systems is application of side coolers or heaters to absorption and desorption columns respectively (39,40).

Fundamental research has shown the benefit of reduced driving forces in chemical processes. In a chemical process, driving forces for heat transfer (temperature), mass transfer, and chemical reaction (19,41) generally result in thermodynamic irreversibility, by which the process consumes more energy than ideally required (31,41). However, a chemical process with reasonable capital cost must have finite driving forces to expend some thermodynamic availability (exergy) and consume more energy compared to an ideal process.

Although it is not possible to have a thermodynamically reversible process, however, by proper design and operation it is possible to minimise the system exergy losses (31,42). Reducing excess driving forces will induce energy savings to the process. As mentioned earlier, CO_2 capture based on absorption/desorption is an important technological option for CO_2 capture from power plant flue gases. Quantitative models based on up-to-date realisation of vapour-liquid equilibrium and mass transfer rate are useful tools to develop and evaluate optimal design of economic processes. Optimal absorber and stripper design is critical in developing energy and cost efficient processes. For instance, optimising the solvent regeneration process is a crucial step in lowering the operational cost as it accounts for more than two thirds of energy consumed by the CO_2 capture process. In following alternative process cognations to optimise absorption and stripping process are presented.

2.2.1. Absorber Intercooling

CO_2 absorption using aqueous amines is usually associated with considerable amount of heat release due to reactions between CO_2 and the solvent by which the absorber column is led to act as both a chemical reactor and a heat exchanger. This heat is usually released in the liquid phase and will raise the liquid temperature and causes further heat transfer to the gas phase. Usually, the greater part of absorption and therefore the heat liberation occurs near the bottom of the column where the gas stream contains the highest amount of CO_2, thus the cool incoming gas absorbs heat from the rich solvent near the bottom of the column and subsequently transfers this heat to the cool lean solvent near the top of the column. The formation of a temperature bulge inside the absorber column is a result of the consecutive heat transfers between liquid and gas streams in the column (43). The magnitude, location and shape of the temperature bulge depend on the heat of reaction, the relative amount of liquid to gas, and where in the absorber column the CO_2 is mainly absorbed (43).

Absorber intercooling is a common strategy to improve the CO_2 absorption process especially when the heat of reactions involved cause an increase in the solvent temperature affecting the vapour pressure of dissolved species (32). Intercoolers are often used in absorbers to cool down flowing solvent that has been heated through the release of the heat of absorption at column locations above the intercooler (30). Intercooling benefits the absorption equilibria by reducing the temperature gradient between solvent and gas. Improved equilibrium in the absorber column will subsequently reduce the amount of solvent required for the same removal rate and thus may results in the reduction in energy required for solvent regeneration (30). Intercooling if used appropriately will provide internal conditions compatible with proper or required absorption process (44). According to a study, when the temperature rise is higher than 17 °C, the absorber column requires intercooling between stages to remove the heat of absorption to retain the operating condition close to the initial conditions (44). However, the effectiveness of using an intercooler is dependent on the location at which the highest temperature rise occurs.

There have been few numbers of studies investigating optimum conditions to employ intercoolers along the absorber columns or identifying process conditions at which intercoolers will be most useful. In one study, Coggan and Bourne (45) experimentally studied the absorption of ammonia into water and demonstrated that the optimal intercooler location was at a column location in the absorber above an equilibrium 'pinch' resulting from a temperature build-up, as long as the heat-carrying capacity (flow rate times specific heat capacity) of the liquid exceeded that of the gas. Conversely, the optimal location was at a column location below such a pinch for cases where the heat-carrying capacity of the gas exceeded that of the liquid (30,45). Plaza (32) extensively studied the application of absorber intercooling for 9 m MEA and 8 m piperazine (PZ) for a range of lean loadings and showed that absorber intercooling is most effective at critical liquid-to-gas ratios, i.e. when the temperature bulge without intercooling occurs in the middle of the column. Plaza (32) only studied the effectiveness of absorber intercooling on the absorber column performance, and the results presented by do not include benefits in terms of regeneration energy requirements.

Sachde and Rochelle (46) studied the possible solvent capacity and mass transfer benefits of using absorber intercooling for 90 % CO_2 capture with 8 m PZ for three different flue gas resources with 4 to 27 % mole CO_2 concentrations. Their study concluded regardless of the flue gas CO_2 concentration the absorber intercooling is most effective when is used at intermediate or mid-loading range lean loadings, whilst at extreme loadings (either low or high) results show negligible potential benefits from intercooling. In terms of CO_2 concentration, their findings revealed that intercooling offers the greatest potential when used for 4 % CO_2 concentration (equivalent of natural gas fired applications). Like Plaza's (32) studies, Sachde and Rochelle (46) studies did not include the benefits in terms of solvent regeneration energy requirements. In addition, there is no study of this kind to evaluate the effectiveness of incorporating absorber intercooling when using an aqueous solution of 30 wt. % MEA (equivalent of 7 m MEA) as solvent.

2.2.2. Advanced Stripper Configurations

In stripper columns, temperature differences are the dominant driving force. Thus, an effective way to reduce this driving force is by reducing the temperature differences between the rich solvent and the operating temperature (34). Schach *et al.* (34) studied the potential benefits of replacing conventional strippers by inter-heated columns. They showed that in conventional strippers there are considerably large thermal driving forces at several locations resulting in excessive expenditure of exergy and thermal energy. Their analysis of the stripper equilibrium and operating lines showed that equilibrium can be reached at only one point in a conventional stripper and that is the top where the rich solvent enters the column.

The stripper operation is often determined by the rich-end pinch which leads to great driving forces inside the column, by which more energy than required will be consumed at the lean-end i.e. at the bottom of the column (19). Oyenekan (19) suggests that by providing a condition to equally distribute driving forces from the rich-end to the lean-end, the reboiler duty will be reduced. Therefore, to reduce the exergy losses of a stripper column and improve its overall performance, more complexity has to be imposed on the process. One method to increase the complexity of the system could be entering the rich solvent to the stripper column via several points.

Previously, a number of research studies have explored various alternative process configurations and optimisation of CO_2 capture processes (31,34,36-38,40-42,47-52). One of the best configurations proposed earlier with PZ will be evaluated in this thesis with MEA. The potential for energy saving therefore exists and design and operation of energy efficient amine based CO_2 capture will have a substantial effect on the overall plant energy consumption and operating costs.

Complex configurations had previously been proposed to improve the energy efficiency of stripping columns. For example, Leites *et al.* (31) proposed several complex configurations that incorporate a combination of stripper column inter-heating and split-flow and a multi-feed arrangement at varying temperature. The original idea of the rich solvent split flow was

suggested and patented by Johnson and Eisenberg (53,54). They modified the stripping process by splitting the rich solvent into two streams downstream of the absorber. One is passed without further heating to the top of the stripper column while the other is passed to an intermediate point in the stripper column after being pre-heated in the lean/rich cross heat exchanger. Their suggested scheme however showed some energy deficiency where a portion of the rich solvent enters the column top with no prior preheating. Preheating the rich solvent to a temperature close to the stripper operating temperature is crucial to avoid the condensation of water vapour that would otherwise take place at the condenser, which causes an increase in the energy requirement (42).

Van Wagener and Rochelle (55) evaluated the benefits of increasing process reversibility by introducing more complexity to the system using multi-stage flash and inter-heated stripping. They showed using the inter-heated configuration improves the performance of the stripper column by approximately 8 % based on total equivalent work.

Furthermore, their study confirmed that increasing pressure will typically yield better performance in terms of energy consumption due to more reversible operation. Madan (48) showed stripper columns with various complex configurations perform better than a conventional one. His results showed that an advanced flash stripper with rich solvent split flow entering the column at different temperature levels offers the best performance. Later, Lin *et al.* (47) developed advanced configurations incorporating thermal integration based on excess regeneration heat and rich solvent split flow and studied the improvement brought by these modifications for 8 m piperazine (PZ) and 9 m MEA. They showed that the proposed configurations provide 10 % less equivalent work for 8 m PZ and 6 % for 9 m MEA when compared to a simple stripper. However, in their study solvent rich loading and lean loading were chosen arbitrary. So their results do not represent benefits for 90% CO_2 capture rate. The advanced flash stripper proposed by Lin was performed as expected when tested with 5 m PZ in a 0.1 MW pilot plant (56).

Recent work in industry has shown interest in the development of more complex configurations with higher efficiency. MHI examined more efficient heat recovery from the stripper column and studied an interheated stripper column (57). The MHI configuration attained a more reversible process in the stripper column by recycling a portion of the heat available in the lean solvent back into the column. Previously, Barchas and Davis (58) also claimed substantial saving in steam requirement for solvent regeneration when the total rich solvent is preheated to the stripper temperature before entering the column, with only a minor increase in equipment costs. However, the temperature of rich solvent before and after the proposed modification was not disclosed.

2.3. Thermal Integration

Newly built, i.e. greenfield, power plants can benefit greatly from the advantage of optimised process integration measures to reduce the efficiency penalty associated with their integration with post-combustion capture processes, although retrofitted plants can enjoy this option to the extent that their thermodynamic cycle allows. In addition to optimal supply of heat and auxiliary power, an optimal integration includes utilisation of waste heat from capture and compression units into the water/steam cycle of the power plant.

Pfaff *et al*. (59) suggested various thermal integration alternatives to optimise the waste heat utilisation from capture process to a greenfield power plant. For example, preheating the entire condensate by recovering the waste heat available at the stripper overhead condenser or compressor intercoolers will slightly increase the overall efficiency. Likewise, recovering the waste heat available in the intercoolers of compressor unit has a positive effect on plant overall net efficiency (13,15,20-22,59,60). Another possible alternative is pre-heating of combustion air with the stripper overhead condenser. Cousins *et al*. (23) studied several process configurations and they concluded that it is possible to reduce the energy required by a capture plant but, normally, at the expense of increasing plant complexity.

All options have to be compared based on their economic performance prior to their implementation. However, the simplicity of the process and its flexibility and integrity at part-load operations are vital to allow the power plant to adapt in variable electricity generation mix.

2.3.1. Steam Turbine Integration

While a standalone steam generator can be used to supply the steam required for solvent regeneration, to maximise efficiency, it is preferable to extract steam from the steam turbine. The steam requirements vary by solvent and some design parameters.

Supplying the steam will fundamentally change the design and operational concept of the steam turbine, by which the operation of base-load and off-design modes of the power plant cycle will be influenced. Depending on solvent type, overall system efficiency and capture rate, the extraction of steam is in the range of 40-50 % of the total flow (9,15,61). However, if the regeneration energy of the solvent is very high, it may reach up to 79 % (62).

The topic of integrating the steam turbine and the capture plant is widely discussed in the literature (12,26,27,59,60,63-67) reinforcing the notion that extracting steam from the steam turbine has a significant impact. Not only the energy of the extracted steam for the use in the stripper will result in the turbine to generate less electricity, but also it eventually brings considerable design implications on the low pressure part of the steam turbine especially after the extraction point.

This concept is further developed, and it became evident that the optimum route to extract steam for stripping the solvent is from the crossover pipe that transports steam from the intermediate pressure (IP) section of the steam turbine to the low pressure (LP) section (12,26,27,59,60,63-67). Nevertheless, extraction within the LP section of the turbine prior to its last expansion stage with the extraction pressure set as close as possible to that required in the reboiler (considering intervening pressure drops) would be a good alternative. However,

the latter option is dependent on the steam turbine inherent design and might not be suitable for retrofit options.

Mimura *et al*. (20,21) studied the thermodynamic integration between a post-combustion CO_2 capture and a natural gas fired power plant. They have shown that in order to lower the power loss by steam extraction it is important to lower the extraction pressure and to effectively utilise the heat available in the condensate returned from the capture plant into the power cycle. These findings were later developed further by Gibbins and Crane (22), mainly for coal based power plants.

In earlier studies performed by Alstom Power Inc. (62), the technical, economics and feasibility of implementing CO_2 capture to an existing coal power plant were evaluated. For an amine plant with 96 % capture rate, nearly 79 % of the total steam from the IP/LP crossover pipe was extracted and expanded through a new back pressure steam turbine. Hence, the exhaust steam from the new back-pressure LP turbine (at 450 kPa) provides the heat required in the reboiler. The remaining 21 % of the IP steam is eventually expanded through the existing LP turbine. Although the reported gross output reduction is about 28 %, the investment cost required for additional back pressure steam turbine were realised to be very high. Consequently, the levelised cost of energy and the unit cost of CO_2 removal were uneconomic.

Later, Ramezan *et al*. (15) performed a follow-up study and evaluated the technical and economic feasibility of integrating an amine process at various capture rates into a coal power plant. Their studies showed that extraction steam at 320 kPa would result in the most economical operation of the reboiler. The gross and net power output reductions were calculated at 16 % and 30 %, respectively, at 90 % CO_2 capture rate. Their study supported that steam extraction from the IP/LP crossover pipe offers a more attractive and economical solution to integrate an amine process into a power plant with no necessity of an additional back-pressure steam turbine.

Some studies have pointed out that the optimum supply pressure (considering pressure drops in piping and valves) is about 360 kPa withdrawing from the IP/LP crossover pipe between intermediate (IP) and low pressure (LP) cylinders (61). Later, Pfaff *et al*. (59) analysed the effect of steam pressure at the extraction point on the efficiency penalty associated with the integration of a post-combustion CO_2 capture (MEA) into a Greenfield state-of-art coal power plant. Their study showed that steam extraction at lower pressure (350 kPa vs. 550 kPa) will have a lesser efficiency penalty at the cost of inflexible behaviour at part-load operation. They have concluded that the choice of the IP/LP crossover design pressure has a great impact on the design efficiency.

Sanpasertparnich *et al*. (27) examined the effect of three steam extraction locations from the IP/LP crossover pipe (i.e. 300, 450, and 900 kPa) for a coal power plant. Their results showed that extraction at 300 kPa gives the lowest efficiency penalty despite requiring the highest extracted steam flow rate. They concluded extraction of steam at lower pressure has the advantage of decreasing the efficiency penalty. High flow steam extraction would cause an operational problem especially for the downstream of the extraction point (i.e. LP turbine), thus, extraction pressure selection must be in accordance with the maximum allowable extraction flow rate.

Aroonwilas and Veawab (26) showed for a supercritical coal power plant coupled with post combustion capture, the net power efficiency increased by 2 %-points (from 39 % to 41 %) when a steam pressure of 200 kPa instead of 400 kPa is extracted for MEA regeneration. Lenninberg *et al*. (67) quantified the energy penalty and the reduction in net power output for three IP/LP crossover pressures, i.e. 390, 550, and 700 kPa. Their results showed that the optimal design pressure in the IP/LP crossover depends on the amount of extracted steam and the reboiler temperature. In general, for a high reboiler temperature of the capture process, a power plant with a high design pressure in the IP/LP crossover is beneficial in terms of power loss. Lenninberg *et al*. (67) concluded the process configuration, solvent type and capture unit operation need to be in favour of existing power plant as it is difficult to

design a power plant technically and economically suitable for a given capture plant. Nevertheless, the optimal design pressure is a trade-off between the efficiency penalty and the operational flexibility of the power plants.

It is worthwhile to mention that there are limitations to the amount of steam can be extracted while maintaining reasonable turbine operation, as a certain amount of steam with an adequate pressure level must flow through the turbine, first, to ensure proper angle alignment of the flow within the turbine blades, and second, to keep the turbine blades cool. Hence, if a significant amount of steam is extracted prior to LP section, it possibly results in sub-optimal operation and consequently reduction in overall efficiency (15,68,69). This matter becomes more critical while the turbine is operating at off-design conditions. At times, the turbine is at part load operation, the steam turbine limitation will define the load operation of the capture plant in order to maintain balanced operation.

However, the majority of these concerns can be eliminated if steam turbine manufacturers design turbines considering this degree of steam extraction. Therefore, one may refer this as an industrial research gap (68).

2.4. Flexible Operations

It is important to consider capture plant implementation in power plants from a flexible operation point of view depending on electricity demand and price. Currently, the majority of studies on coupling capture plants and power plants are dominated by analysing a single design point at steady-state conditions. However, steady state models are not sufficient to properly analyse the behaviour of the system under operation and/or optimise its performance (70). Hence, it is important to consider and analyse flexible operation of post-combustion integrated power plants with particular focus on their potential dynamic performance at unsteady conditions.

In practice, flexible operations help electricity network operators to maintain the quality and security of supply. The widespread use of carbon capture technologies in the power

generation sector highlights the concern that flexible operation of power plants integrated with CCS is as valuable and necessary as standalone plants. This implies that capture plants should be developed to certain extents to be capable of withstanding wide operating ranges of power cycle to which they are coupling. There are quite definite and predictable operating ranges that power plant developers expect from a capture plant. Chalmers *et al*. (70) presented a number of flexible operations that all power plants routinely experience during their lifecycle:

- Quick start-up/shutdown (e.g. fast cycling "FACY")
- Quick change in output (load variation)
- Increase in maximum output (maximum continuous operation "MCR")
- Decrease in minimum output
- Fuel switchover
- Bypass operation (at times steam turbine fails operating)

These operational scenarios are further elaborated in reference (70).

Electricity selling price generally varies depending on demand side response, e.g. electricity price at nights is cheaper than that at peak time because of less demand. Besides, implementing CCS plant will definitely result in an increase in the cost of electricity generated. This add-up cost is more obvious at times the electricity selling prices are inherently high. This fact gives rise to the idea to reduce the high electricity price at peak times through the intrinsic flexibility in operation of a CCS-integrated power plant. Gibbins and Crane (22) suggested the idea of a partial or complete shutdown of the capture plant at peak times to reduce the electricity cost at the cost of reducing CO_2 avoidance. Gibbins and Crane (22) defined in a CCS-integrated power plant what the flexibility in operation means for power plant developers, such as:

- They can operate the plant without CCS at peak times (i.e. high demand thus high electricity price),

- Increase or decrease the net power output of the power plant by adjusting both the power plant and the CCS plant operational modes.

These two options are economically feasible only if the electricity selling prices are high enough to compensate the penalty cost of the emitting CO_2 which would be otherwise captured. For example, Chalmers and Gibbins (71) estimated for a coal based power generation mix only when electricity selling price is considered, that it could be economically advantageous to bypass a post-combustion plant when the unit ($/MWh) electricity price is at least two to three times higher than unit penalty cost of emitted CO_2 ($/t$CO_2$) (71).

Being less carbon intensive, natural gas fired plants emit CO_2 at lower rate per MWh of electricity generated. Hence, the CO_2 emission penalty cost associated with flexible operations even at the extreme case of switching capture plant off would be likely be traded off by the economic gain offered by the electricity selling prices.

In general, partial and entire bypass of the capture plant will have a great impact on the flow rate of the steam extracted from the water/steam cycle of power plant. Therefore, it is necessary to consider the impact of steam flow variation on water/steam cycle design.

Bypassing the capture plant with a clutched turbine would be extremely difficult. Assuming the clutched turbine is kept in standby, it would require re-clutching the turbine to handle the steam surplus. For the throttled LP turbine and floating IP/LP crossover pressure, no operational problem is expected with admitting more steam unless the LP turbine is not sized accordingly.

For a MEA-based amine process, the CO_2 capture rate is typically 90 % at which the highest efficiency penalty occurs. By changing it to lower values, the steam required for solvent regeneration will reduce, hence more steam will be available for power generation, thus more net power output (and vice versa). As discussed in section 2.2.4, Ramezan *et al*. (15) evaluated the effect of various CO_2 capture levels on the performance of a retrofitted coal

power plant with a conventional MEA-based amine process. Their results showed that by changing the CO_2 capture level from 90 % to 30 %, the net power output will increase by approximately 30 %, and concluded that a 10 % reduction in CO_2 capture rate equates to nearly an 11 % reduction in levelised cost of electricity and a 4 % reduction in the CO_2 capture cost.

These results stress the importance and attractiveness of flexible operation for power plants developers. Although results published by Ramezan *et al.* (15) properly demonstrated the trend of change, the behaviour of the capture and the power plant are yet to be described. For example, the operational limitations and the response time of the capture plant to cope with the change in the steam flow entering the reboiler must be analysed. In addition, how CO_2 capture rate varies during transient operation of the power plant, such as start-up, shut-down and load changes, are unclear. These pseudo-steady state operations highly emphasize the need and necessity for dynamic simulation of CCS-integrated power plants.

The bigger context of flexibility in operation is related to diurnal and seasonal variations in electricity demand and pricing. Assuming that CO_2 capture systems operate continuously at full-load and permanently consume a significant portion of power plants generation capacity is indeed ignoring dynamic operations in response to definite load variations. Cohen *et al*. (72) studied the effect of post-combustion plant on daily and yearly electricity demand fluctuations for a power grid in the U.S. Their studies showed flexible operation of the capture plant will benefit the plant operators in terms of electricity selling price at peak time and eliminate the need for building new electricity generation capacity to compensate the security in supply for capture plant deployment.

There are constraints that restrict flexible operations of post combustion plants. For instance, increased thermal interdependency between capture plant and power plant to increase the overall thermal efficiency will likely increase the complexity of the system and thus limit the flexibility in operation. Finally, operational flexibility of a plant is a trade-off between its overall performance (measured as overall efficiency) and associated complexity.

2.5. Conclusions & Remarks

For natural gas fired power plant applications, CO_2 capture based on chemical absorption/desorption using aqueous solution of 30 wt. % is the best near term option for decarbonisation. The various operational considerations for this process were discussed and areas of challenge hindering the commercialisation of this technology were addressed. This process has a major drawback of high heat requirement for solvent regeneration. In order to address this issue, alternative process configurations and/or process modifications have been introduced. Two promising alternative processes for absorber and stripper columns were discussed, which are called: advanced absorber intercooling (recycled intercooling), advanced flash stripper and advanced reboiled stripper, and the research gap associated with their future development were addressed. These alternative configurations improve the CO_2 capture process overall efficiency. These benefits are associated with increase in the process complexity.

Another challenge of incorporating CO_2 capture process into power plant cycle is related to the steam supply by the power plant for the solvent regeneration process. Providing the steam will fundamentally change the design and operational concept of the steam turbine, by which the operation of base-load and off-design modes of the power plant cycle will be influenced. This topic has been widely discussed in the literature. The optimum location to extract the steam is from the crossover pipe that transport steam form the IP steam turbine to the LP steam turbine section at the pressure around 300 to 400 kPa. Flexible operation is another topic that has been widely discussed in the literature. In addition, another issue on the incorporation of CO_2 capture processes into natural gas fired power plants in related to the fact that the integration might cause limitation on the power plant flexible operation as natural fired power plant are envisaged to be used for peak load operations in addition to base load operations. A number of solutions were introduced to manage the power plant flexible operation especially at peak times. These options with their impact were addressed in this chapter. A good number of studies concluded that operational flexibility of a plant is a

trade-off between its overall performance (measured as overall efficiency) and associated complexity.

2.6. List of References

(1) Bosch, H. *Solvents and reactors for acid gas treating*, The University of Twente, PhD. Dissertation. 1989.

(2) Veldman, R.; Ball, T. Improve gas treating. *Chemical Engineering Progress* 1991 (87) 67-72.

(3) Sartori, G.; Ho, W. S. Gas Treating with Solvents. *Separation Technology Symposium* 1985, Princeton, NJ.

(4) Lawal, A.; Wang, M.; Stephenson, P.; Koumpouras, G.; Yeung, H. Dynamic modelling and analysis of post-combustion CO_2 chemical absorption process for coal-fired power plants. *Fuel* 2010 (89) 2791–2801.

(5) Rao, A. B.; Rubin, E. S.; A technical, economic, and environmental assessment of amine-based CO_2 capture technology for power plant greenhouse gas control. *Environmental Science and Technology* 2002 (36) 4467–4475.

(6) Oyenekan, B. A.; G. T. Rochelle. Energy Performance of Stripper Configurations for CO_2 Capture by Aqueous Amines. *Ind Eng Chem Res* 2006 (45) 2457-2464.

(7) DOE/NETL. *Carbon Dioxide Capture and Storage RD&D Roadmap*. US Department of Energy, National Energy Technology Laboratory, 2010.

(8) Romeo, L.; Bolea, I.; Escosa, J. Integration of Power Plant and Amine Scrubbing to Reduce CO_2 Capture Costs. *Applied Thermal Engineering* 2008 (28) 1039–1046

(9) Peeters, A.N.M.; Faaij, A.P.C.; Turkenburg, W.C. Techno-economic analysis of natural gas combined cycles with post-combustion CO_2 absorption, including a detailed evaluation of the development potential. *International journal of greenhouse gas control* 2007 (1) 396–417

(10) Alie, C.; Douglas, P.; Croiset, E. *Simulation and optimisation of a coal-fired power plant with integrated CO_2 capture using MEA scrubbing*. PhD Dissertation, Department of Chemical Engineering,. University of Waterloo, Waterloo, Ontario, Canada, 2003.

(11) Freund, P.; Davison, J. *General Overview of Costs*. IPCC Workshop on Carbon Dioxide Capture and Storage. Geneva, Switzerland. 2002.

(12) Wiley, D. E.; Ho, M. T.; Donde, L. Technical and economic opportunities for flexible CO_2 capture at Australian black coal fired power plants. *Energy Procedia* 2010 (4) 1893–1900,

(13) Kothanadaraman, A.; Nord L.; Bolland O.; Herzog H.; McRae G. Comparison of Solvents for Post-combustion Capture of CO_2 by Chemical Absorption. *Energy Procedia* 2009 (1) 1373–1380

(14) Chalmers, H.; Gibbins, J. Initial evaluation of the impact of post-combustion capture of carbon dioxide on supercritical pulverized coal power plant part load performance. *Fuel* 2007 (86) 2109–2123,

(15) Ramezan, M.; Skone, T.; Nsakala, N.; Liljedahl, G.; Gearhart, L.; Hestermann, R.; Rederstorff, B. *Carbon Dioxide Capture from Existing Coal-Fired Power Plants*. US Department of Energy. Report DOE/NETL-401/110907, November 2007.

(16) Roberts, C. A.; J. R. Gibbons. Potential for Improvement in Power Generation with Post-Combustion Capture of CO_2, *7^{th} International Conference on Greenhouse Gas Control Technologies* 2004.

(17) Goto, K.; Yogo K.; Higashii T. A review of efficiency penalty in a coal-fired power plant with post-combustion CO_2 capture. *Applied Energy* 2013 (111) 710–720,

(18) Ammann, J.; Bouallou, Ch. CO_2 Capture from Power Stations Running with Natural Gas (NGCC) and Pulverized Coal (PC): Assessment of a New Chemical Solvent Based on Aqueous Solutions of N-MethylDiEthanolAmine + TriEthylene TetrAmine. *Energy Procedia* 2009 (1) 909 – 916,

(19) Oyenekan, B.A. *Modeling of strippers for CO_2 capture by aqueous amines*. PhD Dissertation, The University of Texas at Austin, 2007.

(20) Mimura, T.; Shimojo, S.; Suda, T.; Iijima, M.; Mitsuoka, S. Research and development on energy saving technology for flue gas carbon dioxide recovery and steam system in power plant. *Energy Conversion Management* 1995 (36) 397-400.

(21) Mimura, T.; Simayoshi, H.; Suda, T.; Iijima, M.; Mituoka, S. Development of energy saving technology for flue gas carbon dioxide recovery in power plant by chemical absorption method and steam system. *Energy Conversion Management* 1997 (38) 57-62.

(22) Gibbins, J.; Crane, R. Scope for reductions in the cost of CO_2 capture using flue gas scrubbing with amine solvents. Proceedings of the Institution of Mechanical Engineers, Part A. *Journal of Power and Energy* 2004 218: 231.

(23) Cousins, A.; Wardhaugh, L.; Feron, P. Preliminary analysis of process flow sheet modifications for energy efficient CO_2 capture from flue gases using chemical absorption. *Chemical Engineering Research and Design* 2011 (89) 1237-1251.

(24) Chowdhury, F. A.; Yamada, H.; Higashii, T.; Goto K.; Onoda M. CO_2 capture by tertiary amine absorbents: A performance comparison study. *Industrial & Engineering Chemistry Research* 2013 (52) 8323–8331,

(25) Rochelle, G. T. Innovative Stripper Configurations to Reduce the Energy Cost of CO_2 Capture. *Second Annual Carbon Sequestration Conference* 2003, Alexandria, VA,

(26) Aroonwilas, A.; Veawab, A. Integration of CO_2 capture unit using single- and blended amines into supercritical coal-fired power plants: Implications for emission and energy management. *International Journal of Greenhouse Gas Control* 2007 (1)143–150,

(27) Sanpasertparnich, T.; Idem, R.; Bolea, I.; De Montigny D.; Tontiwachwuthikul P. Integration of post-combustion capture and storage into a pulverized coalfired power plant. *International Greenhouse Gas Control* 2010 (4) 499–510,

(28) Page, S.C.; Williamson, A.G.; Mason, I.G.; Carbon capture and storage: fundamental thermodynamics and current technology. *Energy Policy* 2009, 37, 3314‑3324.

(29) Gottlicher, G. *The Energetics of Carbon Dioxide Capture in Power Plants*. U.S. Department of Energy, National Energy Technology Laboratory, 2004.

(30) Thompson, R.; King, C.J. Energy Conservation in Regenerated Chemical Absorption Processes. *Chemical Engineering and Processing* 1987, 21, 115-129,

(31) Leites, I.L.; Sama, D.A.; Lior, N. The theory and practice of energy saving in the chemical industry: some methods for reducing thermodynamic irreversibility in chemical technology processes. *Energy* 2003, 28, 55–97,

(32) Plaza, J.M. *Modelling of Carbon Dioxide Absorption using Aqueous Monoethanolamine, Piperazine and Promoted Potassium Carbonate*. PhD Dissertation, The University of Texas at Austin, 2011.

(33) Sachde, D.; Rochelle, G.T. Absorber intercooling configurations using aqueous Piperazine for capture from sources with 4 to 27 % CO_2. *Energy Procedia* 2014, 63, 1637-1656,

(34) Schach, M.O.; Schneider, R.; Schramm, H.; Repke, J.U. Techno-economic analysis of post-combustion processes for the capture of carbon dioxide from power plant flue gas. *Industrial & Engineering Chemistry Research* 2010, 49, 2363–2370,

(35) Karimi, M.; Hillestad, M.; Svendsen, H.F. Investigation of intercooling effect in CO_2 capture energy consumption. *Energy Procedia* 2011, 4, 1601–1607,

(36) Jassim, M.S.; Rochelle, G.T. Innovative absorber/stripper configurations for CO_2 capture by aqueous monoethanolamine. *Industrial & Engineering Chemistry Research* 2005, 45, 2465–2472.

(37) Amrollahi, Z.; Marchioro Ystad, P.A.; Ertesvag, I.S.; Bolland, O. Optimized process configurations of post-combustion CO_2 capture for natural-gas-fired power plant – Power plant efficiency analysis. *International Journal of Greenhouse Gas Control* 2012, 8, 1–11,

(38) Amrollahi, Z.; Ertesvag, I.S.; Bolland, O. Optimized process configurations of post-combustion CO_2 capture for natural-gas-fired power plant—Exergy analysis. *International Journal of Greenhouse Gas Control* 2011, 5, 1393–1405.

(39) Naka, Y.; Terashita, M. An intermediate heating and cooling method for a distillation column. *Journal of Chemical Engineering of Japan* 1980, 13, 2, 123-129,

(40) Tobiesen F. A.; Svendsen, H. F. Study of a Modified Amine-Based Regeneration Unit. *Ind. Eng. Chem. Res.* 2006, 45, 2489-2496.

(41) Van Wagener, D.H. *Stripper Modeling for CO_2 Removal Using Monoethanolamine and Piperazine Solvents*. PhD Dissertation. The University of Texas at Austin, 2011.

(42) Sama, D.A. The use of the Second Law of thermodynamics in the design of heat exchangers, networks, and Processes. *Proceeding of the International Conference on Energy Systems and Ecology* 1993, 1–24.

(43) Kvamsdal, H .M.; Rochelle, G. T. Effects of the Temperature Bulge in CO2 Absorption from Flue Gas by Aqueous Monoethanolamine. *Industrial & Engineering Chemistry Research* 2008, (47) 867-875.

(44) Coker, A. K. *Ludwig's Applied Process Design for Chemical and Petrochemical Plants*. Vol. 2, 4th Edition, Gulf Professional Publishing, 2010.

(45) Coggan, G. C.; Bourne, J.R. The Design of Gas Absorbers with Heat Effects Part 11: Methods for Improving Separation. *Transactions of the Institution of Chemical Engineers* 1969, (47) T160.

(46) Sachde, D.; Rochelle, G.T. Absorber intercooling configurations using aqueous piperazine for capture from sources with 4 to 27 % CO_2. *Energy Procedia* 2014, (63) 1637-1656,

(47) Lin, Y-J; Madan T.; Rochelle G.T. Regeneration with Rich Bypass of Aqueous Piperazine and Monoethanolamine for CO_2 Capture. *Ind. Eng. Chem. Res.* 2014, 53, 4067-4074.

(48) Madan, T. *Modelling of Stripper Configurations for CO_2 Capture using Aqueous Piperazine*. MSc. Dissertations. The University of Texas at Austin, 2013.

(49) Lin Y-J.; Rochelle G.T. Optimization of Advanced Flash Stripper for CO_2 Capture using Piperazine. *Energy Procedia* 2014, 63, 1504–1513.

(50) Oyenekan, B.A.; Rochelle, G.T. Alternative stripper configurations for CO_2 capture by aqueous amines. *AIChE* 2007, 53 (12), 3144–3154.

(51) Shoeld, M. *Purification and separation of gaseous mixtures*. 1934, Patent No. US 1971798, The Koppers Company of Delaware.

(52) Rochelle, G.T. Amine scrubbing for CO_2 capture. *Science* 2009, (325) 1652-1654.

(53) Johnson, R.R.; Eisenberg, B. *Amine regeneration process*. 1979, Patent No CA 1117461 A1, Exxon Research and Engineering Company.

(54) Eisenberg, B.; Johnson, R.R. *Heat exchanging, acid gas absorption*. 1979, Patent No US 4152217 A, Exxon Research and Engineering Company.

(55) Van Wagener, D.H.; Rochelle, G.T. Stripper configurations for CO_2 capture by aqueous monoethanolamine. *IChemE* 2011, 89, 1639−1646,

(56) Chen, E. Pilot Plant Results for 5 m piperazine with the advanced flash stripper. Presented at *PCCC3*, Regina Saskachewan, Sept 2015.

(57) Yagi, Y.; Mimura, T.; Iijima, M.; Ishida, K.; Yoshiyama, R.; Kamijo, T.; Yonekawa, T. Improvements of carbon dioxide capture technology from flue gas. *GHGT-7* 2005, 1139–1145.

(58) Barchas, R.; Davis, R. The KERR-MCGEE/ABB LUMMUS CREST technology for the recovery of CO_2 from stack gases. *Energy Conversion and Management* 1992, (33) 333–340.

(59) Pfaff, I.; Oexmann, J.; Kather, A. Optimised integration of post-combustion CO_2 capture process in greenfield power plants, *Energy* 2010 *(*35) 4030-4041,

(60) Metz, B.; Davidson, O.; Coninck, H.; Loos, M.; *Meyer, L. IPCC Special Report on Carbon Dioxide Capture and Storage. Intergovernmental Panel on C*limate Change, Cambridge University Press, NY 10013-2473, USA, 2005

(61) Report 2007/4. *CO_2 capture ready plants*. International Energy Agency Greenhouse Gas R&D Program (IEAGHG), 2007.

(62) Liljedahl, G. N.; Gupta, J. C.; Marion, J. L.; Fugate, M. *Engineering Feasibility and Economics of CO_2 Capture on an Existing Coal-Fired Power Plant: Technical Report*. Alstom Power, Inc., Windsor, CT. Power Plant Labs, DE-FC26-99FT40576, 2001,

(63) Gibbins, J.; Crane, R.I. Scope for reductions in the cost of CO_2 capture using flue gas scrubbing with amine solvents. Proceedings of the Institution of Mechanical Engineers, Part A. *Journal of Power and Energy* 2004, (218) 231-239.

(64) Lucquiaud, M; Chalmers, M; Gibbins J. Capture-ready supercritical coal-fired power plants and flexible post-combustion CO_2 capture. *Energy Procedia* 2009 (1) 1411–1418,

(65) Lucquiaud, M; Gibbins J. Effective retrofitting of post-combustion CO_2 capture to coal-fired power plants and insensitivity of CO_2 abatement costs to base plant efficiency. *International Journal of Greenhouse Gas Control* 2011(5) 427–438,

(66) Lucquiaud, M; Gibbins, J. Steam cycle options for the retrofit of coal and gas power plants with post-combustion capture. *Energy Procedia* 2011 (4)1812–1819.

(67) Linnenberg, S.; Liebenthal, U.; Oexmannm J.; Kather, A. Derivation of power loss factors to evaluate the impact of post-combustion CO_2 capture processes on steam power plant performance. *Energy Procedia* 2011 (4) 1385–1394,

(68) Hildebrand, A.N. *Strategies for Demonstration and Early Deployment of Carbon Capture and Storage: A Technical and Economic Assessment of Capture Percentage*. PhD Dissertation, Massachusetts Institute of Technology, 2009.

(69) Pfaff, I.; Oexmann, J.; Kather, A. Optimised integration of post-combustion CO_2 capture process in Greenfield power plants. *Energy* 2010, 35 4030-4041,

(70) Chalmers, H.; Lucquiaud, M.; Gibbins, J.; Leach, M. Flexible operation of coal power plants with post-combustion capture of carbon dioxide. *Journal of Environmental Engineering* 2009, vol. 135, No. 6.

(71) Chalmers, H.; Gibbins, J. Initial evaluation of the impact of post-combustion capture of carbon dioxide on supercritical pulverised coal power plant part load performance. *Fuel* 2007, 86 (14) 2109–2123.

(72) Cohen, S.M.; Rochelle, G.T.; Webber, M.E. Turning CO_2 capture on and off in response to electric grid demand: a baseline analysis of emissions and economics. *Journal of J Energy Resources and Technologies* 2010 (132) 3-8,

(73) Kvamsdal, H. M.; Jakobsen, J. P.; Hoff, K. A. Dynamic modeling and simulation of a CO_2 absorber column for post-combustion CO_2 capture. *Chemical Engineering Proceedings* 2009, 48 (1) 135-144,

(74) Patino-Echeverri, D; Hoppock, D. C. Reducing the energy penalty costs of post-combustion CCS systems with amine-storage. *Environmental Science Technologies* 2012 (46) 1243–1252,

Chapter 3

Modelling Methodology

Models are indispensable tools for research and development. They play a crucial role in the creation and use of processes and help to increase our comprehension of them. A model itself is a simplification of reality, and the effectiveness of a model lies on its ability to capture enough details to be realistic. This chapter presents fundamental concepts, cornerstones and details used to develop a thermodynamic model of the CO_2 capture process using aqueous solutions of monoethanolamine (MEA) as solvent. At first the process description of the system is presented, then the chemistry and kinetics of CO_2 reaction with aqueous MEA are defined, and finally the details of the thermodynamic framework used to represent the CO_2-H_2O-MEA system are described. The importance of this chapter cannot be overstated as the research discussed in this thesis is a contributor to tackle climate change by decarbonising power plants flue gases.

3.1. Post-Combustion CO_2 Capture with MEA

Among methods proposed to remove CO_2 from power plant flue gases, the CO_2 absorption/stripping with a circulating chemical solvent is currently considered as the most viable solution. This process can be placed at the tail end of existing or new fossil fuel based power plants with minor modification within the power plants processes. Design of a CO_2 absorption/stripping process using chemical solvents is a function of many variables such as flue gas conditions, e.g. CO_2 concentration, temperature, pressure, other impurities present, etc., solvent conditions, e.g. type and concentration, construction material, e.g. packing type and column shape, and system configuration. Systems with near atmospheric pressure, which is the interest of this thesis, require relatively active solvents with high absorption capacity to react with CO_2. Amines are commonly considered for such applications with

MEA as the industry standard. Figure 3-1 shows the typical set up for a CO_2 absorption/stripping system using aqueous MEA as circulating solvent.

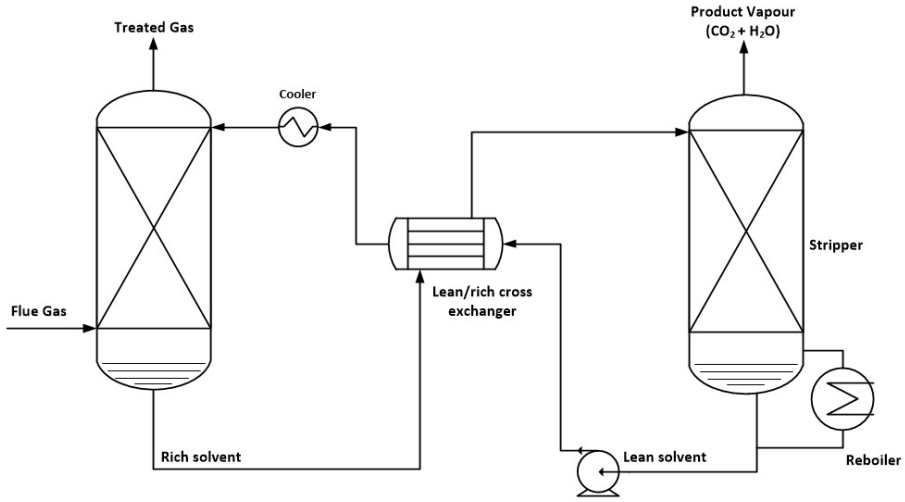

Figure 3-1. MEA based CO_2 absorption/stripping process

Before entering the absorber column, the flue gas should be free from SO_2 and NO_2 as these constituents affect the absorption process by forming heat stable salt with MEA. The recommended concentrations of SO_2 is below 10 part per million by volume (ppmv) (2). Contrary to natural gas flue gases that are free from SO_2, coal fired flue gases contain SO_2, the SO_2 removal is usually achieved by passing the flue gas through a flue gas desulphurisation (FGD) unit. If NO_x is present in the flue gas, it could be removed using selective catalytic reduction (SCR) or selective nonanalytic reduction (SCNR).

In a natural gas-fired power plant, flue gas temperature at the gas turbine exhaust is around 100-120°C, and is required to be cooled before entering the absorber column. Cooling typically is done by passing the flue gas through a direct contact cooling (DCC) unit which is a packed column where water is fed from the top and counter-currently contacted with the flue gas that is fed at the bottom. The flue gas exits the DCC from the top and enters a blower to be slightly pressurised to overcome the passage and packing pressure drop through the absorber column.

Typically, absorbers are packed columns. Packing provides sufficient surface area for CO_2 and solvent to contact and react. Flue gas enters the absorber column below the packing section and counter-currently contacts with the lean solvent that enters above the packing section. CO_2 is absorbed into the aqueous MEA solvent through reversible chemical reactions to form a rich solvent. In a MEA-based system, the absorber operates at a temperature around 40 °C. Therefore, it is recommended that the flue gas and circulation solvent temperatures at the absorber inlet be around 40 to 50 °C. Rich solvent leaves the column at the bottom and treated gas discharges to atmosphere from the top. Before the treated gas leaves the absorber column, it passes through a demister to retain carried over liquid droplets, and then a washing section to further reduce amine losses. In a MEA-based system, the solvent loading can be defined as the molar ratio of CO_2 to MEA in a unit of aqueous solution of the solvent. After leaving the absorber column, the rich solvent is pumped through the cross heat exchanger before being fed to the stripper column. at the cross heat exchanger, the rich solvent is heated by the hot lean solvent, coming from the stripper column. Before proceeding to the absorber column, the lean solvent is further cooled down to typically 40°C in a trim cooler.

The stripper column is also a packed column, and the rich solvent enters the stripper above the packed section. The stripping steam is generated at the bottom of the column by partial evaporation of the liquid solvent in the reboiler where the external heat is provided usually in the form of steam. This heat reverses the chemical equilibrium between MEA and CO_2, and the released product vapour, i.e. CO_2 and water vapour, leaves the stripper at the top. The hot lean solvent leaves the stripper column at the bottom and flows through the cross heat exchanger and the trim cooler to enter the absorber column.

The product vapour released from the stripper enters an overhead condenser where its water vapour is taken out before the remaining CO_2 is compressed in a multi-stage compression unit up to a pressure of 120-150 bar, suitable to transport to suitable storage sites or use in

enhanced oil recovery (EOR) applications. The condensed water is routed back to the stripper column after being stabilised in the reflux drum.

3.1.1. MEA Solution Concentration

MEA is a primary amine and a primary alcohol. Its melting point is at 10.3 °C and its boiling point is at approximately 170°C (1). It is an economic solvent and it has long been the industry standard for non-selective removal of acid gases such as CO_2 and H_2S due to its low cost per mole of amine, high heat of absorption, high absorption capacity, and high rates of reaction (2,3). Low degradation resistance is a downside of this solvent (3).

Choosing an appropriate concentration of MEA solvent is usually made practically on the basis of operating experience (4). Typical concentration of aqueous MEA is in the range of 15 to 30% wt. %. Early application of aqueous MEA for CO_2 removal dates back to 1949 (5). During 1970-1980, Dow chemical and Union Carbide used a 30 wt. % aqueous solution of MEA to produce CO_2 for EOR applications (6, 7). In 1992, ABB Lummus Crest/Kerr McGee used 20 wt. % aqueous solution of MEA in a CO_2 removal process (8). Recently, higher concentrations, e.g. up to 40 wt. %, have been proposed to improve the absorption capacity. Increasing the solvent concentration will generally result in reducing the recirculating solvent flow rate and therefore the plant operational cost, however, higher concentrations are associated with higher risk of corrosion and more corrosion inhibitors are required (9). Unless otherwise stated, throughout this thesis an aqueous solution of 30 wt. % MEA (or equivalent of 7 molar (m) MEA) is used as solvent.

3.2. Chemistry of CO_2 Reaction with Aqueous MEA Solution

In aqueous solutions the extent of electrolyte dissociation is governed by chemical equilibrium. Electrolytes that dissociate completely are referred to as strong electrolytes, and electrolyte species that partially dissociate in aqueous solutions are referred to as weak electrolytes. The compounds of interest in this thesis are characterised as weak electrolytes, as CO_2 is a weak acid electrolyte and MEA is a weak organic base electrolyte (10). These

two weak electrolytes when reacting in aqueous solutions partially ionise, and/or partially dissociate as described in Reactions 3-1 to 3-7.

When gaseous CO_2 absorbs into an aqueous solution of MEA (denoted here as RNH_2) and reacts with it, the following reactions take place (11):

Ionisation of water:

$$\mathrm{H_2O} \xleftrightarrow{K_1} \mathrm{OH^-} + \mathrm{H^+} \tag{3-1}$$

Dissociation of dissolved CO_2 through carbonic acid:

$$\mathrm{CO_2} + \mathrm{H_2O} \xleftrightarrow{\mathrm{k_{H_2O}},\mathrm{K_2}} \mathrm{HCO_3^-} + H^+ \tag{3-2}$$

Bicarbonate formation:

$$\mathrm{CO_2} + \mathrm{OH^-} \xleftrightarrow{k_{OH^-}} \mathrm{HCO_3^-} \tag{3-3}$$

Dissociation of bicarbonate:

$$\mathrm{HCO_3^-} + \mathrm{H_2O} \xleftrightarrow{k_{HCO_3^-},K_3} \mathrm{CO_3^{2-}} + \mathrm{H_3O^+} \tag{3-4}$$

Carbamate formation from MEA and CO_2 reaction:

$$\mathrm{CO_2} + \mathrm{RNH_2} + \mathrm{B} \xleftrightarrow{k_4 k_{-4} K_4} \mathrm{RNH_2^+COO^-} + \mathrm{BH^+} \tag{3-5}$$

Carbamate reversion to becarbonate (hydrolysis reaction):

$$\mathrm{RNHCOO^-} + \mathrm{H_2O} \xleftrightarrow{K_6} \mathrm{RNH_2} + \mathrm{HCO_3^-} \tag{3-6}$$

MEA protonation:

$$RNH_2 + H_3O^+ \xleftrightarrow{k''_{RNH_2} k_9 K_5} RNH_3^+ + H_2O \quad (3\text{-}7)$$

$RNH_2^+COO^-$ and RNH_3^+ are carbamate and protonated MEA, respectively. The base (B) in Reaction 3-5 can be either RNH_2, H_2O, OH^-, or a combination of bases present in the system. Reactions 3-1 and 3-7 are normally considered to be instantaneous. The direct reaction of CO_2 with water (Reaction 3-2) is a very slow reaction when compared with the reaction involved in carbamate formation (Reaction 3-5).

3.2.1. Mechanism of CO_2 Reaction with Aqueous MEA

Reactions between CO_2 (being a weak acid gas) and MEA solution (being a weak base solution), as presented in Reactions 3-5, have been usually described by using either a two-step zwitterion mechanism suggested by Danckwerts (12), or a one-step termolecular mechanism proposed by Crooks and Donnellan (13). In the following these mechanisms and their differences are described.

3.2.1.1. Zwitterion Mechanism

In this mechanism it is suggested that in the first step, CO_2 reacts reversibly with MEA and forms an unstable zwitterion, as expressed by Reaction 3-8. The unstable zwitterion may either reverse back to CO_2 and MEA, or becomes de-protonated by a base present in the system to form carbamate in the second step as expressed by Reaction 3-9 (12,14,15):

$$CO_2 + RNH_2 \xleftrightarrow{k_1, k_{-1}} RNH_2^+COO^- \quad (3\text{-}8)$$

$$RNH_2^+COO^- + B \xleftrightarrow{k_B, k_{-B}} BH^+ + RNHCOO^- \quad (3\text{-}9)$$

The combination of Reactions 3-8 and 3-9 will give Reaction 3-5.

The zwitterion mechanism is mostly used to describe the reactions between CO_2 with a primary (such as MEA) or secondary amines in both aqueous and non-aqueous solutions (12,15-17).

3.2.1.2. Termolecular Mechanism

In this mechanism, it is assumed that the reaction between CO_2 and MEA is a single-step reaction where the initial product is not a zwitterion and instead a loosely-bound encounter complex as the intermediate, that can be represented as (16):

$$\mathrm{RNH_2 \ldots B + CO_2 \leftrightarrow RNHCOO^- + BH^+} \qquad (3\text{-}10)$$

The loosely-bound complex breaks up to form the original reactant molecules, i.e. MEA, CO_2, and the base, although a small fraction of it reacts with a molecule of water or MEA to produce ionic products. However, the production of bond and charge separation takes place only in the second step. Crooks and Donnellan (14) stated that their proposed termlecular mechanism may be regarded as a limiting case of the zwitterion mechanism when $k_{-1} \gg k_B[B]$.

3.2.2. Equilibrium Constants

Equilibrium constants govern the dissociation of weak electrolytes in an aqueous solution, and they are defining inputs to the vapour-liquid equilibra of the solution (11). The equilibrium constant as a function of temperature is proposed by Austgen *et al*. (17) as:

$$ln(K) = C_1 + \frac{C_2}{T} + C_3 Ln(T) + C_4 T \qquad (3\text{-}11)$$

Table 3-1 presents the values of constants C_1, C_2, C_3, and C_4 for different reactions (17).

Table 3-1. Temperature dependencies of the equilibrium constant (17)

Reaction	**C_1**	**C_2**	**C_3**	**C_4**	**Temperature Range**
Reaction (3-1)	132.899	-13445.9	-22.4773	0.0	0-225°C
Reaction (3-2)	231.465	-12092.10	-36.7816	0.0	0-225°C
Reaction (3-4)	216.049	-12431.7	-35.4819	0.0	0-225°C
Reaction (3-6)	2.1211	-8189.38	0.0	-0.007484	0-50°C
Reaction (3-7)	2.8898	-3635.09	0.0	0.0	25-120°C

The thermodynamic framework used in the electrolyte Non Random Two liquid (e-NRTL) model, i.e. the model used in Aspen plus for all simulations carried out in this thesis and will be presented in following sections, is based on two types of equilibria: chemical reaction dissociation equilibria, and vapour-liquid phase equilibria for molecular species (17). Molecular electrolytes react or dissociate in the liquid phase to produce ionic species to the extent governed by chemical equilibria (17). The equation governing chemical equilibria may be expressed as:

$$K = \prod_i \alpha_i^{v_i} \tag{3-12}$$

Where α_i is the activity coefficient of species i. The following sections provide a thorough description of the thermodynamic framework governing the CO_2-H_2O-MEA system.

3.3. Thermodynamic Model

Design of a CO_2 absorption-desorption system with aqueous MEA solution requires knowledge of the vapour-liquid equilibria (VLE) of the CO_2-H_2O-MEA system (17,18). To properly model the CO_2 absorption/desorption process a rigorous thermodynamic model to accurately interpolate and extrapolate experimental vapour-liquid equilibria data of the CO_2-H_2O-MEA system is required (17,18). An ideal thermodynamic model of CO_2-H_2O-MEA should accurately represent the phase equilibria between the vapour and liquid phases, as well as the chemical reaction equilibria existing within the liquid phase (19).

Because of difficulty in presenting activity coefficients in concentrated electrolyte solutions, early VLE models for weak electrolytes were based on empirical models that lacked representation of physical interactions (17). Empirical models are based on experimentally fitted parameters, and since these models use less complex calculations than theoretical models they do not properly estimate the composition of the liquid phase. These models usually fail to predict conditions outside the range of the experimental data used for parameter fitting (17).

One of the first widely used empirical models for amine solutions was proposed by Kent and Eisenberg (20). This model presents H_2S and CO_2 equilibrium partial pressures over aqueous solutions of MEA and diethanolamine (DEA). The model assumes all activity coefficients and vapour-phase fugacity coefficients are unity, and forces a fit between experimental data and the model predicted values by employing apparent equilibrium constants in the equations (17). This model is still used for CO_2 capture modelling. Deshmuck and Mather (21) developed a more rigorous model to calculate the solubility of H_2S and CO_2 in MEA solutions. The model seems to be more accurate than the Kent-Eisenberg Model as it estimates the activity and fugacity coefficients that are used in calculating the liquid phase equilibrium constants and in the application of Henry's law to the VLE. However, this model is known to be complicated (17).

Gabrielsen *et al*. (22) used a simple approach to describe the VLE of CO_2 in single aqueous solution of MEA, DEA and methyldiethanolamine (MDEA) by taking into account only one chemical equilibrium reaction and assuming ideal gas and ideal liquid properties. The model uses four experimentally-regressed parameters to describe the partial pressure of CO_2 in the relatively narrow range of conditions experienced in the CO_2 removal from power plants flue gases across a relatively narrow temperature range.

Contrary to empirical models, semi-empirical models rely mainly on theoretical assumptions. However, they also suggest parameter adjustment via experimental data. Several semi-empirical excess Gibbs energy models and/or activity coefficient models have

been developed that are suitable for aqueous electrolyte systems with conditions typical of industrial application (10). The application of Pitzer's excess Gibbs energy model (23) is generally limited to single-solvent, aqueous systems. For this model, the solute-solute binary interaction parameters are as unknown function of solvent composition. To properly model an aqueous amine system, it is required to consider the amine-water systems as a mixed solvent system of variable composition (24). One of the most accurate models was developed by Austgen *et al*. (18) to represent VLE in H_2S and CO_2 in an aqueous amine system. The model uses the e-NRTL model developed by Chen and Evans (25) to represent activity coefficients in CO_2-H_2O-amine. This model has been successfully used to correlate experimental VLE data for different types of amine solutions over a wide range of applications and proved to produce highly accurate results (26). Activity coefficient models and equation of state are the main semi-empirical models for electrolyte systems. Activity coefficient models represent liquid phase properties and the equations of state describe the vapour phase properties. These two models are usually combined to represent VLE in electrolyte solutions.

3.4. Chemical Equilibria & Phase Equilibria

Figure 3-2 shows the chemical and phase equilibria in a closed loop of a weak electrolyte system, of which the CO_2-H_2O-MEA system is an example. In a closed system at constant pressure and temperature, phase equilibria governs the distribution of molecular species between the liquid and vapour phase. In such systems ionic species are normally considered as non-volatile and they will be present only in the liquid phase. Chemical equilibria govern the distribution of an electrolyte in the liquid phase between the molecular and ionic forms. Physical and chemical equilibria are highly coupled in such systems. Equality of chemical potentials is the fundamental criterion for phase and chemical equilibrium (27).

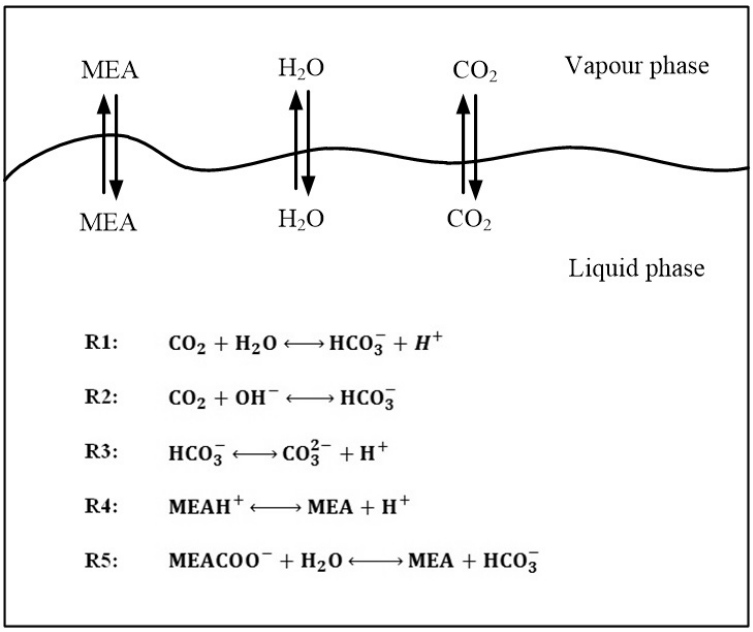

Figure 3-2. Schematic representation of chemical and phase equilibria in a closed loop of a weak electrolyte system

According to Gibbs theory, phase equilibria are attainable when at the same temperature and pressure the chemical potential of each species is the same in all phases (28). For a vapour-liquid system at isothermal and isobaric conditions, the Phase equilibria can be expressed as:

$$\mu_i^v = \mu_i^l \tag{3-13}$$

Where μ_i^v and μ_i^l are the chemical potential of species *i* in the vapour and liquid phase, respectively. The chemical potential of species *i* present in phase *a* is defined by:

$$\mu_i^a = \left(\frac{\partial G^a}{\partial n_i}\right)_{T,P,n_{j\neq i}} \tag{3-14}$$

Where G^a is the total Gibbs free energy of the species *i* in phase *a*, n_i is the number of moles of species *i*, T is the uniform temperature of the closed system, and P is the uniform pressure. The subscript $n_{j\neq i}$ implies the number of moles of all species, except the i^{th} component, are held constant.

3.5. Rigorous Vapour-Liquid Equilibrium (VLE) Models for the CO_2-H_2O-MEA System

In theory, the vapour-liquid equilibria for the solvent species are expressed as (19,28):

$$y_i\hat{\phi}_i P = x_i\gamma_i\phi_i^{sat}P_i^{sat}exp\left(\frac{v_s(P-P_s^{sat})}{RT}\right) \quad (3\text{-}15)$$

Eq. 3-15 accurately describes the VLE of solvent molecules; however it fails for supercritical components, i.e. components that are gaseous at normal conditions, as the saturation pressure does not apply to them (21). An equivalent form of Eq. 3-15, based on Henry's constant is usually used to express vapour-liquid equilibria for the supercritical components as (10,19):

$$y_i\hat{\phi}_i P = x_i\gamma_i\left(\frac{H_i^m}{\gamma_i^\infty}\right)exp\left(\frac{\bar{v}_{i-m}^\infty(P-P_m^{sat})}{RT}\right) \quad (3\text{-}16)$$

Where,

$$\ln\left(\frac{H_i^m}{\gamma_i^\infty}\right) = \sum_s w_s \ln\left(\frac{H_{i-s}}{\gamma_{i-s}^\infty}\right) \quad (3\text{-}17)$$

With:

$$w_s = \frac{x_s\left(v_s^{*l}\right)^{2/3}}{\sum_{s'} x_{s'}\left(v_s^{*l}\right)^{2/3}} \quad (3\text{-}18)$$

Where H_i^m is the Henry's constant of solute *i* in all solvent components, $\bar{v}_{i-m}^\infty$ is the partial molar volume of solute *i* at infinite dilution in the solvent mixture at the system temperature and saturation pressure of of the solvent mixture (P_m^{sat}), γ_i^∞ is the activity coefficient of solute *i* at infinite dilution in the solvent, H_{i-s} is Henry's constant of solute *i* in solvent s, γ_{i-s}^∞ is the activity coefficient of solute *i* at infinite dilution in pure solvent s. w_s is the apparent volume fraction of solvent s.

The partial molar volume of the supercritical component, e.g. CO_2, at infinite dilution in water was estimated by the correlation of Brelvi and O'Connel (29). The general form of Brelvi-O'Connel (BO) correlation can be expressed as (19,30):

$$v_{i,s}^{\infty} = f(v_i^{BO}, v_s^{BO}, v_s^{sat}) \tag{3-19}$$

With:

$$v_k^{BO} = v_{1,k} + v_{2,k}T \qquad (k = i, s) \tag{3-20}$$

Where v_i^{BO} and v_s^{BO} are the characteristic volume of the supercritical component *i* and the solvent s, respectively, v_s^{sat} is the saturated liquid volume of the solvent that can be calculated using the Rachett model (31). $v_{1,k}$ and $v_{2,k}$ are the correlation parameters for component k.

The exponential term in Eq. 3-40, called the Poynting correction, can be neglected when used for systems operating at low to moderate pressures (28,32), therefore the equivalent of Eq. 3-16 for supercritical components (Henry components) can be expressed as (19):

$$y_i \hat{\phi}_i P = x_i \gamma_i \left(\frac{H_i^m}{\gamma_i^{\infty}}\right) \tag{3-21}$$

A rigorous VLE model of electrolyte systems requires accurate descriptions of fugacity coefficients and activity coefficients in addition to Henry constants for Henry components.

To effectively describe the VLE, accurate values of fugacity coefficients and activity coefficients in addition to Henry's constants for henry components are required.

3.5.1. Models for Fugacity Coefficient

Fugacity coefficient can be calculated from PVT data using a cubic Equation of State (EoS) available in the literature (28). Cubic equations of state usually have volume terms raised to the first, second, and third power. Equations of state are suitable to be applied for liquid-

vapour equilibria as only two phases are involved in the process. A general form of available cubic EoS can be expressed by a five-parameter formula ($b, \Phi, \eta, \delta, \varepsilon$) as (33):

$$P = \frac{RT}{V-b} - \frac{\Phi(V-\eta)}{(V-b)(V^2+\delta V+\varepsilon)} \quad (3\text{-}22)$$

The parameters are model dependant. They can be constant values (including zero) or a function of temperature and/or composition.

The Redlich-Kwong (RK) equation of state (34), a modification of this model by Soave (35), called the Redlich-Kwnog-Soave (RKS) equation of state, and the Peng-Robinson Equation of State (36), are the most commonly used equations to represent the non-ideal equilibrium behaviour of gas-phase in CO_2-H_2O-MEA systems. The expression of the three mentioned cubic equations of states are:

Redlich-Kwong (RK) EoS (34):

$$P = \frac{RT}{V-b} - \frac{a}{T^{1/2}\,V(V+b)} \quad (3\text{-}23)$$

Redlich-Kwnog-Soave (RKS) EoS (35):

$$P = \frac{RT}{V-b} - \frac{a(T)}{V(V+b)} \quad (3\text{-}24)$$

Peng-Robinson (PR) EoS (36):

$$P = \frac{RT}{V-b} - \frac{a(T)}{V(V+b)+b(V-b)} \quad (3\text{-}25)$$

Where the parameter a represents the strength of the attractive forces between molecules and the parameter b is related to the molecule size. Values of these two parameters in terms of

critical properties were determined by forcing the EoS to satisfy the condition of criticality as (10):

$$a = 0.427480\frac{R^2T_c^2}{P_c} \quad (3\text{-}26)$$

$$b = 0.086640\frac{RT_c}{P_c} \quad (3\text{-}27)$$

Spear *et al*. (37) showed the Redlich-Kwong equation of state is a reliable model to calculate the vapour-liquid critical properties of binary mixtures. Chueh and Prausnitz (38,39) also confirmed that the Redlich-Kwong equation can be reliably predict both vapour and liquid properties. Soave (35) used the Soave-Redlich-Kwong equation to calculate the vapour pressures of a number of hydrocarbons and some binary systems and compared the results with experimental data. Soave's modification fitted the experimental (vapour-liquid) curve well and it was able to predict the phase behaviour of mixtures in the critical region. Han *et al*. (40) confirmed the Peng-Robinson equation of state was reliable for predicting vapour-liquid equilibrium in hydrogen and nitrogen containing mixtures. Harstad *et al*. (41) also showed that the Peng-Robinson equation of state could be used to determine a fairly accurate and computationally efficient correlation of high pressure fluid mixtures used in rocket engines and gas turbines.

The Peng-Robinson and Redlich-Kwong-Soave equations of state are widely used in industry and recommended for hydrocarbon processing applications such as petrochemical processes, refinery, and gas processing. Results of the Peng-Robinson model are comparable with those of the Redlich-Kwong-Soave equation of state. The Redlich-Kwong equation-of-state is applicable to calculate vapour phase thermodynamic properties of systems at low to moderate pressures (maximum pressure 10 bar) for which the vapour-phase non-ideality is small (19).

3.5.2. Models for Activity Coefficient

The activity coefficient of a system can be determined if a model to calculate the system excess Gibbs energy is available. Most of excess Gibbs energy models available for electrolyte systems, such as CO_2-H_2O-MEA systems, usually are a combination of short-range interaction and long-range electrostatic interactions as expressed below (42):

$$G^E = G^{E,SR} + G^{E,LR} \quad (3\text{-}28)$$

Where $G^{E,SR}$ and $G^{E,LR}$ are the short-range and the long-range contributions to the system excess Gibbs energy.

Usually, the short-range interactions are represented by local composition models such as the universal quasi-chemical (UNIQUAC) equation of Abraham and Prausnitz (43), or the non-random two-liquid equation of Renon and Prausnitz (44). Representation of long-range electrostatic interactions in most models is based on a version of the equation originally proposed by Debye and Huckel (28). Guggenheim (45) extended the original Debye-Huckel (DH) equation, and the extended equation was further improved by Pitzer (46,47) which is known as the Pitzer-Debye-Huckel (PDH) equation. By taking the PDH equation into consideration, Eq. 3-28 can be re-expressed as (48,49):

$$G^E = G^{E,SR} + G^{E,PDH} \quad (3\text{-}29)$$

The activity coefficient for any species, ionic or molecular, solute or solvent is derived from the partial derivative of the excess Gibs energy with respect to mole number. Taking the derivative of Eq. 3-29 in line with the definition of the activity coefficient provides:

$$\ln \gamma_i = \ln \gamma_i^{SR} + \ln \gamma_i^{PDH} \quad (3\text{-}30)$$

Two widely used rigorous models for the excess Gibbs energy are the extended UNIQUAC model (electrolyte-UNIQUAC model) and the electrolyte-NRTL model (42). In following

the electrolyte-NRTL (e-NRTL) model will be further discussed as this is the model used in this thesis.

3.5.2.1. Electrolyte Non-Random-Two-Liquid (e-NRTL) Model

The electrolyte non-random, two liquid (e-NRTL) model was first proposed by Chen *et al*. (49,50) to represent the excess Gibbs Energy of aqueous electrolyte systems and later extended by Mock *et al*. (51) for mixed solvent electrolyte systems. Chen and Song (52) have generalised this model for mixed solvent systems using a segment interaction concept, and Bollas *et al*. (53) refined this model by using a derivative of general expressions for activity coefficient correlations.

The original model proposed by Chen *et al*. (49,50) is based on two fundamental assumptions about the liquid framework of electrolye systems (51):

1- The local composition of cations around a central cation is zero, and the local composition of anions around a central anion is zero. This means repulsive forces between ions of like charge are assumed to be extremely large (the like-ion repulsion assumption).
2- The distribution of cations and anions around a central molecule is such that the net local ionic charge is zero (the local electro-neutrality assumption).

The original e-NRTL model assumes the excess Gibbs energy is the sum of two expressions (51): One expression is derived from the NRTL equation (44) to represent the local interaction contribution produced by all short-range and long-range interactions that occurs between all neighbouring species. Another expression is the Pitzer-Debye-Huckel (PDH) equation (46) which represents the long-range interaction contribution produced by the long-range ion-ion electrostatic interactions beyond the immediate neighbourhood of a central ion. However, a refined and recent development of the e-NRTL model includes a third expression, called the Born term (54), to represent the excess Gibbs energy for transfer from infinite dilution in mixed-solvent to infinite dilution in aqueous phase. The reason for adding

the third expression is that the reference stage chosen for ionic species in the context of a mixed solvent electrolyte system is the ideal dilute state in water only (17).

Austgen *et al*. (17) developed a rigorous VLE model based on the e-NRTL model to represent activity coefficients of all species, ionic and molecular, in acid-gas-MEA-H_2O and acid gas-DEA-water systems. In this model both water and alkanolamine were regarded as solvents, therefore the model treats the solution as a mixed-solvent system (water-alkanolamine system). The model rigorously represents chemical equilibria and mass balance and allows determining of all liquid-phase ionic and molecular species. The liquid-phase activity coefficients are represented with the e-NRTL model (49,50), modified for mixed solvents electrolyte solution (55) considering both short-range and long-range interactions between all true species in the liquid phase. The vapour-phase fugacity coefficients are represented using the Redlich-Kwong equation of state modified by Soave (35). This model provides vital information such as interface VLE, bulk interface driving forces, and true liquid species which makes it particularly suitable for kinetic studies and for design and simulation based on rates of mass transfer rather than equilibrium (56). This model is probably the most sophisticated and thermodynamically rigorous framework to model aqueous electrolyte systems, including aqueous alkanolamine, e.g. MEA, for CO_2 capture (56,57). This model is the Aspen Plus® recommended model for electrolyte CO_2-H_2O-MEA systems.

In the e-NRTL model for mixed solvent electrolyte systems, the excess Gibbs energy has three contributions as follows (17,19,56):

$$G^{ex^*} = G^{ex^*,PDH} + G^{ex^*,BORN} + G^{ex^*,LC} \quad (3\text{-}31)$$

And such that:

$$\ln \gamma^{ex^*} = \ln \gamma^{*PDH} + \ln \gamma^{*BORN} + \ln \gamma^{*LC} \quad (3\text{-}32)$$

Where the superscript * denotes an unsymmetrical reference state.

As mentioned earlier, the expression for the long-range interaction contribution in based on the Pitzer-Debye-Huckel (PDH) formula (46). The PDH formula, normalised to mole fraction of unity for solvent and zero for electrolytes, is expressed as (46):

$$G^{ex^*,PDH} = -RT\left(\sum_i x_i\right)\left(\frac{1000}{M_s}\right)^{1/2}\left(\frac{4A_\varphi I_x}{\rho}\right)\ln\left(1+\rho I_x^{1/2}\right) \quad (3\text{-}33)$$

Where x_i is mole fraction of species i, M_s is the molecular weight of the solvent, ρ is the *closest approach* parameter, A_φ is Debye-Huckel parameter and I_x is the ionic strength of the mixture based on mole fraction. The Debye-Huckel parameter and the ionic strength are expressed as (46):

$$A_\varphi = \left(\frac{1}{3}\right)\left(\frac{2\pi N_A d}{1000}\right)^{1/2}\left(\frac{e^2}{DkT}\right)^{3/2} \quad (3\text{-}34)$$

$$I_x = \frac{1}{2}\sum_i x_i Z_i^2 \quad (3\text{-}35)$$

Where, N_A is Avogadro's number, d is the mass density of solvent, e is electron charge, D is the Dielectric constant of solvent, k is Boltzmann constant, T is temperature and z_i is charge number of ion i.

3.6. Conclusions & Remarks

This chapter provides a review of the chemistry and kinetics of CO_2 reactions with MEA and the thermodynamic concept that have been applied to model the vapour-liquid equilibra of the CO_2-H_2O-MEA system. Also in this chapter a brief review of relations between chemical potential, activity and fugacity coefficient and excess Gibbs energy functions was provided. The e-NRTL model to represent the excess Gibbs energy of aqueous electrolyte systems was also introduced in this chapter. A review of the rigorous e-NRTL model developed by Austgen *et al*. (17) to represent activity coefficients of all species, ionic and molecular, in acid-gas-MEA-H_2O and acid gas-DEA-water systems was also provided. This model is the

Aspen Plus® recommended model for electrolyte CO_2-H_2O-MEA systems which is the basis of the CO_2 absorption/desorption process model developed and applied in this thesis. In this version of the e-NRTL model both water and alkanolamine were regarded as solvents, therefore the model treats the solution as a mixed-solvent system (water-alkanolamine system). The model rigorously represents chemical equilibria and mass balance and allows determining of all liquid-phase ionic and molecular species. The liquid-phase activity coefficients represented with the e-NRTL model which are modified for mixed solvents electrolyte solution by considering considering both short-range and long-range interactions between all true species in the liquid phase. The vapour-phase fugacity coefficients are represented using the Redlich-Kwong equation of state modified by Soave. This model provides vital information such as interface VLE, bulk interface driving forces, and true liquid species which makes it particularly suitable for kinetic studies and for design and simulation based on rates of mass transfer rather than equilibrium. This model is probably the most sophisticated and thermodynamically rigorous framework to model aqueous electrolyte systems, including aqueous alkanolamine, e.g. MEA, for CO_2 capture.

3.7. List of References

(1) Plaza J.M., “Modeling of Carbon Dioxide Absorption using Aqueous Monoethanolamine, Piperazine and Promoted Potassium Carbonate”, PhD Dissertation, The University of Texas at Austin, 2011

(2) IEA Greenhouse Gas R&D Programme, Improvement in power generation with post-combustion capture of CO_2. 2004.

(3) Chen, X., “Carbon Dioxide Thermodynamics, Kinetics, and Mass Transfer in Aqueous Piperazine Derivatives and Other Amines”, PhD Dissertation, The University of Texas at Austin, 2011

(4) Kohl-gas purification 5th edition

(5) Reed, R.., 1949. Method of and Apparatus for the Separation of Acidic Gases from Gaseous Mixtures

(6) Chapel, D.G.., Mariz, C.., Ernest, J., 1999. Recovery of CO_2 from Flue Gases: Commercial Trends. Canadian Society of Chemical Engineers Annual Meeting

(7) Butwell K.F., Kubek D.J., “Process for CO_2 removal”, Patent No US 4184855 A, 1980, Union Carbide Corporation,

(8) Barchas, R. and Davis, R., “The Kerr-McGee/ABB Lummus Crest Technology for the Recovery of CO, from Stack Gases”, 1992, Energy Conversion and Management, 1992, 33, No. 5-8, 333-340,

(9) DuPart, M.S., Bacon, T.R., Edwards, D.J., “Understanding corrosion in alkalonamine gas treating plants. Part 1: Proper mechanism diagnosis optimizes amine operations”, Hydrocarbon Processing, 1993, 75-80.

(10) Austgen, D.M., “A model of vapour-liquid equilibria for acid gas-alkanolamine-water systems”, PhD Dissertation, The University of Texas at Austin, 1989.

(11) Aboudheir, A., Tontiwachwuthikul, P., Chakma, A., Iem, R., “Kinetics ofthe reactive absorption of carbon dioxide in high CO_2-loaded, concentrated aqueous monoethanolamine solutions”, Chemical Engineering Science, 2003, 58, 5195 – 5210.

(12) Danckwerts, P.V., “The reaction of CO_2 with ethanolamines”, Chemical Engineering Science, 1979, 34, 443–446.

(13) Crooks, J.E., Donnellan, J.P., “Kinetics and mechanism of the reaction between carbon dioxide and amines in aqueous solution”, Journal of Chemical Society of Perkin Transactions II, 1989, 331–333.

(14) Glasscock, D.A., Critchfield, J.E., Rochelle G.T., “Absorption of carbon dioxide in mixtures of MDEA with MEA or DEA”, Chemical Engineering Science, 1991, 46, 2829–2845.

(15) Mahajani, V.V., Joshi, J.B., “Kinetics of reactions between carbon dioxide and alkanolamines”, Gas Separation & Purification, 1988, 50-64.

(16) Vaidya, P.D., Kenig, E.Y. “CO_2-Alkanolamine reaction kinetics: A Review of Recent studies”, Chemical Engineering & Technology, 2007, 30, 1467-1474.

(17) Austgen, D.M., Rochelle, G.T., Peng, X., Chen, C.C., “Model of Vapor-Liquid Equilibria for Aqueous Acid Gas-Alkanolamine Systems Using the Electrolyte-NRTL Equation”, Industrial & Engineering Chemistry Research, 1989, 28, 1060.

(18) Austgen, D.M., Rochelle, G.T., Chen, C.C., “Model of vapour-liquid equilibria for aqueous acid gas-alkanolamine systems, 2: Representation of H_2S and CO_2 solubility in aqueous MDEA and CO_2 solubility in aqueous mixtures of MDEA and MEA or DEA”, Industrial & Engineering Chemistry Research, 1991, 30, 543−555.

(19) Aspen Technology, “Aspen Physical Property System, V 7.3”, Aspen Technology, Inc., Burlington, MA, 2011.

(20) Kent R., Eisenberg, B., “Better data for amine treating”, Hydrocarbon Processing, 1976, 55, 87-90.

(21) Deshmukh, R., Mather, A., “A mathematical model for equilibrium solubility of hydrogen sulphide and carbon dioxide in aqueous alkanolamine solutions”, Chemical Engineering Science, 1981, 36, 355-362.

(22) Gabrielsen, J., Michelsen, M., Stenby, E., Kontogeorgis, G., “A model for estimating CO_2 solubility in aqueous alkanolamines”, Industrial & Engineering Chemistry Research, 2005, 44, 3348-3354.

(23) Pitzer, K.S., “Thermodynamics of Electrolytes. I: Theoretical Basis and General Equations”, The Journal of Physical Chemistry, 1973, 77, 268-277.

(14) Versteeg, G.F., van Dijck, L.A., van Swaaij, P.M., “On the kinetics between CO_2 and alkanolamines both in aqueous and non-aqueous solutions: An overview”, Chemical Engineering Communications, 1996, 144, 113–158.

(25) Chen, C.C., Evans, L. B., “A Local Composition Model for the Excess Gibbs Energy of Aqueous Electrolyte Systems”, AIChE Journal, 1986, 32, 444-454.

(26) Jou, F.Y., Mather, A.E., Otto F.D., “The solubility of CO_2 in a 30 mass percent monoethanolamine solution”, The Canadian Journal of Chemical Engineering, 1995, 73, 140-147.

(27) De Nevers, N., “Physical and Chemical Equilibrium for Chemical Engineers”, 2nd Edition, John Wiley and Sons, Inc., Hoboken, New Jersey, 2002.

(28) Smith, J.M., Van Ness, H.C., Abbott, M.M., *Introduction to Chemical Engineering Thermodynamics*, 7th Eddition, McGraw Hill, New York, 2005.

(29) Brelvi, S.W., O'Connell, J.P., “Correspondling states correlations for liquid compressibility and partial molal volumes of gases at infinite dilution in liquids”, 1st Edition, John Wiley and Sons, Inc., Hoboken, New Jersey, 1972.

(30) Yan, Y.Z., Chen, C.C., “Thermodynamic Modelling of CO_2 Solubility in Aqueous Solutions of NaCl and Na_2SO_4”, The Journal of Supercritical Fluids, 2010, 55, 623-634.

(31) Rackett, H.G., “ Equation of state for saturated liquids”, Journal of Chemical and Engineering Data, 1970, 15, 514-517.

(32) Zhang, Y., Chen, C.C., “Thermodynamic Modeling for CO_2 Absorption in Aqueous MDEA Solution with Electrolyte NRTL Model”, Industrial & Engineering Chemistry Research, 2011, 50, 163-175.

(33) Abbott, M.M., “Cubic Equations of State: An Interpretive Review”, American Chemical Society, 1979, 182, 47-70.

(34) Redlich, O., Kwong, J.N.S., “On the Thermodynamics of Solutions. V. An Equation of State. Fugacities of Gaseous Solutions”, Chemical Reviews, 1949, 44 (1), pp 233–244.

(35) Soave, G., “Equilibrium constants from a modified Redkh-Kwong equation of state”, Chemical Engineering Science, 1972, 27, 1197-1203.

(36) Peng, D.Y., Robinson, D.B., “A New Two-Constant Equation of State”, Industrial & Engineering Chemistry Fundamentals, 1976, 15, 59-64.

(37) Spear, R.R., Robinson, J.R.L., Chao, K.C., “Critical States of Mixtures and Equations of State”, Industrial & Engineering Chemistry Fundamentals, 1969, 8, 2-8.

(38) Chueh, P.L., Prausnitz, J.M., “Vapour-Liquid Equilibria at High Pressures: Vapour-Phase Fugacity Coefficients in Nonpolar and Quantum-Gas Mixtures”, Industrial & Engineering Chemistry Fundamentals, 1967, 6, 492-498.

(39) Chueh, P.L., Prausnitz, J.M., “Vapour -Liquid Equilibria at High Pressures: Calculation of Partial Molar Volumes in Nonpolar Liquid Mixtures”, AIChE Journal, 1967, 13, 1099-1107.

(40) Han, S.J., Lin, H.M., Chao, K.C., “Vapour-Liquid Equilibrium of Molecular Fluid Mixtures by Equation of State”, Chemical Engineering Science, 1988, 43, 2327-2367.

(41) Harstad, K.G., Miller, R.S., Bellan, J., “Efficient High-Pressure State Equations”, AIChE Journal, 1997, 43, 1605-1610.

(42) Kontogeorgis, G.M., Folas, G.K., *Thermodynamic Models for Industrial Applications: From Classical and Advanced Mixing Rules to Association Theories*, John Wiley and Sons, Inc., Hoboken, New Jersey, 2010.

(43) Abrams, D.S., Prausnitz, J.M., “Statistical Thermodynamics of Liquid Mixtures: A New Expression for the Excess Gibbs Energy of Partly or Completely Miscible Systems”, AIChE Journal, 1975, 21: 116-128.

(44) Renon, H., Prausnitz, J.M., “Local composition in thermodynamic excess functions for liquid mixtures”, AICHE Journal, 1968, 14, 135-44.

(45) Guggenheim, E.A., “The specific thermodynamic properties of aqueous solutions of strong electrolytes”, The London, Edinburgh, and Dublin Philosophical Magazine and Journal of Science, 1935, 19, 588-643.

(46) Pitzer, K.S., “Electrolytes, from Dilute Solutions to Fused Salts,” Journal of American Chemical Society, 1980, 102, 2902-2906.

(47) Pitzer, K.S., “ Thermodynamics of Electrolytes, I. Theoretical basis and general equations”, The Journal of Physical Chemisrty, 1973, 77, 268-277.

(48) Li, Y.G., Mather, A.E., “Correlation and Predicton of the Solubility of CO_2 in a Mixed Alkanolamine Solution”, Industrial & Engineering Chemistry Research, 1994, 33, 2006-2015.

(49) Chen, C.C., Britt, H.I., Boston, J.F., Evans, L.B., “Local Composition Model for Excess Gibbs Energy of Electrolyte Systems: Part I: Single solvent, single completely dissociated electrolyte systems”, ALChE Journal 1982, 588-596.

(50) Chen, C.C., Evans, L.B., “A Local Composition Model for the Excess Gibbs Energy of Aqueous-Electrolyte Systems”. AIChE Journal, 1986, 32, 444-454.

(51) Mock, B., Evans, L.B., Chen, C.C., “Thermodynamic representation of phase equilibria of mixed-solvent electrolyte systems”, AlChE Journal, 1986, 32, 1655-1664.

(52) Chen, C.C., Song, Y., “Generalized electrolyte-NRTL model for mixed-solvent electrolyte systems”, AlChE Journal, 2004, 50, 1928-1941.

(53) Bollas, G.M., Chen, C.C., Barton, P.I., “Refined electrolyte-NRTL model: Activity coefficient expressions for application to multi-electrolyte systems”, AlChE Journal, 2008, 54, 1608-1624.

(54) Robinson, R.A., Stokes, R.H., Electrolyte Solutions, 2nd Edition, Butterworth & Co.: London, 1970.

(55) Scauflaire, P., Richards, D., Chen, C.C., “Ionic activity coefficients of mixed solvent electrolyte systems”, AIChe Journal, 1989.

(56) Liu, Y., Zhang, L., Watanasiri, S., “Representing Vapor-Liquid Equilibrium for an Aqueous MEA-CO_2 System Using the Electrolyte Nonrandom-Two-Liquid Model”, Industrial & Engineering Chemistry Research, 1999, 38, 2080-2090.

(57) Chen, C.C., Mathias, P.M., “Applied Thermodynamics for Process Modeling”, AIChE Journal, 2002, 48, 194–200.

(58) Chen, C.C., “Toward Development of Activity Coefficient Models for Process and Product Design of Complex Chemical Systems”, Fluid Phase Equilibrium, 2006, 241, 103–112.

Chapter 4

CO_2 Capture Model Development & Validation

This chapter describes the development of a rate-based model of CO_2 absorption/desorption process using 7m (30 wt. %) MEA as solvent in Aspen Plus® V.8.4, and presents validation results of the model using experimental data reported from two different pilot plants: The UK Carbon Capture and Storage Research Centre/Pilot Scale Advanced Capture Technology (UKCCSRC/PACT) CO_2 capture plant located at Sheffield, UK, and the MEA-based pilot plant at the University of Kaiserslautern, located in Kaiserslautern, Germany.

4.1. Modelling Approaches

There are two main approaches to describe mass transfer equations of a chemical based absorption/desorption process: the equilibrium-based approach and the rate-based approach. These two approaches are described below.

4.1.1. Equilibrium-based Modelling Approach

The traditional method to model and design a reactive absorption process has usually been based on the stage equilibrium models (1). In this method, the packed column is divided into a user-defined number of segments or theoretical stages. The equilibrium stage model assumes that the vapour stream leaving a stage is in thermodynamic equilibrium with the liquid stream leaving the same stage (1,2). This method is useful in carrying out preliminary process simulations and has been widely used in various process simulation tools. However, in reactive absorption processes thermodynamic equilibrium is rarely achieved and separation takes place due to the mass transfer between vapour and liquid phases (2,3). Deviation from equilibrium is usually taken into account through the use of efficiencies, such as Murphree efficiencies and stage efficiency called the HETP (height equivalent to a

theoretical plate) (2,4). However, for a reactive absorption process this approach generally fails since the absorption always take place in multi-component mixtures (1-4).

4.1.2. Rate-based Modelling Approach

The rate-based approach is a more complex and physically consistent approach to describe a reactive absorption process (1,5,6). This approach aims to take into account the actual rates of multi-component mass and heat transfer and chemical reactions (1). In rate-based models, mass transfer at the liquid and vapour interface can be described using the two-film theory (7) or the penetration/surface renewal model (8). Usually the use of the two-film theory is advantageous since a broad range of correlations is available in the literature for numerous types of processes. In the two-film theory, as shown in Figure 4-1, it is assumed that the liquid and vapour phases both are comprised of thin film and bulk regions, and all of the resistance to heat and mass transfer is concentrated in laminar thin films adjacent to the phase interface, and that transfer occurs within these films by steady-state molecular diffusion only. The liquid and vapour bulk regions are assumed to have a uniform composition (1). The Maxwell-Stefan equations are used to describe the multi-component diffusion in the films (1,9). The rate-based model also requires additional considerations at liquid and vapour interface and process hydrodynamics that includes correlations for hold-up, pressure drop and interfacial area (10).

On the other hand, in the equilibrium-based approach, each theoretical stage is assumed to be composed of a well-mixed liquid and vapour phases being in phase equilibrium with each other. The latter assumption is basically an approximation as these two phases are never in equilibrium in a real system. (4,11).

The rate-based modelling approach is rigorous and reliable and offers higher accuracy over the commonly used equilibrium-based approach (4,11). Therefore, the Rate-based approach was adapted in this thesis to model the CO_2 absorption and stripping processes.

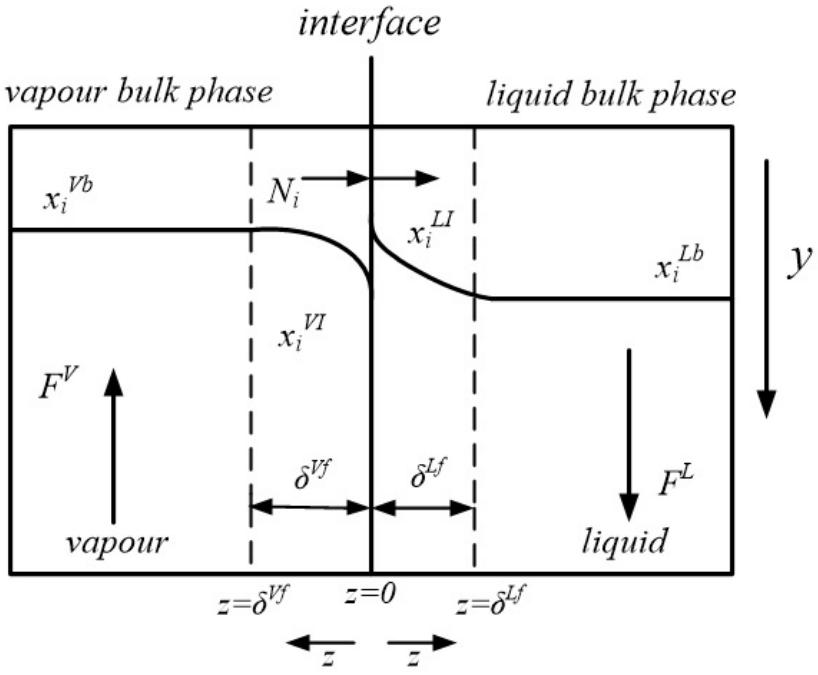

Figure 4-1. Schematic illustration of the two-film theory

4.2. Aspen Plus® RateSep™ Modelling Framework

In this thesis, the CO_2 absorption/desorption model and any modification of it are developed in Aspen Plus® RateSep™. Aspen RateSep™ is an extension of Aspen RateFrac with rate-based capabilities to rigorously simulate reactive multi-stage separation systems (12). In the RateSep model, it is assumed that the separation is a result of mass transfer between contacting phases and the equilibrium is only achieved at the vapour-liquid interface (12). Aspen RateSep divides packed columns into a defined number of theoretical stages, and uses the Maxwell-Stefan multi-component mass transfer equation with the approximate solution proposed by Alopaeus *et al*. (13) to describe mass transfer at the vapour-liquid interface. In Aspen RateSep, Separate balance equations are considered for each distinct phase, and heat and mass transfer resistances are determined according to the two-film theory (4) with respect to interfacial fluxes (12). Furthermore, Aspen RateSep allows film discretization for the nonhomogeneous film layer which is a useful tool to develop an accurate concentration profile in the film for fast reactions (12). Equations used in the film model include chemistry

and thermodynamics of electrolyte systems and are combined with diffusion and reaction rate kinetics.

The column hydrodynamics are represented with specific correlations for vapour-liquid interfacial area, mass transfer coefficients, pressure drop, and liquid hold-up. Figure 4-2 shows a schematic illustration of CO_2 mass transfer across the vapour-liquid interface film. As shown in Figure 4-2, the liquid film is discretised into multiple film segments to accurately model the non-homogeneous film layer (12), film discretisation will be explained in following sections.

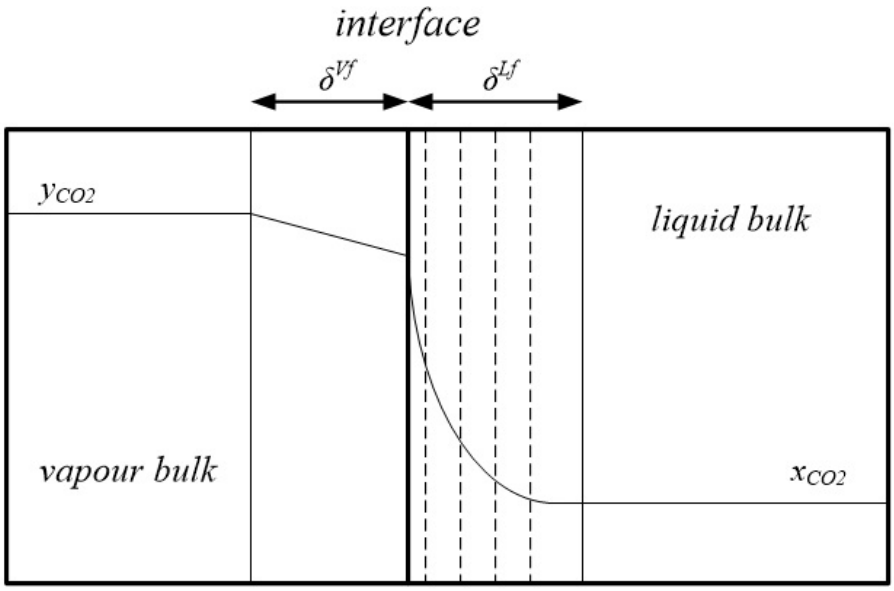

Figure 4-2. schematic illustration of CO_2 mass transfer across the vapour-liquid interface film

4.2.1. Film Reactions

To properly model the CO_2 absorption process, reactions taking place in the film and their effects on mass transfer are required to be taken into consideration. When reaction rates are very slow it is possible to simplify the model by using either a single film segment, or eliminate the film entirely (10). However, in many cases, it is required to differentiate existing reaction regimes and their effect on physical mass transfer. The Hatta number H_a, which represents the ratio of the maximum possible rate of reaction rate to rate of mass transfer (14), can be used as an indicator to evaluate the rate of reaction. For instance, low

Hatta number indicates slow kinetics, and if the Hatta number is greater than 3, at near the vapour-liquid interface, the flux of CO_2 is controlled by reaction kinetics and the diffusion of untreated CO_2 is negligible (10). The Hatta number is expressed as:

$$H_a = \frac{\sqrt{D_{CO_2} k_f [AM]}}{k^{\circ}_{CO_2}} \tag{4-1}$$

Where D_{CO_2} is the binary diffusion of CO_2 in the solvent, k_f is the forward rate constant controlling the absorption reaction, $[AM]$ is the amine concentration and $k^{\circ}_{CO_2}$ is the physical mass transfer coefficient.

There is a simple approach to simply take into account reactions at the boundary layers by employing a factor in models, called the enhancement factor (10). A more rigorous approach is to discretise the boundary layer to represent the nonlinear concentration profile. Rates of reactions will be affected by discretising the film. Discretisation if applied efficiently will assure a proper representation of the phenomena taking place in the boundary layer without unduly extending the computational time or reducing the accuracy of results. Discretisation is crucial in CO_2 capture modelling as there are number of fast reactions taking place in the system. Different boundary layer discretisation approaches have been suggested by various authors (2,3,15-17). Film discretisation is used in this thesis.

Aspen RateSep™ provides a number of options for film discretisation. In the following these options are described (18):

4.2.1.1. No Film

When this option is selected for a phase, the model assumes there is no film resistance in that phase and performs an equilibrium phase calculation of the phase.

4.2.1.2. Film

By selecting this option, the model performs diffusion resistance calculations and ignores any reaction calculation for this film of that phase.

4.2.1.3. Filmrxn

In this case, the model uses the reaction condition factor to calculate compositions and temperatures that will be used in the reaction rate evaluation. The reaction condition factor varies between zero to one, where one is the bulk condition and zero is the interface condition. This is an adjustable factor and can be specified by the user.

4.2.1.4. Discrexn

This is the most robust option that Aspen RateSep™ offers to represent reactions taking place in the vapour-liquid interface film. By selecting this option, the film is discretised into distinct segments and species concentrations in each discrete point are calculated to obtain a reliable concentration profile across the film. This option requires the user to set the number of discretisation points and the ratios of discretisation. The discretisation ratio is the ratio of two adjacent film segments. In CO_2 absorption/stripping applications, discretisation of the Interface film will provide a proper presentation of the enhancement effect of the carbamate reaction in the absorption of CO_2 (10).

4.2.2. Flow Models

The flow model is a key input for a rate-based model. Aspen RateSep™ offers four flow models to determine bulk properties that are required to calculate reaction kinetics and energy and mass fluxes (18). Figure 4-3 shows the flow models available in Aspen RateSep™ to determine bulk properties.

4.2.2.1. Mixed Flow Model

This is the default flow model in Aspen RateSep™. In this model both vapour and liquid phases are well-mixed. Within each phase, bulk properties are assumed to be the same as the

outlet conditions of that phase when leaving the stage. This model is recommended for tray contactors; however, it can also be used for packed columns (18).

4.2.2.2. Counter-Current Flow Model

This model can be used when vapour and liquid are counter-current. By using this model, within each phase, bulk properties are calculated as an average of the inlet and outlet properties. This model provides more accurate results for packing, but is more computationally intensive. It is recommended for structured packing (10,18). This flow model is adapted in this thesis for the absorber column simulations.

4.2.2.3. VPlug Flow Model

In this model the liquid phase is assumed to be well-mixed and the vapour phase is plug flow. In this model the liquid phase properties in each stage are assumed to be similar to conditions at which the liquid phase leaves that stage, and the vapour phase properties are calculated as described in the counter-current model. This model assumes the stage pressure for each phase is their pressure when leaving that stage. This flow model is adapted in this thesis for the stripper column simulations.

4.2.2.4. VPlug-P_{avg} Flow Model

This flow model is similar to the VPlug model except an average pressure of the phase at the inlet and outlet of a stage, represented as P_{avg}, is used for bulk properties calculations instead of the outlet pressure.

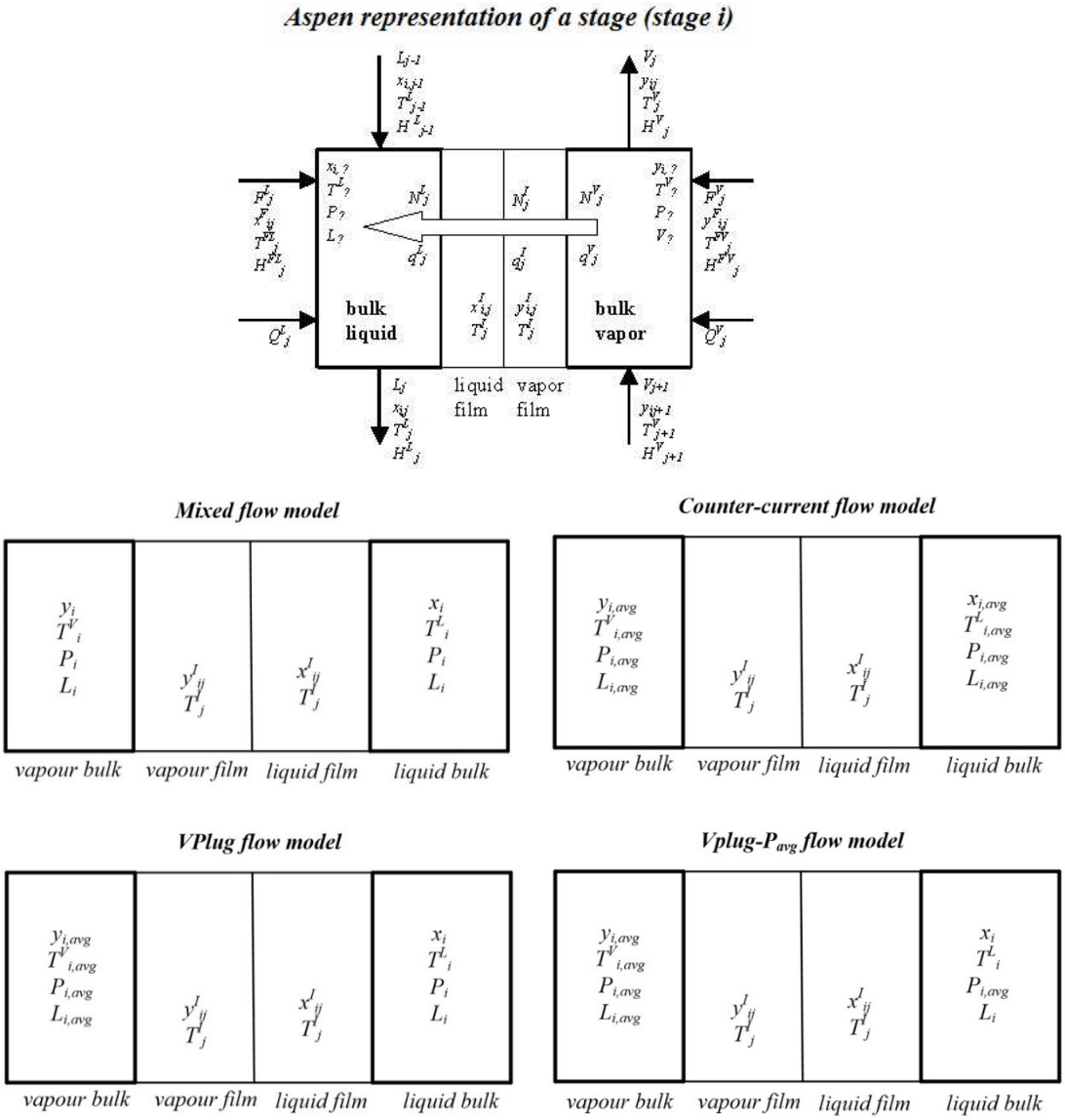

Figure 4-3. Flow model options available in Aspen Plus® RateSep™

4.3. CO_2 Capture Model Development

The rate-based model of CO_2 absorption/desorption was developed within the Aspen Plus® RateSep™ modelling framework. Figure 4-4 shows the developed Aspen flowsheet of this model. The model was developed by implementing a thermodynamic framework to accurately represent the CO_2-H_2O-MEA system, followed by proper description of kinetics of CO_2 reaction with the MEA solution, and suitable transport properties affecting the heat and mass transfer.

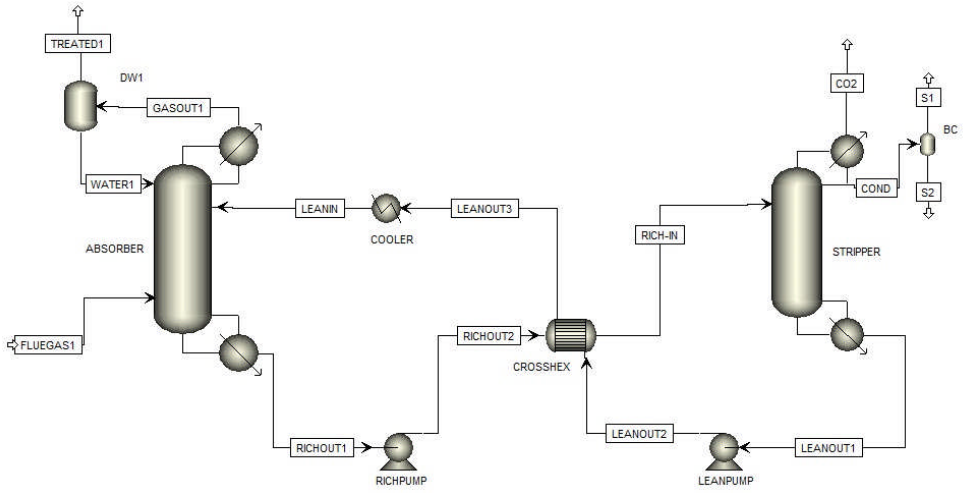

Figure 4-4. Developed rate-based model of CO_2 absorption/desorption in Aspen RateSep

4.3.1. Thermodynamic Framework

The model used in Aspen RateSep for the thermodynamic properties is based on the work by Zhang *et al*. (12). The model uses the asymmetric electrolyte Non-Random-Two-Liquid (e-NRTL) activity coefficient model to account for the liquid phase non-ideality, and the Redlich-Kwong (RK) equation of state for the vapour phase. The model has been validated by Zhang *et al*. (12) against experimental data available in open literature. The absorber model comprises both equilibrium and kinetic rate-based controlled reactions, while the stripper model comprises equilibrium rate-based controlled reactions. In the absorber column, the reactions that involve CO_2 were described with a kinetic model. The equilibrium reactions describing the solution chemistry of CO_2 absorption with MEA, which are integral components of the thermodynamic model, are expressed as (12):

$$2H_2O \leftrightarrow H_3O^+ + OH^- \quad (4\text{-}2)$$

$$CO_2 + 2H_2O \leftrightarrow HCO_3^- + H_3O^+ \quad (4\text{-}3)$$

$$HCO_3^- + H_2O \leftrightarrow H_3O^+ + CO_3^{2-} \quad (4\text{-}4)$$

$$MEAH^+ + H_2O \leftrightarrow MEA + H_3O^+ \quad (4\text{-}5)$$

$$MEACOO^- + H_2O \leftrightarrow MEA + HCO_3^- \quad (4\text{-}6)$$

The equilibrium constants (K) for reactions 4-2 to 4-6 are calculated from the reference state Gibbs free energy for each participating component (19,20)

$$-RT \ln K_J = \Delta G_j^{\circ} \quad (4\text{-}7)$$

Where, R is the universal gas constant, T is the system temperature in Kelvin, and ΔG_j° is the reference state Gibbs energy change for reaction j.

4.3.2. Reaction Kinetics Model

The formation of carbamate and bicarbonate are kinetically limited, and the forward and reverse reactions are expressed as follows (21):

$CO_2 + OH^- \rightarrow HCO_3^-$ (4-8)

$HCO_3^- \rightarrow CO_2 + OH^-$ (4-9)

$MEA + CO_2 + H_2O \rightarrow MEACOO^- + H_3O^+$ (4-10)

$MEACOO^- + H_3O^+ \rightarrow MEA + CO_2 + H_2O$ (4-11)

In Aspen plus, reaction rates for Reaction 4-8 to 4-11 are described by power law expressions (12):

$$r_j = k_j^0 exp(-\frac{E_j}{R}\left[\frac{1}{T} - \frac{1}{298.15}\right]) \prod_{i=1}^{N} (C_i)^{a_{ij}} \quad (4\text{-}12)$$

Where r_j is the rate of reaction for reaction j, k_j^0 is the pre-exponential factor, T is the system temperature in Kelvin, n is the temperature factor, E_j is the activation energy, R is the universal gas constant, C_i is the concentration of species i, and a_{ij} is the reaction order of component i in reaction j. Table 4-1 summarises kinetic expressions of MEA carbamate and bicarbonate reactions used in RateSep™ for absorber and stripper models (21).

Table 4-1. Kinetic rate expressions of MEA carbamate and bicarbonate reactions used in RateSep absorber and stripper model (21)

Related species	Reaction direction	Reaction kinetics
HCO_3^-	Forward	$r_{(4-7)}\left(\frac{kmol}{m^3 s}\right) = 1.33 \times 10^{17}\left(\frac{kmol}{m^3 s}\right) exp\left(-\frac{55.38\ \left(\frac{kJ}{mol}\right)}{R\ (\frac{kJ}{mol.K})}\left[\frac{1}{T}-\frac{1}{298.15}\right]\right)\alpha_{CO_2}\alpha_{OH^-}$
HCO_3^-	Reverse	$r_{(4-8)}\left(\frac{kmol}{m^3 s}\right) = 6.63 \times 10^{16}\left(\frac{kmol}{m^3 s}\right) exp\left(-\frac{107.24\ \left(\frac{kJ}{mol}\right)}{R\ (\frac{kJ}{mol.K})}\left[\frac{1}{T}-\frac{1}{298.15}\right]\right)\alpha_{HCO_3^-}$
$MEACOO^-$	Forward	$r_{(4-9)}\left(\frac{kmol}{m^3 s}\right) = 3.02 \times 10^{14}\left(\frac{kmol}{m^3 s}\right) exp\left(-\frac{41.2\ \left(\frac{kJ}{mol}\right)}{R(\frac{kJ}{mol.K})}\left[\frac{1}{T}-\frac{1}{298.15}\right]\right)\alpha_{MEA}\alpha_{CO_2}$
$MEACOO^-$	Reverse (absorber)	$r_{(4-10)}\left(\frac{kmol}{m^3 s}\right) = 5.52 \times 10^{23}\left(\frac{kmol}{m^3 s}\right) exp\left(-\frac{69.05\ \left(\frac{kJ}{mol}\right)}{R\ (\frac{kJ}{mol.K})}\left[\frac{1}{T}-\frac{1}{298.15}\right]\right)\frac{\alpha_{MEACOO^-}\alpha_{H_3O^+}}{\alpha_{H_2O}}$
$MEACOO^-$	Reverser (stripper)	$r_{(4-10)}\left(\frac{kmol}{m^3 s}\right) = 6.56 \times 10^{27}\left(\frac{kmol}{m^3 s}\right) exp\left(-\frac{95.24\ \left(\frac{kJ}{mol}\right)}{R\ (\frac{kJ}{mol.K})}\left[\frac{1}{T}-\frac{1}{298.15}\right]\right)\frac{\alpha_{MEACOO^-}\alpha_{H_3O^+}}{\alpha_{H_2O}}$

4.3.3. Transport Property Models

In RateSep™, computable models are required to account for transport properties to solve correlations of heat transfer, mass transfer, interfacial area, liquid holdup, pressure drop, etc. (12,20,21) Table 4-2 summarises the models with their literature references used in Aspen RateSep™ for transport property calculations.

Table 4-2. Transport property models used in Aspen Plus for the CO_2 capture model (12,20,21)

Property	Model used
Mass transfer at vapour-liquid interface	Two-film theory
Thermo-physical property model	Ying and Chen model
Liquid density	Clarke density model
Gas density	Redlich-Kwong equation of state
Liquid viscosity	Jones-Dole electrolyte correction model
Gas Viscosity	Chapman−Enskog model with Wilke approximation
Thermal conductivity of the liquid	Riedel electrolyte correction model
Surface tension of the liquid solution	Onsager-Samaras model
Diffusivity of CO_2 in H_2O and MEA-H_2O solutions	Wilke-Chang diffusivity model

4.4. CO_2 Capture Model Validation

To validate the developed model, results of two pilot plant experiments were used: (1) the UKCCSRC/PACT CO_2 pilot plant located at Sheffield, UK, and (2) the CO_2 capture pilot plant at the Laboratory of Engineering Thermodynamic in TU Kaiserslautern, Germany (22). In the following, results of the model and their comparisons with the respective experimental data are described.

4.4.1. UKCCSRC/PACT CO_2 Pilot Plant Model

The design of the UKCCSRC/PACT CO_2 capture plant is based on the design of a standard amine-based CO_2 capture plant. It consists of an absorber and stripper column in a closed loop. The Plant uses an aqueous solution of MEA with 30 wt. % as solvent and operates with the flue gases provided by a 100 kW_e micro gas turbine located at the plant. Figure 4-5 shows the process flow diagram (PFD) of the PACT pilot plant. The process description of the plant is provided in Chapter 5. Table 4-3 summarises the UKCCSRC/PACT pilot plant process design specifications.

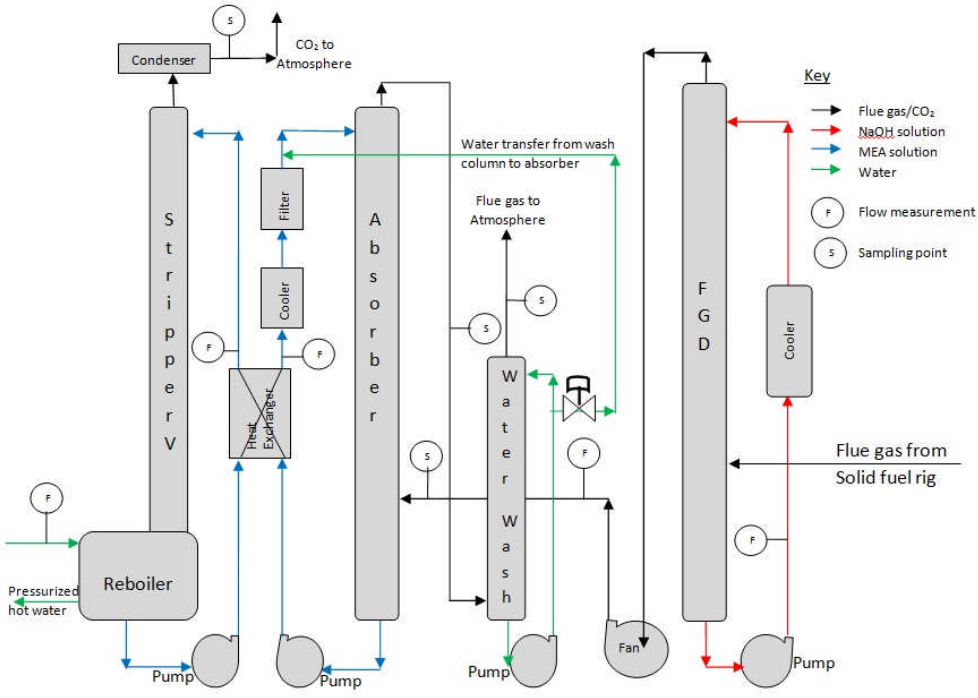

Figure 4-5. The UKCCSRC/PACT CO_2 capture pilot plant process flow diagram

Table 4-3. The UKCCSRC design specifications

Parameter	Specification
Flue gas source	Turbec T100 micro gas turbine + CO_2 feed from CO_2 storage tank
CO_2 concentration in the flue gas	5.5-9.9 mole %
Flue gas flow rate in the absorber	400 Nm^3/h
Flue gas temperature at the absorber inlet	~ 40 °C
Solvent type	7 mole MEA aqueous solution
Solvent flow rate	~ 400-1200 (kg/h)
Solvent temperature at the absorber inlet (°C)	40 °C
Column packing in absorber, stripper, water washing sections	Koch IMTP25 random packing
Material of packing	metal
Diameter of columns (absorber, stripper, water wash sections)	0.30 m
Height of packing	
Absorber	8 m
Stripper	8 m
Water wash	1.2 m
Pressure in the absorber	Atmospheric pressure
Pressure in the stripper	120 – 300 kPa absolute
Temperature of cooling water	5-10 °C

Table 4-4 provides a summary of the key features and sub-models used in Aspen to develop the Pilot-scale CO_2 capture flow sheet in Aspen Plus® V8.4.

Table 4-4. Key design parameters and Aspen Sub-models used in developing UKCCSRC/PACT CO_2 pilot plant model in Aspen Plus V.8.4

Parameter	Absorber column	Stripper column
Modelling approach	Rate-based approach	Rate-based approach
Number of theoretical stages	20	20
Mass transfer coefficient model	Onda *et al*. 1968 (24)	Onda *et al*. 1968
Interfacial area model	Onda *et al*. 1968	Onda *et al*. 1968
Liquid hold-up model	Stichlmair *et al*. (25)	Stichlmair *et al*.
Flooding method (pressure drop calculation model)	Stichlmair *et al*.	Stichlmair *et al*.
Heat transfer coefficient model	Chilton and Colburn (4)	Chilton and Colburn
Film resistance options	"Film" for vapour phase, "Discrxn" for Liquid phase	"Film" for vapour phase, "Discrxn" for Liquid phase
Liquid film discretisation	Discretisation points = 5 Discretisation ratio of 5	Discretisation points = 5 Discretisation ratio of 5
Flow model	VPlug	VPlug

Experimental results presented in Table 4-5 were used to verify the accuracy and reliability of the developed rate-based model. For these tests, the concentration of CO_2 in flue gas at the absorber inlet was varied in steps from 5.5% to 9.9%. The plant is capable of treating a flue gas flow rate of 250 Nm^3/h; for these tests the flue gas flow rate was maintained at around 210 Nm^3/h and its temperature was controlled at 40°C. The solvent flow rate was varied to change the liquid to gas (L/G) ratio corresponding to different CO_2 concentrations. The temperature of lean solvent at the absorber inlet was controlled at 40°C. The control mechanism of the plant kept the lean solvent flow constant to fix the L/G ratio in the absorber, for a particular test. However, the rich solvent flow rate was varied in order to control the levels in the stripper and the absorber. Pressurised hot water was used as the reboiler heat source and it flow rate was controlled at 7.43m^3/h. the CO_2 removal rate was maintained constant at nearly 90% throughout the test campaigns.

Table 4-5. Process characteristics of experimental tests carried out in PACT pilot plant with variable flue gas CO_2 concentration (23)

Test campaign	**Unit**	**Case#1**	**Case#2**	**Case#3**	**Case#4**	**Case#5**
CO_2 in flue gas (after CO_2 injection)	Vol (%)	5.5	6.6	7.7	8.3	9.9
Solvent flow	kg/h	400	488	567	604	721
Flue gas flow to capture plant	kg/h	210	210	210	210	210
Flue gas Temperature	°C	40	40	40	40	40
Lean solvent temperature	°C	40	40	40	40	40
Rich solvent concentration	(wt. %)	30.8	27.8	30.6	27.5	29.1
Lean solvent concentration	(wt. %)	31.9	29.9	31.7	29.8	30.5
Rich loading	(mol/mol)	0.388	0.399	0.411	0.417	0.443
Lean loading	(mol/mol)	0.165	0.172	0.183	0.18	0.204
Degree of regeneration	(%)	57.5	56.9	55.5	56.8	54.0
Liquid to Gas ratio	(kg/kg)	1.55	1.88	2.17	2.3	2.73
Solvent to CO_2 ratio	(kg/kg)	19.9	20.6	21.1	20.7	21.7
Specific Reboiler duty	($MJ/kgCO_2$)	7.1	7.4	6.0	6.1	5.3
Stripper bottom temperature	(°C)	110.39	108.75	109.65	108.83	108.83
CO_2 removal rate	%	90.8	90.3	90.0	90.2	90.8

Tables 4-6 and 4-8 present the verification results:

Table 4-6. Comparison of experimental and simulation results of operating parameters

Description		Rich solvent CO_2 loading (mol /mol)	Solvent temperature at reboiler (°C)	Captured CO_2 flow rate (kg/h)	Reboiler heat duty (kW)
Case#1	Experiment	0.388	110.4	20.2	40.0
(5.5% CO_2)	Simulation	0.394	110.0	20.3	41.77
Case#2	Experiment	0.399	108.8	23.76	48.6
(6.6% CO_2)	Simulation	0.411	108.5	24.3	45.6
Case#3	Experiment	0.411	109.7	26.9	45.0
(7.7% CO_2)	Simulation	0.414	109.8	28.7	48.9
Case#4	Experiment	0.417	108.8	29.2	49.4
(8.3% CO_2)	Simulation	0.426	108.8	30.6	49.6
Case#5	Experiment	0.443	108.8	33.2	48.5
(9.9% CO_2)	Simulation	0.443	108.8	36.1	50.3

The absolute deviation of a simulated result from the experimental one was calculated using Eq. 4-13:

$$\text{Deviation (\%)} = \frac{\left|i_{experiment} - i_{simulation}\right|}{i_{experiment}} \times 100 \quad (4\text{-}13)$$

The mean absolute deviation values of parameters compared in Table 4 are in the range of 0.15 % to 4.7 % which are within an acceptable range.

To characterise the process independent of scale, performance parameters as defined in Table 4-7 were used.

Table 4-7. Parameters to characterise the plant performance independent of the scale

Parameter	Definition
CO_2 removal rate	$\psi_{CO_2} = m_{CO_2}^{TG} / m_{CO_2}^{FG}$
Degree of regeneration (mol/mol)	$\Delta x_{reg} = \left(x_{CO_2}^{rich} - x_{CO_2}^{lean}\right)/x_{CO_2}^{lean}$
Specific regeneration energy requirement (kJ/kg CO_2)	$Q_{specific} = Q_{reboiler} / m_{CO_2}$
Absorption capacity (kg/kg)	$C_{abs} = m_{CO_2}/m_L$

Where, $m_{CO_2}^{TG}$ is the CO_2 mass fraction in the treated gas at the absorber outlet, $m_{CO_2}^{FG}$ is the CO_2 mass fraction in the flue gas at the absorber inlet, $x_{CO_2}^{rich}$ is the rich solvent CO_2 loading. $x_{CO_2}^{lean}$ is the lean solvent CO_2 loading, $Q_{reboiler}$ is the reboiler heat duty, m_{CO_2} is the mass flow rate of CO_2 captured, and m_L is the mass flow rate of lean solvent.

The mean absolute deviation values of parameters compared in Table 4-8 are in the range of 1.1 % to 5.0 % which are within an acceptable range.

Table 4-8. Comparison of experimental and simulation results of performance parameters

Case		ψ_{CO_2} (%)	Δx_{reg} (%)	$Q_{specific}$ (kJ/kg CO_2)	C_{abs} (g/kg)
Case#1	Experiment	90.8	57.5	7.1	50.3
(5.5% mole CO_2)	Simulation	94.9	58.1	7.3	50.7
Case#2	Experiment	90.3	56.9	7.4	48.6
(6.6% mole CO_2)	Simulation	94.7	58.2	6.8	49.8
Case#3	Experiment	90.0	55.5	6.0	47.5
(7.7% mole CO_2)	Simulation	96.0	55.8	6.1	50.6
Case#4	Experiment	90.2	56.8	6.10	48.2
(8.3% mole CO_2)	Simulation	95.0	57.7	5.8	50.6
Case#5	Experiment	90.8	54.0	5.30	46.1
(9.9% mole CO_2)	Simulation	94.1	54	5.0	50.1

The experimental liquid to gas ratio and therefore the associated specific heat duty for the UKCCSRC/PACT CO_2 capture pilot plant are sub-optimal. This fact highlights the need for further modelling studies to be carried out to propose more efficient operating conditions to operate the pilot plant. As results of the developed rate-based model showed good agreement

with the experimental results, the model was therefore used for further studies to propose process modifications and optimal operating conditions at which the PACT pilot plant should operate more efficiency in the future. This topic is discussed in the Chapter five of this thesis.

4.4.2. TU Kaiserslautern Pilot Plant Model

To validate the model, a comprehensive collection of experimental results, published by Notz *et al*. (22), which were carried out at the Laboratory of Engineering Thermodynamics in TU Kaiserslautern, Germany were used. The collection is comprised in total of 47 experiments categorised into 13 different variation group studies for which only one parameter was varied. The aim of these experimental tests was to provide a comprehensive systematic study to understand the influence of process parameters on the CO_2 capture unit performance.

All 47 tests were used to validate the developed rate-based model. Tables 4-11 to 4-23 show comparisons of key performance results calculated by the model with those of the experiments for all 13 groups. Furthermore, Figures 4-6 to 4-18 present comparisons of the absorber and stripper temperature profiles with those of the corresponding experiments for all groups. The process flow diagram (PFD) of each experiment, containing details of the experimental results can be found in Reference (22).

The pilot plant consists of an absorber column and stripper column in a closed-loop arrangement and uses a 30 wt. % aqueous solution of MEA as solvent. All columns were packed with the Sulzer Mellapak 250Y structured packing with the inner diameter of columns being 125 mm. The heights of packing in the absorber and stripper columns are 4.2 and 2.52 m, respectively. The absorber column operated with a flue gas flow rate between 30 and 150 kg/h and a lean solvent flow rate between 50 and 280 kg/h. The flue gas is provided by a gas burner operating in two modes to produce flue gas with a CO_2 partial pressure of 3.6-13.4 kPa. The flue gas is then cooled to a temperature in the range of 44–47°C and saturated with water in a pre-washer before entering the absorber. To reach higher CO_2

partial pressures, captured CO_2 from the stripper top was recycled. The validity of each test was verified by checking the mass balance of CO_2 in flue gas and solvent streams that was reported to be within ±5%. Table 4-9 summarises the UT Kaiserslautern CO_2 capture pilot plant design specifications. The process description of the pilot plant and further details about its set up, operations, and results are provided by Notz *et al*. (22).

Table 4-10 provides a summary of the key features and sub-models used in Aspen Plus® to develop the flow sheet of the UT Kaiserslautern CO_2 capture pilot plant.

Table 4-9. Summary of the TU Kaiserslautern CO_2 capture pilot plant characteristics data (22)

Parameter	**Specification**
Flue gas source	Natural gas burner + CO_2 feed from gas bottles + CO_2 recycle from stripper
CO_2 partial pressure in the flue gas	36–134 mbar
Diameter of columns (absorber, stripper, washing section, pre washer)	125 mm
Column internals in absorber, stripper, washing sections, pre washer	Structured packing Sulzer Mellapak 250.YTM
Height of packing	
Absorber	4.20 m
Stripper	2.52 m
Washing sections in absorber and stripper	0.42 m
Pre washer	0.84 m
Flue gas flow rate in the absorber	30–110 kg/h
Solvent flow rate	~50–350 kg/h
Liquid load in the absorber	~4–28.5 $m^3/(m^2\ h)$
Pressure in the absorber	Atmospheric pressure
Pressure in the desorber	1–2.5 bar (absolute)
Electric heat duty of the reboiler	0–30 kW
Temperature of cooling water	~5-10 °C

Table 4-10. Key design parameters and Aspen Sub-models used in developing UT Kaiserslautern pilot plant model in Aspen Plus V.8.4

Parameter	**Absorber column**	**Stripper column**
Modelling approach	Rate-based approach	Rate-based approach
Number of theoretical stages	20	20
Mass transfer coefficient model	Bravo *et al*. 1985 (26)	Bravo *et al*. 1985
Interfacial area model	Bravo *et al*. 1985	Bravo *et al*. 1985
Liquid hold-up model	Bravo *et al*. 1985	Bravo *et al*. 1985
Flooding method (pressure drop calculation model)	Sulzer in-built correlation in Aspen	Sulzer in-built correlation in Aspen
Heat transfer coefficient model	Chilton and Colburn (4)	Chilton and Colburn (4)
Film resistance options	"Film" for vapour phase, "Discrxn" for Liquid phase	"Film" for vapour phase, "Discrxn" for Liquid phase
Liquid film discretisation	Discretisation points = 5 Discretisation ratio of 5	Discretisation points = 5 Discretisation ratio of 5
Flow model	VPlug	VPlug

Group A.1: Variation of the solvent flow rate at flue gas flow rate of 71.2 kg/h with CO_2 partial pressure of 54.7 mbar with CO_2 removal rate of 76% (Associated experiments: 1, 4, 34, 35, 36, 37, 38, and 39).

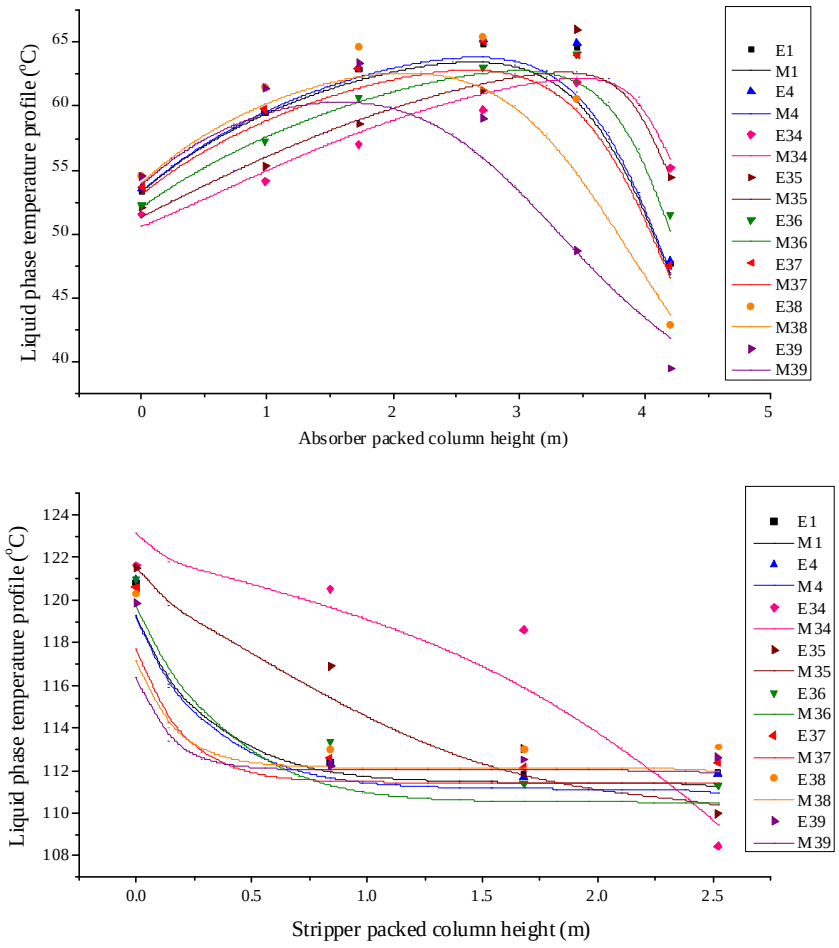

Figure 4-6. Comparison of the absorber (top) and stripper (bottom) temperature profiles calculated by the model with those of the pilot plant experiments of Group A.1

Table 4-11. Comparison of simulation results and pilot plant performance parameters of Group A.1

Experiment number (as per Notz *et al.* (22))	**Rich loading** (mol CO_2/mol MEA)		**Captured CO_2** (kg/h)		**Specific heat duty** (MJ/kg CO_2)	
	Experiment	Model	Experiment	Model	Experiment	Model
E#1	0.386	0.386	4.67	4.77	5.01	5.16
E#4	0.397	0.395	4.83	5.06	5.05	4.90
E#34	0.417	0.444	4.41	4.82	4.85	4.36
E#35	0.411	0.437	4.57	4.79	4.27	4.37
E#36	0.393	0.410	4.46	4.67	4.68	4.54
E#37	0.398	0.408	4.41	4.40	5.11	4.85
E#38	0.385	0.399	4.52	4.52	5.40	4.99
E#39	0.400	0.401	4.48	4.37	5.23	4.76

Group A.2: Variation of the solvent flow rate at the flue gas flow rate of 70.8 kg/h with CO_2 partial pressure of 53.7 mbar with CO_2 removal rate of 88 % (Associated experiments: 40, 41, 42, 43, 44, and 45).

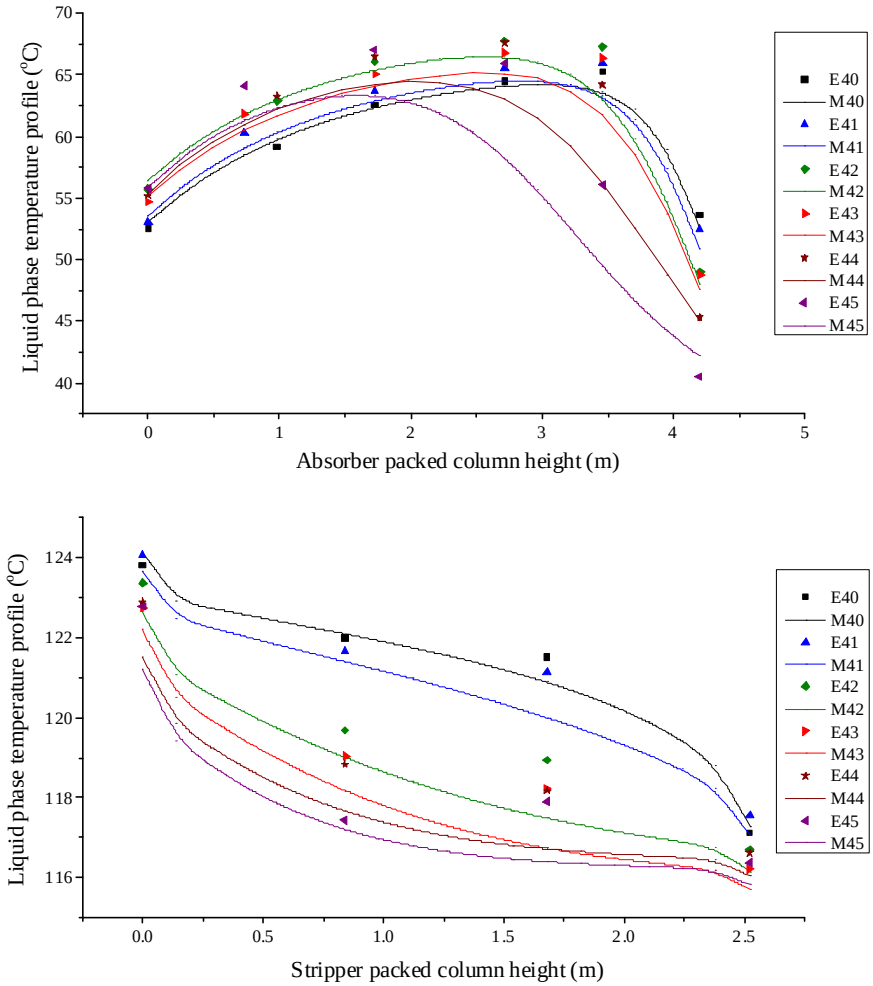

Figure 4-7. Comparison of the absorber (top) and stripper (bottom) temperature profiles calculated by the model with those of the pilot plant experiments of Group A.2

Table 4-12. Comparison of simulation results and pilot plant performance parameters of Group A.2

Experiment number (as per Notz *et al.* (22))	**Rich loading** (mol CO_2/mol MEA)		**Captured CO_2** (kg/h)		**Specific heat duty** (MJ/kg CO_2)	
	Experiment	Model	Experiment	Model	Experiment	Model
E#40	0.297	0.292	5.27	5.35	10.24	9.74
E#41	0.297	0.290	5.27	5.42	9.76	8.97
E#42	0.310	0.312	5.26	5.57	7.16	7.36
E#43	0.318	0.318	4.98	5.26	6.87	7.06
E#44	0.314	0.309	5.01	5.20	7.18	7.34
E#45	0.318	0.314	4.98	5.37	6.87	7.17

Group A.3: Variation of the solvent flow rate at flue gas flow rate of 99.6 kg/h with CO_2 partial pressure of 57.1 mbar with CO_2 removal rate of 75% (Associated experiments: 15, 16, 17, 18, and 19).

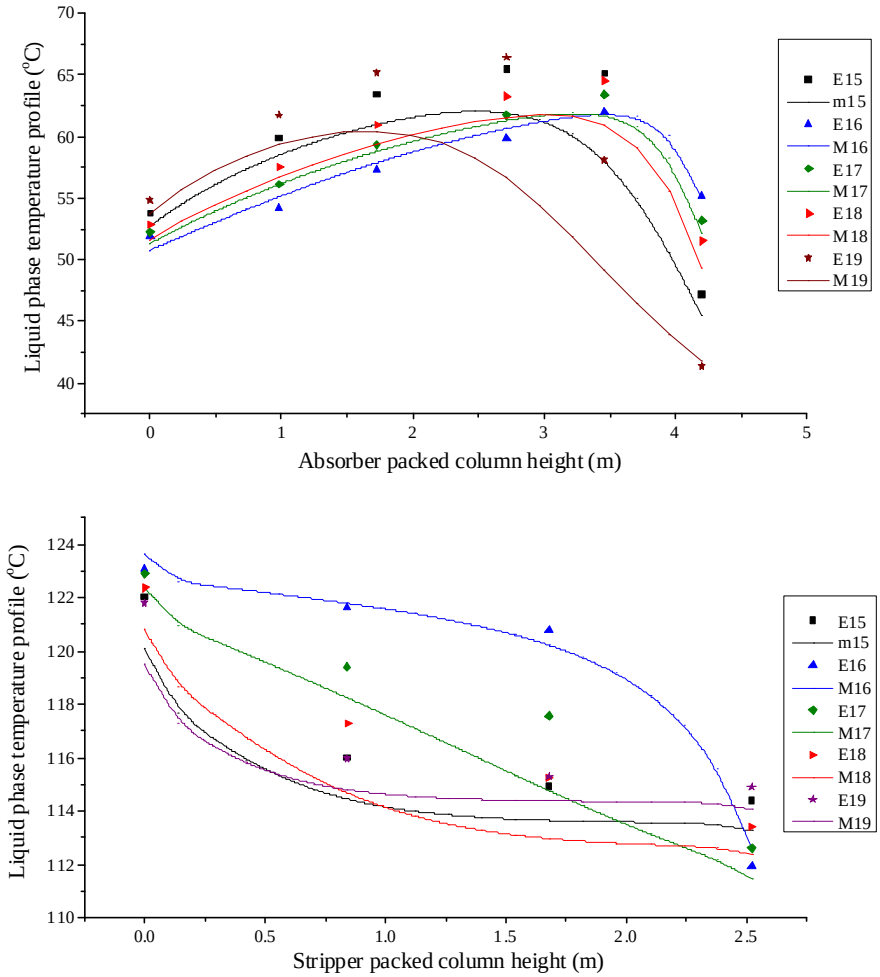

Figure 4-8. Comparison of the absorber (top) and stripper (bottom) temperature profiles calculated by the model with those of the pilot plant experiments of Group A.3

Table 4-13. Comparison of simulation results and pilot plant performance parameters of Group A.3

Experiment number (as per Notz *et al.* (22))	**Rich loading** (mol CO_2/mol MEA)		**Captured CO_2** (kg/h)		**Specific heat duty** (MJ/kg CO_2)	
	Experiment	Model	Experiment	Model	Experiment	Model
E#15	0.359	0.354	6.34	6.13	5.81	5.78
E#16	0.414	0.410	6.37	6.60	7.38	6.33
E#17	0.371	0.383	6.38	6.59	5.47	5.20
E#18	0.387	0.380	6.43	6.22	5.35	5.00
E#19	0.354	0.340	6.43	5.99	6.27	6.08

Group A.4: Variation of the solvent flow rate at flue gas flow rate of 75.5 kg/h with CO_2 partial pressure of 107.5 mbar with CO_2 removal rate of 54% (Associated experiments: 2, 28, 29, 30, 31, 32, and 33)

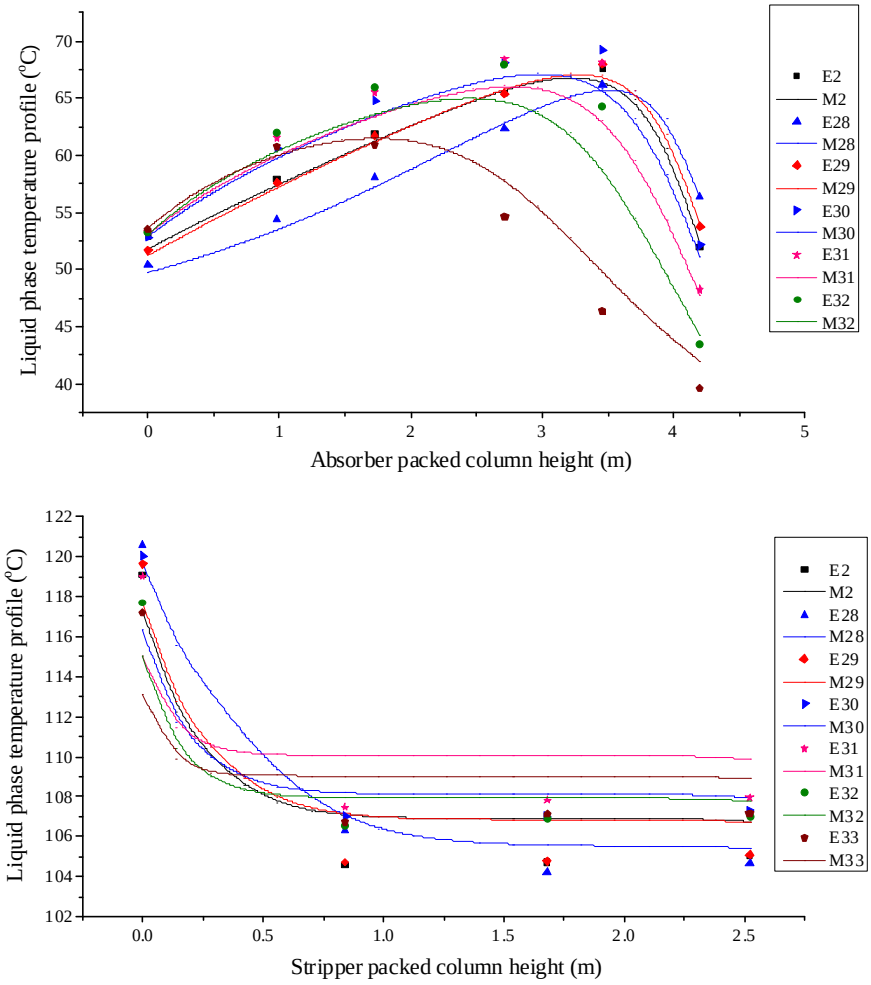

Figure 4-9. Comparison of the absorber (top) and stripper (bottom) temperature profiles calculated by the model with those of the pilot plant experiments of Group A.4

Table 4-14. Comparison of simulation results and pilot plant performance parameters of Group A.4

Experiment number (as per Notz *et al.* (22))	**Rich loading** (mol CO_2/mol MEA)		**Captured CO_2** (kg/h)		**Specific heat duty** (MJ/kg CO_2)	
	Experiment	Model	Experiment	Model	Experiment	Model
E#2	0.464	0.474	6.11	6.79	3.98	3.49
E#28	0.470	0.480	6.63	6.88	3.68	3.72
E#29	0.465	0.474	6.64	7.19	3.92	3.52
E#30	0.459	0.464	6.67	7.01	4.38	4.07
E#31	0.454	0.465	6.71	6.69	4.30	3.66
E#32	0.449	0.459	6.61	6.95	4.57	4.22
E#33	0.441	0.461	6.60	6.49	4.35	3.87

Group B: Variation of the stripper pressure (Associated experiments: 1, 4, 10, 11, and 12).

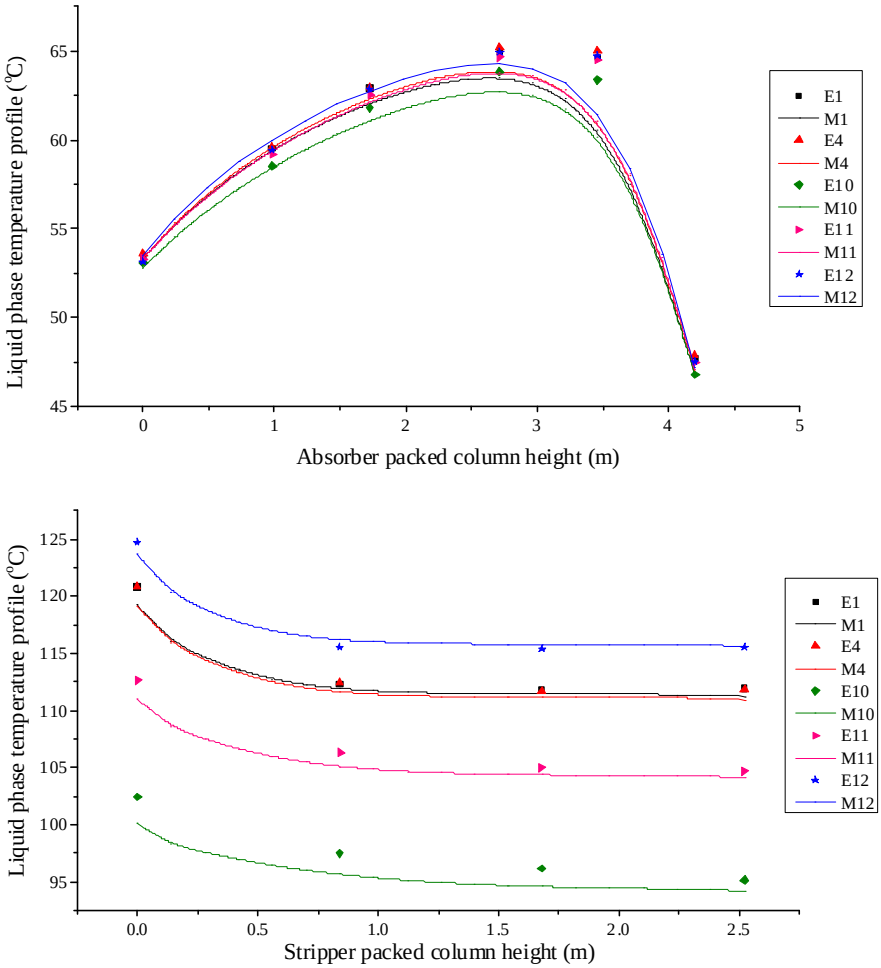

Figure 4-10. Comparison of the absorber (top) and stripper (bottom) temperature profiles calculated by the model with those of the pilot plant experiments of Group B

Table 4-15. Comparison of simulation results and pilot plant performance parameters of Group B

Experiment number (as per Notz *et al.* (22))	**Rich loading** (mol CO_2/mol MEA)		**Captured CO_2** (kg/h)		**Specific heat duty** (MJ/kg CO_2)	
	Experiment	Model	Experiment	Model	Experiment	Model
E#1	0.386	0.386	4.67	4.77	5.01	5.16
E#4	0.397	0.395	4.83	5.06	5.05	4.90
E#10	0.402	0.415	4.34	4.12	5.65	5.94
E#11	0.396	0.405	4.59	4.97	5.12	4.86
E#12	0.372	0.383	4.76	5.22	4.91	4.81

Group C.1: Variation of the MEA mass fraction at the flue gas CO_2 partial pressure of 55.5 mbar (Associated experiments: 1, 4, 24, and 25).

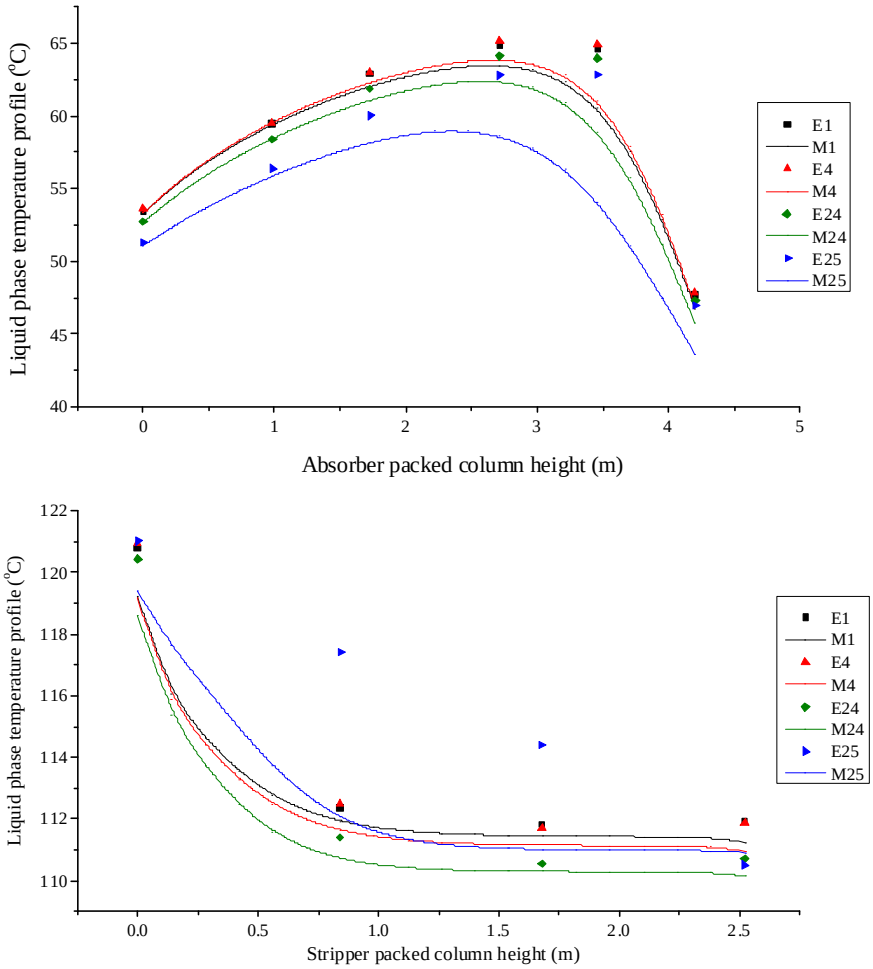

Figure 4-11. Comparison of the absorber (top) and stripper (bottom) temperature profiles calculated by the model with those of the pilot plant experiments of Group C.1

Table 4-16. Comparison of simulation results and pilot plant performance parameters of Group C.1

Experiment number (as per Notz *et al*. (22))	**Rich loading** (mol CO_2/mol MEA)		**Captured CO_2** (kg/h)		**Specific heat duty** (MJ/kg CO_2)	
	Experiment	Model	Experiment	Model	Experiment	Model
E#1	0.386	0.386	4.67	4.77	5.01	5.16
E#4	0.397	0.395	4.83	5.06	5.05	4.90
E#24	0.392	0.394	4.57	4.54	5.11	5.02
E#25	0.435	0.402	4.19	3.53	5.46	5.40

Group C.2: Variation of the MEA mass fraction at the flue gas CO_2 partial pressure of 109.5 mbar (Associated experiments: 2, 26, and 27).

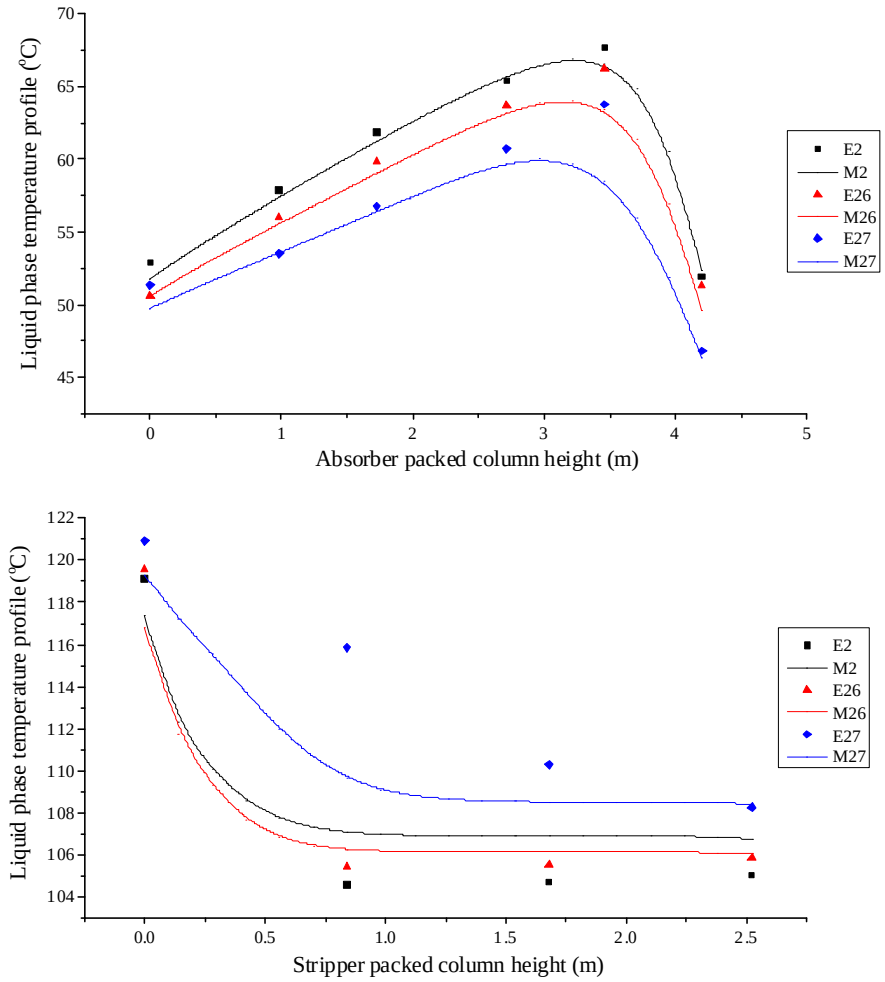

Figure 4-12. Comparison of the absorber (top) and stripper (bottom) temperature profiles calculated by the model with those of the pilot plant experiments of Group C.2

Table 4-17. Comparison of simulation results and pilot plant performance parameters of Group C.2

Experiment number (as per Notz *et al.* (22))	**Rich loading** (mol CO_2/mol MEA)		**Captured CO_2** (kg/hr)		**Specific heat duty** (MJ/kg CO_2)	
	Experiment	Model	Experiment	Model	Experiment	Model
E#2	0.464	0.474	6.11	6.79	3.98	3.49
E#26	0.475	0.473	5.89	5.79	4.13	3.82
E#27	0.501	0.468	5.03	4.48	4.77	4.73

Group D: Variation of the lean solvent temperature (Associated experiments: 1, 4, 20, and 21)

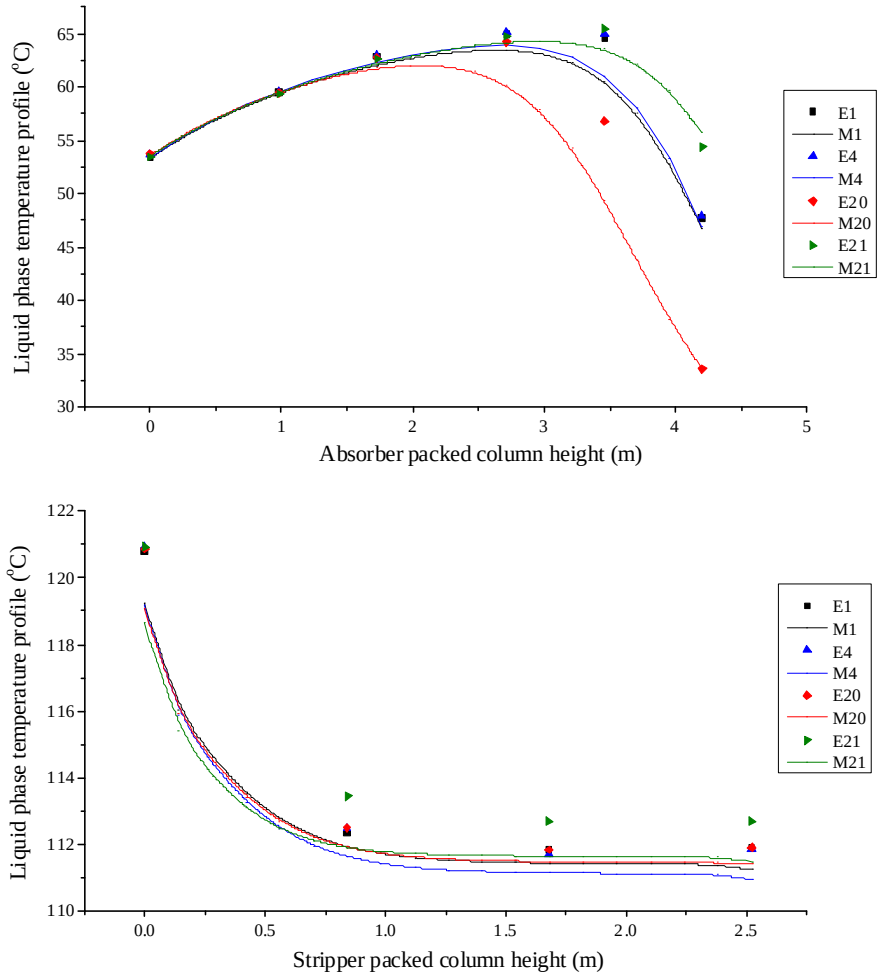

Figure 4-13. Comparison of the absorber (top) and stripper (bottom) temperature profiles calculated by the model with those of the pilot plant experiments of Group D

Table 4-18. Comparison of simulation results and pilot plant performance parameters of Group D

Experiment number (as per Notz *et al.* (22))	**Rich loading** (mol CO_2/mol MEA)		**Captured CO_2** (kg/h)		**Specific heat duty** (MJ/kg CO_2)	
	Experiment	Model	Experiment	Model	Experiment	Model
E#1	0.386	0.386	4.67	4.77	5.01	5.16
E#4	0.397	0.395	4.83	5.06	5.05	4.90
E#20	0.395	0.389	4.71	4.77	5.10	4.93
E#21	0.400	0.395	4.64	4.64	5.18	4.64

Group E: Variation of the CO_2 partial pressure in the flue gas (Associated experiments: 1, 2, 3, 4, 5, and 6).

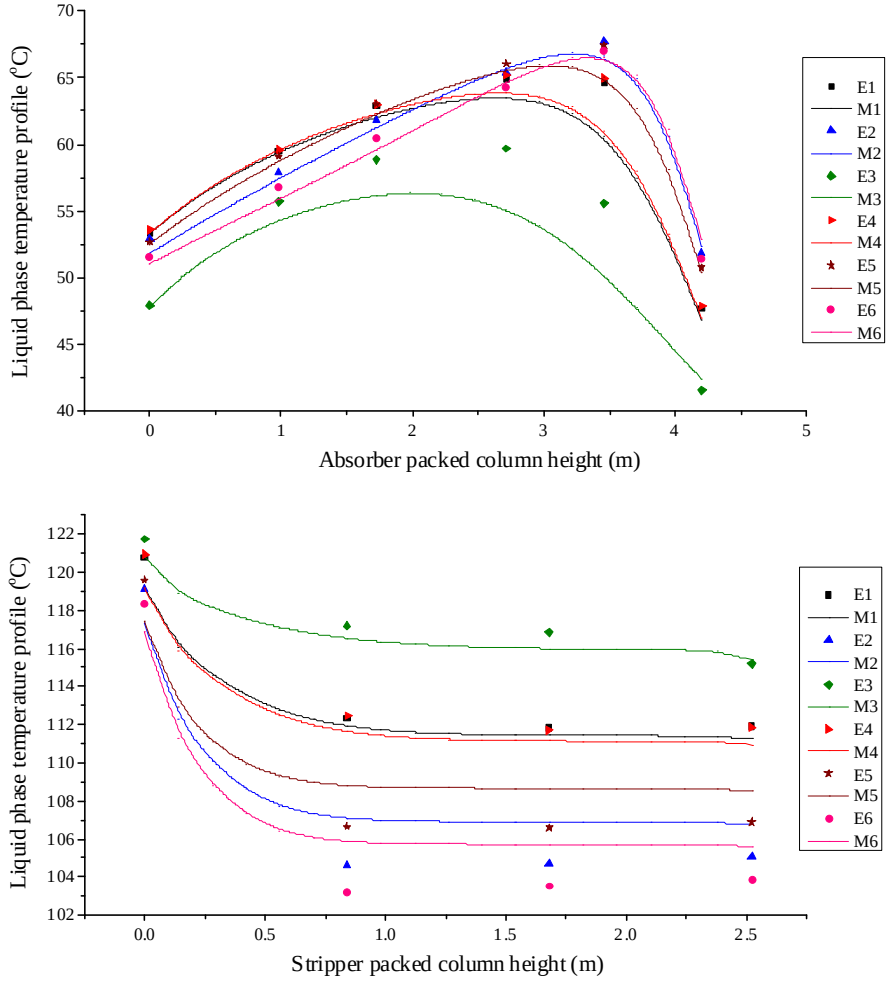

Figure 4-14. Comparison of the absorber (top) and stripper (bottom) temperature profiles calculated by the model with those of the pilot plant experiments of Group E

Table 4-19. Comparison of simulation results and pilot plant performance parameters of Group E

Experiments number (as per Notz *et al.* (22))	**Rich loading** (mol CO_2/mol MEA)		**Captured CO_2** (kg/h)		**Specific heat duty** (MJ/kg CO_2)	
	Experiment	Model	Experiment	Model	Experiment	Model
E#1	0.386	0.386	4.67	4.77	5.01	5.16
E#2	0.464	0.474	6.11	6.79	3.98	3.49
E#3	0.308	0.313	3.35	3.41	7.18	7.55
E#4	0.397	0.395	4.83	5.06	5.05	4.90
E#5	0.446	0.458	5.65	6.20	4.19	3.99
E#6	0.464	0.483	6.24	6.82	3.85	3.48

Group F: Variation of the fluid dynamic load in the absorber column (Associated experiments: 1, 4, 13, 14, and 15).

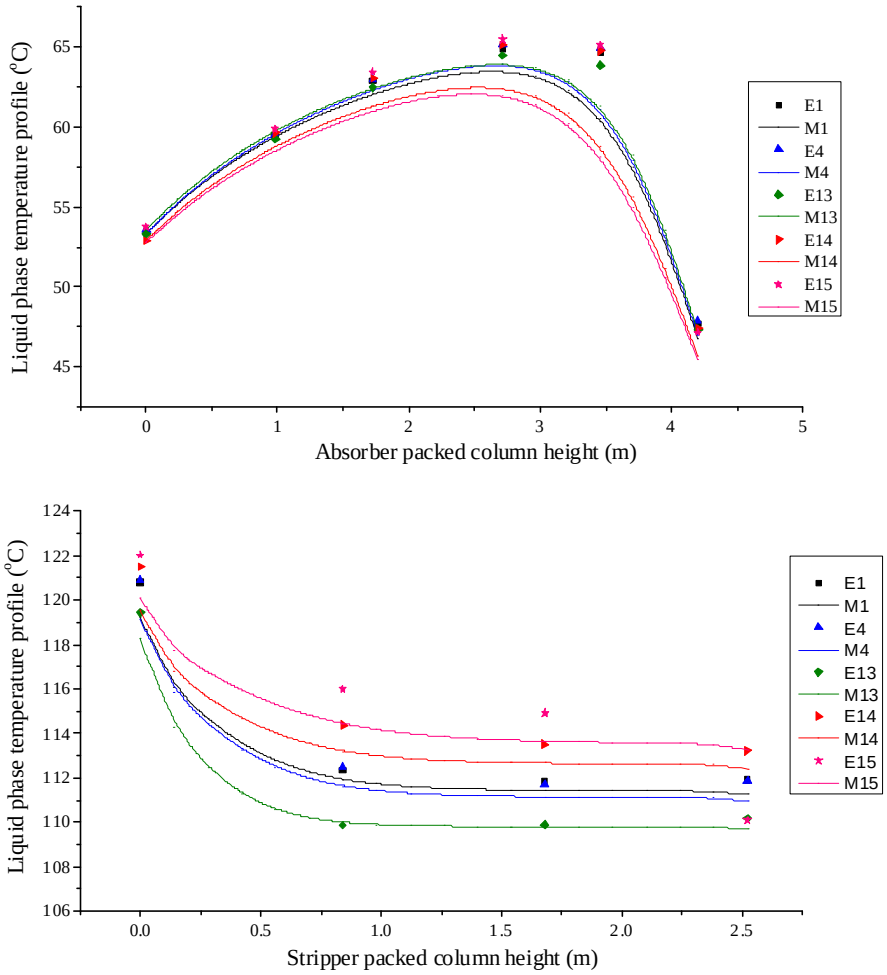

Figure 4-15. Comparison of the absorber (top) and stripper (bottom) temperature profiles calculated by the model with those of the pilot plant experiments of Group F

Table 4-20. Comparison of simulation results and pilot plant performance parameters of Group F

Experiment number (as per Notz *et al*. (22))	**Rich loading** (mol CO_2/mol MEA)		**Captured CO_2** (kg/h)		**Specific heat duty** (MJ/kg CO_2)	
	Experiment	Model	Experiment	Model	Experiment	Model
E#1	0.386	0.386	4.67	4.77	5.01	5.16
E#4	0.397	0.395	4.83	5.06	5.05	4.90
E#13	0.400	0.409	3.53	3.74	4.52	4.72
E#14	0.369	0.370	5.41	5.30	5.48	5.36
E#15	0.359	0.354	6.34	6.13	5.81	5.78

Group G.1: Variation of the CO_2 removal rate at the flue gas with CO_2 partial pressure of 54.6 mbar (Associated experiments: 1, 4, 37, 42, 43, 46, and 47).

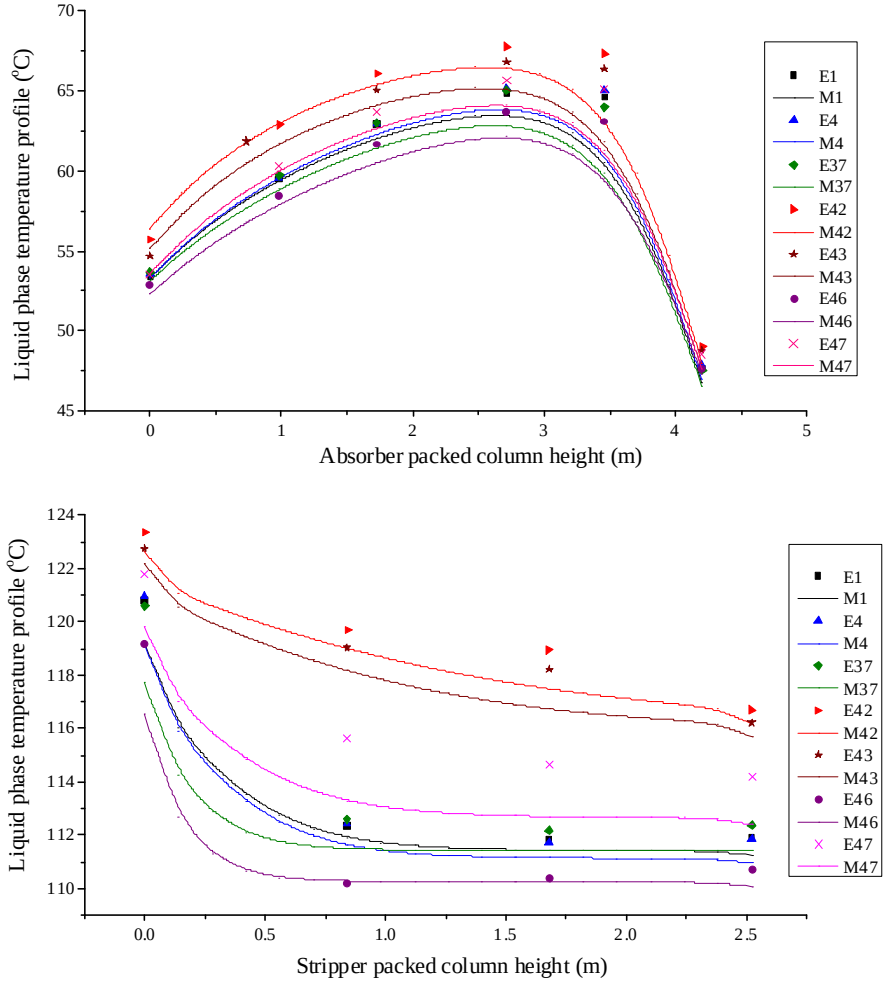

Figure 4-16. Comparison of the absorber (top) and stripper (bottom) temperature profiles calculated by the model with those of the pilot plant experiments of Group G.1

Table 4-21. Comparison of simulation results and pilot plant performance parameters of Group G.1

Experiment number (as per Notz *et al*. (22))	**Rich loading** (mol CO_2/mol MEA)		**Captured CO_2** (kg/h)		**Specific heat duty** (MJ/kg CO_2)	
	Experiment	Model	Experiment	Model	Experiment	Model
E#1	0.386	0.386	4.67	4.77	5.01	5.16
E#4	0.397	0.395	4.83	5.06	5.05	4.90
E#37	0.398	0.408	4.41	4.40	5.11	4.85
E#42	0.310	0.312	5.26	5.57	7.16	7.36
E#43	0.318	0.318	4.98	5.26	6.87	7.06
E#46	0.417	0.424	4.01	3.86	4.68	4.22
E#47	0.366	0.379	4.86	4.58	5.50	5.60

Group G.2: Variation of the CO_2 removal rate at the flue gas with CO_2 partial pressure of 109.6 mbar (Associated experiments: 1, 4, 37, 42, 43, 46, and 47).

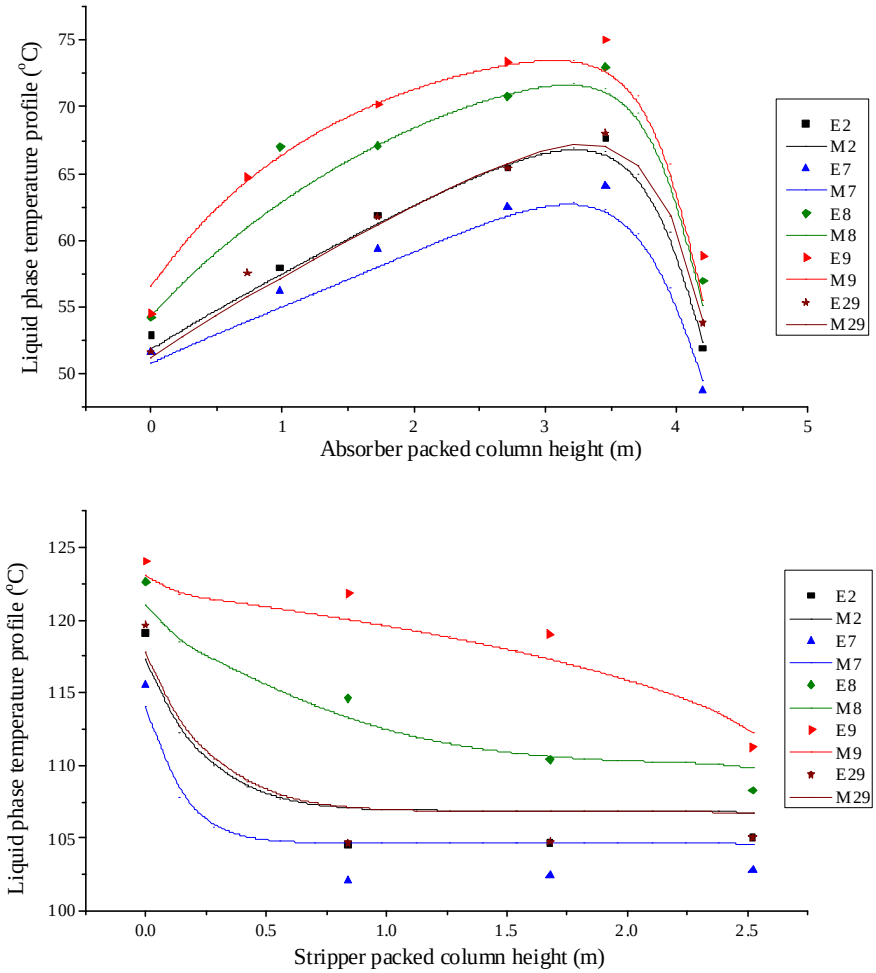

Figure 4-17. Comparison of the absorber (top) and stripper (bottom) temperature profiles calculated by the model with those of the pilot plant experiments of Group G.2

Table 4-22. Comparison of simulation results and pilot plant performance parameters of Group G.2

Experiment number (as per Notz *et al.* (22))	**Rich loading** (mol CO_2/mol MEA)		**Captured CO_2** (kg/h)		**Specific heat duty** (MJ/kg CO_2)	
	Experiment	Model	Experiment	Model	Experiment	Model
E#2	0.464	0.474	6.11	6.79	3.98	3.49
E#7	0.478	0.482	4.82	5.07	3.91	3.47
E#8	0.444	0.448	9.06	9.32	4.22	3.84
E#9	0.393	0.396	10.56	10.60	5.49	5.27
E#29	0.465	0.474	6.64	7.19	3.92	3.52

Group H: Variation of the flue gas temperature (Associated experiments: 1, 4, 22, and 23)

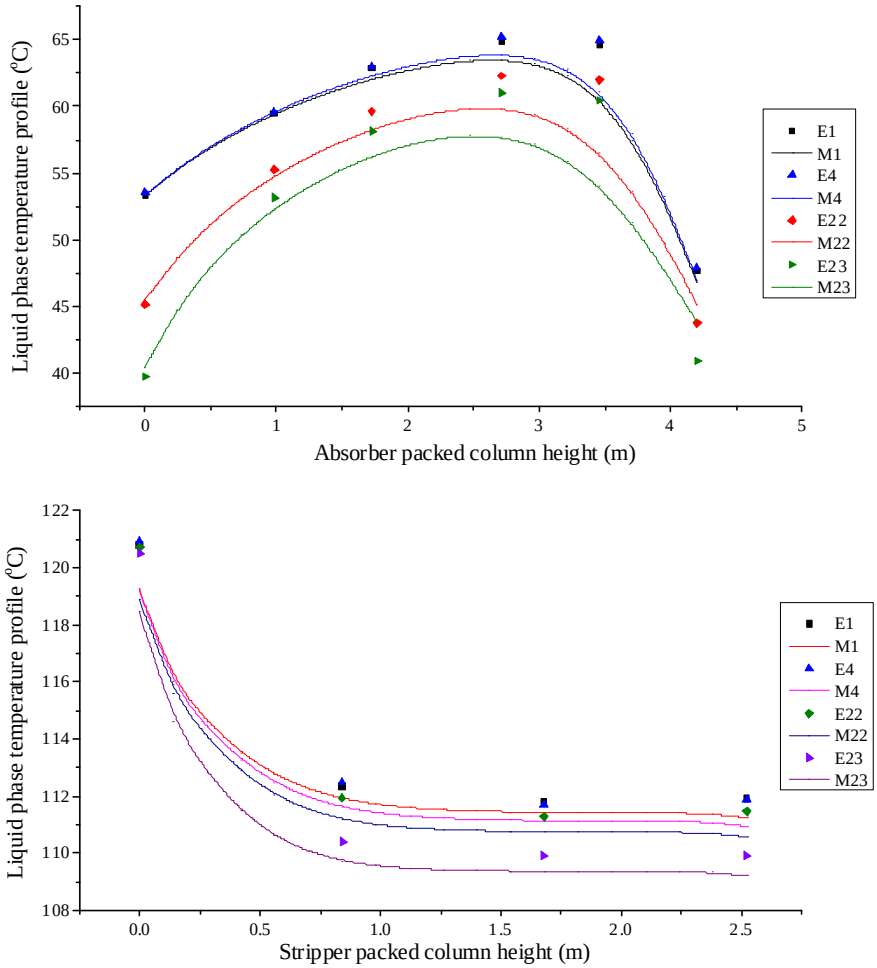

Figure 4-18. Comparison of the absorber (top) and stripper (bottom) temperature profiles calculated by the model with those of the pilot plant experiments of Group H

Table 4-23. Comparison of simulation results and pilot plant performance parameters of Group H

Experiment number (as per Notz *et al.* (22))	**Rich loading** (mol CO_2/mol MEA)		**Captured CO_2** (kg/hr)		**Specific heat duty** (MJ/kg CO_2)	
	Experiment	Model	Experiment	Model	Experiment	Model
E#1	0.386	0.386	4.67	4.77	5.01	5.16
E#4	0.397	0.395	4.83	5.06	5.05	4.90
E#22	0.389	0.397	4.80	4.93	5.10	4.85
E#23	0.393	0.403	4.73	4.78	5.11	5.03

It is evident from Tables 4-11 to 4-23 and Figures 4-6 to 4-18 that the model predictions are in good agreement with the experimental results. The average absolute deviation of the model results for the rich CO_2 loading, the captured CO_2 mass flow rate and the specific heat duty are 2.31 %, 4.59 % and 5.69 %, respectively, when compared with results of 47 experiments. It is important to note that Notz *et al*. (22) reported a maximum uncertainty of 2% for rich CO_2 loading, 6 % for the heat duty and 5 % for the CO_2 capture rate. Reported uncertainties associated with the CO_2 capture rate and the reboiler duty of experiments are relatively high. As the specific heat duty is calculated using these two parameters (as described in Table 4-5), therefore it is meaningful to conclude that these relatively high uncertainties may have been manifested in the relatively high deviation of the specific heat duty calculated by the model. The confidence gained by the reasonable agreement between the model results and experimental data allows the validated model to be applied for large scale design of the CO_2 capture process suitable to integrate with a commercial-scale natural gas fired combined cycle power plant. This topic is discussed in Chapter six of this thesis.

4.5. Conclusions & Remarks

A rate-based model of the CO_2 capture process using a 30 wt. % aqueous solution of MEA as solvent has been developed in Aspen Plus® V. 8.4. The thermodynamic framework, kinetics and transport property models used to develop the model were described. The rate based model was validated at pilot scale using experimental data obtained from two pilot plants: (1) the UKCCSRC/PACT CO_2 pilot plant, and (2) the pilot plant at the Laboratory of Engineering Thermodynamics in TU Kaiserslautern. The model predictions were in good agreement with each pilot plant data.

The experimental liquid to gas ratio and therefore the associated specific heat duty for the UKCCSRC/PACT CO_2 capture pilot plant are sub-optimal. This fact highlights the need for further modelling studies to be carried out to propose more efficient operating conditions to operate the pilot plant. As results of the developed rate-based model showed good agreement

with the experimental results, the model was therefore used for further studies to propose process modifications and optimal operating conditions at which the PACT pilot plant should operate more efficiency in the future. This topic is discussed in the Chapter five of this thesis.

The model predictions of the 47 experimental cases of the CO_2 capture pilot plant at the Laboratory of Engineering Thermodynamics in TU Kaiserslautern showed good agreement with the experimental results with average absolute deviations of 2.31%, 4.59% and 5.69%, respectively for the rich CO_2 loading, the captured CO_2 mass flow rate and the specific heat duty. The confidence gained by the reasonable agreement between the model results and experimental data allowed the validated model to be applied for large scale design of the CO_2 capture plant suitable to integrate with a commercial-scale natural gas fired combined cycle power plant. This topic is discussed in Chapter six of this thesis.

4.6. List of References

(1) Kenig, E., Kucka, L., Gorak, A., “Rigorous Modelling of Reactive Absorption Processes”, Chemical Engineering Technology, 2003, 26, 631-646.

(2) Asprion, N., “Non-equilibrium rate-based simulation of reactive systems: Simulation model, heat transfer, and influence of film discretization”, Industrial & Engineering Chemistry Research, 2006, 45, 2054-2069.

(3) Asprion, N., “Simulation of Mass Transfer in Reactive Absorption”, in: Marquardt, W., Pantelides, C. (Eds.), 16th European Symposium on Computer Aided Process Engineering and 9th International Symposium on Process System Engineering. Elsevier B.V.

(4) Taylor, R., Krishna, R., “Multicomponent Mass Transfer”, Wiley series in Chemical Engineering. 1993, John Wiley & Sons, New York City,

(5) Seader, J.D., “The rate-based approach for modelling staged separations”, Chemical Rngineering Progress, 1989, 85, 41–49.

(6) Katti S.S., “Gas-liquid-solid systems: an industrial perspective”, Trans IChemE Journal, 1995, 73, 595–607.

(7) Kenig, E.Y., “Modelling of multicomponent mass transfer in separation of fluid mixtures”, VDI-Verlag, Dusseldorf 2000.

(8) Danckwerts, P.V., Gas-Liquid Reactions, McGraw Hill, New York 1970.

(9) Hirschfelder, J.O., Curtiss, D.F., Bird, R.B., “Molecular Theory of Gases and Liquids”, WILEY, New York, 1964.

(10) Plaza, J.M., “Modelling of Carbon Dioxide Absorption using Aqueous Monoethanolamine, Piperazine and Promoted Potassium Carbonate”, PhD Dissertation, The University of Texas at Austin, 2012.

(11) Taylor, R., Krishna, R., Kooijman, H., “Real-World Modelling of Distillation”, Chemical Engineering Progress Journal, 2003, 99, 28–39.

(12) Zhang, Y., Chen, H., Chen, C.C., Plaza, J.M., Dugas, R., Rochelle, G.T., “Rate-Based Process Modeling Study of CO_2 Capture with Aqueous Monoethanolamine Solution”, Industrial & Engineering Chemistry Research, 2009, 48, 9233-9246.

(13) Alopaeus, V., Aittamaa, J., Norden, H.V., “Approximate High Flux Corrections for Multicomponent Mass Transfer Models and Some Explicit Methods”, Chemical Engineering Science, 1999, 54, 4267–4271.

(14) Vaidya, P., Kenig, E., “Gas-Liquid Reaction Kinetics: A Review of Determination Methods”, Chemical Engineering Communications, 2007, 194, 1543-1565.

(15) Kucka, L., Muller, I., Kenig, E., Gorak, A., “On the Modelling and Simulation of sour gas absorption by aqueous amine solutions”, Chemical Engineering Science, 2003, 58, 3571-3578.

(16) Chen, E., “Carbon Dioxide Absorption into Piperazine Promoted Potassium Carbonate using Structured Packing”, PhD. Dissertation, The University of Texas at Austin, 2007.

(17) Tobiesen, F.A., Svendsen, H.F., Juliussen, O., “Experimental validation of a rigorous absorber model for CO_2 postcombustion capture”, AIChE Journal, 2007, 53, 846-865.

(18) ASPEN, User Online Documentation. 2008.

(19) Aspen Plus, “Rate-Based Model of the CO_2 Capture Process by MEA using Aspen Plus”, Aspen Technology, Inc.,

(20) Zhang, Y., Que H., Chen, C.C., “Thermodynamic modelling for CO_2 absorption in aqueous MEA solution with electrolyte NRTL model”, Fluid Phase Equilibria, 2011, 311, 67–75.

(21) Zhang, Y., Chen, C-C. “Modeling CO_2 Absorption and Desorption by Aqueous Monoethanolamine Solution with Aspen Rate-based Model”, Energy Procedia, 2013, 37, 1584−1596.

(22) Notz, R., Mangalapally, H.P., Hasse, H., “Post Combustion CO_2 Capture by Reactive Absorption: Pilot Plant Description and Results of Systematic Studies with MEA.” International Journal of Greenhouse Gas Control, 2012, 6, 84-112,

(23) Akram, M., Ali, U., Best, T., Blakey, S., Finney, K. F., Pourkashanian, M., “Performance evaluation of PACT Pilot-plant for CO_2 capture from gas turbines with Exhaust Gas Recycle”, International Journal of Greenhouse Gas Control 2016 (47) 137–150.

(24) Onda, K., Takeuchi, H., Okumoto, Y., “Mass transfer coefficients between gas and liquid phases in packed columns”, Journal of Chemical Engineering of Japan, 1968, 1, 56–62.

(25) Stichlmair, J., Bravo, J.L., Fair, J.R., “General Model for Prediction of Pressure Drop and Capacity of Counter-Current Gas/Liquid Packed Columns”, Gas Separation and Purification Journal, 1989, 3, 19-28.

(26) Bravo, J.L., Rocha, J.A., Fair, J.R., “Mass Transfer in Gauze Packing”, Hydrocarbon Proceeding, 1985, 91-95.

Chapter 5

UKCCSRC/PACT CO_2 Capture Plant Performance Evaluation & Optimisation

This chapter presents the performance evaluation and optimisation of the UKCCSRC/PACT CO_2 capture plant, which will be called the PACT pilot plant for simplicity throughout this chapter, using the verified rate-base model described in Chapter 4.

5.1. Introduction

During the model verification using the PACT pilot plant experimental data, which was described thoroughly in Section 4.4 of Chapter 4, simulated CO_2 removal rates were on average converged to nearly 95 % in all five experimental cases whilst those of the experiments were around 90 %. The constant difference of nearly 5 % between the simulated and experimental CO_2 removal rate indicates that the mass transfer efficiency in the absorber column is sub-optimal, and points out the possibility of poor solvent distribution over the absorber packed column. Furthermore, the specific regeneration energy requirement corresponding to each experiment is sub-optimal and considerably higher than what has been reported to be attainable in industry to date, i.e. (3.2-4.2 MJ per kg of CO_2 captured using 30 wt. % MEA solvent (1)). These two issues underscore the need for further modelling work to be carried out to identify the appropriate system modifications and operating conditions by which the pilot plant may operate more efficiently in the future. As the results of the developed model showed good agreement with the experimental data, the model was therefore employed in further studies.

To determine optimal operating conditions for the PACT pilot plant, a number of parametric studies were carried out via modelling. Several parameters have been identified and varied over a given range of lean solvent CO_2 loading, i.e. 0.165 to 0.30, to evaluate their effects on

the pilot plant energy requirement. The optimum lean solvent CO_2 loading was determined using the total equivalent work concept.

The main conclusions of this work should also hold for other plants of this type that employ an aqueous solution of 30 wt. % MEA as the solvent.

5.2. Pilot Plant Process Description

The design of the PACT pilot plant is based on a standard amine-based CO_2 capture plant, and Figure 5-1 shows its process flow diagram. The one ton per day CO_2 capture plant uses 7 m MEA as solvent and operates with the flue gas provided by a 100 kW_e micro gas turbine (Turbec T100). The micro gas turbine, which is a combined heat and power unit, consists of a centrifugal compressor, radial turbine and high speed generator, which all are mounted on one shaft (2). Natural gas burns in the combustor and the hot flue gas expands through the turbine diffuser with an average CO_2 concentration of 1.6 % (on a molar basis; all subsequent CO_2 concentration percentages are on a molar basis unless otherwise stated). To attain a flue gas with conditions similar to that of a natural gas fired combined cycle power plant, i.e. 4 to 6 % CO_2 concentration, the turbine flue gas was mixed with CO_2 gas from a CO_2 storage tank. The flue gas CO_2 concentration was then increased in four steps up to 9.9 % to resemble flue gas conditions similar to a gas turbine with an exhaust gas recirculation (EGR) cycle at various recycle rates. The experiments presented in this study were carried out by injecting only pure CO_2 gas to the flue gas stream without adding any other traces such as NO_x or SO_2.

The pressure of the flue gas is increased by a booster fan before entering the absorber column. The typical 40 °C flue gas temperature at the absorber inlet was achieved by controlling the gas turbine heat exchanger bypass flow rate. An orifice plate flow meter along with temperature and pressure indicators measures the flue gas conditions at the absorber inlet. The flue gas flow rate throughout the experiments was constant due to plant

operating conditions. However, the solvent flow rate was varied with the variation of the flue gas CO_2 partial pressure to maintain a fixed CO_2 removal rate.

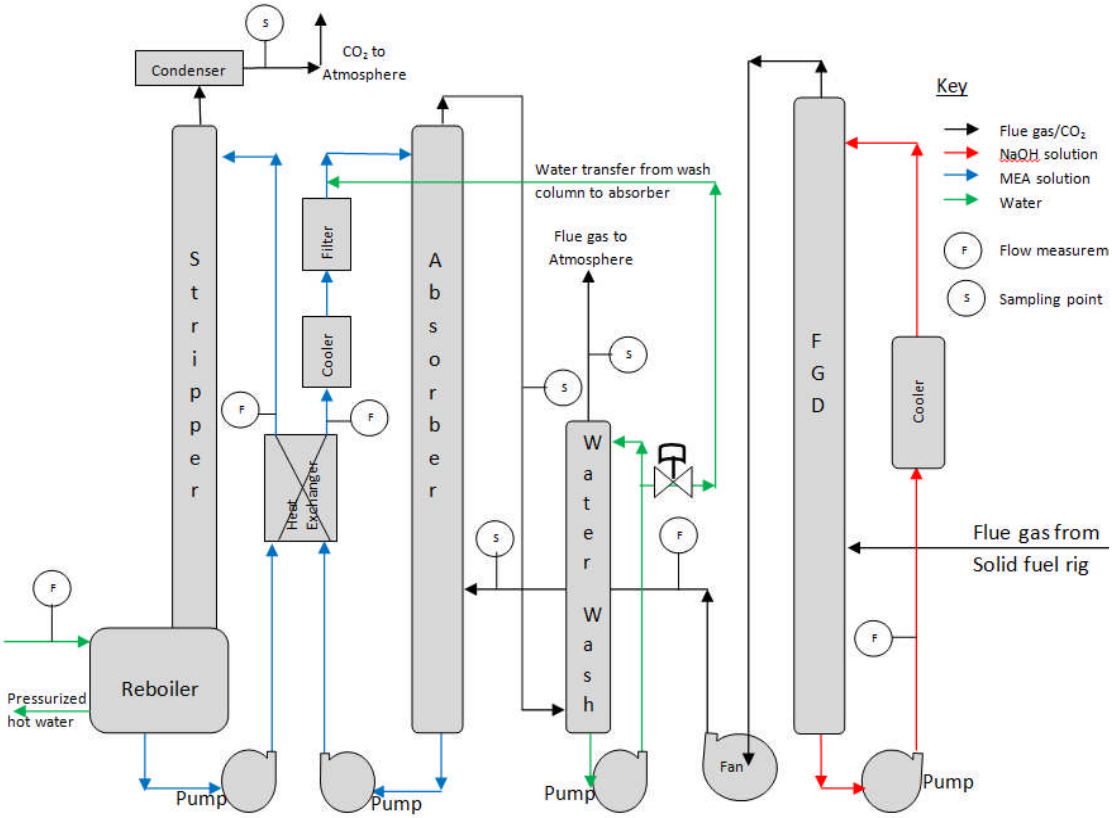

Figure 5-1. the process flow diagram of the UKCCSRC/PACT CO_2 capture pilot plant

The pilot plant consists of a packed absorber column, a packed water-wash column, and a packed stripper column constructed in a similar fashion to the absorber column with an air-cooled condenser and a reflux drum at the top. Columns are packed with INTALOX Metal Tower Packing (IMTP) No. 25 random packing due to its low cost and ease of installation. Table 5-1 summarises the pilot plant design specifications. Heat integration of the regenerated and rich solvent is realised via a plate type heat exchanger, and further cooling of the lean solvent prior entering the absorber column is achieved by an air-cooled induced draft cooler.

Table 5-1. The UKCCSRC design specifications

Parameter	**Specification**
Flue gas source	Turbec T100 micro gas turbine + CO_2 feed from CO_2 storage tank
CO_2 concentration in the flue gas	5.5-9.9 %
Flue gas flow rate in the absorber	250 Nm^3/h
Flue gas temperature at the absorber inlet	~ 40 °C
Solvent type	7 mole MEA aqueous solution
Solvent flow rate	~ 400-1200 kg/h
Solvent temperature at the absorber inlet	40 °C
Column packing in absorber, stripper, water washing sections	Koch IMTP25 random packing
Material of packing	metal
Diameter of columns (absorber, stripper, water wash sections)	0.30 m
Height of packing	
Absorber	8 m
Stripper	8 m
Water wash	1.2 m
Pressure in the absorber	Atmospheric pressure
Pressure in the stripper	120 – 300 kPa absolute

The counter-current contact of the flue gas entering the absorber column below the packing section with the lean solvent solution entering above the packing section results in the absorption of CO_2 by the solvent. Before the treated gas leaves the absorber column, it has to pass a demister to retain carried over liquid droplets. To further reduce amine losses, the flue gas leaving the absorber enters the wash column where it is treated with water to remove droplets of amine before exiting to atmosphere.

The temperature and mass flow rate of the lean solvent entering the absorber column are controlled. A Coriolis flow measurement device measures the lean solvent flow rate, and the required flow rate is controlled by a proportional control valve. The lean solvent temperature is measured by a thermocouple at the absorber inlet and controlled by opening of the valve bypassing the lean solvent across the lean solvent air-cooler. A Coriolis flow measurement device measures the rich solvent flow rate leaving the absorber column. The composition of

the rich solvent can be determined by analysis of a liquid sample taken downstream of the rich solvent pump. To ensure the plant steady state operation, the rich solvent level in the absorber sump is controlled by the rich amine pump.

Before being fed to the stripper column, the rich solvent is pumped through the cross heat exchanger to be heated up by the hot lean solvent leaving the stripper column, and both stream temperatures at the heat exchanger inlet and outlet are measured. The rich solvent enters the stripper column above the packed section, and the product vapour leaves the stripper from the top. The stripping steam is generated at the stripper bottom by partial evaporation of the liquid solvent in the reboiler, with the heat required in the reboiler being provided by pressurised hot water. The mass flow rate, inlet and outlet temperatures of the hot water are measured and recorded to calculate the heat required for solvent regeneration. The hot lean solvent leaves the stripper from the bottom and flows through the cross heat exchanger and the air-cooler to enter the absorber column. The composition of the lean solvent can be determined by analysis of a liquid sample taken downstream of the lean solvent pump.

To obtain temperature profiles for the absorber column, temperature was measured along the whole length of the absorber column at different locations of 2m, 3.3m, 5.1m, and 6.8m in height from the gas entry point. Along the stripper, temperature was recorded at 0.3m (bottom), 3.8m (middle) and 7.5m (top) heights from the bottom of the stripper.

Two Servomex analyzers – a Servomex 4900 for O_2 and low level CO_2 measurement, as well as a Servomex 2500 for high level CO_2 measurement were used to analyse the flue gas composition at the following locations: inlet of the absorber, exit of the absorber, exit of the wash column and CO_2 concentration at the exit of the stripper. The Servomex 4900 draws samples from three locations (absorber inlet, absorber outlet, wash column outlet) alternately. The switchover happens every 5 minutes and is controlled by a Programmable Logic Controller (PLC) through solenoid valves. In order to avoid condensation problems, the temperature of the heated sampling lines was maintained at 150 °C in all cases. The

sampling points have been equipped with coalescence filters to remove droplets of water carried over by the gas. The alkalinity of the solvent is determined analytically by titrating samples with HCl solution, while the CO_2 loading of the lean and rich solutions are determined via titrating samples with NaOH solution. The control of the pilot plant is done via programmable logic controllers (PLCs) while data acquisition and logging are performed with LABVIEW® interfaced with MS Excel®.

5.3. Methodology

The verified rate-based model of the CO_2 absorption/desorption process described in Chapter 4 was used to simulate and evaluate the performance of the PACT pilot plant over a range of lean loading from 0.165 to 0.30 at steady state condition to identify optimal operating conditions in terms of energy consumption which will be used for future operations of the PACT pilot plant. The CO_2 removal rate of 90% was targeted using the flue gas condition of the experiment 1 (case#1) with 5.5 % CO_2 as summarised in Table 5-2 with 30 wt. % MEA solution as solvent. This flue gas condition was chosen for this study as it is similar to a typical flue gas of natural gas fired applications with 3-5 % CO_2.

Table 5-2. The base-case performance characteristics

Parameter	**Value**
Total flue gas mass flow rate	260 kg/h
Flue gas temperature at absorber inlet	40 °C
Flue gas pressure at absorber inlet	~ 125 kPa
Flue gas composition	
N_2	74.74 %
O_2	16.6 %
CO_2	5.5 %
H_2O	3.16 %

5.3.1. Process Evaluation

To evaluate the energy performance of the PACT pilot plant, the total equivalent work concept is used in addition to the specific regeneration energy requirement. This concept

estimates the total electrical work penalty that would be imposed on the power plant by operating the CO_2 capture plant. Eq. 5-1 shows the three main contributors to the total equivalent work (3):

$$W_{eq} = W_{heat} + W_{comp} + W_{pump} \quad (5\text{-}1)$$

Where, W_{eq} is the total equivalent work, W_{heat} is the regeneration heat equivalent work, W_{comp} is the compression equivalent work and W_{pump} is the pump equivalent work. The equivalent electrical penalty associated with solvent regeneration, called the regeneration heat equivalent work, is calculated using the Carnot efficiency method, as represented by Eq. 5-2 (3):

$$W_{heat} = \eta_{turbine}\left(\frac{T_{reb} + \Delta T - T_{sink}}{T_{reb} + \Delta T}\right) Q_{reb} \quad (5\text{-}2)$$

Where, $\eta_{turbine}$ is the Carnot efficiency, T_{reb} is the solvent temperature at the reboiler, ΔT is the temperature difference between hot and cold streams at the reboiler, T_{sink} is the cooling water temperature, and Q_{reb} is the reboiler heat duty. Assumptions made for Eq. 2 include a 90 % efficiency to account for non-ideal expansion in steam turbines (4), an approach temperature of 5 °C for the steam side in the reboiler section, and a sink temperature of 40 °C.

The compression work is the work required to compress the captured CO_2 from the stripper pressure (P_{in}), to the storage pressure, e.g. 15 MP (150 bar), and calculated using Eq. 5-3 (5).

$$W_{comp} = -3.48\ln(P_{in}) + 14.85, \qquad 1 < P_{in}\,(bar) < 20 \quad (5\text{-}3)$$

Assumptions made for Eq. (3) include a compression ratio of 2 or less for each compression stage, a compressor polytropic efficiency of 86 %, inter-stage cooling to 40 °C with knocked out water between stages with zero pressure drop (5).

The pump work includes only the required head at the efficiency of the pump, e.g. 75 %, to move and circulate the solvent from the absorber to the pressure of the stripper and vice versa. The flue gas blower work is excluded from this calculation, assuming the flue gas pressure at the absorber inlet is sufficiently high to overcome the passage and packing pressure drops. The Aspen Plus pump block is used to calculate the pump work.

5.4. Performance Evaluation

Specific regeneration energy and total equivalent work were chosen as parameters independent of scale to evaluate and compare the plant energy performance. Four areas of improvement were identified to be explored: solvent lean loading, cross heat exchanger logarithmic mean temperature difference (LMTD), stripper operating pressure, and replacement of the current packing, i.e. IMTP25, with a more efficient packing, i.e. Sulzer Mellapak 250Y.

5.4.1. Lean Solvent CO_2 Loading

The stripper energy consumption is strongly dependant on the lean solvent CO_2 loading. For a given rich loading, if lean loading increases, the amount of steam required per unit of produced CO_2 will be reduced. Increasing lean loading can be achieved by increasing solvent circulating rate with respect to the targeted CO_2 removal rate. The lean solvent CO_2 loading used in the PACT pilot plant for this case was 0.165. To find an optimum lean loading, a range of lean loading from 0.165 to 0.30 was studied. Table 5-3 presents the required solvent flow rate calculated by the model for each lean loading to achieve 90 % CO_2 removal rate using the flue gas condition presented in Table 5-2.

The reboiler duty at each lean loading was calculated using the model. Then the specific regeneration energy requirement and the total equivalent work for each lean loading were calculated. As shown in Figure 5-2, the minimum total equivalent work occurs at a CO_2 loading of 0.23. The specific regeneration energy requirement at this loading is 5.13 MJ/kg CO_2 to achieve a 90 % CO_2 removal rate, compared to the base-case with 0.165 lean loading, where the specific regeneration energy requirement is 7.1 MJ/kg CO_2. The nearly 15 % reduction in the specific regeneration energy requirement is associated with a nearly 39 % higher circulating solvent flow rate. Studying the absorber design performance suggests the absorber column is capable of handling the excess solvent flow rate. The additional operational cost associated with the increased pumping power is very small compared to the gain associated with the reduction in the steam requirement.

Table 5-3. Required solvent flow rate to achieve 90 % CO_2 removal rate with the base-case flue gas composition with IMTP25 random packing material

Lean loading (mol CO_2/mol MEA)	**Solvent flow rate (kg/h)**	**Liquid to gas ratio (L/G) (kg/kg)**
0.165	340.7	1.32
0.18	363.4	1.41
0.2	400.8	1.55
0.21	420.3	1.63
0.22	447.7	1.73
0.23	475.3	1.84
0.24	508.7	1.97
0.25	549.2	2.12
0.26	601.1	2.32
0.28	752.3	2.91
0.3	954.4	3.69

Although changing the lean loading to a higher value resulted in reducing the specific regeneration energy, the pilot plant energy performance is still sub-optimal and requires further modifications.

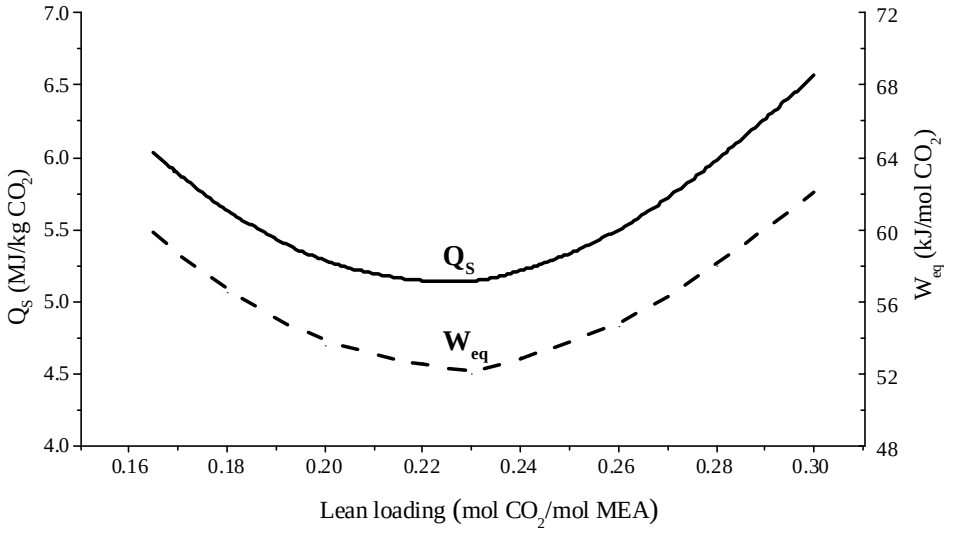

Figure 5-2. optimisation of lean loading for minimum total equivalent work with 125 kPa stripper pressure, 20 °C LMTD in cross heat exchanger, and IMTP25 random packing material

5.4.2. Cross Heat Exchanger Performance

The rich solvent inlet temperature to the stripper is determined by the performance of the cross heat exchanger. This performance can be defined using the log mean temperature difference (LMTD) concept. In general, a lower LMTD is associated with higher capital cost for a given heat load, and the pilot plant cross heat exchanger currently operates with a 20 °C LMTD. To evaluate the extent to which a better performing heat exchanger will improve the plant energy performance, three different heat exchanger design specifications were analysed, corresponding to 20, 10 and 5° LMTD. Figure 5-3 shows the variation of specific regeneration energy requirement and total equivalent work with lean loading when the stripper column operates at 125 kPa.

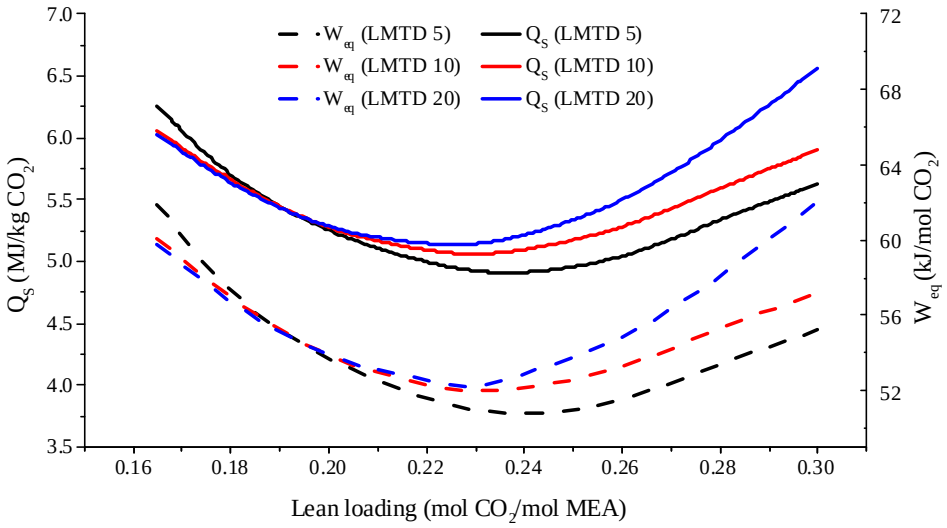

Figure 5-3. Specific regeneration energy requirement and total equivalent work variations with lean loading with 125 kPa stripper pressure, and IMTP25 random packing material, with 5, 10, 20 °C LMTD in cross heat exchanger.

The results show that the plant energy performance improves by up to 14 % across the range of lean loading by lowering the LMTD from 20 to 5 °C. Comparing the plant energy performance at the optimum lean loading, i.e. 0.23, suggests that having a 5 °C LMTD across the cross heat exchanger results in approximately 5 % reduction in the solvent regeneration energy requirement with almost 13 °C increase in the rich solvent temperature at the stripper inlet in relation to the base case with 20 °C LMTD. These findings suggest one way to improve the pilot plant energy performance is by replacing the cross heat exchanger with a high performing heat exchanger designed to operate with 5 °C LMTD. However, this benefit is associated with an additional cost of acquiring a larger heat exchanger. The studies discussed in the following sections are performed assuming the cross heat exchanger operates with a 5 °C LMTD.

5.4.3. Stripper Operating Pressure

It is possible to increase the stripper operating pressure and therefore its operating temperature by increasing the reboiler operating temperature via increasing the pressure of heat source, e.g. the boiler pressure (1). Currently the stripper operating pressure is 125±5

kPa when measured at the top of the column, and it was designed to operate at pressures up to 300 kPa. Figure 5-4 shows the effect of varying the stripper pressure from 125 to 250 kPa on total equivalent work and specific regeneration energy requirements across the range of lean loading from 0.165 to 0.30 assuming 90 % CO_2 removal rate, 5 °C LMTD at the cross heat exchanger, and 5 °C temperature approach across the reboiler.

As shown in Figure 5-4, the specific energy requirement reduces with increasing the stripper pressure. Increasing the operating pressure from 125 to 250 kPa is associated with nearly a 17 % reduction in the specific regeneration energy consumption at their optimum lean loading. Operating at higher pressures in general reduces the CO_2 compression energy requirement although this is not considered for this pilot plant energy study. It appears increasing the stripper operating pressure is a meaningful way to enhance the pilot plant energy performance.

However, increasing the pressure will increase the solvent temperature at the reboiler and throughout the column. The thermal degradation of MEA occurs mainly in the stripper packing and reboiler due to exposure to high temperature (6). Davis and Rochelle (6) studied the thermal degradation of MEA and indicated that thermal degradation is minor when the solvent temperature at reboiler temperature is held below 110 °C but it accelerates above 130 °C. Figure 5-5 shows the variation of the solvent temperature at the reboiler with the stripper operating temperature. By considering a degradation threshold of 120 °C, based on data provided in Figure 5, 180 kPa pressure appears to be the most suitable operating pressure in order to gain benefits by operating the stripper at higher pressure and avoid a higher risk of solvent degradation and minimise corrosion problems.

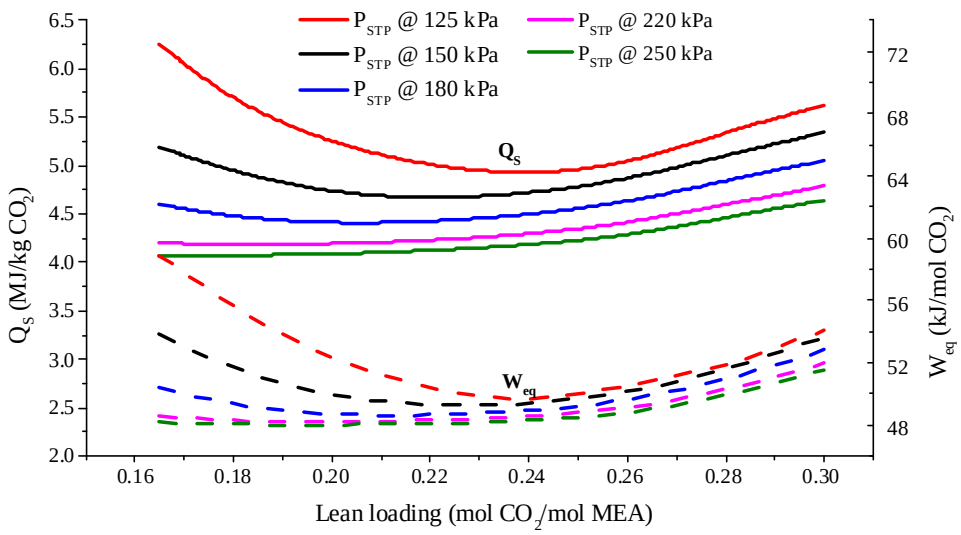

Figure 5-4. Specific regeneration energy requirement and total equivalent work variation with lean loading at various stripper operation pressure (125 kPa (red), 150 kPa (black), 180 kPa (blue), 220 kPa (magenta) and 250 kPa (green)) with 5 °C LMTD in cross heat exchanger, 5 °C temperature approach across the reboiler, and IMTP25 random packing material.

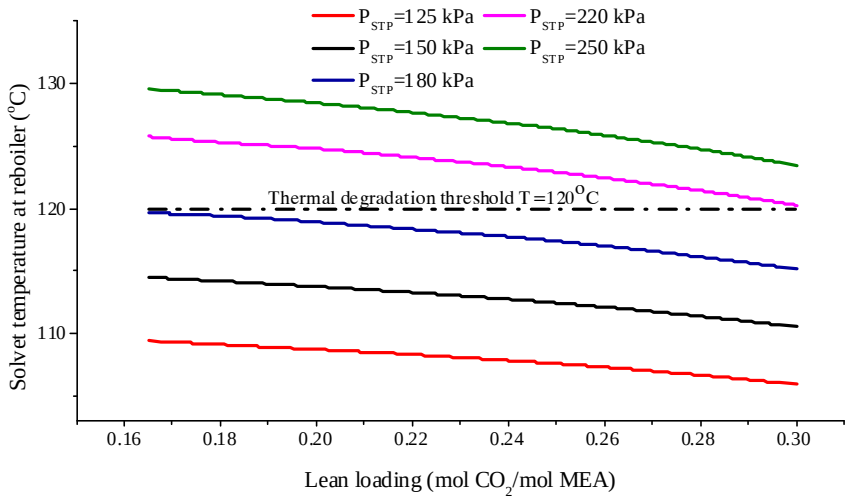

Figure 5-5. the variation of solvent temperature at the reboiler section with lean loading at various stripper operation pressures (125 kPa (red), 150 kPa (black), 180 kPa (blue), 220 kPa (magenta) and 250 kPa (green)) with 5 °C LMTD in cross heat exchanger, 5 °C temperature approach across the reboiler, and IMTP25 random packing material.

The lean loading at which the total equivalent work is minimised when the stripper operates at the pressure of 180 kPa is 0.21, provided a 5 °C LMTD in the cross heat exchanger and a 5 °C approach temperature across the reboiler. The solvent temperature at the optimum lean

loading is 118.7 °C with the specific regeneration energy requirement of 4.4 MJ/kg CO_2. This amount of specific regeneration energy requirement is nearly 28 % lower than what has been currently recorded from the pilot plant operation. Table 5-4 summarises the proposed operating conditions to improve the energy performance of the PACT pilot plant to achieve 90 % CO_2 removal rate using IMTP25 random packing in all packed columns.

Table 5-4. Summary of proposed operating conditions for optimum operation of the PACT pilot plant to achieve 90 % CO_2 removal rate from typical natural gas fired flue gases when using the IMTP25 random packing

Parameter	**Specification**
Packing material	IMTP25 random packing
Flue gas temperature at absorber inlet	40 °C
Liquid to gas ratio	1.64 (kg/kg)
Lean solvent temperature at absorber inlet	40 °C
Lean loading	0.21 (mol CO_2/mol MEA)
Stripper pressure	180 kPa
Cross heat exchanger LMTD	5 °C
Reboiler approach temperature	5 °C

5.4.4. Packing Material

It may not be fully advantageous to find conditions to optimally operate a CO_2 capture plant if is not associated with an efficient packing material. There are mainly two different types of packing materials used in a CO_2 capture processes: random packing and structured packing. The pilot plant is currently packed with the IMTP25 random packing. Difficulties to achieve uniform distribution at the outset and the risk of maldistribution close to the column wall are problems typically reported for random packing, while structured packing materials are specifically designed to avoid such problems (7). Compared to random packing, structured packing has in general better mass transfer efficiency, good wettability and lower pressure drop (8). To further improve the energy performance of the PACT pilot plant with the fixed absorber design, i.e. height and diameter, and CO_2 removal rate, the current packing material should be replaced by a more efficient and better performing packing material from structured packing categories, such as Sulzer Mellapak 250Y. This

modification will result in a reduction in the amount of circulating solvent required to achieve 90 % removal rate for a given lean loading due to the improved mass transfer efficiency in the absorber column. The lower solvent flow rate will therefore require less stripping steam to regenerate, as well as better performance of the stripper column itself by changing the packing material. All these will lead the pilot plant to operate with lower specific generation energy requirement. Table 5-5 summarises the solvent flow rate required to achieve 90 % CO_2 removal rate for the range of lean loading with the base-case flue gas compositions when replacing all the packing with the Sulzer Mellapak 250Y structured packing.

Table 5-5. Required solvent flow rate to achieve 90 % CO_2 removal rate with the base-case flue gas composition with Sulzer Mellapak 250Y structured packing, and the comparison with those for the IMTP25 random packing material

Lean loading (mol CO_2/mol MEA)	**Lean solvent flow rate (kg/h)**		**Reduction in required solvent flow rate (%)**
	Mellapak 250Y	IMTP25	
0.165	283.2	340.7	16.9
0.18	297.6	364.5	18.3
0.2	319.3	401.3	20.4
0.21	331.0	420.3	21.2
0.22	344.2	447.7	23.1
0.23	358.5	475.3	24.6
0.24	373.8	373.8	26.9
0.25	390.5	390.5	29.2
0.26	408.9	408.9	32.1
0.28	452.4	452.4	39.8
0.3	509.9	509.9	46.7

As presented in Table 5-4, the significant reduction in the required solvent flow at higher lean loading confirms the poor mass transfer efficiency of random packing at higher liquid to gas ratios. When using the Sulzer Mellapak 250Y structured packing, the simulation results also confirmed the stripper operating pressure of 180 kPa is the best option in terms of energy performance with respect to a 120°C thermal degradation threshold. Figure 5-6 shows the variation of total equivalent work and specific regeneration energy requirement with lean

loading when using the Sulzer Mellapak 250Y structured packing with the stripper pressure of 180 kPa, 5 °C LMTD in the cross heat exchanger and 5 °C temperature approach at the reboiler. The curves related to the IMTP25 random packing with similar operating conditions were added for comparison.

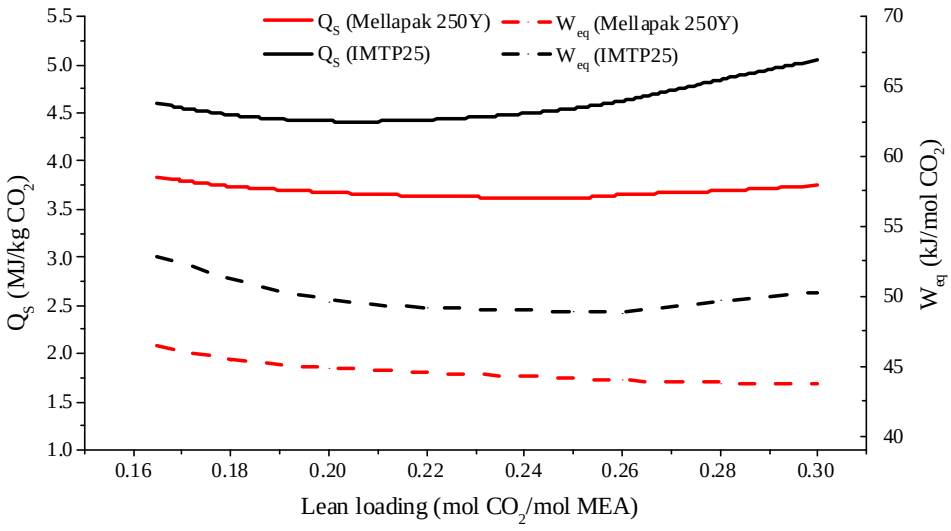

Figure 5-6. Optimisation of the lean loading for minimum total equivalent work and the specific regeneration energy requirement with the Sulzer Mellapak 250Y structured packing (black) and the IMTP25 random packing (red) to achieve 90 % CO_2 removal rate with the stripper pressure of 180 kPa

The minimum total equivalent work occurs at lean loading of 0.26 with a specific regeneration energy requirement of 3.64 MJ/kg CO_2, implying a nearly 39 % reduction in the specific regeneration energy requirement when compared with the current pilot plant operating condition to achieve 90 % CO_2 removal rate. The highest solvent temperature at the reboiler at the optimised lean loading is 107 °C. The specific regeneration energy requirement after changing the packing type is suitability within the industry range of 3.2 to 4.2 MJ/kg CO_2. The optimum operating condition using the Mellapak 250Y structured packing provides a 15 % reduction in the specific regeneration energy requirement compared to that provided by the optimum operating condition with the IMTP25 random packing. Table 5-6 summarises operating conditions to suitably improve the energy performance of

the PACT pilot plant to achieve 90 % CO_2 removal rate for typical gas turbine flue gases when replacing all packing with the Sulzer Mellapak 250Y structured packing.

Table 5-6. Summary of the proposed operating condition for an optimum operation of the UKCCSRC/PACT CO_2 capture pilot plant to achieve 90 % CO_2 removal rate from typical natural gas fired flue gases when using the Sulzer Mellapak 250Y structured packing

Parameter	**Specification**
Packing material	Sulzer Mellapak 250Y structured packing
Flue gas temperature at absorber inlet	40 °C
Liquid to gas ratio	1.58 (kg/kg)
Lean solvent temperature at absorber inlet	40 °C
Lean loading	0.26 (mol CO_2/mol MEA)
Stripper pressure	180 kPa
Cross heat exchanger LMTD	5 °C
Reboiler approach temperature	5 °C

5.5. Conclusions & Remarks

A rate-based model to simulate the CO_2 capture process using an aqueous solution of 30 wt.% MEA as solvent has been developed in Aspen Plus® Version 8.4 and validated using results of 5 experimental studies carried out at the UKCCSRC/PACT pilot plant in Sheffield, UK. The developed model was then used to assess the performance of the pilot plant in terms of energy consumption, and to propose new operating conditions to operate the pilot plant optimally in future. A number of performance parameters have been identified and varied for a given range of lean solvent CO_2 loading from 0.165 to 0.30 (mol CO_2/ mol MEA) to evaluate their effects on the plant energy performance. Two sets of operating conditions with two different packing materials were finally suggested to improve the pilot plant energy performance.

For the pilot plant to efficiently achieve 90 % CO_2 capture from flue gases with 5.5 % CO_2, typical of a natural gas fired applications, the following modifications were suggested:

- A more efficient cross heat exchanger has the potential to improve the stripper performance by providing the rich solvent with a temperature closer to its bubble point at the stripper inlet. Simulation results showed a nearly 5 % reduction in the specific regeneration energy requirement associated with the rich solvent being heated up by further 13 °C when using a 5 °C LMTD cross heat exchanger instead of the current one with a 20 °C LMTD.

- Considerable energy savings can be achieved by increasing the lean loading level, provided that the absorber column is capable of operating at higher liquid rates, which is achievable for the case of the PACT pilot plant. Simulation results have shown that by solely increasing the lean loading from 0.165 to 0.23, with no other change of the pilot plant operating condition, the specific regeneration energy requirement was reduced by nearly 15 %. The additional cost associated with the 28 % increase in the solvent flow rate is insignificant compared to the energy gain realised in the regeneration process.

- The stripper operating pressure also has a significant effect on the regeneration energy performance. Simulation results showed that by increasing the stripper pressure from 125 to 180 kPa the specific regeneration energy requirement will reduced by 28 %. The optimum lean loading to realise this gain is at 0.21 with a 118.7 °C solvent temperature at the reboiler section, which is reasonably below the thermal degradation threshold of MEA solvents.

- An efficient and modern packing material can contribute to significantly improve the overall performance of the PACT pilot plant by providing higher mass transfer efficiency, lower pressure drop and more efficient liquid and gas distributions. Simulation results suggest replacing the existing packing material with higher performing structured packing, e.g. Sulzer Mellapak 250Y will result in a nearly 40 % reduction in the specific regeneration energy when compared with the plant existing conditions. The proposed operating condition with the Sulzer Mellapak

250Y structured packing outperformed the condition proposed with the IMTP25 random packing by nearly 15 %.

The main conclusions of this work should also hold for other plants of this type that employ 30 wt. % MEA solution as solvent.

5.6. List of References

(1) Tobiesen, F.A., Svendsen, H.F., “Study of a Modified Amine-Based Regeneration Unit”, Industrial and Engineering Chemistry Research, 2006 (45) 2489-2496.

(2) Turbec, A.B., Technical description–T100 microturbine system, 2000, Turbec Company. Italy.

(3) Oyenekan, B.A. Modeling of strippers for CO_2 capture by aqueous amines. PhD Dissertation, The University of Texas at Austin, 2007.

(4) Lucquiaud M., Patel P., Chalmers H., Gibbins J., “Retrofitting CO_2 capture ready fossil plants with post-combustion capture. Part 1: Requirements for natural gas combined cycle plants using solvent-based flue gas scrubbing” Energy 2009, 223-213.

(5) Lin, Y-J.; Rochelle, G.T. Approaching a reversible stripping process for CO_2 capture. Chemical Engineering Journal 2016 (283) 1033–1043.

(6) Davis, J. and Rochelle, G., “Thermal Degradation of MEA at Stripper Conditions”, Energy Procedia,Proceedings of GHGT- 9 Conference, 16-20 November, 2008, Washington DC, USA

(7) Billet, R., 1995, Packed Towers, VCH, Weinheim, Germany.

(8) Sulzer Chemtech, 2015. Structured Packing for distillation, absorption and reactive distillation. Sulzer Chemtech Ltd., Switzerland.

Chapter 6

Process Design of Large-scale CO_2 Capture for Natural Gas Combined Cycle Power Plant Applications

This chapter focuses on the process design of MEA-based post combustion CO_2 capture process (PCC) with CO_2 compression unit to be incorporated into a 650 MW natural gas combined cycle (NGCC) power plant, and assesses the performance viability of the integrated NGCC-PCC at power plant full- and part-load operations in terms of net power plant output and efficiency. The process simulation of the NGCC power plant and the methodology applied to size a large-scale PCC plant are thoroughly explained. The PCC plant energy requirements, including the energy required for CO_2 compression, at various power plant load operations are determined. Furthermore, the performance of the NGCC plant, especially the LP steam turbine, during non-capture operation are studied as there will be a considerable amount of steam available at the LP turbine inlet at those times. Issues require careful considerations for the NGCC plant in case of non-capture operation are also addressed. Moreover, the potential impact on the performance of the LP and IP steam turbine sections and the condenser during the non-capture operation are discussed.

6.1. Introduction

Natural gas combined cycle (NGCC) power plants fitted with post combustion CO_2 capture (PCC) are projected to operate as mid-merit plants in the future of the decarbonised energy market. This projection stems from an inherent characteristic of the NGCC plants of being flexible in operation and able to rapidly change their output power. Therefore, it is expected that the NGCC-PCC plants will continue to operate flexibly for a range of operational loads; and therefore compliment the intermittent electricity generation of other low carbon plants to securely maintain the quality of electricity supply. Therefore, the suitability of these plants to

operate in peak power, and especially mid-merit markets should be assessed at the design stage by carefully evaluating their part load behaviours and responses, and the implications of them being decoupled temporarily from the CO_2 capture plant.

There is a limited amount of information available on the additional constraints that limit the power plant flexibility with PCC, in terms of start-up; shut down and part load performances (1). To improve the flexibility of fossil-fuelled power plants fitted with PCC, the following suggestions have been evaluated and published in the public domain:

- Application of solvent storage to postpone the solvent regeneration process to a later time, allowing the power plant to increase or decrease load as per its original ramp up/down rates (2-9),
- Temporary shutdown of the CO_2 capture plant in order to benefit from fluctuating electricity prices by avoiding the need for steam supply for solvent regeneration (2,5,7,9),
- Varying the CO_2 capture rate with respect to electricity market price and cost related to the CO_2 emissions (2,5,8,9).

Although the above mentioned alternatives allow the plant to generate extra power, or operate with their original ramp up/down rates when required, all of them require extra capital investment in terms of additional equipment or over-sized capacity of some major units (1,10). In contrast, although there are limits to its flexibility constrained by design, operation and control of the chemical processes involved, the post combustion CO_2 capture process is capable of following the load of the power plant via using advanced control systems (1,11,12). A key factor will then be to impose appropriate operational procedures on the capture plant performance at times when flexible operation is necessary (2,11). Having satisfied this requirement, another aspect that needs to be fulfilled before delivering flexibility in power generation with PCC in place is the operability of the power plant in general, and the low-pressure (LP) steam turbine section in particular at times that the CO_2 capture unit is temporarily shut down. Since no steam is required for solvent regeneration,

such conditions correspond to a substantial increase in the steam flow available at the LP turbine cylinder. This option requires the balance of the plant to be appropriately designed and sized to accommodate the increased steam flow in the LP turbine and the cold end i.e. condenser. Moreover, the generator must be sized accordingly to handle the extra electricity generation during non-capture operation (2,9,13).

In the following sections, the model development and verification of a nominal 650 MW NGCC power plant in Aspen Plus® V.8.4 are explained. This power plant is considered as the reference power plant in this thesis. A large-scale PCC plant is designed to capture 90% of the power plant flue gases at the plant full load operation, and the design methodology explained. The large-scale PCC process is also modelled in Aspen Plus® using the verified developed CO_2 capture model described in Chapter 4. Furthermore, the methodology used to simulate a multi-stage compression system in Aspen Plus® applied to compress the produced CO_2 from the stripper pressure to a pressure suitable for transportation and storage, e.g. 15 MPa is explained. Finally, the impact of incorporating a CO_2 capture process into a large-scale NGCC power plant is evaluated at power plant full- and part-load operations in terms of plant net power output and efficiency. The operational impact and considerations at non-capture operation are also addressed.

6.2. Standard NGCC Configuration & Performance Study

This section provides details of a nominal 650 MW NGCC power plant simulation and verification at full load operation and simulations at part load operations, and served as the reference power plant for this thesis. The focus is on the power plant main performance parameters, e.g. plant net power output, plant net efficiency, that will be affected by incorporating a CO_2 capture plant. The power plant simulation was performed in Aspen Plus V.8.4 based on a plant, denoted as DoE-2013-Case#1a in this thesis, originally defined and modelled by DoE/NETL (14) using GT-PRO and THERMOFLEX simulation software (15). Applying GT-PRO for a combined cycle power plant simulations reflects a realistic

performance of existing technologies, and the results can be considered highly reliable at both full-load and part-load operations (16). In the following, the details of the power plant simulation and verification are described in detail.

6.2.1. NGCC Power Plant Model Development

A steady state model of the nominal 650 MW_e NGCC power plant was developed in Aspen Plus® V.8.4, that is comprised of three integrated sub-models: the gas turbine model, the heat recovery steam generator (HRSG) model, and the steam turbine model.

6.2.1.1. Gas Turbine Cycle

The topping cycle is based on two General Electric 7 Frame (GE 7F.05) gas turbines with an ISO output of 211 MW when firing natural gas. Ambient air and natural gas are combined in the dry Low NO_x burner that is operated to control the rotor inlet temperature at 1359 °C. The flue gas exits the turbine at 604 °C and passes into the HRSG (15). Natural gas is the main fuel in the DoE-2013-Case#1a and its composition is presented in Table 6-1.

Table 6-1.Natural gas composition (15)

Component	**Mole fraction (%)**
Methane (CH_4)	93.1
Ethane (C_2H_6)	3.2
Propane (C_3H_8)	0.7
n-Butane (C_4H_{10})	0.4
Carbon Dioxide (CO_2)	1.0
Nitrogen (N_2)	1.6
Fuel LHV (kJ/kg)	47220
Fuel HHV (kJ/kg)	52314

The composition of the incoming air to gas turbine compressors and the exhaust gases at gas turbine outlets is provided in Table 6-2.

Table 6-2. Air and exhaust gas compositions (15)

Components	Air (mole-fraction)	Exhaust gas (mole-fraction)
Ar	0.92	0.89
CO_2	0.03	4.04
H_2O	0.099	8.67
N_2	77.32	74.31
O_2	20.74	12.09

6.2.1.2. Water/Steam Cycle

The bottoming cycle (Rankine cycle) uses a single reheat 16.5 MPa / 566 °C / 566 °C steam cycle. The steam generation section is two identical triple-pressure with reheat HRSGs, each comprises HP, IP and LP steam drums, economisers, super-heaters, and reheat sections. Each HRSG generates steam at three pressure levels, as provided in Table 6-3. The IP steam after the IP superheater is mixed with the hot reheat stream from the reheat section of each HRSG and the combined flow from each HRSG are merged into one main steam line and admitted to the IP cylinder of the steam turbine. The gas turbine exhaust gas exits each HRSG at 88 °C and passes to stacks (15).

Table 6-3. Steam pressure levels of the HRSG section of Doe-2013-Case#1a (15)

Stream	Pressure (MPa)	Temperature (°C)
HP steam	16.5	566
IP steam	2.48	566
Reheat cycle	2.48	566
LP steam	0.34	292

The steam turbine comprises three sections: HP section, IP section, and one double flow LP section. All sections are connected to one generator by a common shaft. Similar to gas turbine generators, the efficiency of the steam turbine generator is 98.6% (15). The low-pressure steam at the LP turbine outlet, exit the turbine downward into the condenser (15).

The combined cycle power plant generates a net output of 634 MW_e at a net plant efficiency of 57.8 % on a LHV basis. The overall plant performance as per DoE's report is summarised in Table 6-4 which includes expected auxiliary power consumptions (14).

Table 6-4. DoE-2013-Case#1a NGCC power plant performance summaries (14)

Parameter	**Value**
Gas turbine gross power output (MW_e)	420.8
Steam turbine gross power output (MW_e)	229.7
Total gross power output (MW_e)	650.5
Total auxiliary power consumptions (MW_e)	16.5
Net plant power output	634
Net plant efficiency based on HHV (%)	51.8
Net plant efficiency based on LHV (%)	57.4
Net plant heat rate based on HHV (kJ/kWh)	6946
Net plant heat rate based on LHV (kJ/kWh)	6269
Fuel consumption (kg/h)	84161

6.2.1.3. Gas Turbine Cycle Simulation Details

Figure 6-1 shows the gas turbine flowsheet developed in Aspen Plus. In the gas turbine cycle, the incoming air enters the combustor after passing through the compressor, and mixes with the fuel, i.e. natural gas before entering the combustion chamber. The combustion by-product gases, i.e. flue gases, at high pressure and temperature enter the turbine and expand up to nearly atmospheric pressure. The net difference between the work generated by the turbine shaft and the work consumed by the compressor is the available work for generating electricity in the generator. As shown in Figure 6-1, Input streams to the gas turbine flowsheet model are the incoming air and the fuel. The data related to these streams are presented in Table 6-5 with the compositions presented in Tables 6-1 and 6-2.

Table 6-5. Input streams for the gas turbine simulation model

Stream	Mass Flow (tonne/h)	Pressure (MPa)	Temperature (°C)
Incoming air	3622.82	0.101	15
Natural gas	84.161	2.76	38

The gas turbine was modelled in Aspen Plus® V.8.4 using the Peng-Robinson equation of state to determine thermodynamic properties of the components and mixtures in the process. The isentropic efficiencies of the turbine and the compressor polytropic efficiency were set to 90% and 85%, respectively (15). The compressor compression ratio was set to 17 (15). The combustion process was modelled based on the minimisation of the Gibbs free energy, representing a phase and chemical equilibrium.

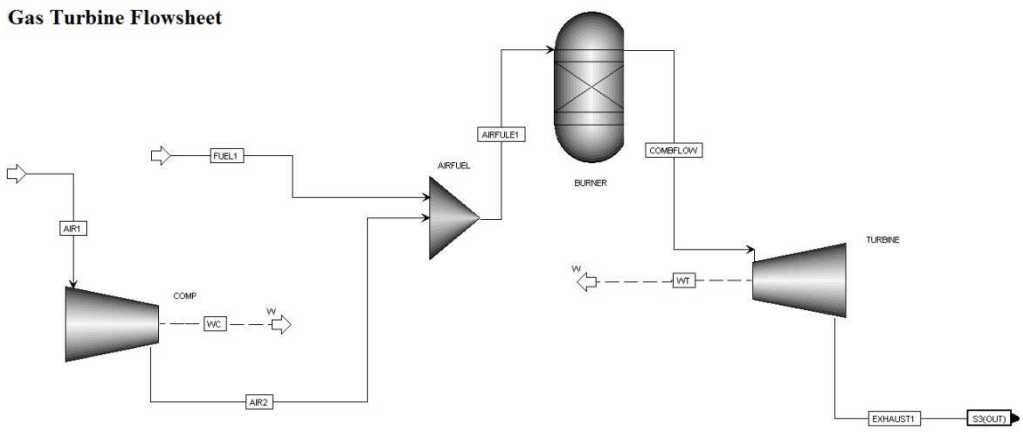

Figure 6-1. The gas turbine flowheet developed in Aspen Plus®

6.2.1.4. Water/Steam Cycle Simulation Details

The water/steam cycle comprises two sub-model simulations: the heat recovery steam generator (HRSG) simulation and the steam turbine simulation, as shown in Figure 6-2, and 6-3, respectively. The hot flue gases at the gas turbine discharge enter the HRSG. HRSG heat exchangers recover the sensible heat of flue gases to produce superheated steam at three different pressure levels. The total condensate stream enters the HRSG cold end and its

temperature is increased by recovering a portion of the flue gas heat. The preheated condensate divides into three streams as high pressure (HP), intermediate pressure (IP) and low pressure (LP) feedwater streams. After being pressurised by feedwater pumps, each stream enters the HRSG to recover a portion of flue gas heat to produce superheated steam. The generated steam at three pressure levels expands through three stages in the steam turbine: at the HP turbine from 16.5 to 2.4 MPa, at the IP turbine from 2.4 to 0.38 MPa, followed by an LP turbine from 0.38 MPa to 4.8 kPa. The LP steam turbine is a condensing steam turbine. The steam from the HP turbine exit returns to the HRSG to gain additional heat from the flue gas, and after combining with the IP generated steam enters the IP section of the steam turbine.

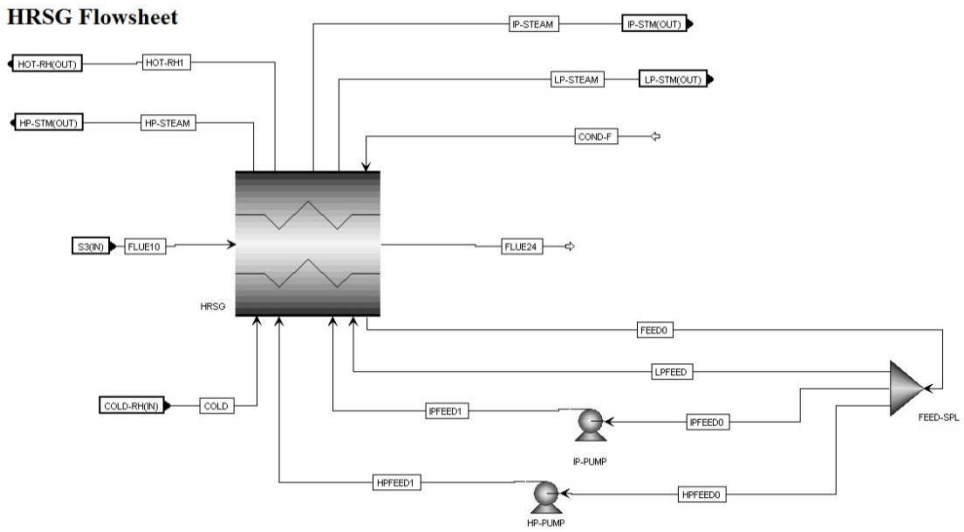

Figure 6-2. The HRSG flowsheet developed in Aspen Plus®

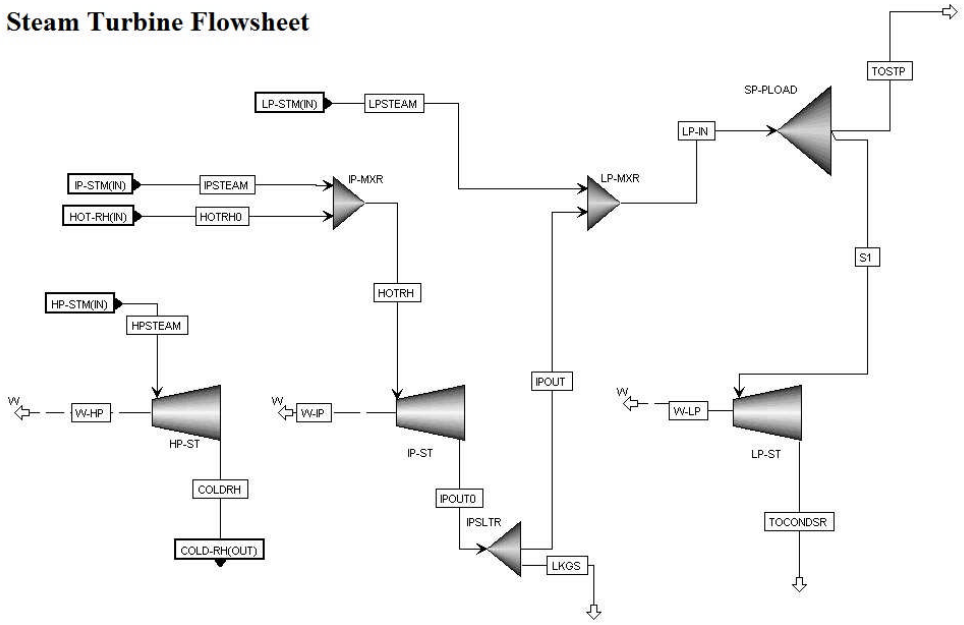

Figure 6-3. The steam turbine flowsheet developed in Aspen Plus®

Input streams to the HRSG flowsheet model are the main condensate stream, the flue gas stream from the gas turbine outlet, the cold reheat stream, and HP, IP and LP feedwater streams. The data related to these streams are presented in Table 6-6. Input streams to the steam turbine flowsheet model are the main HP steam, the hot reheat steam, the IP and the LP steam. These streams are originally the output streams of the HRSG simulation flowsheet from which some drains or miscellaneous streams are deducted to supply steam for the plant internal consumers such as gland steam condenser, seal steam, etc.

The HRSG section was modelled as a multi-stream heat exchanger, and the steam cycle is modelled in Aspen Plus® V.8.4 using steam table, i.e. STEAM-TA, property package. The STEAM-TA property package model is applicable for pure water and steam streams with temperature ranges of 273.15 K to 1073 K, with the maximum pressure of 1000 bar. This method is the default property method for the free-water phase, when free-water calculations are performed. For process calculations, the accuracy of this method is adequate (17). The isentropic efficiency of the HP, IP and LP steam turbine were set as 88.03, 92.37, and 93.67 %, respectively (15).

Table 6-6. Input streams of the HRSG simulation model

Stream	Mass Flow (tonne/h)	Temperature (°C)	Pressure (MPa)
Total condensate at HRSG inlet	579.52	32.7	0.4
LP feedwater	74.48	141.7	0.38
IP feedwater	103.02	227.8	2.80
HP feedwater	402.02	352.4	17.50
Cold reheat	385.37	310.6	2.74
Exhasut Gas from the GT outlet	3706.92	603.3	0.105

6.2.2. NGCC Power Plant Model Verification

The NGCC power plant was simulated at full load in Aspen Plus® V.8.4 as described above. In the Gas turbine cycle, the simulated gross power output of two gas turbines and the power consumed by the two air compressors are 857.21 and 430.55 MW, respectively. By taking into account the efficiency of the gas turbine generators as 98.6 % as specified in the DoE report (15), the simulated gas turbine cycle gross power output is 420.7 MW_e. For the steam turbine section, the simulated work output of HP, IP and LP steam turbine are 49.96, 79.67, and 102.14 MW, respectively, providing a total work output of 231.78 MW for the steam turbine section. By considering the efficiency of the steam turbine generator as 98.6 % as specified in the DoE report (15), the simulated steam turbine gross power output is 228.5 MW_e. Comparing the simulation results against data provided by the DoE shows an excellent agreement, the maximum deviation from the DoE data was less than 1%. Table 6-7 presents the comparison of the plant key performance parameters of the simulation model against those of the DoE-2013-Case#1a.

Table 6-7. Plant performance summary of the simulation model vs. DoE-2013-Case#1a

Key Performance Parameter	DoE data	Simulation results	Deviation (%)
Gas Turbine Gross Power	420.8	420.7	0.02
Steam Turbine Gross Power	229.7	228.5	0.52
Total Gross Power (MW_e)	650.5	649.2	0.20
Total Auxiliary power consumption (MW_e)	16.5	16.5	N.A.
Total Net Power (MW_e)	634	632.7	0.21
Net Plant Efficiency based on LHV (%)	57.4	57.31	0.16
Net Plant Heat Rate based on LHV (kJ/kWh)	6269	6281.2	0.19

6.2.3. NGCC Power Plant Simulation at Part Loads

The part load simulations of the Doe-2013-Case#1a for 90, 80, 70 and 60 % of the GT full load were performed in GT-PRO V.21 and then replicated in Aspen Plus V.8.4. To reduce the GT load in a combined cycle arrangement, the fuel and air mass flows must be simultaneously decreased while maintaining a high turbine exit temperature to ensure high steam cycle efficiency. Reduction in the gas turbine load leads to the reduction of pressures and mass flow rates in the water/steam cycle. The preferred method to control a combined cycle at part loads down to 50% is the sliding pressure control mode. This method ensures good utilisation of the exhaust energy and therefore relatively higher efficiency at part loads. Below 50% load, the live steam pressure should be held constant by means of a number of steam turbine inlet valves that introduce considerable throttling losses and thus higher stack losses (18). In these, the NGCC part loads were designed based on purely sliding pressure operation. Table 6-8 summarises the full and part load results of the reference power plant at ISO condition based on the Aspen Plus simulation. As mentioned earlier, the power plant part loads are defined according to the gas turbine load varying from 100% to 60%.

Table 6-8. Full and part load simulation of the reference NGCC power plant

GT load (%)	**100**	**90**	**80**	**70**	**60**
GTs output (MW_e)	420.80	380.80	339.60	298.00	256.40
ST output (MW_e)	229.7	224.1	215.4	206.5	195.7
Gross plant power output (MW_e)	650.5	604.9	555.0	504.5	452.1
Auxiliary power consumption (MW_e)	16.5	16.5	16.3	16	15.8
Net plant power output (MW_e)	634	588.4	538.7	488.5	436.3
Net power plant electrical efficiency (%)	57.4	56.75	55.84	54.86	53.67
Flue gas flow rate (tonne/h)	3706.82	3481.80	3313.52	3021.30	2783.88
Flue gas flow relative to full-load case (%)	100	93.93	89.40	81.50	75.10
N_2	74.39	74.4	74.41	74.43	74.45
O_2	12.37	12.39	12.43	12.48	12.55
CO_2	3.905	3.896	3.88	3.856	3.822
H_2O	8.434	8.417	8.386	8.34	8.275
Ar	0.895	0.895	0.895	0.895	0.895
Total steam flow to LP turbine (tonne/h)	579.54	558.96	532.35	507.20	480.12

These data will be used to assess the performance of a large-scale CO_2 capture plant designed to capture 90% of the power plant flue gases. The details of the CO_2 capture plant design and its performance evaluation at power plant full and part loads are described in following sections.

6.3. Post Combustion CO_2 Capture (PCC) Process Design

The process description of the MEA-based post combustion CO_2 Capture (PCC) was provided in Chapter 3, Section 3.1. Absorption and stripping processes are usually carried out in vertical, cylindrical columns in which devices such as plates or packing materials are placed. The gas and liquid streams normally flow counter-currently and the devices, e.g. packing elements, serve to provide the contacting and development of interfacial surface through which mass transfer takes place (19).

The design procedure of absorber and stripper columns is a combination of chemical engineering science and successful past practiced experiences. The column packed diameter for a defined liquid and gas flow rates is usually determined based on two criteria:, first, the pressure drop characteristics of the packing material, i.e. the maximum pressure drop that the packing is capable of handling, and second, the approach to maximum capacity prior experiencing flooding phenomena in the packing material. The fractional approach to flooding depends on the packing material and is usually in the range of 70 to 85 % of the flooding point velocity (20,21). The packed column height is determined with respect to the degree of separation, i.e. CO_2 removal rate for the application in hand, which involves the calculation of mass-transfer parameters such as heights of transfer units (HTU) or the height equivalent to a theoretical plate (HETP), which the latter method is the preferred approach.

6.3.1. Packed Column Diameter Calculations

Flooding normally represents the maximum capacity condition for packed column, and determines the minimum possible diameter of the packed column (19). Usually the cross sectional of packed column are designed to accommodate gas velocities for 60 to 80 % of the flooding point velocity (19). This range varies with the type of packing used in the column. For instance, for structured packing this range is between 70 to 80 % of the flooding point velocity (20,21)). Eq. 6-1 represents the relationship between the column diameter and the gas stream superficial velocity as:

$$D = \sqrt{\frac{4G}{\pi U_s}} \qquad (6\text{-}1)$$

Where D is the column diameter, G is the gas mass flow rate, and U_s is the gas stream superficial velocity. The superficial velocity is related to the column packing capacity factor as expressed in Eq. 6-2 as (19-20):

$$C_s = U_s \left[\frac{\rho_G}{(\rho_L - \rho_G)}\right]^{1/2} F_P^{1/2} v^{1/2} \quad (6\text{-}2)$$

Where, C_s is the capacity factor, ρ_G and ρ_L are gas and liquid densities, respectively, F_p is the packing factor, and v is the kinetic viscosity of liquid. The capacity factor of packed columns is a function of the flow parameter (F_{LG}) and the pressure drop per unit of height of packing (ΔP). The flow parameter is defined as (19):

$$F_{LG} = \frac{L}{G}\left(\rho_G / \rho_L\right)^{1/2} \quad (6\text{-}3)$$

Where, L is the liquid mass flow rate.

The packing factor (F_p) is empirically determined for each packing and is provided by the vendor. The Pressure drop is usually determined based on the generalised pressure drop correlation (GPDC) curves/charts that are vendor-specific for each type of packing. GPDC charts of a number of popular packing types, including those have been used in this thesis, are available in Aspen Plus® simulation software, which were used for columns diameter sizing and pressure drop calculations.

6.3.2. Packed Column Height Calculations

Packed column height calculation normally involves determination of the number of theoretical equilibrium stages or plates N. Therefore, when packed columns are used in distillation or dilute-gas absorption and stripping systems, it is a common practice to rate efficiency of the column packing in terms of the height of packing equivalent to the one theoretical plate (HETP) (19, 22,23). The HETP of packed column for a stage j (of N identical stages) is expressed as (19):

$$HETP_j = \frac{\ln \lambda_j}{\lambda_j - 1}\left(HTU_{G,j} + \lambda_j HTU_{L,j}\right) \quad (6\text{-}4)$$

Where, λ_j is the stripping factor for stage j, $HTU_{G,j}$ is the height of transfer units for the gas phase, and $HTU_{L,j}$ is the height of transfer units for the liquid phase. These three parameters are defined as (19):

$$\lambda_j = \frac{m_j G_j}{L_j} \tag{6-5}$$

$$HTU_{G,j} = \frac{u_{G,s}}{k_{G,j} a_{e,j}} \tag{6-6}$$

$$HTU_{L,j} = \frac{u_{L,s}}{k_{L,j} a_{e,j}} \tag{6-7}$$

Where, m_j is the local slope of the equilibrium line for stage j, G_j and L_j are local flow rates of gas and liquid streams in stage j, respectively, $u_{G,s}$ and $u_{L,s}$ are the superficial velocities of gas and liquid phases, respectively. $k_{G,j}$ and $k_{L,j}$ are the local mass transfer coefficient for gas and liquid phases, respectively, and $a_{e,j}$ is the effective interfacial area per unit volume of the packed section in stage j. the total packed height required for a certain degree of separation is the summation of HTEP of N stages comprising the column packed height. The total column packed height of absorber and stripping column with N identical theoretical stages are determined as (19):

$$Z_{Absorber} = \sum_{j=1}^{N} HTEP_j \tag{6-8}$$

$$Z_{Stripper} = \sum_{j=1}^{N} HTEP_j \tag{6-9}$$

6.3.3. Large Scale CO_2 Capture Plant Design

The developed CO_2 absorption/desorption model described in Chapter 4, that was verified using the comprehensive pilot plant results, published by Notz et al. (24), using Sulzer Mellapak 250Y structured packing, was used to simulate a large scale CO_2 capture process suitable to capture 90% CO_2 of the aforementioned NGCC flue gas at full load. Figure 6-4 provides a schematic overview of the integrated NGCC-PCC plant with a CO_2 compression unit. In this figure, the CO_2 capture plant is outlined by the dashed rectangular box.

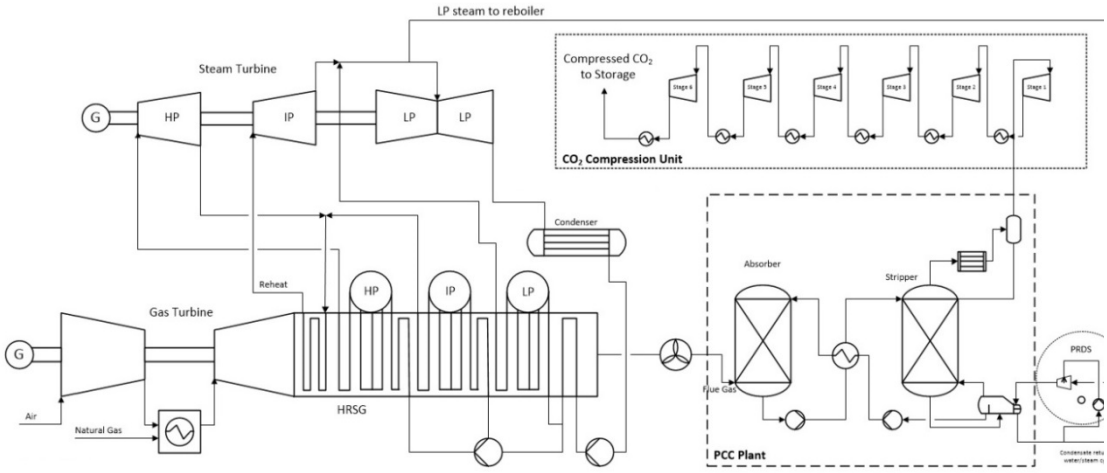

Figure 6-4. Schematic overview of a NGCC-PCC plant including CO_2 compression unit

Based on the knowledge gained from several studies on large-scale post-combustion CO_2 capture plants (25-28), and chemical engineering principles as described above (29-31), the process configuration, equipment sizes and energy requirement of the large-scale PCC with 90% CO_2 removal rate were determined. The capture plant was designed under the assumption that the NGCC flue gas is free from NO_x and SO_2. An aqueous solution of 30 wt. % MEA was used as the solvent with the lean loading of 0.21 based on the energy performance study explained in Chapter 5. The absorber operating pressure is atmospheric and the stripper operating pressure was set as 180 kPa based on the energy performance study explained in Chapter 5. The rich CO_2 loading was determined using Aspen Plus based on the optimum absorber packed column height when using the optimum liquid to gas ratio.

The optimum liquid to gas ratio, based on mass, required to provide 90% capture rate at the design load was determined using the following formula (27):

$$F_{\mathrm{Lean}} = \frac{F_{\mathrm{FG}} x_{\mathrm{CO_2}} \varphi_{\mathrm{CO_2}}}{100 z(\alpha_{\mathrm{rich}} - \alpha_{\mathrm{lean}})} \left(\frac{M_{\mathrm{MEA}}}{44.009} \left[1 + \frac{1 - \omega_{\mathrm{MEA}}}{\omega_{\mathrm{MEA}}} \right] + z.\alpha_{\mathrm{Lean}} \right) \quad (6\text{-}10)$$

Where, F_{Lean} is the mass flow rate of the lean solvent, F_{FG} is the mass flow rate of the flue gas, $x_{CO_2}$is the mass fraction of CO_2 in the flue gas, $\varphi_{CO_2}$is the percentage of CO_2 in the flue gas that is recovered, M_{MEA} is the molar mass of MEA, α_{rich} and $\alpha_{lean}$are the lean and the rich solvent CO_2 loading, respectively, $\omega_{MEA}$is the mass fraction of the MEA in the unloaded solution, and z is the number of equivalents per mole of the amine (z is 1 for MEA).

To design the PCC plant suitable for the 650 NGCC plant, two absorber and two stripper columns were considered (one absorber and one stripper per gas turbine). As explained earlier, the design principle to determine the diameter was based on the flooding limitations and the highest economical pressure drop to ensure a stable operating condition with proper liquid and gas distributions. Recommended pressure drop for packed columns ranges from 147 to 490 Pa (15 to 50 millimetres water) per meter packing (31). Besides, the gas load corresponding to the maximum operating capacity should in general be 5 to 10% below the flooding point (32). In addition to the liquid and gas flow properties, the latter parameter is sensitive to the type of packing (32). To ensure a reliable operation, the diameter of the absorber column was then fine-tuned to ensure a 70-75% approach to flooding for the Sulzer Mellapak 250Y packing. This value also corresponds to that of the pilot scale validated model. A similar method was applied for the stripper column. Table 6-9 summarises the geometrical details of the Sulzer Mellapak 250Y packing.

Table 6-9. Geometrical details of columns packing (29,33)

Packing Geometry	**Sulzer Mellapak 250Y**
Specific surface area (m^2/m^3)	256
Void fraction (%)	98.7
Packing factor (m^{-1})	66
Side dimension corrugation (m)	0.0171
Corrugation angle (°)	45
Crimp height (m)	0.012

In general, columns with very large diameters are not recommended. To date, the maximum diameter for an absorber column under operation is 18.2 m (60 ft) reported by Reddy et al. (34). The absorber diameter was calculated to be 15 m. Table 6-10 summarises key design parameters of a large-scale CO_2 capture process to remove 90% CO_2 of the 650 MW NGCC power plant flue gases.

Table 6-10. Design specification of the large-scale PCC process

Parameter	**Value**
Number of Absorber columns	2
Packing material	Sulzer Mellapak 250Y
Absorber column diameter (m)	15
Absorber column height (m)	20
Absorbent	MEA
Absorbent concentration (wt. %)	30
Absorber column pressure (top stage) (kPa)	101.6
Treated gas temperature at absorber exit (◦C)	35
Lean solvent temperature at absorber inlet (◦C)	40
Flue gas temperature at absorber inlet (◦C)	40
Flue gas pressure at absorber inlet (kPa)	113.8
Number of Stripper columns	2
Packing material	Sulzer Mellapak 250Y
Stripper column diameter (m)	9
Stripper column height (m)	20
Stripper column pressure (top stage) (kPa)	180
Stripper condenser temperature (◦C)	35
Lean/rich cross heat exchanger approach temperature (°C)	5

6.3.4. Large Scale CO_2 Capture Performance at NGCC Part Loads

Details of the PCC process simulation at the NGCC flue load were explained above, and its design parameters were summarised in Table 6-10. Steady state simulations of the PCC performance at the power plant part loads were obtained using the respective flue gas characteristics specified in Table 6-8. For all load cases, the flue gas is assumed to be cooled down to 40°C prior to entering the absorber column. At part loads, the liquid to gas ratios were adjusted to maintain the CO_2 capture rate at 90%. The details of the PCC simulation at part loads are provided in Table 6-11, and the PCC process at full load is also summarised in this table for comparison.

Table 6-11. PCC process simulation at full and part load operations

GT load (%)	**100**	**90**	**80**	**70**	**60**
CO_2 capture efficiency (%)	90	90	90	90	90
CO_2 captured (tonne/h)	2x103.17	2x96.60	2x91.35	2x82.80	2x75.63
Liquid to gas mass ratio	1.00	0.985	0.980	0.972	0.963
Lean solvent CO_2 loading	0.21	0.21	0.21	0.21	0.21
Rich solvent CO_2 loading	0.4761	0.4764	0.4766	0.4770	0.4773
Absorber fraction to flooding (%)	0.73	0.69	0.65	0.59	0.54
Absorber average pressure drop (Pa/m)	221.6	189.3	169.7	140.2	118.7
Stripper fraction to flooding (%)	0.33	0.31	0.30	0.27	0.24
Stripper liquid hold-up (m^3)	3.71	3.60	3.52	3.37	3.24
Reboiler energy requirement (MW_{th})	104.6	97.8	93.0	85.2	77.6
Specific reboiler duty (MJ/kg CO_2)	3.64	3.65	3.66	3.70	3.70
Solvent temperature at stripper discharge (°C)	117.4	117.4	117.4	117.4	117.4

6.3.4.1. Steam Requirements for Solvent Regeneration

The main thermodynamic interface between the NGCC and PCC is the large amount of steam to be used for solvent regeneration. The steam is extracted from the IP/LP crossover pipe as there the steam is available at a pressure close to that required at the reboiler (12,35-37). A 10°C approach temperature is assumed in the reboiler to ensure reliable operation and avoid polymerisation of carbamate ions, i.e. thermal degradation of the solvent. Provided an

equilibrium solvent temperature of 117.2°C at the bottom of the stripper in all load cases, as presented in Table 6-11, a saturated steam at 250 kPa is constantly required in the reboiler. By assuming 10% pressure losses in the branch pipe passage from the crossover pipe to the reboiler inlet, the minimum pressure required at the extraction point is calculated to be 275 kPa, provided the stripper pressure at all load cases is kept constant. The extracted steam is assumed to be routed to the reboiler section via a combined pressure reducing with de-superheating system (PRDS). The water required for de-superheating is provided by recycling a portion of condensate from the reboiler outlet on the hot side. This integration is defined by a dotted circle in Figure 6-4. This method has two benefits, first, by recycling a portion of the condensate at the temperature close to the steam saturation temperature, the sensible heat required to heat up the de-superheating water is minimised; second, a portion of the required steam is complimented by the evaporation of the condensate in the de-superheater, resulting in less steam to be extracted. Calculations revealed that approximately 13% of the steam required in the reboiler is provided by the evaporation of the recycled condensate. For all load cases, the extracted steam flow rate and parameters associated with the PRDS are provided in Table 6-12.

Table 6-12. PCC steam requirements for solvent regeneration at full and part loads

GT load (%)	**100**	**90**	**80**	**70**	**60**
Total steam required in both reboilers (kg/h)	345.2	322.8	306.9	281.2	256.3
Steam pressure at reboiler (kPa)	250	250	250	250	250
Steam temperature at reboiler inlet (°C)	127.4	127.4	127.4	127.4	127.4
Total extracted steam (kg/h)	301.2	281.2	268.1	246.3	224.1
Steam pressure at extraction point (kPa)	337	323	310	295	279
Steam temperature at extraction point (°C)	284.80	286.60	283.10	279.30	282.80
Condensate required for de-superheating (kg/h)	44	41.6	38.8	34.9	32.2

6.3.4.2. PCC Auxiliary Consumption

The auxiliary consumption includes the electricity required to run the solvent circulating pump, make-up pumps, cooling water pumps, flue gas blowers and any other rotary

equipment involved in the process, with the flue gas blowers as the major consumer. Table 6-13 provides the PCC electricity consumption at various loads.

Table 6-13. CO_2 compression unit electricity consumption at full and part loads

GT load (%)	**100**	**90**	**80**	**70**	**60**
PCC auxiliary power consumption (MWe)	15.9	15.3	14.5	14.1	13.3

6.4. CO_2 Compression Unit

The produced CO_2 with high purity, i.e. > 98 mol. % CO_2, is expected to be compressed to 11 to 15 MPa to be transported for storage (1,38). This is achieved by means of a multi-stage compression train with intermediate cooling, and then followed by a pump as a final step to deliver the CO_2 product in liquid phase for storage (1).

It is confirmed that the compression process does not add a specific constraint on the integrated plant capabilities to operate flexibly and change loads, as the compressors ramp rates, depending on their types, vary in the order of a few seconds (1). However, similar to the GT main air compressors, at low loads, i.e. less than 70% of the design load, a portion of the compressed CO_2 must be recycled to maintain the unit operability at the expense of higher auxiliary electricity consumption.

CO_2 compression consumes a great amount of electricity to operate, that needs to be supplied by the power plant (39). To calculate the CO_2 compression auxiliary power consumption, a six-stage centrifugal compression unit with intermediate coolers was modelled in Aspen Plus V8.4. Figure 6-5 shows the simulation flowsheet developed in Aspen Plus®.

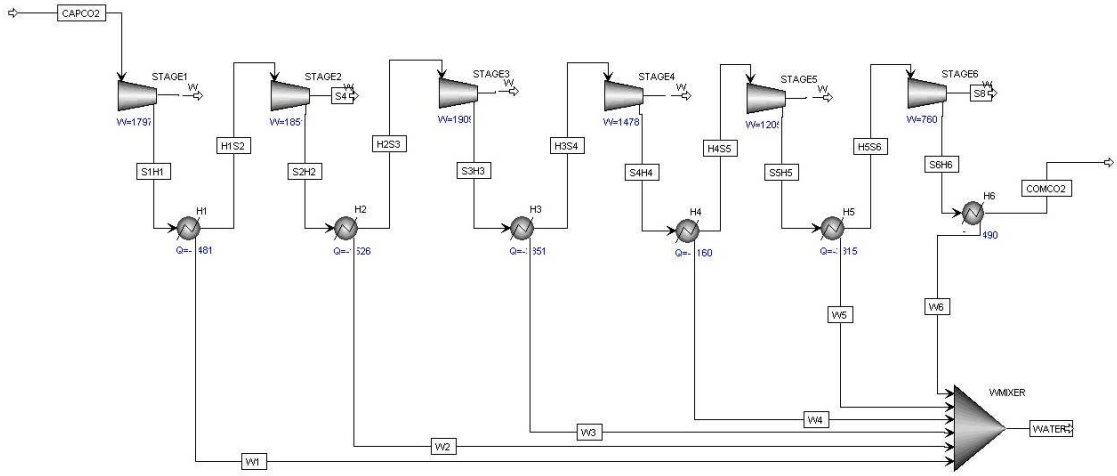

Figure 6-5. The CO_2 compression unit flowsheet in Aspen Plus®

The validity of the CO_2 compression model was ensured by comparing its results with data available in the public domain (14). The compression train is outlined in Figure 6-4 by a dotted rectangular shape. Table 6-14 summarises the auxiliary power consumption of the CO_2 compression unit at various loads.

Table 6-14. Energy requirements of the CO_2 compression unit at plant full and part load operations

GT load (%)	**100**	**90**	**80**	**70**	**60**
CO_2 compression electricity consumption (MWe)	18	16.9	15.8	14.5	13.2

6.5. Integrated NGCC-PCC Performance at Part Loads

Table 6-15 provides the performance details of the NGCC plant integrated with the PCC at part loads evaluated by taking into account the data from CO_2 capture and CO_2 compression units as described above.

Table 6-15. Design and off-design loads of the NGCC power plant with CO_2 capture plant

GT load (%)	**100**	**90**	**80**	**70**	**60**
GTs output (MW_e)	420.80	380.80	339.60	298.00	256.40
ST output (MW_e)	184.7	180.0	173.4	168.2	160.7
Gross plant power output (MW_e)	605.5	560.8	513.0	466.2	417.1
Auxiliary power consumption (MW_e) (Inc. power plant + capture plant + compression plant)	52.4	50.3	48.0	45.9	43.4
Net power plant power output (MW_e)	553.1	510.5	465	420.3	373.7
Total power loss due to PCC integration (MW_e)	79	76.3	72.3	66.9	61.5
Net Plant Thermal efficiency (%)	50.10	49.37	48.33	47.33	46.1
Efficiency penalty (%-point)	7.15	7.38	7.52	7.54	7.59

6.6. PCC Performance Evaluation at NGCC Full & Part Load Operations

In this section the PCC performance in terms of overall energy consumption and solvent circulation rate at the power plant part loads are evaluated and compared with those at the power plant full load operations. In addition, the hydraulics of the absorber and stripper columns in terms of pressure drop, packing wettability and mass transfer efficiency are explored.

6.6.1. Specific Energy Requirement

The specific energy requirement for solvent regeneration at various NGCC operational loads were calculated using simulation results as presented in Table 6-11. At each load, the liquid to gas ratio was adjusted to maintain the CO_2 capture efficiency at 90%, resulting in reducing the liquid to gas ratio to nearly 0.96 at the GT 60% load from its value of 1.00 at the full load. The reduction in the flue gas and circulating solvent flow rates at part loads results in lower auxiliary power consumption. This effect is more pronounced at the GT 60% load where the auxiliary power consumption reduced by nearly 18% compared to the full load operation. However, the specific energy required for solvent regeneration does not follow the same trend at part loads. Although the energy required in the reboiler in general decreases, the reboiler specific energy increases. This is partly due to the change in the liquid to gas

ratio from its design value, and partly because of the increased rich solvent CO_2 loading at part loads. The rich solvent CO_2 loadings at part loads were also provided in Table 6-11. Despite a counter-intuitive behaviour that might have been expected due to the relatively lower CO_2 composition in the flue gas at part loads, the slight increase in the solvent CO_2 loading at the end of the absorption process might be due to the improved efficiency in the absorber column. The improved efficiency in the absorber simulation is because of relatively smaller HETP at lower loads. As Table 6-16 presents, the average HETP of the absorber column at the GT 60% load is reduced by 5.6% compared to that of the GT full load.

Table 6-16. Variation of the absorber column HETP with NGCC load variations

GT load (%)	**100**	**90**	**80**	**70**	**60**
Absorber column average HETP (m)	0.420	0.414	0.410	0.402	0.396

In general, for structured packing such as Sulzer Mellapak 250Y, HETP increases with liquid and vapour loadings, and the load effect on the HETP is more due to liquid rather than vapour loads (30). Furthermore, at higher liquid flow rates, more gas is entrained down the bed, causing the mass transfer efficiency to drop. Due to the structural characteristics of structured packing that limit lateral movement of fluids, at higher gas flow rates, more gas will be carried downstream, which is unfavourable for the column efficiency (30,40). At part loads, the flue gas and circulating solvent flow rates are simultaneously reduced, whilst the liquid load reduction is more pronounced to maintain the CO_2 capture rate at 90%. This might be a reason for the improved efficiency, i.e. lower HETP, and hence higher CO_2 rich loading at lower GT loads. All above statements are valid under the assumption that the absorber packed column is evenly wet and uniformly distributed at all loads.

For a given lean solvent CO_2 loading, higher rich solvent CO_2 loading means more energy is required for solvent regeneration. Despite the lean CO_2 loading being a fixed design parameter at all loads, the rich CO_2 loading increased at part loads. To retain the lean CO_2

loading at the bottom of stripper column, therefore more specific energy was consumed in the reboiler.

6.6.2. Column Hydraulics

The reduction in the flue gas mass flow rate is the major challenge that a CO_2 capture plant experiences at power plant part loads, as this is a crucial design value for the PCC. The hydraulics of the absorber and stripper columns should therefore be suitable to withstand various operational conditions. To examine the operability of the PCC at part loads, a number of operational parameters were considered for detailed evaluation.

6.6.2.1. Liquid Distribution

The process design of the PCC is at the NGCC full-load operation, this means that the CO_2 capture plant is designed for the highest possible flue gas and circulating solvent flow rates. As described previously, sizing of packed columns at their design points was achieved by maintaining the column fractional approach to flooding at a reasonable level of 70-75%. Therefore, the risk of flooding in the columns at part loads is not a concern, whereas the risk of poor irrigation, and uneven flow distribution (maldistribution) and hence dry patch formation is more prominent.

Uneven flow distribution affects the packed column efficiency (30). It occurs when the liquid and/or vapour flows are low and when less liquid is delivered to some areas than to others, causing a drop in mass transfer (30,41). For an absorber to operate properly, the lean solvent flow rate entering the column must be high enough to effectively wet the packing to facilitate the mass transfer between the gas and liquid streams (42). The minimum superficial liquid flow rate ($L_{\mathrm{sfr}_{\mathrm{min}}}$) that is required to wet the packing effectively is calculated using the following equation (42):

$$L_{\mathrm{sfr}_{\mathrm{min}}} = MWR.\rho_{\mathrm{L}}.\alpha \qquad (6\text{-}11)$$

Where, *MWR* is the minimum wetting rate of the absorber packing, ρ_{L} is the solvent density entering the absorber column, and α is the surface area to volume ratio of the absorber packing. The superficial liquid flow rate at each load case ($L_{\mathrm{sfr}_{\mathrm{load}}}$) is calculated using the following equation (42):

$$L_{\mathrm{sfr}_{\mathrm{load}}} = \frac{L_{\mathrm{mol}_{\mathrm{load}}} . M_{\mathrm{MEA}}}{A_{\mathrm{Abs}}} \tag{6-12}$$

Where, $L_{\mathrm{mol}_{\mathrm{load}}}$ is the molar flow rate of the lean solvent at various GT loads, M_{MEA} is the solvent molecular weight, and A_{Abs} is the absorber column cross sectional area. Figure 6-6 shows the variation of the absorber column superficial value at various loads and their comparison with the minimum value.

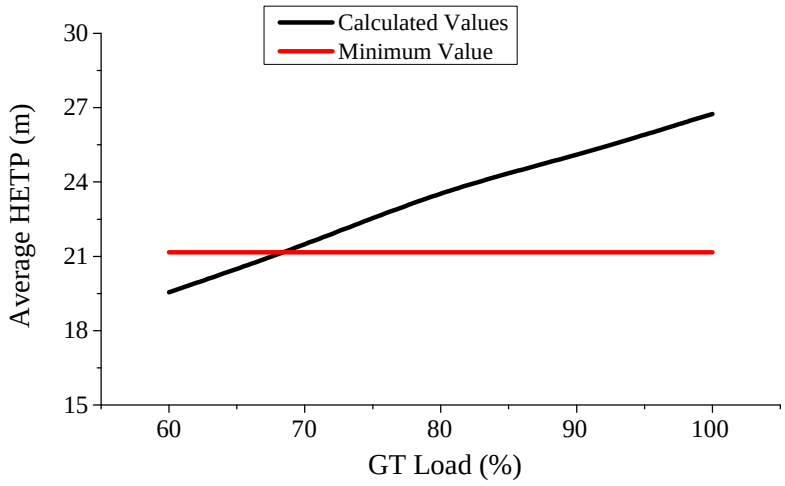

Figure 6-6. Absorber column liquid superficial value at various GT loads in comparison with its minimum value

The comparison confirmed there is sufficient liquid flow to wet the packing using the current design conditions up to 70% of the GT load, whilst the absorber operation at GT 60% load is at the risk of under wetting. One solution to mitigate this risk is to increase the lean solvent flow rate to meet the minimum requirement. Calculations showed that the lean solvent mass flow rate must increase by approximately 6% to maintain the minimum liquid load in the absorber column at the GT 60% load. To maintain the CO_2 capture rate at 90%, a solution is

for the lean solvent CO_2 loading at this particular case to increase to 0.23 from the design value of 0.21.

6.6.2.2. Vapour Distribution

Reduction in the flue gas flow rate at part loads results in the reduction in its velocity through the packed bed which will promote the risk of uneven vapour distribution in the absorber column. In general, the packing pressure drop places a resistance in the flue gas path that helps spread the vapour radially. If the pressure drop is too low, the flue gas will tend to channel through the bed, leading to poor mass transfer (30). There is a common practice to design a packed column for a pressure drop not smaller than 15 mm of water per meter of packing height. When there is a likelihood of foaming, this value must be reduced (31). Simulations showed that the pressure drop of the absorber packed column is in the range of 22 to 12 mm of water per meter of packing, where the lowest pressure drop corresponds to the 60% GT load. The packing material used in the absorber is the sulzer Mellapak 250Y which is categorised as a low-pressure gauze packing with a very low operational pressure drop (33). Thus, the uneven vapour distribution in the absorber column at the 60% GT load is less likely to be a risk with the applied packing material.

6.6.2.3. Column Operability

There is a reliable region for packed columns to operate at variable liquid and gas flow rates. Kister (30) defined an operational curve for packed columns and suggested that for a reliable operation at various liquid and gas flow rates, the absorber and stripper column efficiencies must be independent of gas and liquid flow rates, while the column pressure drop uniformly increases with gas flow rate. Thus, for absorber and stripper columns to cope with power plant part loads, their efficiencies should not vary with load changes. To verify this, the efficiency characteristic curves of the absorber and stripper columns operating at various loads is plotted and shown in Figure 6-7. The vertical axis is the average HETP of the column as the efficiency representative, and the horizontal axis is the GT load. As

shown, the HTEP demonstrates a constant trend at various loads, confirming that both absorber and stripper columns operate reliably at part loads down to 60% GT load.

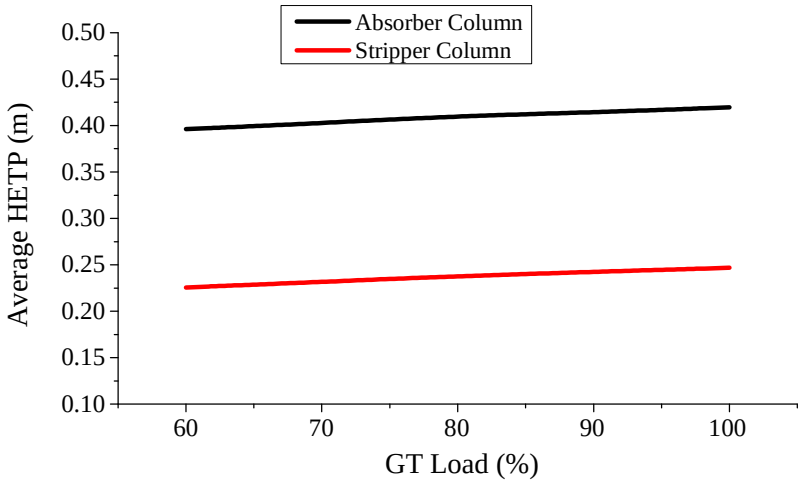

Figure 6-7. Absorber and stripper columns average HETP at various GT loads

There are other parameters that may be studied to confirm a reliable operation of PCC plants at part loads that are beyond the scope of this study. for example, the higher oxygen content in the flue gas at part loads has a potentially negative impact on the solvent degradation rate and the unit operation. it is therefore worthwhile to study and seek alternative inhibitors to protect the unit against likely corrosion and degradation risks at part loads where O_2 content in flue gas increases (1).

6.7. Integrated NGCC Performance Evaluations at Part Loads

In the second part, the impact of the PCC integration on the NGCC at part loads in terms of the net power output and net efficiency penalty were presented. In addition, the impact of the integration on the steam turbine at part loads was described. Finally, the drawbacks of the non-capture operation on the performance of the integrated NGCC especially on the steam turbine were investigated.

6.7.1. NGCC Net Plant Efficiency

Based on the simulation results of the NGCC at part loads while integrated with the PCC, the net plant efficiency of the integrated NGCC-PCC plant and the associated efficiency penalty were calculated at full and part loads and presented in Table 6-17. As expected, the net plant efficiency of the reference NGCC at part loads drops by 2-3% points (1) as a result of operating the equipment at loads different from their design point.

Table 6-17. NGCC net plant efficiency at various GT loads when integrated with the PCC

Net plant efficiency	**GT Load (%)**				
	100	**90**	**80**	**70**	**60**
Reference NGCC (%)	57.4	56.75	55.84	54.86	53.67
NGCC+PCC (%)	50.25	49.37	48.33	47.33	46.09
Efficiency penalty (%-point)	7.15	7.38	7.51	7.53	7.58

The efficiency penalty associated with the integration of the PCC and NGCC increases by reducing the GT load, which is due to inefficiencies associated with the CO_2 desorption in the stripper column. Also, for the NGCC-PCC plant, the reduction of the steam turbine efficiency is more pronounced at lower loads. In fact, the significantly light-load operation of the steam turbine at part loads promotes the rate of the efficiency drop. In this study, the efficiency of the CO_2 compression unit was assumed constant for all load cases. In practice, compressor efficiency will reduce with reducing the load which will have an additional impact on their auxiliary power consumption, and thus on the net plant efficiency and the efficiency penalty.

6.7.2. Steam Turbine Performance

By studying the LP steam pressure at the IP/LP crossover pipe presented in Table 6-12, it is evident that the pressure requirement of the steam to be extracted can be met for all load cases. In addition, the evaluations confirmed that the throttling loss associated with the steam extraction is minimal as the pressure of steam in the IP/LP pipe is close to that required in

the reboiler. To reach a part-load capability below 60% GT load, a higher design crossover pipe pressure would be required. For example, in a study performed by Pffaf et al. (13) on a greenfield coal power plant, a design pressure of 700 kPa was suggested for the crossover pipe if part-load capability of 40% is required. A reduction of 50 kPa on the design pressure of IP/LP crossover pipe results in nearly 0.2% point gain in the plant net efficiency at the expense of restricted part-load operation (13). Therefore, it is useful to identify an efficient part-load limit with IP/LP pressure evaluations. In this work, the efficient part-load limit is around 60% as the crossover pressure at this load rate has a marginal difference with the minimal required pressure at the interface point.

6.7.3. Impact of Non-Capture Operation

NGCC plants equipped with PCC should be designed to operate with variable steam extraction rates, possibly down to zero, to adjust both desired CO_2 capture efficiency and power output whenever required. There are conditions in which it is economically beneficial to operate without PCC, for example at times of high electricity demand. Also, there are conditions where operation without CO_2 capture is inevitable, for example during an interruption in the operation of the PCC or the CO_2 compression unit. In either case, the steam which is otherwise used for the solvent regeneration must be utilised in the LP turbine to generate electricity. This means that nearly double the amount of steam is available to enter to the LP turbine cylinder at power plant full load operation. This will have a considerable impact on the performance of the steam turbine in general and on the LP and IP turbines and the cold end in particular.

In coal power plants, the impact of variable steam flow rates through the LP turbine is manageable via using a synchronous self-shifting (SSS) clutch that entirely disconnects one of the LP steam turbines depending on the heat required in the PCC plant (43). While in NGCC plants, usually only one double-flow LP steam turbine is used and therefore there is no flexibility in terms of possibility to shut down an LP turbine (43).

It is worth to note that the design of LP steam turbines capable of operating under large variations of steam flow is a not a new technology, and examples of such turbines can be found in combined heat and power (CHP) plants (42,44). To shed light on the requirements and performance of an LP steam turbine operating with large variations of steam flow, it is useful to review some of the steam turbine theories. At any given load, the steam turbine has approximately constant volume flow. This helps the velocity vectors to remain unchanged and so does the efficiency (45). The steam mass flow through the steam turbine at any off-design, e.g. operation without the PCC, can be calculated using the Law of Cones (46):

$$\frac{\dot{m}_{\mathrm{s}}}{\dot{m}_{\mathrm{s},0}} = \frac{\bar{V}.p_{\mathrm{a}}}{\bar{V}_0.p_{\mathrm{a},0}}\sqrt{\frac{p_{\mathrm{a},0}.v_{\mathrm{a},0}}{p_{\mathrm{a}}.v_{\mathrm{a}}}}\sqrt{\frac{1-\left[\frac{p_{\mathrm{w}}}{p_{\mathrm{a}}}\right]^{\frac{n+1}{n}}}{1-\left[\frac{p_{\mathrm{w},0}}{p_{\mathrm{a},0}}\right]^{\frac{n+1}{n}}}} \qquad (6\text{-}13)$$

Where, $\dot{m}_{\mathrm{s}}$ is the steam mass flow, p is the pressure, v is the specific volume, $\bar{V}$ is the average swallowing capacity, and n is the polytropic exponent. The suffix 0 is the design point, suffixes a and w denote at the ST inlet and outlet respectively. For the condensing LP turbine, where the pressure ratio is low and the ratio of swallowing capacity is almost 1, the above equation can be simplified as below and used to determine the relation between the live steam pressure and steam mass flow rate (47):

$$\frac{\dot{m}_{\mathrm{s}}}{\dot{m}_{\mathrm{s},0}} = \sqrt{\frac{p_{\mathrm{a},0}.v_{\mathrm{a},0}}{p_{\mathrm{a}}.v_{\mathrm{a}}}} \Rightarrow \frac{p_{\mathrm{a}}}{p_{\mathrm{a},0}} = \left[\frac{\dot{m}_{\mathrm{s}}}{\dot{m}_{\mathrm{s},0}}\right]^2\frac{\rho_{\mathrm{a},0}}{\rho_{\mathrm{a}}} \qquad (6\text{-}14)$$

Where, ρ is the steam density. If the NGCC plant operates at full load while the PCC is shut down, the steam mass flow rate to the LP turbine cylinder increases by 108%. Using equation (6-14), it is estimated the inlet pressure of the LP turbine will consequently increase from 337 to nearly 700 kPa. This will have an impact on the IP turbine too, since the exit pressure at the IP outlet increases, and the steam volumetric flow decreases substantially by approximately 52%, leading to an efficiency impact. One suggested solution to minimise the

impact of the non-capture operation is that during the PCC shutdown, the power plant operates at a lower load with the net power output equivalent to that of the power plant full load operation while integrated with the CO_2 capture plant (13). Therefore, for this application, the suggested part load operation to minimise the impact of the PCC shut down will be at the GT load of nearly 85%. Nevertheless, for this option, the IP/LP crossover pressure will increase to 627 kPa.

In addition to the above, the condenser back-pressure will rise as a consequence of the increased steam flow, if the cooling water mass flow rate is kept constant at the expense of higher outlet temperature. However, in the case of environmental limitations leading to the higher outlet temperature being not viable, the heat load rise in the cold end demands more cooling water which results in higher electricity consumption in the cooling water system, given the cooling water pumps are capable to operate at higher mass flow rates. Moreover, some provisions must be considered in the steam turbine generator to handle the surplus electricity generations. All these scenarios will definitely have a negative impact on the efficiency. If an NGCC power plant is designed to operate in a CO_2 capture integrated scheme, it is not beneficial to operate in a standalone mode, apart from emergency periods mentioned earlier.

6.8. Conclusions & Remarks

Steady state simulation of a natural gas combined cycle power plant and a post combustion CO_2 capture unit was carried out in Aspen Plus V8.4. Simulations were made at full and part loads for two process options with and without CO_2 capture. The considered option to provide the heat for the solvent regeneration was the steam extraction at IP/LP crossover pipe for all cases. Part load cases were studied at GT load of 90, 80, 70 and 60%. The results confirmed the performance viability of the NGCC-PCC plant at full and part loads down to the 60% load. By adjusting the solvent circulation rate to lower values, except for the GT 60% load, the CO_2 capture with 90% capture rate was achievable at part loads. The study of

the absorber column hydraulics showed that in order to have a reliable operation at the 60% load, the minimum liquid load required in the absorber packed column led to an increase of 6% in the circulating solvent flow rate. A suggested solution to retain the CO_2 capture rate at 90% at this load is to increase the lean solvent CO_2 loading to 0.23 from its design value of 0.21.

Simulation results confirmed that there is sufficient steam available at the IP/LP crossover pipe to provide the steam required for the solvent regeneration at part loads up to 60% GT load. Moreover, the study of the IP/LP crossover pressure showed that the throttling loss related to the steam extraction is minimal as the pressure of the steam in the crossover pipe is close to that required in the reboiler. However, to reach a part load capability below the 60% GT load, a higher design pressure for the crossover pipe would be required. An analysis of net plant efficiency for the two process options revealed that at full load, the efficiency penalty associated with the CO_2 capture operation is 7.15% point at full load and will increase to 7.6% point at 60% GT load.

The study of the absorber column performance and the mass transfer efficiency revealed that at part loads, due to relatively lower load of gas and liquid in the column, the mass transfer efficiency slightly improves and leads to a slightly higher rich solvent CO_2 loading at the column discharge. This improvement however showed a negative effect on the stripper performance in terms of the specific energy required by the reboiler.

An evaluation was made to study the impact of non-capture operation on the LP steam turbine. the results showed that if the NGCC plant operates at full load while the PCC is off, the steam flow available at the LP turbine increases by 108%, which will result in an increase on the LP turbine inlet pressure from 337 to nearly 700 kPa. The increase on the LP inlet pressure will affect the IP turbine as well, leading to the turbine efficiency drop. To minimise the impact of non-capture operation, it is suggested to operate the power plant at a lower load with the net power output equivalent to that of the NGCC full load operation while fitted with the PCC unit (13). Specifically for this study, calculations showed that the

suggested part load operation to minimise the impact of non-capture operation will be at the GT load of nearly 85%.

In addition to the IP and LP turbine performance, the non-capture operation will affect the condenser operating pressure due to the rise of the coolant temperature as a consequence of the increased steam flow, leading to a drop in the plant net power output. Moreover, to make the plant capable of operating without capture, some provision must be considered in the steam turbine generator to handle the surplus electricity generation. These evaluations suggest that if an NGCC plant is designed to operate in a CO_2 capture integrated scheme, it is not beneficial to operate in a standalone mode, apart from inevitable situations such as CO_2 capture plant or CO_2 compression unit trip.

6.9. List of References

(1) IEAGHG, 2012. Operating Flexibility of Power Plants with CCS, June, 2012.

(2) Chalmers, H., Gibbins, J., 2007. Evaluation of the impact of post-combustion capture of carbon dioxide on supercritical pulverised coal power plant part load performance. Fuel 86, 2109–2123.

(3) Odenberger, M., Johnsson, F. 2010. Pathways for the European electricity supply system to 2050—The role of CCS to meet stringent CO_2 reduction targets. International Journal of Greenhouse Gas Control 4, 327–340

(4) Davidson, J. 2009. The need for flexibility in power plants with CCS. Workshop on Operating Flexibility of Power Plants with CCS, Imperial College, London, 11-12 of November.

(5) Chalmers, H., Chen, C., Lucquiaud, M., Gibbins, J., Strbac, G., 2006. Initial Evaluation of Carbon Capture Plant Flexibility. 8th International Conference on Greenhouse Gas Control Technologies: Trondheim, Norway..

(6) Chalmers, H., Leach, M., Lucquiaud, M., Gibbins, J., 2009. Valuing flexible operation of power plants with CO_2 capture. Energy Procedia 1, 4289−4296.

(7) Haines, M.R., Davidson, J.E., 2009. Designing Carbon Capture power plants to assist in meeting peak power demand. Energy Procedia 1, 1457–1464.

(8) Lucquiaud, M., Chalmers, H., Gibbins, J., 2007, Potential for flexible operation of pulverised coal power plants with CO_2 capture", Material Science and Engineering for Energy Systems 2 (3), 175–180.

(9) Chalmers, H., Lucquiaud, M., Gibbins, J., Leach, M., 2009. Flexible operation of coal fired power plants with postcombustion Capture of Carbon Dioxide. J. Environ. Eng. 135, Special Issue: Recent Developments in CO_2 Emission Control Technology, 449–458,

(10) Patino-Echeverri, D., Hoppock, D.C., 2012. Reducing the energy penalty costs of post combustion CCS systems with amine-storage. Conventional Science & Technology 46, 1243-1252.

(11) Department of Energy and Climate Change, CCS Cost Redution Taskforce. London, UK, May 2013.

(12) Jensen, J.N., 2009. Experience with the CASTER/CESAR Pilot Plant. Workshop on operating flexibility of power plants with CCS, Imperial College, London, 11-12 of November.

(13) Pfaff, I., Oexmann, J., Kather, A., 2010. Optimised integration of post-combustion CO_2 capture process in greenfield power plants. Energy 35, 4030-4041.

(14) National Energy Technology Laboratory, 2013. Current and Future Technologies for Natural Gas Combined Cycle (NGCC) Power Plants. DOE/NETL-341/061013, U.S. Department of Energy, Office of Fossil Energy.

(15) Thermoflow. (2011). GT PRO and THERMOFLEX Version 21.0: Sudbury, Massachusetts. www.thermoflow.com

(16) Jordal, K., Ystad, P.A.M., Anantharaman, R., Chilukawa, A., Bolland, O., 2012. Design-point and part-load considerations for natural gas combined cycle plants with post combustion capture. International Journal of Greenhouse Gas Control 11, 271–282.

(17) Aspen Technology, Inc (2009), "Aspen Physical Property System: physical property method" Cambridge, MA, USA

(18) Kehlhofer, R., Rukes, B., Hannemann, F., Stirnimann, F., 2009. Combined-cycle gas & steam turbine power plants. Third ed. PennWell Books, Tulsa, Oklahoma, USA.

(19) Perry's Chemical Engineers' Handbook, 8th ed.; Green, D. W., Perry, R. H., Eds.; McGraw-Hill: New York, 2007.

(24) Notz, R., Mangalapally, H.P., Hasse, H., 2012. Post Combustion CO2 Capture by Reactive Absorption: Pilot Plant Description and Results of Systematic Studies with MEA. International Journal of Greenhouse Gas Control, 6, 84-112.

(25) Kvamsdal, H.M., Hetland, J., Haugen, G., Svendsen, H.F., Major, F., Karstad, V., Tjellander, G., 2010. Maintaining a neutral water balance in a 450MWe NGCC-CCS power system with post-combustion carbon dioxide capture aimed at offshore operation. International Journal of Greenhouse Gas Control 4, 613–622.

(26) Lawal, A., Wang, M., Stephenson, P., Okwose, O., 2012. Demonstrating full-scale post-combustion CO_2 capture for coal-fired power plants through dynamic modelling and simulation. Fuel 101, 115-128.

(27) Agbonghae, E.O., Hughes, K.J., Ingham, D.B., Ma, L., Pourkashanian, M., 2014. Optimal Process Design of Commercial-Scale Amine-Based CO_2 capture Plants. Industrial & Engineering Chemistry Research 53, 14815−14829.

(28) Biliyok, C., Yeung, H., 2013. Evaluation of natural gas combined cycle power plant for post-combustion CO_2 capture integration. International Journal of Greenhouse Gas Control 19, 396-405.

(29) Green, D.W., Perry, R.H., 2008. Perry's Chemical Engineer's handbook. Eighth ed. McGraw-Hill, New York, USA.

(30) Kister, H., 1992. Distillation Design. First ed. McGraw-Hill, New York, USA.

(31) Sinnott, R.K., Towler, G., Towler, 2009. Chemical Engineering Design. Fifth ed. Elsevier, Oxford, USA.

(32) Aspen Plus Simulation Software V.8.4,, "Maximum Capacity Calculations for Packing", Aspen Technology, Inc.

(33) Sulzer Chemtech. Structured Packings for distillation, absorption and reactive distillation. Sulzer Chemtech Ltd. Switzerland.

(34) Reddy, S., Scherffius, J., Freguia, S., Fluor's Econamine FG PlusSM Technology: An Enhanced Amine-Based CO_2 Capture Process. 2003. Second National Conference on Carbon Sequestration National Energy Technology Laboratory/Department of Energy, Alexandria, VA, May 5-8.

(35) Gibbins, J.R., Crane, R.I., 2004. Scope for reductions in the cost of CO_2 capture using flue gas scrubbing with amine solvents. Proceedings of the Institution of Mechanical Engineers, Part A: Journal of Power and Energy 218, 231-239.

(36) Lucquiaud, M., Chalmers, M., Gibbins, J., 2009. Capture-ready supercritical coal-fired power plants and flexible post-combustion CO_2 capture. Energy Procedia 1, 1411–1418.

(37) Linnenberg, S., Liebenthal, U., Oexmann, J., Kather, A., 2011. Derivation of power loss factors to evaluate the impact of post-combustion CO_2 capture processes on steam power plant performance. Energy Procedia 4, 1385–1394.

(38) Luo, X., Wang, M., Chen, J., 2015. Heat integration of natural gas combined cycle power plant integrated with post-combustion CO_2 capture and compression. Fuel 151, 110–117.

(39) Luo, X., Wang, M., Oko, E., Okezue, C., 2014. Simulation-based techno-economic evaluation for optimal design of CO_2 transport pipeline network. Applied Energy 132, 610–620.

(40) Kurtz, D.P., McNulty, K.J., Morgan, R.D., 1991. Stretch the Capacity of High-Pressure Distillation Columns. Chem. Eng. Prog. 87, 43-49.

(41) Kister,, H.Z., 1990. Distillation operation. First ed. McGraw Hill. New York, USA.

(42) Office of Air Quality Planning and Standards Research, 2002. EPA Air Pollution Control Cost Manual. Sixth ed. United States Environmental Protection Agency, Triangle Park, North Carolina, USA.

(43) Thern, M., Jordal, K., Genrup, M., 2014. Temporary CO_2 shut down: Implications on low pressure steam turbine design and efficiency. Energy Procedia 51, 14-23.

(44)Bellamy, N., 2009. CHP Plant – optimum efficiency, total flexibility", Power Gen Europe, Cologne, Germany, May 26-28.

(45) Bolland, O., Thermal power generation, 2010. Department of Energy and Process Engineering, Norwegian University of Science and Technology.

(46) Stodola, A., Loewenstein, L.C., 1945. Steam and gas turbines, P. Smith, New York, USA.

(47) Flatebo, O., 2012. Off-design Simulations of Offshore Combined Cycles, Master Thesis, Department of Energy and Process Engineering, Norwegian University of Science and Technology.

Chapter 7

Absorber Intercooling

Absorber intercooling has been recognised as one process modification technique to improve the CO_2 absorption process and therefore reduce the overall energy requirement of a CO_2 capture process. This chapter presents the study to determine the benefit of using two absorber intercooling configurations, i.e. in-and-out" intercooling and "recycled" intercooling, for natural gas fired applications when using MEA solvent for range of lean loading from 0.15 to 0.42 (mol CO_2/mol MEA). The developed rate-based model presented in Chapter 4 was used to determine operating conditions at which the use of absorber intercooling is meaningful and promising in terms of capital and energy requirements.

7.1. Introduction

CO_2 absorption using aqueous amines is usually associated with a considerable amount of heat liberation due to reactions between CO_2 and the solvent by which the absorber column is led to act as both a chemical reactor and a heat exchanger. This heat is usually released in the liquid phase and will rise the liquid temperature and causes further heat transfer to the gas phase. Absorber intercooling is usually used to cool down flowing solvent that has been heated through the release of the heat of absorption at column locations above the intercooler (1). The use of absorber intercooling benefits the absorption equilibria by reducing the column operating temperature and breaking mass transfer pinches (2). Improved equilibrium in the absorber column will subsequently reduce the amount of solvent required for the same removal rate and thus may result in the reduction in energy required for solvent regeneration (1). According to a study, when the temperature rise is higher than 17°C, the absorber column requires intercooling between stages to remove the heat of absorption to retain the operating condition close to the initial conditions (3). However, the effectiveness of using an

intercooler is dependent on several factors, such as flue gas condition, lean solvent CO_2 loading, liquid to gas ratio, flue gas and solvent temperatures at the absorber inlet, etc. In the following text, the benefits of using two difference configurations of absorber intercooling, i.e. “in-and-out” intercooling and “recycled” intercooling, over a range of lean loading from 0.15 to 0.42 were investigated using the flue gas condition and CO_2 capture process described in Chapter 6.

7.2. Evaluation Methodology

The developed CO_2 capture model was used to evaluate the benefits of using absorber intercooling for a range of lean loading from 0.15 to 0.42 on CO_2 absorption efficiency and plant overall energy requirement. All configurations in this study are modelled using structured packing and cylindrical columns. Unless otherwise stated, the packing used in most sections are assumed to be Mellapak 250Y which is categorised as a low-pressure gauze packing with a very low operational pressure drop (4). Absorber simulation with and without intercooling were performed using flue gas conditions presented in Table 7-1 for 650 MW gas fired combined cycle power plant.

Table 7-1. Flue Gas characteristic

Parameter	**Composition (mole fraction %)**
N_2	74.39
O_2	12.37
CO_2	3.905
H_2O	8.434
Ar	0.8952

The stripper packed height was over-specified, i.e. 20 m, resulting in a pinch in all cases. Noting that a practical design of stripper column would use an optimised packing height, over-specification of the stripper packed height in this study confirms the packing was being equally utilised in all cases, without additional height optimization criteria, whilst each case approaching equilibrium, and therefore providing an appropriate estimate for the energy

requirement. To retain a constant compression work, the stripper operating pressure was kept constant at 170 kPa (1.7 bar) in all load cases.

For a column with absorber intercooling, there are three degrees of freedom for optimisation, i.e. lean loading, liquid to gas ratio and the location of the absorber intercooling. Lean loading and therefore the L/G were varied while maintaining the CO_2 removal rate constant. Furthermore, at each lean loading, the absorber packing volume was optimised by varying the height of the packing sections at the top and bottom of the absorber intercooling location. Results were normalized by the moles of CO_2 removed. Lean solvent and flue gas inlet temperatures were 40 °C in all cases. The absorber column diameter was calculated to provide a 75 % approach to flooding, and the column height was determined to satisfy 90 % CO_2 removal rate in all cases. Benefits of two different types of intercooling were investigated: “in-and-out” intercooling (simple intercooling) and “recycled” intercooling (advanced intercooling). For a column with absorber intercooling, there are three degree of freedom for optimisation, i.e. lean loading, liquid to gas (L/G) ratio and the absorber packing volume. For each lean loading there is a fixed liquid to gas ration to maintain the CO2 removal rate constant at 90 %. At each lean loading, the absorber packed volume was optimised by varying the height of the packing sections at the top and bottom of the absorber intercooling location. Results were normalised by the moles of CO2 removed. Lean solvent and flue gas inlet temperatures were 40 °C in all cases. The absorber column diameter was calculated to provide a 75% approach to flooding, and the column height was determined to satisfy 90% CO_2 removal rate in all cases.

7.2.1. In-and-Out Intercooling (Simple Intercooling)

Figure 7-1 shows the process flow diagram (PFD) of an absorber column with in-and-out intercooling. This is the simplest and conventional method of intercooling where the semi-rich solvent exits the absorber column at the end of one packing section and passes through an external heat exchanger (cooler) to cool down to the temperature at which the lean solvent first entered the absorber column at the top. After being cooled, the semi-rich solvent re-

enters the column at the top of the successive section of packing and continues absorbing CO_2 from upcoming flue gases. To simulate this case, the absorber column was modelled using two sections packed with Sulzer Mellapak 250Y structured packing, as shown in Figure 1. The intercooling loop was modelled using "pump-around" option in RateSep™ with no reactions involved where the entire semi-rich flow rate cools down to 40 °C via an external cooler.

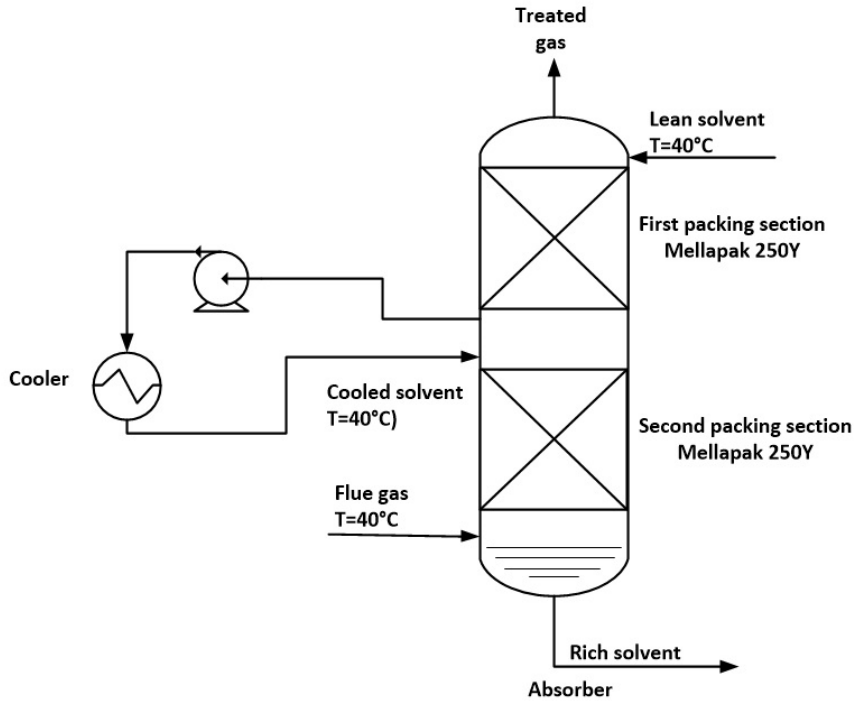

Figure 7-1. The arrangement of an absorber column with in-and-out (simple) intercooler

7.2.2. Recycled Intercooling (Advanced Intercooling)

Figure 7-2 shows the PFD of the absorber column with recycled intercooling. In this configuration, the semi-rich solvent leaves the absorber column at one point, cools in an external cooler to the to the temperature at which the lean solvent first entered the absorber column at the top, and returns back to the column via a higher point which is below the location the lean solvent first entered the column. In this configuration, the absorber packed column was divided into three sections, by which the first and third sections were packed with the Sulzer Mellapak 250Y structured packing, and the middle section (recycled section)

with a coarse structured packing, e.g. Sulzer Mellapak 125Y, to avoid excessive pressure drop due to the high solvent load in in the middle section.

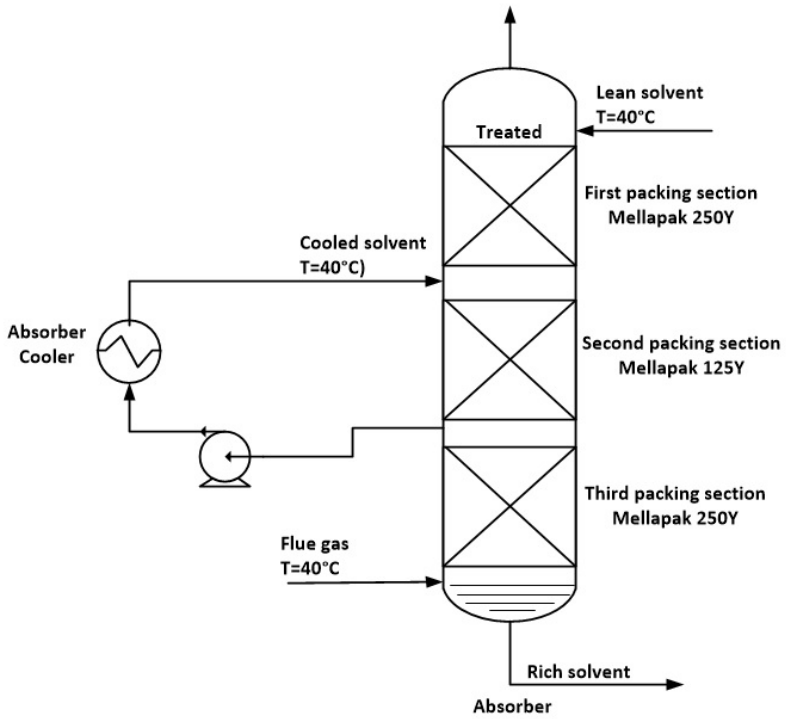

Figure 7-2. The arrangement of an absorber column with recycled (advanced) intercooling

The recycle rate can be varied with respect to the plant design and operational constraints. The recycle rate which is usually 2 to 5 times of the solvent flow rate provides another degree of freedom for optimisation, constrained by flooding criteria, pressure drop, and operational cost (energy required to operate the recycle pump). In general, higher recycle ratios result in cooler and richer solvent at the absorber exit at the expense of higher pumping power and more packing requirement at the middle section of the column. To find an optimal recycle ratio, various recycle ratios, from 1 to 9 times the solvent flow rate, were compared with each other and with the base case, i.e. a simple absorber with no intercooling (no recycle rate). As shown, the change in slope at around the recycle ratio of 3 indicates this may be the optimised ratio for the natural gas application. From a ratio of 3 to a ratio of 10, very little change occurs in both rich solvent temperature and rich loading.

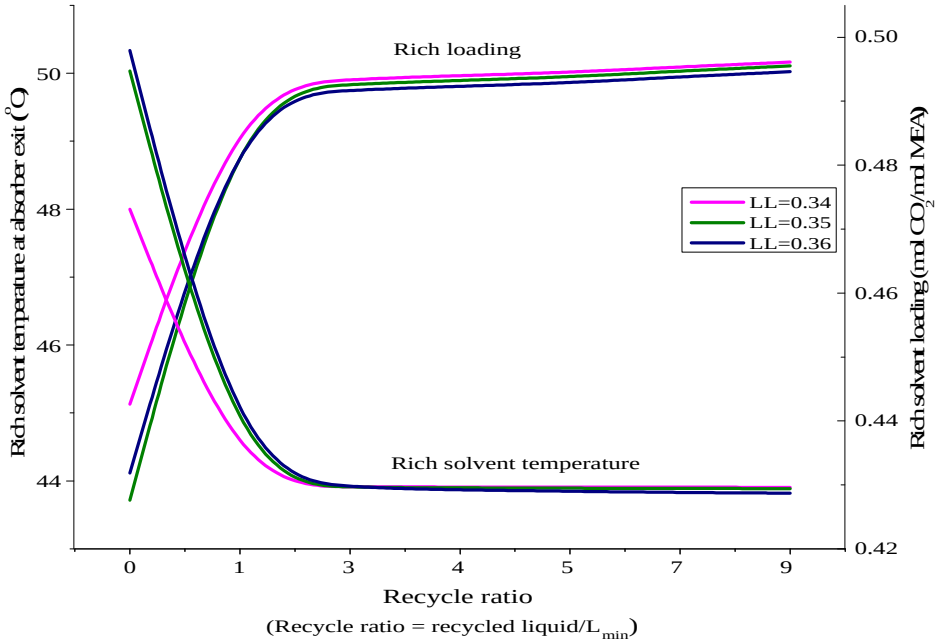

Figure 7-3. Variation of rich solvent loading and temperature at absorber exit with cooling solvent recycle rate for three different lean loading

Figure 7-4 shows the variation of minimum liquid to gas ratio (L/G) with recycle ratio. The change of slope at around the recycle ratio of 3 was also observed in this figure. Therefore, the recycle ratio of 3 was selected as an optimum ratio for the advanced intercooling simulations for the natural gas application.

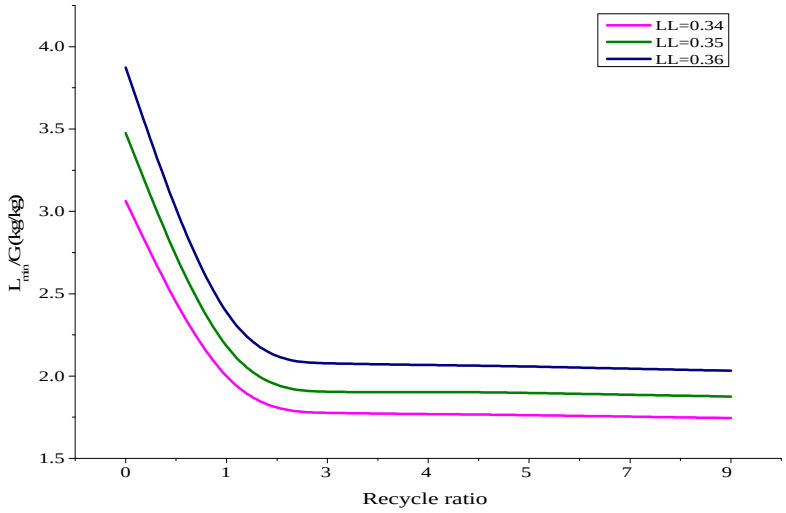

Figure 7-4. Variation of minimum liquid to gas ratio (L_{min}/G) with cooling solvent recycle ratio for three different lean loading

7.2.3. Minimum Solvent Flow Rate (L_{min})

For a fixed lean loading and CO_2 removal rate, the solvent flow rate is a function of the packing area. The liquid flow rate decreases by increasing the packing area until it reaches a minimum. The minimum amount of solvent required to achieve 90 % CO_2 removal rate was calculated for a range of lean loading from 0.15 to 0.42 for the three case studies: (1) an absorber with no intercooling, (2) an absorber with simple intercooling, and (3) an absorber with advanced intercooling. The minimum solvent flow rates were then used to determine the respective minimum liquid-to-gas ratios (L_{min}/G).

For the absorber with no intercooling, for a given lean loading, the minimum solvent flow rate to achieve 90 % CO_2 removal rate was determined assuming an infinity height of packing, e.g. 40 m in the absorber column to assure equilibrium pinch at the rich end of the column (5), provided the fractional approach to flooding was retained at 75 %.

Similarly, for absorbers with simple and advanced intercooling, for a given lean loading, the minimum solvent flow rate to achieve 90 % CO_2 removal rate was determined assuming an infinity height of packing, e.g. 30 m, for each packing section, provided the fractional approach to flooding was kept at 75 %.

The effectiveness of intercooling can be better realised by comparing the minimum solvent flow rate required for a given lean loading in relation to the theoretical minimum solvent flow rate required at that lean loading to attain 90 % CO_2 removal rate. The theoretical minimum solvent flow rate was determined assuming an isothermal absorber where the temperature of the liquid phase throughout the column is the same and equal to the inlet liquid temperature (ideal intercooling) (5). The isothermal absorber was modelled in Aspen Plus® using a flash drum where the lean solvent at a given loading mixes with the pure CO_2 stream with a flow rate equivalent of that in the flue gas and enters the drum at 40°C. Two streams exit the drum: the flashed gas stream and the flashed liquid stream. The flash gas stream is the 10 % remaining of the CO2 flow rate which was not absorbed by the solvent considering a 90 % removal rate, and the flashed liquid stream is the saturated rich solvent at

the end of absorption process. The liquid flow rate required at the inlet to achieve 90 % removal rate was considered as the minimum theoretical solvent flow rate.

Figure 7-5 shows the relation of the minimum solvent flow rates of the three options to the isothermal solvent flow rate for the range of lean loading form 0.15 to 0.42. As shown, the minimum ratio is related to the advanced intercooling option.

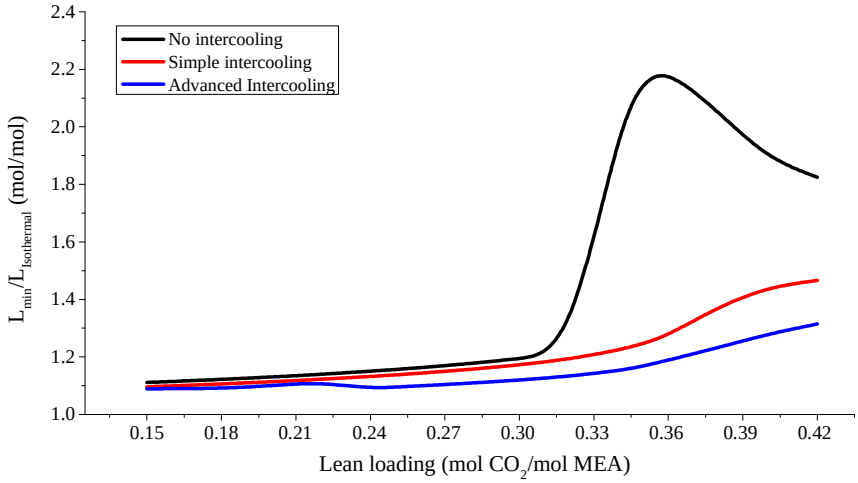

Figure 7-5. The relation of minimum solvent flow rate of simple absorber with no intercooling (black), an absorber with simple intercooling (red) and an absorber with advanced intercooling with the recycle rate of $3xL_{min}$ ((blue) to the isothermal solvent flow rate over a range of lean loading.

Figure 7-6 shows the comparison of the minimum liquid to gas ratios of the isothermal absorber with the absorber with no intercooling, the absorber with simple intercooling, and the absorber with advanced intercooling.

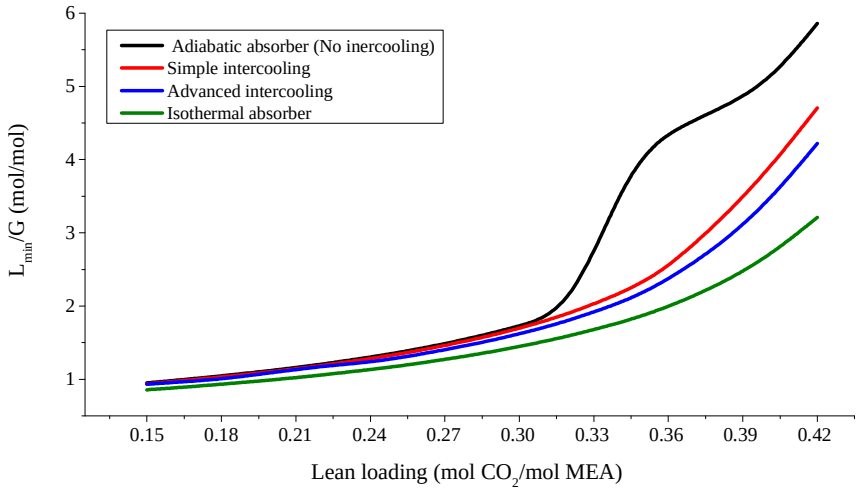

Figure 7-6. Comparison of the minimum liquid to gas ratios (L_{min}/G) of an isothermal absorber

(green), an adiabatic absorber (black), an absorber with simple intercooling (red), and an absorber with advanced intercooling with the recycle rate of $3xL_{min}$ (blue) over a range of lean loading.

As shown in Figures 7-5 and 7-6, the lean loading range at which the application of intercooling is meaningful is from 0.30 and higher. The greatest decrease in solvent requirement was realised at lean loading of .35 at which the simple intercooling and advanced intercooling, respectively, provide 42.4 and 46.1 % reduction in the minimum solvent flow rate when compared to the absorber with no intercooling. At lean loading below 0.30, the effect is less significant, where simple and advanced intercooling, respectively require on average 1.5 and 3.4 % less solvent flow rate when compared with the absorber with no intercooling.

7.2.4. Overall Energy Requirement

Similar to Chapter 5, the total equivalent work concept was used to evaluate and compare the energy requirement of the CO_2 capture process with and without absorber intercooling at various lean loading. Eqs. 5-1 to 5-3 were used to determine the total equivalent work. Assumptions made for each equation are as described in Chapter 5, Section 5.3.1.

7.3. Application of Absorber Intercooling with L_{min}

7.3.1. Effect of Absorber Intercooling on Temperature Bulge

The aqueous solvent enters the absorber column at the top and counter-currently contacts with the flue gas fed to the column at the bottom. As the down-coming solvent absorbs the CO_2, its temperature increases and causes the water to vaporise. Toward the top of the column, the produced water vapour condenses by contacting counter-currently with the cooler solvent, which leads to formation of a pronounced temperature bulge on the gas and liquid temperature profiles along the absorber column (6). Depending on the solvent lean loading and the liquid to gas ratio (L/G), the magnitude and location of temperature bulge vary through the column height. Figure 7-7 shows the magnitude of bulge temperature (T_{Bulge}) at various lean loading for an absorber with no intercooling, with simple intercooling,

and with advanced intercooling. Figure 7-8 shows the location of bulge in relation to the absorber column height. As L/G increases, the location of the bulge moves toward the bottom of the column and its magnitude decreases as more heat has been carried by the solvent due to its relatively higher heat capacity.

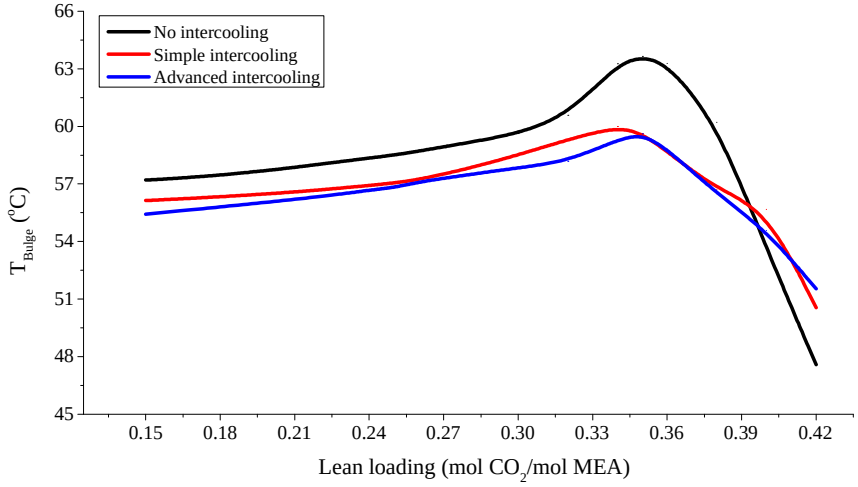

Figure 7-7. Magnitude of bulge temperature (T_{Bulge})for an absorber with no intercooling (black), with simple intercooling (red) and with advanced intercooling with the recycle rate of 3xL_{min} (blue) over a range of lean loading.

As shown in Figure 7-8, at low lean loading (0.15 < lean loading < 0.30), the bulge occurs at the top of the packed column. As lean loading and therefore L/G increases, the location of the bulge moves toward the bottom of the column. The rate of movement is more pronounced for the absorber with no intercooler. Concurrently the magnitude of the bulge temperature ascends by which the greatest temperature bulge occurred at the lean loading of 0.35 in all three cases. After this point, as lean loading increases, the magnitude of temperature bulge descends. The temperature bulge at its peak is located nearly in the middle of the column (H_{Bulge}/H_{total}=0.6) in an absorber with no intercooling, whilst for the absorber with simple intercooling and advanced intercooling, the temperature bulge at its peak occurs nearly at the top of the packed column, i.e. (H_{Bulge}/H_{total}=0.925) and (H_{Bulge}/H_{total}=0.95), respectively.

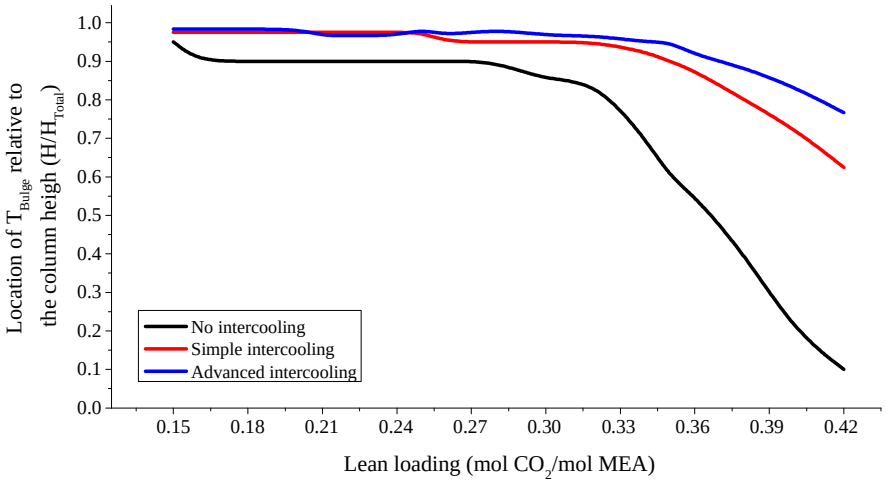

Figure 7-8. The location of bulge temperature (T_{Bulge}) in relation to the column height for an absorber with no intercooling (black), with simple intercooling (red), and advanced intercooling with the recycle rate of $3xL_{min}$ (blue).

As mentioned earlier, an absorber column is typically designed to reach equilibrium at the rich end of the column (rich-end pinch) (5). According to the bulge theory, the greatest absorption rate will occur away from pinch and so does the temperature bulge (6). The temperature bulge basically results in reducing equilibrium driving forces, however, as long as it occurs away from the equilibrium pinch, its effect on the column mass transfer performance should be trivial as the mass transfer performance is focused on the pinch (6).

However, at high L/G ratios where there is excess solvent relative to the inlet gas, the absorber column will reach equilibrium at the lean end of the tower. If the total heat capacity of the liquid (mass times heat capacity) becomes greater than that of the gas, the heat of reaction tends to liberate at the bottom of the column, and this will push the temperature bulge to occur at the rich end. In such cases (of which the CO_2 absorption using MEA is an example), the temperature bulge will have a great negative impact on the mass transfer performance of the column, especially when the pinch and the temperature bulge both occur in the middle of the column (6).

Although due to the high heat capacity of the liquid, the magnitude of temperature bulge tends to lower at high L/G, and as L/G increases, the operating line moves away from equilibrium. This creates a tendency for more CO_2 to be absorbed by the solvent per stage,

resulting in more heat to be liberated at each stage which then causes the equilibrium curve to move upward (6). Depending on the magnitude of L/G, the pinch may occur in the middle of the column or near the top. As can be observed from Figures 7-6 and 7-8, for the absorber with no intercooling, at lean loadings between 0.32 and 0.36, the sharp rise in L/G coincides with the location of temperature bulge being near the middle of the column.

Curves related to the simple and advanced intercooling shown in Figures 7-7 and 7-8 confirm that employing intercooling alters the location as well as the magnitude of the temperature bulge. The maximum bulge temperature after employing simple and advanced intercooling dropped to 60.0 °C and 59.6 °C respectively, compared to 63.6 °C of the non-intercooled case. Concurrently, employing absorber intercooling favours the column mass transfer efficiency by moving the temperature bulge to the top of the column. The location of temperature bulge moves to 0.925 and 0.950 of the total absorber packed height, when simple and advanced intercooling were applied, respectively, compared to 0.60 in the non-intercooled case.

In an absorber with no intercooling, when the temperature bulge occurs near or at the middle of the packed column, it is defined as the critical temperature bulge (6). The liquid to gas ratio associated with this condition is called the critical L/G. In this study, the critical temperature bulge was realised at lean loading of 0.36, with critical L/G of 4.45 (mol/mol). The magnitude and location of the bulge temperature at the critical lean loading are 63.3 °C and H_{Bulge}/H_{Total}=0.55, respectively. At the critical temperature bulge, there is a balance in the enthalpy leaving with the liquid and with the flue gas. At this point, liquid and gas outlet temperatures change rapidly with changing liquid to gas ratio (6). Figure 7-9 shows the variation of liquid (rich solvent) and gas (treated solvent) temperatures when leaving the absorber column of the three cases. As shown, both liquid and gas temperature curves display a smoother trend after employing absorber intercooling. The effect of intercooling on the liquid outlet temperature is more pronounced especially in the advanced intercooling case. This is due to the solvent having in general a cooler temperature profile along the

absorber column after employing intercooling, which results in an increase in the solvent absorption capacity since the absorption capacity of amine solvents for acid gases, e.g. CO_2, increases with lowering operating temperatures. Equally, for a fixed CO_2 removal rate, employment of absorber intercooling is associated with less solvent flow rate requirement. This can be seen by comparing the L_{min}/G of intercooled cases to those of non-intercooled as shown in Figure 7-6.

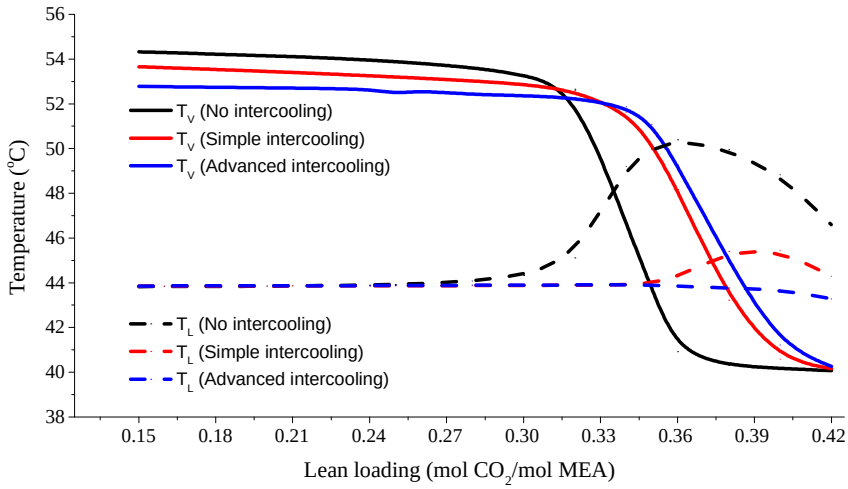

Figure 7-9. Variations of liquid and gas outlet temperature over the range of lean loading for an absorber with no intercooling (black), with simple intercooling (red) and advanced intercooling with the recycle rate of $3xL_{min}$ (blue).

7.3.2. Effect of Absorber Intercooler on CO_2 Absorption rate & Liquid and Gas Temperature Profiles

Figures 7-10 to 7-16 show the CO_2 mass transfer, and the liquid and gas temperatures profiles along the absorber packed column for lean loading of 0.22, 0.28, 0.32, 0.35, 0.36, 0.38, and 0.42, respectively.

At lean loading below the critical lean loading, as shown in Figures 7-10 to 7-12, the relatively low CO_2 loading of the solvent at the top of the column with no intercooling intensifies the CO_2 mass transfer rate toward the top of the column, which led to a large increase in both liquid and gas temperatures at that region. As most of the CO_2 was absorbed at the lean end, and the use of absorber intercooling appears to only intensify the CO_2 mass

transfer rate at its peak and leave the rest of the column unchanged, lowering the operating temperature provides no significant improvement in terms of CO_2 mass transfer rate toward the bottom of the column.

The temperature profile for lean loading near the critical lean loading, as shown in Figures 7-13 to 7-15, is nearly constant across most of the profile as it has reached a mass transfer pinch. At the bottom of the column with no intercooling the low temperature of the flue gas increases slightly the CO_2 mass transfer rate. At these lean loading the absorption efficiency is limited due to the increase in the operating temperature and therefore benefit most from the incorporation of absorber intercooling. As shown, using intercooling significantly improved the CO_2 mass transfer rate, lowered the temperature of the bulge, and the liquid and gas temperature profiles along the column.

Curves shown in Figure 7-16 are for the richest lean solvent with lean loading of 0.42 combined with the highest liquid to gas ratio (L/G=7.2 (mol/mol)). As shown, the column with no intercooling was approached to pinch at the lean end. The CO_2 mass transfer profile showed that most of the removal occurs toward the middle of the column. Intercooled mass transfer profiles show higher removal rates towards the top section of the column. The relatively high liquid to gas ratio with intercooling maintains low temperature profiles throughout the column. Using absorber intercooling does not provide benefits as the intercooled liquid to gas ratios at lean loading higher than the critical lean loading are still excessively high.

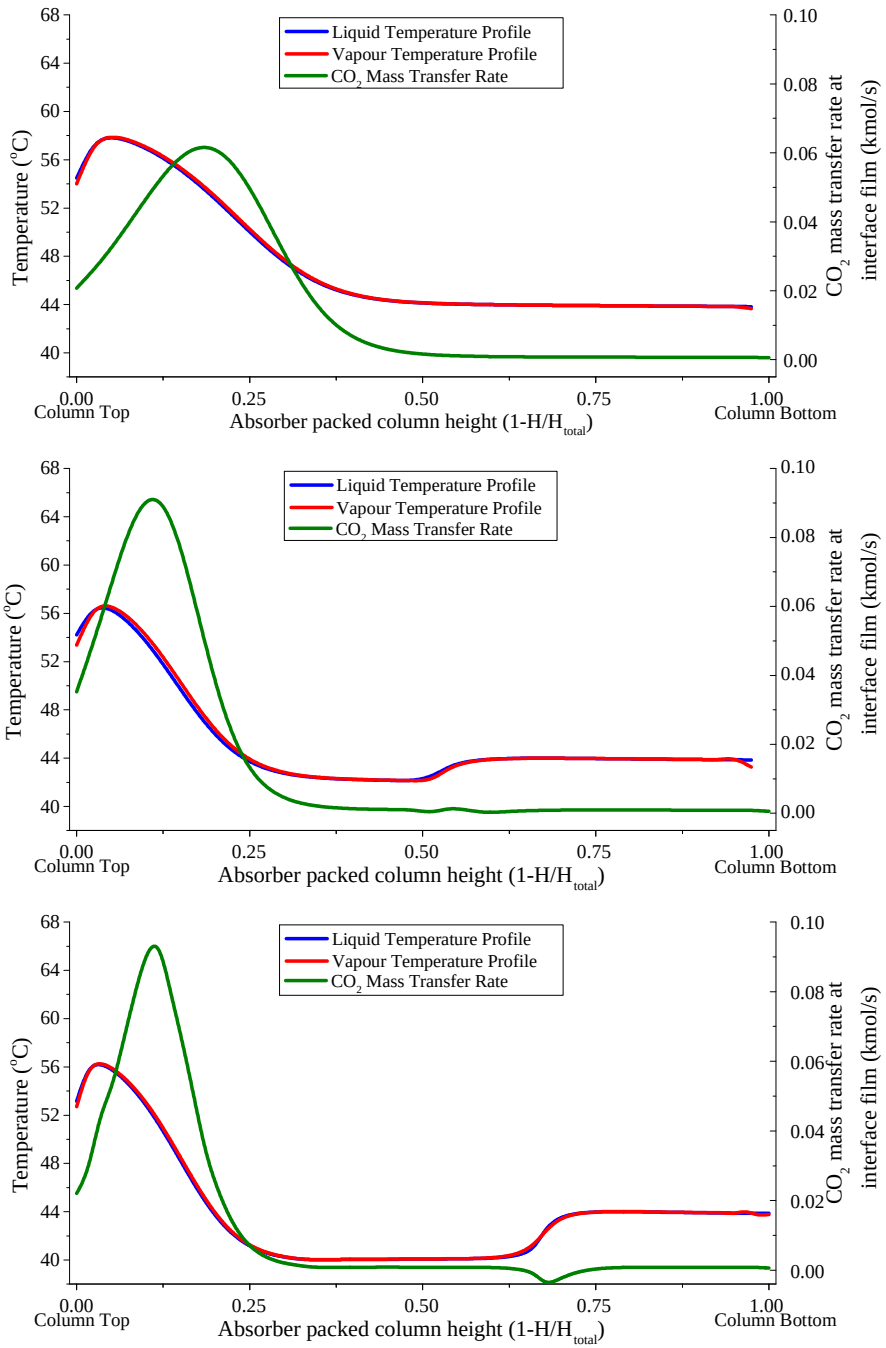

Figure 7-10. Liquid and gas temperature profiles and CO_2 mass transfer rate along the absorber column for lean loading of 0.22 for an absorber with no intercooling (top) with simple intercooling (middle) and with advanced intercooling with the recycle rate of $3xL_{min}$ (bottom)

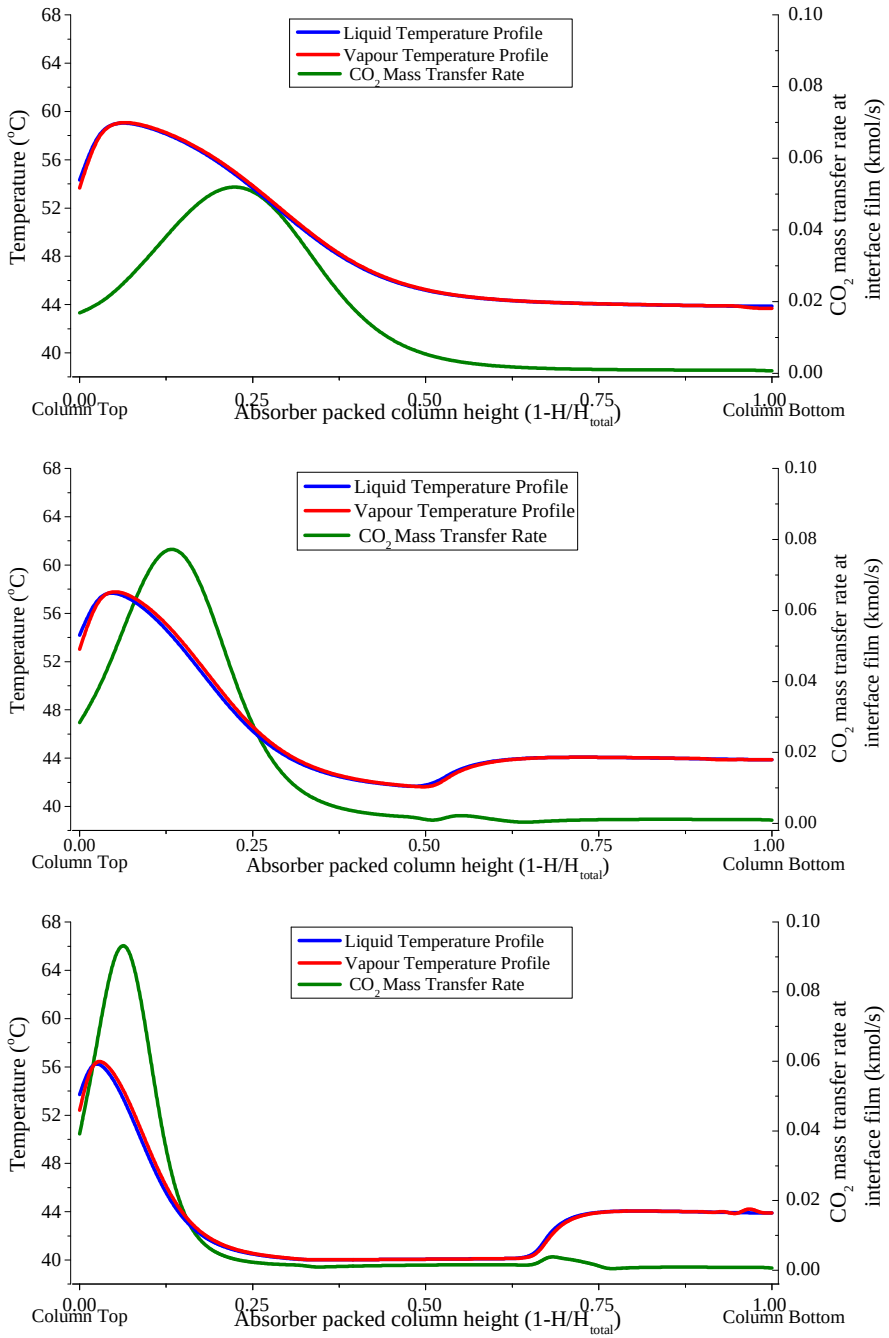

Figure 7-11. Liquid and gas temperature profiles and CO_2 mass transfer rate along the absorber column for lean loading of 0.28 for an absorber with no intercooling (top) with simple intercooling (middle) and with advanced intercooling with the recycle rate of $3xL_{min}$ (bottom)

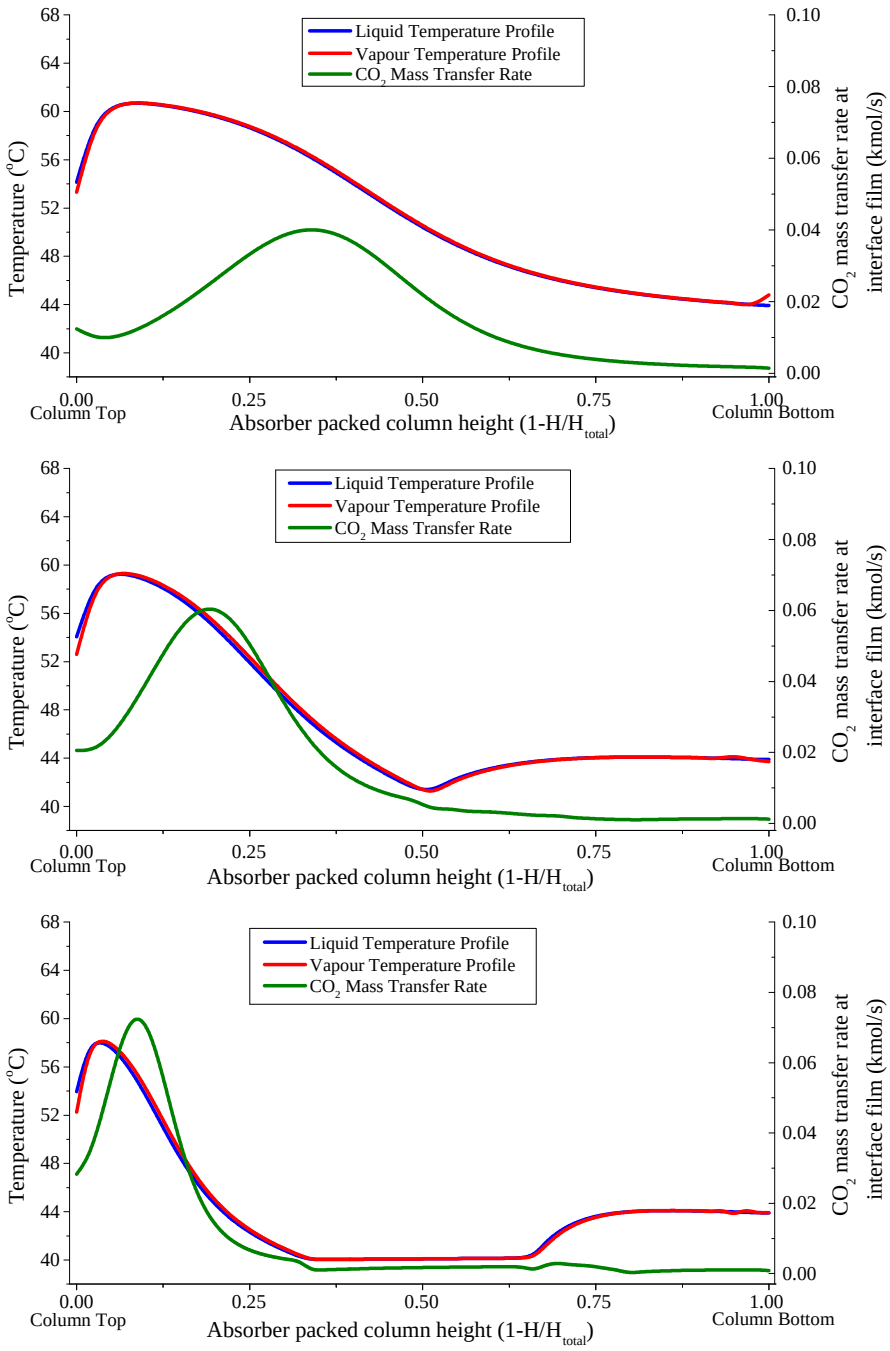

Figure 7-12. Liquid and gas temperature profiles and CO_2 mass transfer rate along the absorber column for lean loading of 0.32 for an absorber with no intercooling (top) with simple intercooling (middle) and with advanced intercooling with the recycle rate of $3xL_{min}$ (bottom)

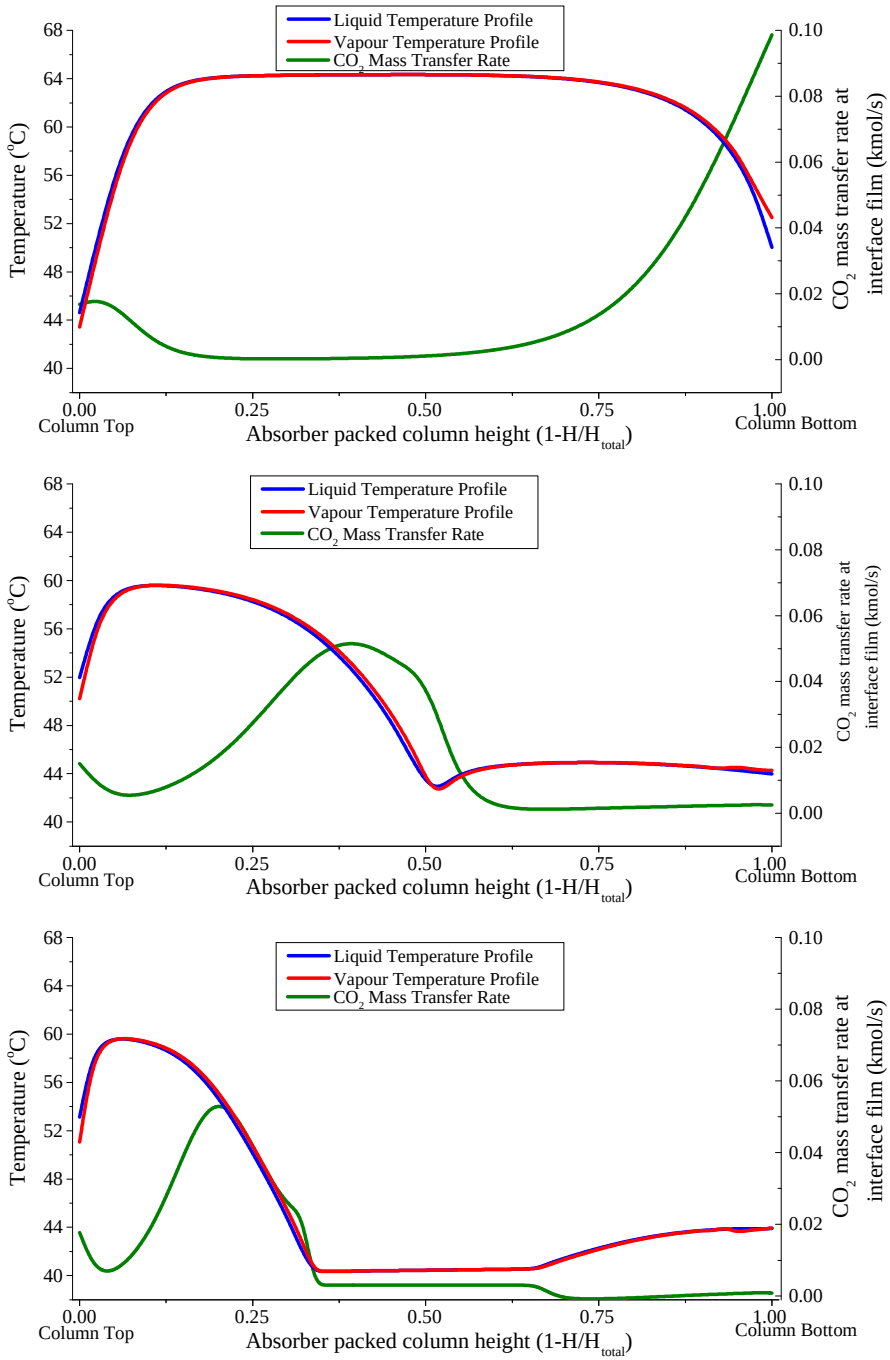

Figure 7-13. Liquid and gas temperature profiles and CO_2 mass transfer rate along the absorber column for lean loading of 0.35 for an absorber with no intercooling (top) with simple intercooling (middle) and with advanced intercooling with the recycle rate of $3xL_{min}$ (bottom)

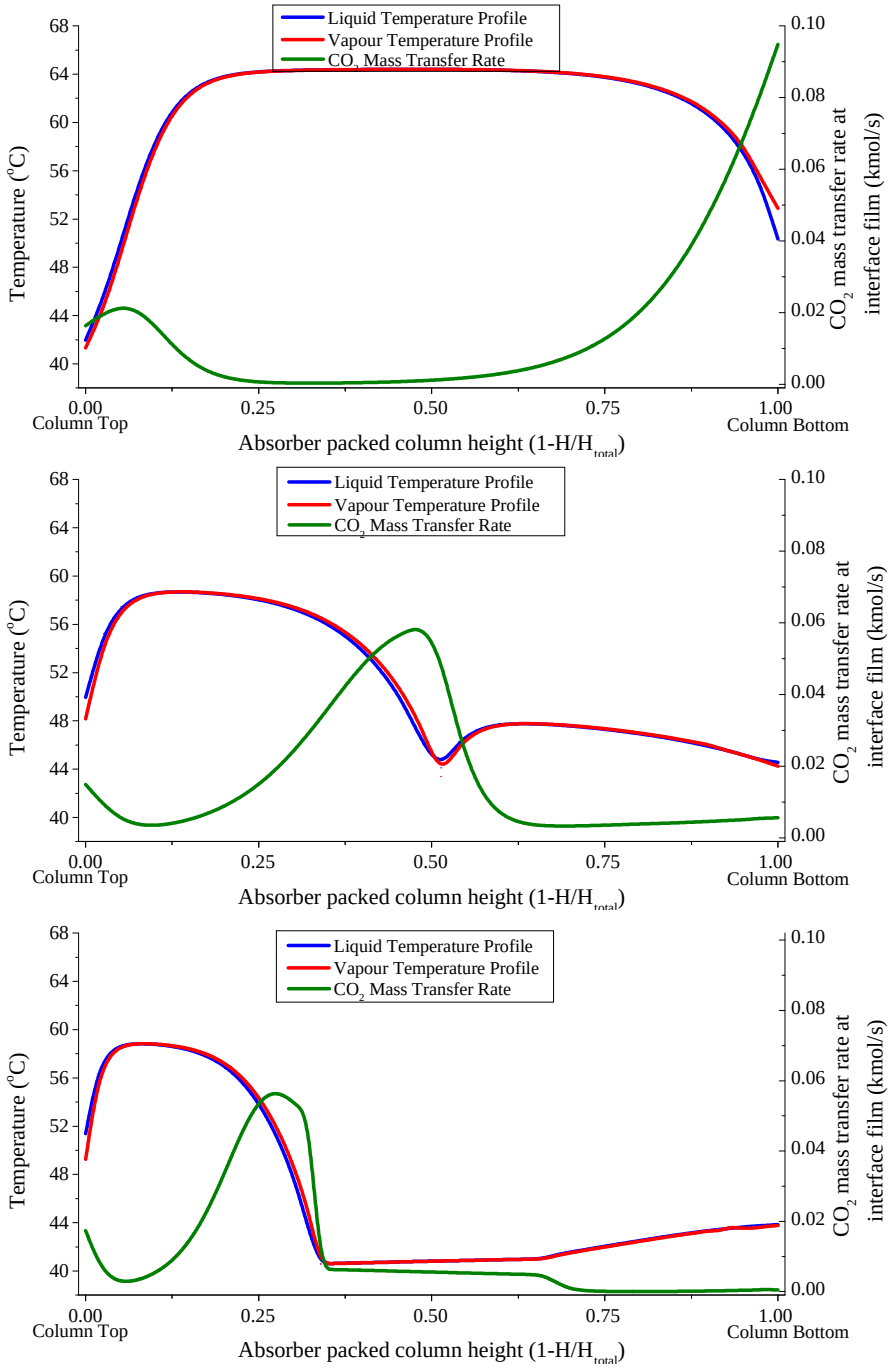

Figure 7-14. Liquid and gas temperature profiles and CO_2 mass transfer rate along the absorber column for lean loading of 0.36 for an absorber with no intercooling (top) with simple intercooling (middle) and with advanced intercooling with the recycle rate of $3xL_{min}$ (bottom)

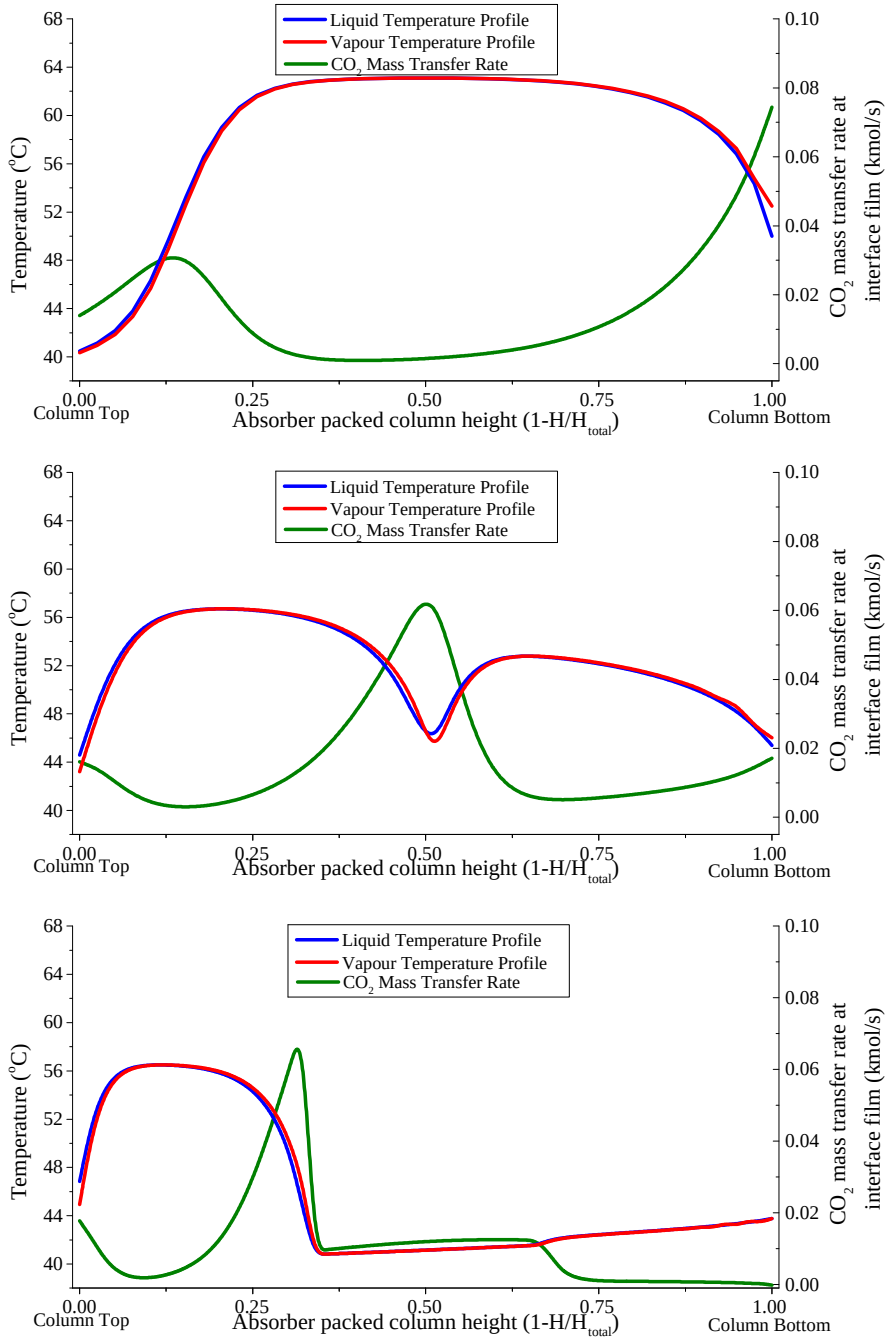

Figure 7-15. Liquid and gas temperature profiles and CO_2 mass transfer rate along the absorber column for lean loading of 0.38 for an absorber with no intercooling (top) with simple intercooling (middle) and with advanced intercooling with the recycle rate of $3xL_{min}$ (bottom)

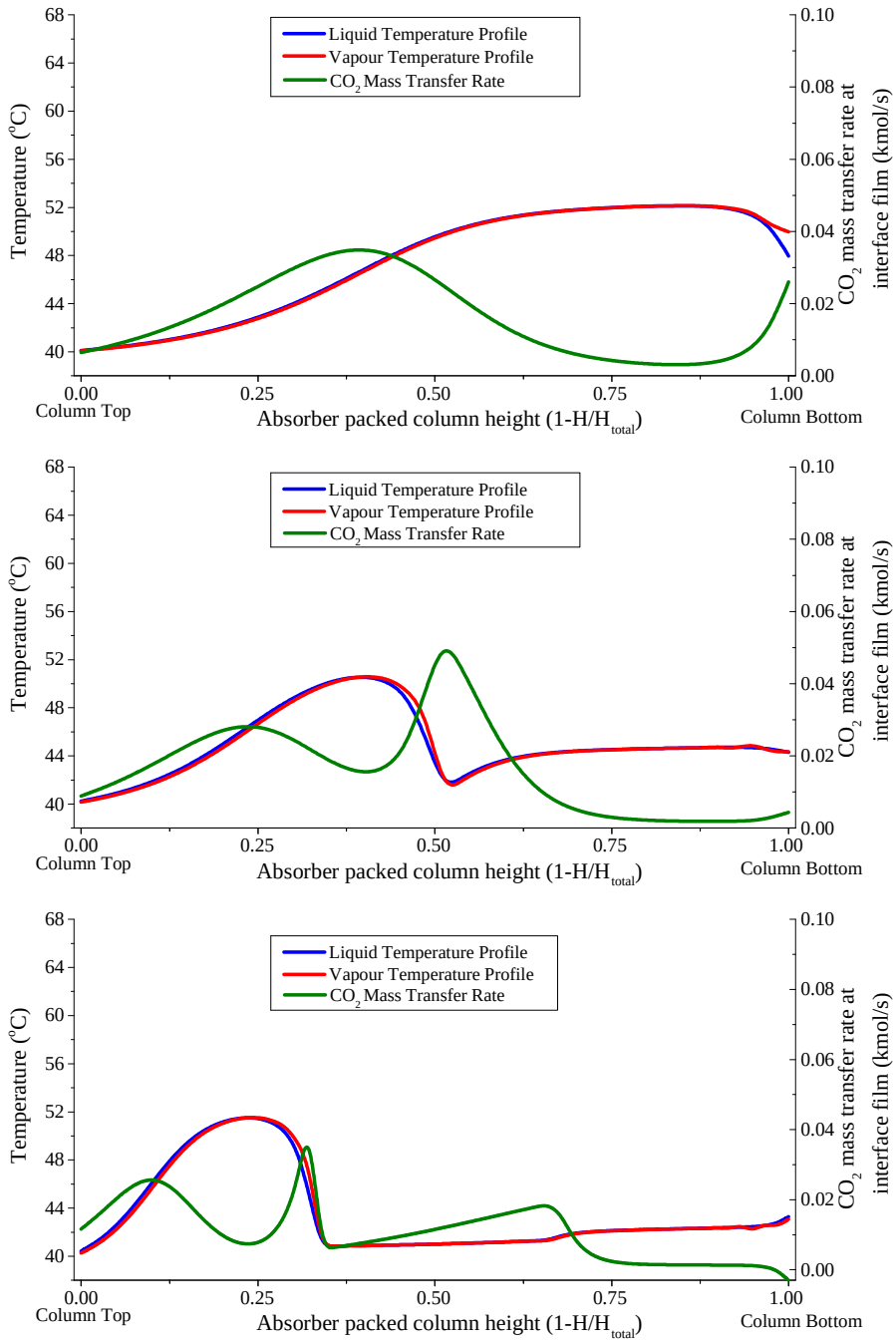

Figure 7-16. Liquid and gas temperature profiles and CO_2 mass transfer rate along the absorber column for lean loading of 0.42 for an absorber with no intercooling (top) with simple intercooling (middle) and with advanced intercooling with the recycle rate of $3xL_{min}$ (bottom)

7.3.3. Effect of Absorber Intercooling on Solvent Absorption Capacity

As mentioned earlier, an amine solvent capacity to absorb acid gases, e.g. CO_2, increases as operating temperature reduces (7). Solvent absorption capacity was defined as the unit of CO_2 removed per unit of lean solvent used. Figure 7-17 shows the variation of solvent absorption capacity with lean loading for the three cases provided the CO_2 removal rate was maintained at 90 %. The solvent absorption capacity of an absorber with no intercooling substantially dropped after lean loading of 0.32 and reached its minimum capacity at 0.36, which is the critical lean loading. After the critical lean loading, a slight improvement in terms of solvent absorption capacity was observed due to the excessive increase in the liquid to gas ratio at those lean loading as shown in Figure 7-6.

As shown in Figure 7-17, the use of absorber intercooling was realised well in terms of solvent capacity at lean loading higher than 0.32, where the advanced intercooling provided the highest improvement. At the critical lean loading, the use of simple and advanced intercooling resulted in improving the overall absorption rate by nearly 75.3 and 88.1 %, respectively. The solvent absorption capacity in general lowers with increasing lean loading due to the limiting capacity imposed to it by the initial CO_2 content in the lean feed.

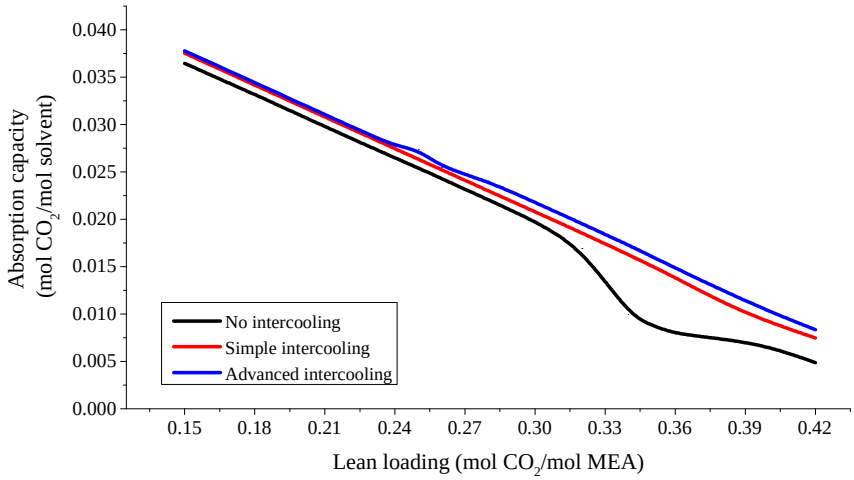

Figure 7-17. Variation of solvent absorption capacity with lean loading for an absorber with no intercooling (black), with simple intercooling (red) and with advanced intercooling with the recycle rate of $3xL_{min}$ (blue)

7.3.4. Effect of Absorber Intercooling on Rich Solvent Loading

Figure 7-18 shows the variation of rich solvent loading with lean loading for an absorber with and without intercooling.

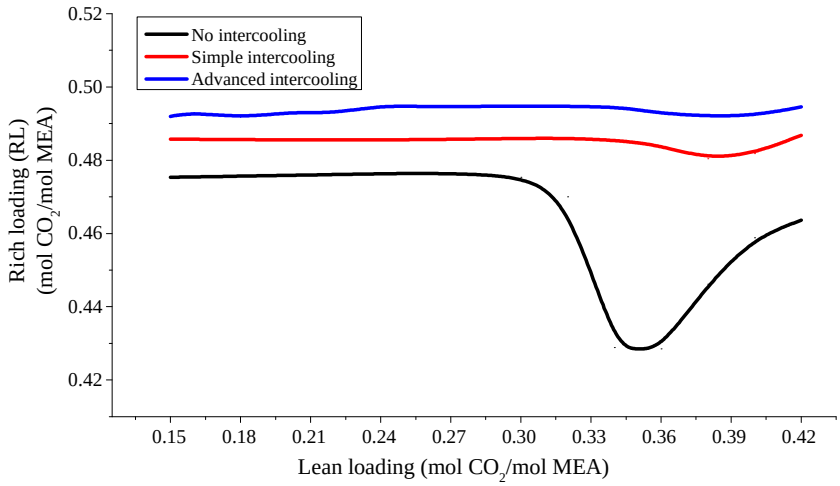

Figure 7-18. Variation of rich solvent loading with lean loading for an absorber with no intercooling (black), with simple intercooling (red) and with advanced intercooling with the recycle rate of $3xL_{min}$ (blue) when using minimum liquid to gas ratio (L_{min}/G)

By considering Figures 7-6, 7-7 and 7-18 together, following results can be concluded:

- At lean loading up to 0.30, the rich loading curve of the absorber with no intercooling is fairly constant with a steady increase of L_{min}/G with lean loading. Using both simple and advanced intercooling slightly uplift the rich loading curve by 2.0 and 3.8 %, respectively, with no noticeable changes in their L_{min}/G curves. At this lean loading range, in all these three options the temperature bulges occur at the column top confirming the effect of using absorber intercooling to be negligible on the mass transfer efficiency and solvent absorption capacity.
- At lean loading from 0.30 to 0.36, a noticeable decline in the rich loading accompanied with a considerable increase in the L_{min}/G were observed in curves of the absorber with no intercooling case. Predictably, this region matches with the lean loading range at which the temperature bulges occur somewhere in the middle of the column. The difference between the L_{min}/G of non-intercooled and intercooled counterparts (for both simple and advanced cases) widens as the critical lean

loading. The significant reduction in the L_{min}/G and remarkable improvement in the rich loading observed in curves related to the simple and advanced intercooling confirm the effectiveness of using intercooling at this lean loading range. Employing simple and advanced intercooling at critical lean loading is associated with 42.0 and 45.6 % reduction in L_{min}/G, respectively, and 12.4 and 14.5 increase in rich loading, respectively.

- At lean loading higher than 0.36, a gradual increase in the rich loading curve with lean loading in the absorber with no intercooling is observed coincided with a sharp rise in the L_{min}/G curve. This region relates with the lean loadings at which the location of temperature bulge is at the bottom of the column. The increase in the L_{min}/G is relatively because of the limited capacity of the lean solvent due to its relatively high initial CO_2 loading.

As shown in Figure 7-18, the increase in rich loading after using simple or advanced intercooling confirms that intercooling in general allows the absorber column to have a closer approach to equilibrium. Furthermore, the increase in rich loading coincides with another advantage of using intercooling, which is less lean solvent flow rate is required compared to that of a column with no intercooling to achieve 90 % CO_2 removal rate for a given lean loading. The rich loading curves related to both simple and advanced intercooling show reasonably steady trend throughout the lean loading range. This is another advantage of using absorber intercooling as the absorber column can operate at higher lean loading and reach a fixed rich loading at the absorber bottom, at the expense of higher solvent flow rate. The benefit of operating an absorber column with intercooler at higher lean loading should be realised by evaluating its energy requirement for solvent regeneration. This will be discussed in following sections.

7.4. Application of Absorber Intercooling with 1.2xL_{min}

As described in previous sections, the lean loading range at which the use of simple and advanced intercooling is beneficial is approximately from 0.30 to 0.38 based on the minimum liquid flow rate (L_{min}) concept. The minimum liquid flow rate to achieve 90 % CO_2 removal rate is determined based on an infinity packing volume, which is not a practical design in terms of plant economics. The optimisation of liquid to gas ratio in terms of plant economics suggests the molar L/G should be about 1.2 to 1.5 times its minimum value in order to avoid using excessive amount of packing (5). Therefore, to properly evaluate the benefits of using absorber intercooling for this range of lean loading in terms of overall energy requirement, the solvent flow rate was set to 1.2 times the minimum liquid solvent flow rate. Based on the new solvent flow rate, the absorber packing dimensions, i.e. each section height and diameter, were optimised.

7.4.1. Effect of Absorber intercooling on Absorber Packing Area with 1.2xL_{min}

Based on the new solvent flow rate, i.e. 1.2xLmin, the packed column dimensions, i.e. height and diameter, of the absorber with no intercooling, with simple intercooling and with advanced intercooling were optimised. Diameters were determined to provide a 75 % fractional approach to flooding, and heights were optimised to satisfy 90 % CO_2 removal ate. Table 7-2 summarises heights and diameters of the three cases for the range of lean loading from 0.30 to 0.38. It is worth to note that columns were comprised of one, two and three packed sections, respectively, absorbers with no intercooling, with simple intercooling and with advanced intercooling.

Table 7-2. Optimised heights (H) and diameters (D) of the three cases for lean loading range of 0.30 - 0.38

Lean loading (mol CO_2/mol MEA)	Absorber without intercooling	Absorber with simple intercooling	Absorber with advanced intercooling
0.30	H=13.6 m, D=16.1 m	Section#1 (H=10.2 m, D=15.9 m) Section#2 (H=3.0 m, D=15.4 m)	Section#1 (H=10 m, D=15.8 m) Section#2 (H=2.3 m, D=14.8 m) Section#3 (H=3.0 m, D=15.4 m)
0.32	H=16.7 m, D=16.4 m	Section#1 (H=10.9 m, D=16.0 m) Section#2 (H=4.0 m, D=15.6 m)	Section#1 (H=10.0 m, D=15.9 m) Section#2 (H=1.1 m, D=15.0 m) Section#3 (H=5.0 m, D=15.5 m)
0.34	H=20.4 m, D=17.6 m	Section#1 (H=10.4 m, D=16.0 m) Section#2 (H=7.0 m, D=15.8 m)	Section#1 (H=10.0 m, D=16.0 m) Section#2 (H=1.7 m, D=15.3 m) Section#3 (H=8.0 m, D=15.7 m)
0.35	H=11.8 m, D=16.8 m	Section#1 (H=11.1 m, D=16.1 m) Section#2 (H=8.0 m, D=15.9 m)	Section#1 (H=11.0 m, D=16.0 m) Section#2 (H=2.0 m, D=15.4 m) Section#3 (H=8.5 m, D=15.9 m)
0.36	H=11.9 m, D=16.9 m	Section#1 (H=11.2 m, D=16.0 m) Section#2 (H=10 m, D=16.1 m)	Section#1 (H=11.0 m, D=16.0 m) Section#2 (H=3.6 m, D=15.6 m) Section#3 (H=9 m, D=16.0 m)
0.38	H=13.7 m, D=17.0 m	Section#1 (H=12.6 m, D=16.1 m) Section#2 (H=8.0 m, D=16.5 m)	Section#1 (H=12.0 m, D=16.0 m) Section#2 (H=7.3 m, D=15.8 m) Section#3 (H=8.0 m, D=16.3 m)

Figure 7-19 shows the required packing area per unit of CO_2 removed (mole/s) to achieve 90 % CO_2 removal rate in an absorber with no intercooling, with simple intercooling, and with advanced intercooling, when using $1.2xL_{min}$ as the solvent flow rates. The required packing area is calculated by multiplying the volume of packing by the specific surface area of the packing which is a geometrical characteristic of the packing material. For the Sulzer Mellapak 250Y and 125Y, the specific surface area is 250 and 125 square metre per volume of packing, respectively (4). For all cases, the volume of packing is calculated based on specifying the fractional approach to flooding to 75 % to determine the diameter, and optimising the height of packing to achieve the 90 % CO_2 removal rate.

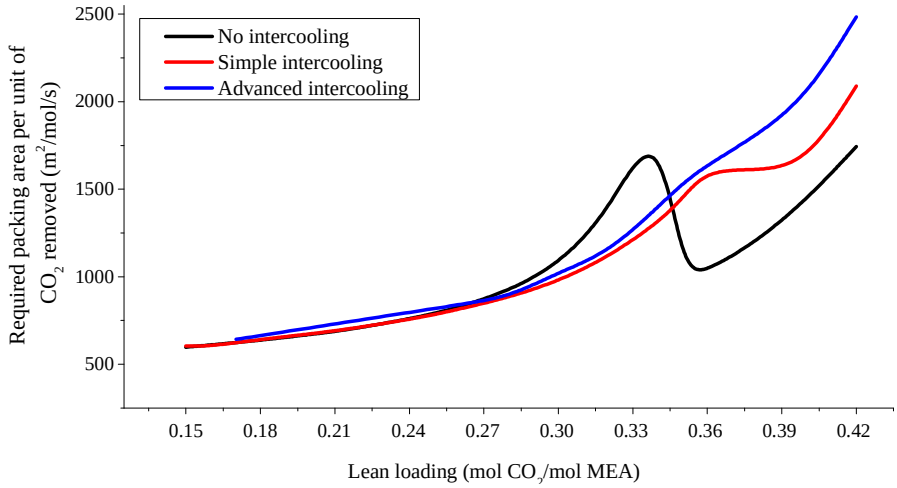

Figure 7-19. Required packing area per unit of CO_2 removed for an absorber with no intercooling (black), with simple intercooling (red), and with advanced intercooling with the recycle rate of 3xL (blue) for a range of lean loading

As shown, the benefit of using simple and advanced intercooling in terms of packing requirements, for 90 % CO_2 removal rate, was only observed for the lean loading range of 0.28 to 0.34. Maximum benefits in terms of absorber packing area was realised at the lean loading of 0.34 with nearly 30.4 and 25.6 % reduction for simple and advanced intercooling, respectively. This range of loading is partially related to the range that earlier confirmed the potential effectiveness of incorporating intercooling in terms of solvent absorption capacity. For the lean loading range of 0.28 to 0.34, the use of advanced intercooling is on average associated with 3.8 % more packing area requirements compared to that when simple intercooling was used.

As observed previously, at lean loadings of 0.35 and above, using absorber intercooling provides significant reduction in the required solvent flow rate and therefore L/G. As shown in Figure 7-19, to achieve these benefits additional packing area is required. In fact, this additional packing area should be spent to reach a higher rich loading at the bottom of the absorber column, as shown in Figure 7-18, when using simple and advanced intercooling. At lean loading 0.36, the use of simple and advanced intercooling, respectively, results in 43 % and 46.8 % reduction in the molar liquid to gas ratio which is associated with, 60 % and 62.2

% increase in the absorber required packing area, respectively. At lean loading below 0.30 the use of absorber intercooling does not change the packing requirement.

7.4.2. Effect of Absorber Intercooling on Total Equivalent Work

Figure 7-20 shows the total equivalent work for a CO_2 capture process with and without absorber intercooling for the range of lean loadings. The compression equivalent work was constant across all cases as the stripper pressure was kept at 17 kPa (1.7 bar). For cases with absorber intercooling (both simple and advanced intercooling cases), the pump equivalent work includes the work required to pump the solvent from the middle of the absorber column to the external cooler and back to the column, in addition to the work required to circulate the solvent through the process.

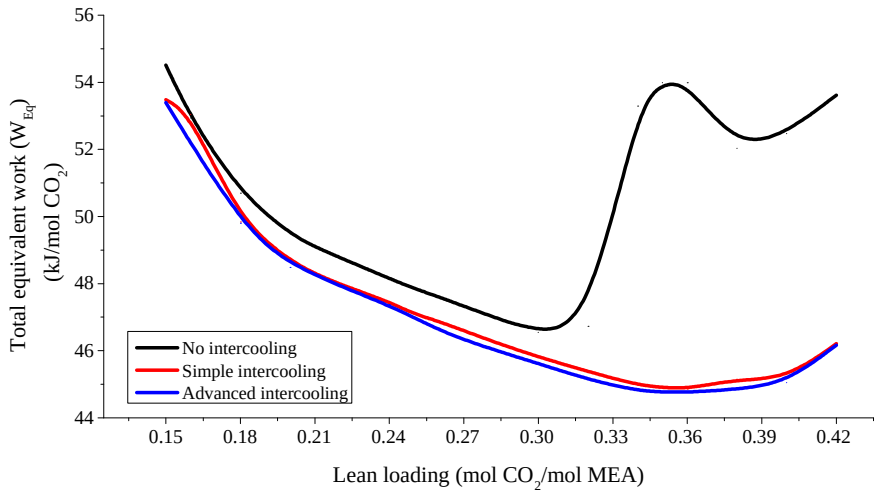

Figure 7-20. Calculated total equivalent work for an absorber with no intercooling (black), with simple intercooling (red), and with advanced intercooling with the recycle rate of 3xL (blue) for a range of lean loading

As shown, the use of absorber intercooling has a positive effect on the total equivalent work especially at lean loading higher than 0.30. By taking Figures 7-6, 7-19, and 7-20 into consideration, it can be realised that the use of absorber intercooling for the lean loading range from 0.30 to 0.34 is associated with reduction in the required solvent flow rate, the required packing area in absorber column and the total equivalent work. These results suggests the lean loading range at which the application of absorber intercooling is

significant and promising is from 0.30 to 0.34 for natural gas fired applications when using an aqueous solution of 30 wt. % MEA as solvent.

at lean loading higher than 0.34, the benefits of incorporating absorber intercooling are a trade-off between benefits in terms of solvent flow rate and total energy requirement, and drawbacks of excess packing area in the absorber column. For instance, according to Figure 7-20 the highest energy saving was realised at the lean loading of 0.36 for nearly 16.9 and 17.1 % by using simple and advanced intercooling, respectively. These reductions respectively are associated with nearly 56.2 and 56.9 % increase in the required packing area in absorber column.

7.5. Conclusions & Remarks

The benefits of using two absorber intercooling configurations in the CO_2 capture unit using an aqueous solution of 30 wt. % MEA as solvent to remove 90 % CO_2 from natural gas fired flue gases for a range of lean loadings from 0.15 to 0.42 were studied. The effect of intercooling on the temperature bulge, liquid flow rate, L/G, rich solvent loading, and solvent absorption capacity were evaluated using the minimum solvent flow rate concept. Benefits of using absorber intercooling in terms of absorber packing area and overall energy requirement were quantified using 1.2 times the minimum solvent flow rate. The total equivalent work concept was used to evaluate the plant overall energy requirement.

In absorbers without intercooling with solvents with lean loading below 0.30, temperature bulges occurred near the top of the column and away from the equilibrium pinch at the rich-end of the column, suggesting the benefit of using absorber intercooling in terms of CO_2 mass transfer and solvent absorption capacity is insignificant. Minor differences in L_{min}/G ratios before and after using simple and advanced intercooling confirmed their minor benefits in this region. The plant overall energy study also showed minor gain in terms of total equivalent work which was associated with a slight increase in absorber total packing area when using simple or advanced intercooling.

At lean loading between 0.30 and 0.36, a remarkable increase in L_{min}/G, followed by a sharp reduction in rich solvent loading were observed in absorbers with no intercooling. At this range of loading, the temperature bulge was positioned somewhere around the middle of the column. Applying simple and advanced absorber intercooling showed significant improvement on both L_{min}/G and rich loading. Studying the packing requirements and energy requirements confirmed the effectiveness of using absorber intercooling in this range. For lean loadings between 0.30 and 0.34, using simple and advanced absorber intercooling will reduce both absorber packing requirements and the plant overall energy requirements. For instance, using simple and advanced absorber intercooling at the lean loading of 0.34 benefited the process by reducing the absorber packing area by nearly 32.0 and 36.6 %, respectively, accompanied by a reduction in the total equivalent work by 15.6 and 15.9 %, respectively.

At lean loading equal to and higher than 0.36, the use of absorber intercooling had positive effects on L_{min}/G and rich loading curves resulting in significant reduction in the plant overall energy requirement in terms of total equivalent work. However, these benefits are associated with the expense of requiring an excessive amount of packing in the absorber packed column.

At lean loading higher than and equal to 0.36, the use of simple and advanced intercooling showed positive effects on L/G and rich solvent loading resulting in significant reduction in the plant overall energy requirement in terms of total equivalent work. At this lean loading range, additional packing area should be provided in the absorber column to allow the increase in the rich solvent CO2 loading at the bottom of the absorber. At 0.36, the use of simple and advanced intercooling is associated with 43 % and 46.8 % reduction on the molar L/G with 60 % and 62.2 % increase in the absorber packing area, respectively.

These findings can be used as a guideline for future application of absorber intercooling for commercial scale natural gas fired flue gas applications (3-5 % mole CO_2 concentration) when using an aqueous solution of 30 wt. % MEA as solvent.

7.6. List of References

(1) Thompson, R.; King, C.J. Energy Conservation in Regenerated Chemical Absorption Processes. *Chemical Engineering and Processing* **1987**, 21, 115-129,

(2) Plaza

(3) Coker, A. K. *Ludwig's Applied Process Design for Chemical and Petrochemical Plants*4th edition. Vol. 2.Gulf Professional Publishing, 2010.

(3) Sulzer Chemtech. *Structured Packings for distillation, absorption and reactive distillation*. Sulzer Chemtech Ltd. Switzerland, 2015.

(4) Perry, R.H.; Green, D.W. *Perry's Chemical Engineers' Handbook*. 8th edition", McGraw-Hill, New York, 2008.

(5) Kvamsdal, H .M.; Rochelle, G. T. Effects of the Temperature Bulge in CO_2 Absorption from Flue Gas by Aqueous Monoethanolamine. *Industrial & Engineering Chemistry Research* **2008**, 47, 867-875.

(6) Kohl, A.; Nielsen, R. *Gas Purification, 5th edition*. Gulf Publishing Company, 1997.

Chapter 8

Advanced Stripper Configurations

This chapter aims to evaluate energy improvements offered by two complex stripper configurations, i.e. advanced reboiled stripper and advanced flash stripper, for natural gas fired applications when using an aqueous solution of 30 wt. % MEA as solvent for a range of lean loading from 0.15 to 0.38 (mol CO_2/mol MEA) with 90 % CO_2 removal rate. The conventional stripping system modelled for the 650 MW combined cycle power plant application as described in Chapter 6 was used as the baseline case to compare the benefits of the advanced configurations. The process description, modelling specifications, and energy performance of advanced stripper configurations and their bypass rate optimisations in proportion to the total rich solvent flow rate for the range of lean loading are described in this chapter.

8.1. Introduction

In a post-combustion CO_2 capture (PCC) process, there are two major energy requirements: electricity to operate the multi-stage compression train to pressurise the produced CO_2, e.g. up to 15 MPa (150 bar) for transport and storage, and energy required in the stripper column in form of heat for solvent regeneration. The energy required for solvent regeneration accounts for more than 60 % of the total energy required by the PCC process and is usually provided as low pressure steam from the power plant steam cycle (1). Studies have shown that the addition of an amine-based CO_2 capture plant to a natural gas combined cycle power plant leads to a net power plant efficiency penalty of 7-11 % (2,3).

The conventional solvent regeneration process is a simple stripper, with a significant loss of exergy as water is condensed from the CO_2-rich product stream (4,5). This process can be replaced by a more complex process which provides better performance. Fundamental

research has shown the benefit of reducing driving forces in a chemical process by adding complexity to its system. In a chemical process, driving forces for heat transfer (temperature), mass transfer, and chemical reaction (4,5) generally result in thermodynamic irreversibility, by which the process consumes more energy than is ideally required (5,6). However, a chemical process with reasonable capital cost must have finite driving forces to expend some thermodynamic availability (exergy) and consume more energy compared to an ideal process. Reducing the process driving forces if applied properly will provide energy savings for the process. However, an excessively small driving force, like an excessively large driving force is harmful for the commercial viability of the process, as it leads to excessive capital cost investment (6,7). Typical stripper columns have very large driving forces in several locations. A stripper column with optimised conditions has large driving forces in the reboiler and bottom section of the packed column and pinches at the top (8). When the rich-end pinches, the driving force at the lean-end is excessively large, causing a loss of available work (4). Introducing more complexity to the process by means of splits, recycles, and multi-pressure stages can reduce the existing driving forces to cut down on total exergy losses (6).

Complex configurations with the objective of reducing the solvent regeneration energy requirements were studied using MEA solvents and have shown promising performance such as matrix stripper, inter-heated stripper, flashed-feed stripper, multi-pressure stripper, vapour recompression system, and multi-pressure stripper with vapour recompression (8,9). Comprehensive cost analysis of these configurations has also demonstrated the superiority of advanced configurations (Karimi et al., 2011=10).

Recently, Lin et al. (11) developed two advanced configurations incorporating thermal integration based on excess regeneration heat and rich solvent split flow, and studied the improvement brought by these modifications for 8 m piperazine (PZ) and 9 m MEA (equivalent of 40 wt. % MEA), and showed that the proposed configurations provide 10 % less equivalent work for 8 m PZ and 6 % for 9 m MEA when compared to a simple stripper

for arbitrarily-chosen rich and lean loadings, i.e. arbitrary CO_2 removal rates, and arbitrary cold-rich bypass rate. The advanced flash stripper proposed by Lin was successfully tested with 5 m PZ in a 0.1 MW pilot plant (12).

The present study aims to evaluate energy improvements offered by the two advanced configurations proposed earlier by Lin et al. (11) for natural gas fired applications when using an aqueous solution of 30 wt. % MEA as solvent for a range of lean loading from 0.15 to 0.38. This study is more comprehensive and advanced compared to the realiser study conducted by Lin et al. for two reasons. First, the degree of regeneration, i.e., the difference between the solvent rich and lean loading across the stripper column for a given lean loading, represents a realistic value corresponding to 90 % CO_2 capture, which is obtained by simulating the absorber column simultaneously, and second, for each lean loading the cold- and warm-rich bypass rates were optimised as a proportion to the total rich solvent flow rate. The description of these two advanced configurations and the methodology used to simulate and quantify their benefits in terms of regeneration energy requirements are described in the following sections.

8.2. Advanced Stripper Configurations

The base case of this study uses a simple stripper as shown in Figure 8-1. The rich solvent enters the stripper at the top after being pre-heated in the lean/rich cross heat exchanger by the hot lean solvent leaving the stripper column at the bottom. The heat exchanger was modelled with rich side flashing and 5 °C LMTD. In the stripper column, the energy required for the solvent regeneration is provided by the reboiler. The regenerated lean solvent returns to the absorber column through the lean/rich cross heat exchanger. The product vapour leaves the column from the top and after being cooled to 40 °C in the overhead condenser is fed to a multi-stage compressor train. The product vapour cooling at the overhead condenser is associated with a loss of latent heat of its excess water vapour.

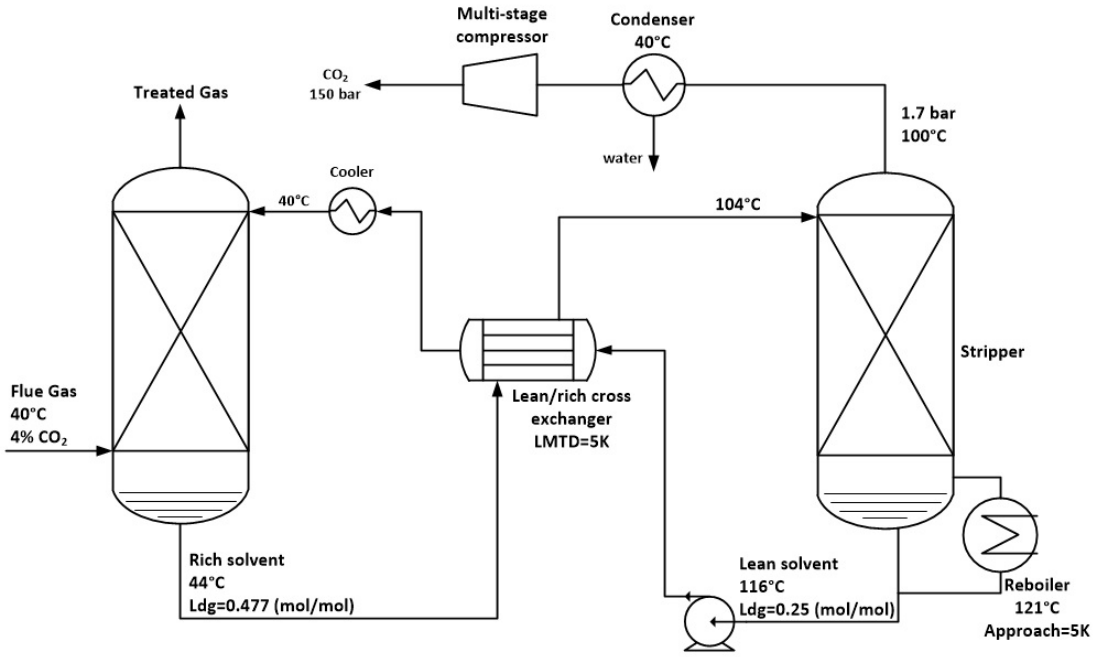

Figure 8-1. The CO_2 capture process with simple stripper for the solvent lean loading of 0.25.

8.2.1. Advanced Reboiled Stripper

Figure 8-2 shows the advanced reboiled stripper with cold rich bypass and warm rich bypass. This configuration is an advanced version of a simple stripper that includes a heat recovery of the latent heat available in the product vapour by the cold rich solvent. In this configuration, the cold rich solvent splits into two streams downstream of the absorber column. One split bypasses the lean/rich cross heat exchanger and enters the cold rich bypass heat exchanger, to partially recover the latent heat available in the product vapour exiting the system. The product vapour usually contains more than 50 % water vapour.

The second stream enters the lean/rich cross heat exchanger and recovers the heat available in the lean solvent leaving the stripper column. Subsequently, a portion of this stream splits further into two streams, and one stream is drawn from the cross heat exchanger at its bubble point (bp) and mixed with the preheated, bypassed rich solvent before entering the stripper column at the top. The remainder of the warm rich solvent heats further up in the cross heat exchanger before entering the stripper column in the middle. The temperature of this stream

is usually higher than the bubble point. Using this arrangement is expected to be more efficient than the conventional practice since it avoids inevitable flashing of the rich solvent at the top of the stripper column due to recovering all the heat available in the hot lean solvent at once at the lean/rich cross exchanger. Using the additional heat exchanger will therefore balance the heat transfer more efficiently and reversibly by making smaller heat transfer driving force between the rich solvent and the product vapour at the top of the column.

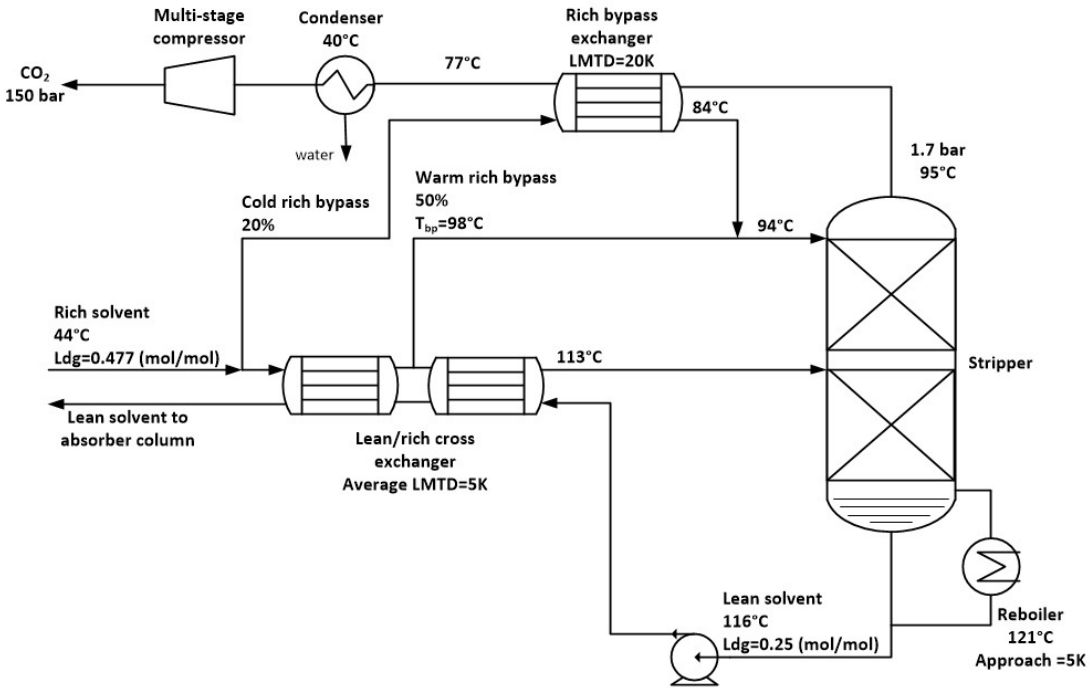

Figure 8-2. The advanced reboiled stripper for the lean solvent loading of 0.25.

8.2.2. Advanced Flash Stripper

Figure 8-3 shows the flowsheet of the advanced flash stripper. This configuration is similar to that of the advanced reboiled stripper, except the reboiler is replaced by a convective steam heater and a flash in the sump of the stripper. In this configuration, one split of the rich solvent downstream of the absorber column bypasses the lean/rich cross heat exchanger and preheats by the hot product vapour exiting the stripper column at the top. The rest of the rich

solvent preheats in the cross heat exchanger, where a portion of it, at its bubble point, is drawn to mix with the preheated cold rich bypass, prior to entering the stripper at the top. The rest of the boiling rich solvent is further heated in the cross heat exchanger before entering the steam heater. The hot flashing rich solvent is then fed into a flash vessel from the bottom where the flashed vapour counter-currently contacts the rich solvent. Since the convective steam heater has less solvent hold-up and residence time at elevated temperature, compared to a reboiler, it will minimise the solvent thermal degradation (11,14).

With respect to process specifications described earlier, the proportion of the cold rich and warm rich solvent flow rates at various lean loadings is subject to optimisation to quantify the highest energy savings offered by each advanced configuration.

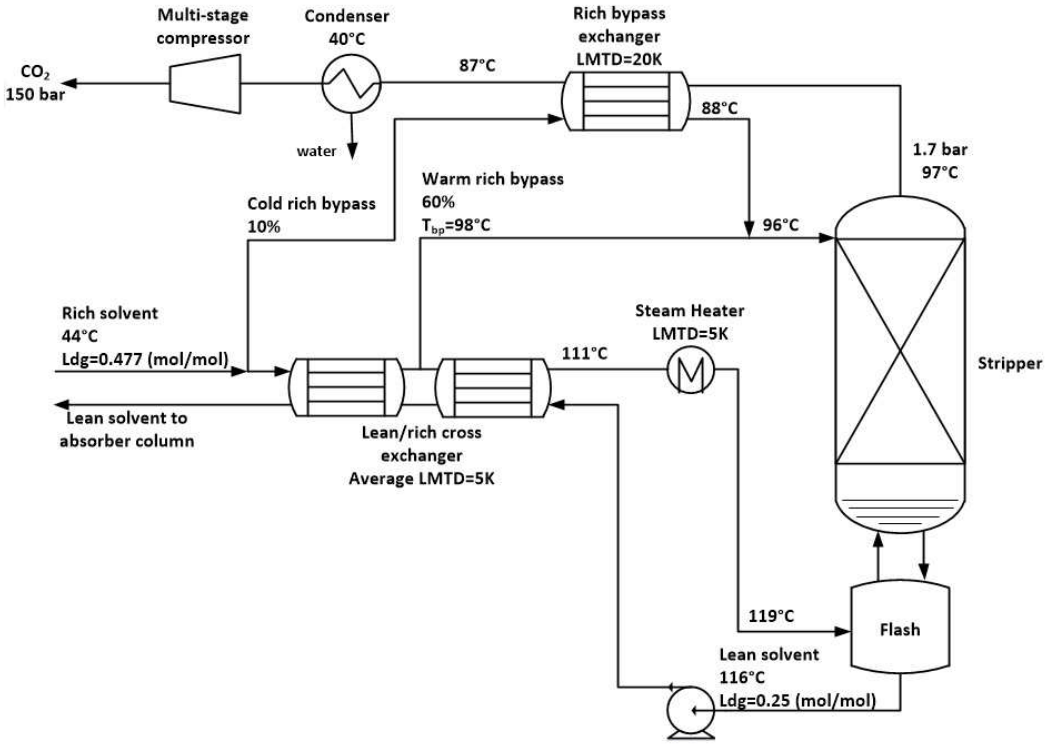

Figure 8-3. The advanced flash stripper for the lean solvent loading of 0.25

8.3. Process Specifications & Evaluations

8.3.1. Process Specifications

The standard CO_2 absorption/desorption process which was modelled and described in Section 6 for a 650 MW natural gas fired combined cycle power plant was used as the reference case to evaluate and quantify energy savings the advanced stripper configurations will offer for natural gas fired applications with 90 % CO_2 removal rate. The analysis started with simulating the CO_2 capture process for a range of lean loading from 0.15 to 0.38 with a fixed flue gas flow rate and compositions, as presented in Table 6-1, as a baseline for comparison against the advanced configurations.

Packed columns were all defined with Sulzer Mellapak 250Y structured packing. The column diameters were specified to give a 75 % approach to flooding. The height of packing was specified as 20 m for both the stripper and absorber, resulting in a pinch for all cases. This excess packing height should provide an accurate estimate of the relative energy use, but will underestimate the actual energy requirement. The stripper pressure was constant at 180 kPa (1.8 bar) for all configurations while lean loading and bottom temperature varied. Table 8-1 summarises the liquid to gas (L/G) ratio and the associated rich loading at the absorber discharge for a range of lean loading while maintain the CO2 removal rate at 90 % when the absorber column is fed with the flue gas described above.

Table 8-1. Predicted absorber and stripper performance (90 % CO_2 removal, with 20 m Sulzer Mellapak 250Y structured packing, solvent and flue gas fed to the absorber at 40 °C, 1.8 bar stripper pressure)

Lean loading (mol CO_2/mol MEA)	**L/G ratio (kg/kg)**	**Rich loading (mol CO_2/mol MEA)**	**Lean solvent temperature at stripper discharge (°C)**
0.15	0.80	0.475	118.5
0.18	0.89	0.476	118
0.20	0.96	0.476	117.5
0.21	1.00	0.476	117
0.25	1.18	0.477	116
0.30	1.53	0.477	114

0.32	1.79	0.471	113
0.36	3.87	0.431	110
0.38	4.14	0.446	109

For all cases, the overall log mean temperature difference (LMTD) of the lean/rich cross heat exchanger, was specified as 5 °C. The LMTD of the rich solvent bypass heat exchanger was set at 20°C. A 5 °C hot side approach was specified on the steam reboiler, and a 5 °C LMTD was specified for the convective steam heater. The process specifications used to simulate the various flow sheets are summarised in Table 8-2.

Table 8-2. Process design specifications used in process simulations

Design specifications	**Advanced Reboiled Stripper**	**Advanced Flash Stripper**
Process simulation tool	Aspen Plus V8.4	
Thermodynamic model	e-NRTL-RK	
Packing type	Sulzer Mellapak 250Y	
Absorber column packed height (m)	20	
Stripper column packed height (m)	20	
Lean/rich cross heat exchanger LMTD (°C)	5	
Cold rich bypass heat exchanger LMTD (°C)	20	
Reboiler approach temperature (°C)	5	-
Steam heater LMTD (°C)	-	5
Stripper pressure (bar)	1.8	

8.3.2. Process Evaluation

As in Chapter 5, the total equivalent work concept was used to evaluate and compare the energy requirement of the CO_2 capture process when using advanced stripper configurations at various lean loading. Eqs. 5-1 to 5-3 were used to determine the total equivalent work. Assumptions made for each equation are as described in Chapter 5, Section 5.3.1.

8.4. Comparison of Stripper Configurations & Discussions

8.4.1. Total Equivalent Work

Total equivalent work is an appropriate indicator to evaluate and compare the advanced configurations against each other and the base case. The calculated overall equivalent work was normalised by the moles of CO_2 removed. For a given lean loading, the optimum equivalent work was quantified by varying the cold and warm rich bypass flow rates. The optimum flow rates are given as their fraction of the total rich solvent flow for a given lean loading. Also, for each advanced configuration, there was an optimum lean loading at which the reduction in the total equivalent work is highest when compared to their respective base case. The total equivalent work of the simple stripper for the range of lean loading from 0.15 to 0.38 is summarised in Table 8-3. These values are the baseline values against which the advanced configurations are compared. For advanced flash and advanced reboiled configurations, the results of optimum cases with their cold and warm rich bypass flow fractions are summarised in Table 8-4 and 8-5, respectively. For each lean loading, the reported optimum cold rich and warm rich bypass fractions are the relative proportion of their flow rates to the total rich solvent flow rate in percentage.

Table 8-3. Performance of the simple stripper for 90 % capture for various lean loading

Lean Loading (mol CO_2/mol MEA)	Regeneration specific heat duty (kJ/mol CO_2)	$\boldsymbol{W_{heat}}$ (kJ/mol CO_2)	$\boldsymbol{W_{comp}}$ (kJ/mol CO_2)	$\boldsymbol{W_{eq}}$ (kJ/mol CO_2)
0.15	183.8	34.8	13.0	48.2
0.18	169.6	32	13.0	45.4
0.20	166.6	31.2	13.0	44.7
0.21	166	31	13.0	44.6
0.25	164.4	30.4	13.0	44.1
0.30	164	29.7	13.0	43.6
0.32	167.2	30	13.0	44.0
0.36	205.3	35.8	13.0	51.1
0.38	197.3	33.8	13.0	49.3

Table 8-4. Optimum results for the advanced flash stripper for 90 % capture rate for various lean loading

Lean Loading (mol CO_2/mol MEA)	Cold rich bypass (%)	Warm rich bypass (%)	Specific heat duty (kJ/mol CO_2)	$\mathbf{W_{heat}}$ (kJ/mol CO_2)	$\mathbf{W_{comp}}$ (kJ/mol CO_2)	$\mathbf{W_{eq}}$ (kJ/mol CO_2)
0.18	10	75	160.1	34.4	13.0	47.9
0.20	20	60	151.9	29.2	13.0	42.7
0.21	30	50	143.4	27.4	13.0	40.9
0.25	10	60	138.0	25.5	13.0	39.2
0.30	15	35	136.1	24.3	13.0	38.2
0.32	10	35	140.9	24.9	13.0	39.0
0.36	10	15	182.0	31.3	13.0	46.6
0.38	10	10	178.1	30.1	13.0	45.6

Table 8-5. Optimum results for the advanced reboiled stripper for 90 % capture for various lean loading

Lean Loading (mol CO_2/mol MEA)	Cold rich bypass (%)	Warm rich bypass (%)	Specific heat duty (kJ/mol CO_2)	$\mathbf{W_{heat}}$ (kJ/mol CO_2)	$\mathbf{W_{comp}}$ (kJ/mol CO_2)	$\mathbf{W_{eq}}$ (kJ/mol CO_2)
0.15	35	50	170.6	32.3	13.0	45.7
0.18	30	55	148.3	27.9	13.0	41.4
0.20	30	50	143.3	26.9	13.0	40.4
0.21	30	50	140.3	26.2	13.0	39.8
0.25	20	50	136.6	25.3	13.0	39.0
0.30	20	35	139.7	25.3	13.0	39.2
0.32	20	30	147.7	26.5	13.0	40.5
0.36	15	10	190.0	33.1	13.0	48.5
0.38	13	12	185.5	31.8	13.0	47.3

As shown in Table 8-4, the results for the advanced flash stripper at the lean loading of 0.15 could not be obtained because the optimum theoretically occurs when the total bypass exceeds 85 % of the total rich solvent flow. This means that the total heat required for the solvent regeneration should be provided by the remaining rich solvent flow (i.e. less than 15 % of the total rich solvent flow), resulting in a significant rise in the rich solvent temperature after the convective steam heater (i.e. more than 180 °C). This temperature is excessive and would result in thermal degradation of the amine. In principle, for the convective steam heater, the highest acceptable operating temperature with respect to the solvent thermal degradation is 135-140 °C, while, for the reboiler application this limit is 120-125°C. The

calculated results show that the lean loading of 0.18 is the limit for the advanced flash stripper, as at this loading the rich solvent temperature after the steam heater is 138° C. Although at this loading the regeneration specific heat duty of the advanced flash stripper is smaller than that of the simple stripper, however, from the total equivalent work point of view, at this loading the advanced flash stripper offers no energy savings. In fact, the total equivalent work of the advanced flash stripper is nearly 6 % higher than that of the simple stripper. This finding offers another limit than the solvent thermal degradation for the applicability of the advanced flash stripper. From the total equivalent work viewpoint, the lowest lean loading at which the advanced flash stripper is capable of providing energy savings in terms of overall equivalent work is 0.20.

Figure 8-4 and 8-5 present graphically the regeneration specific heat duty and the total equivalent work of the advanced configurations and a comparison to the simple stripper.

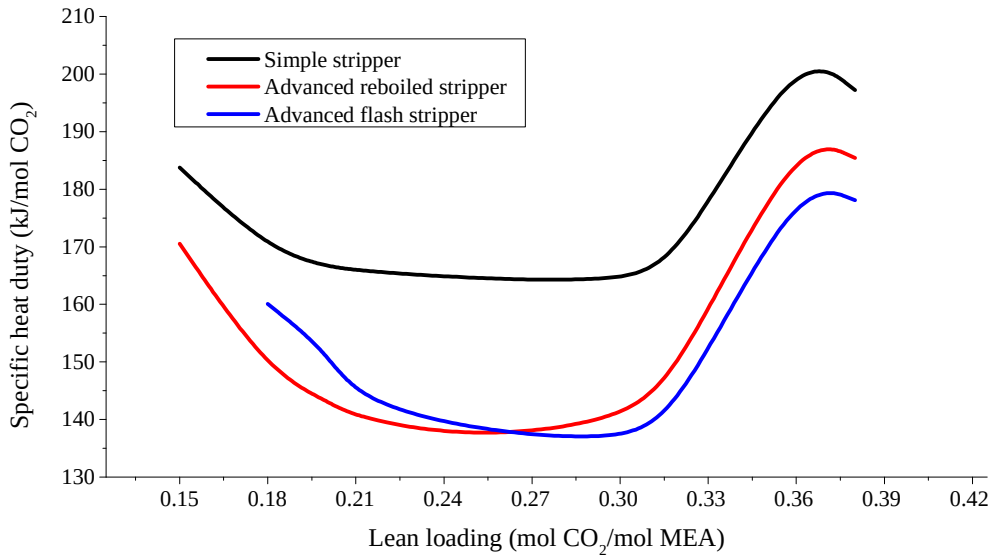

Figure 8-4. Comparison of the regeneration specific heat duty of advanced configurations for a range of lean loading.

Adding complexity improves the stripper energy requirements. The advanced reboiled stripper requires 6 to 16.9 % less heat duty than the simple stripper, which is 4.1 to 11.7 % less total equivalent work, where the lean loading associated with the highest and lowest

improvements is 0.25 and 0.38, respectively. Likewise, for the advanced flash stripper, the improvement in specific heat duty varies from 8.8 to 17 %, and in total equivalent work varies from 4.4 to 12.4 % at the lean loading of 0.30 and 0.20, respectively.

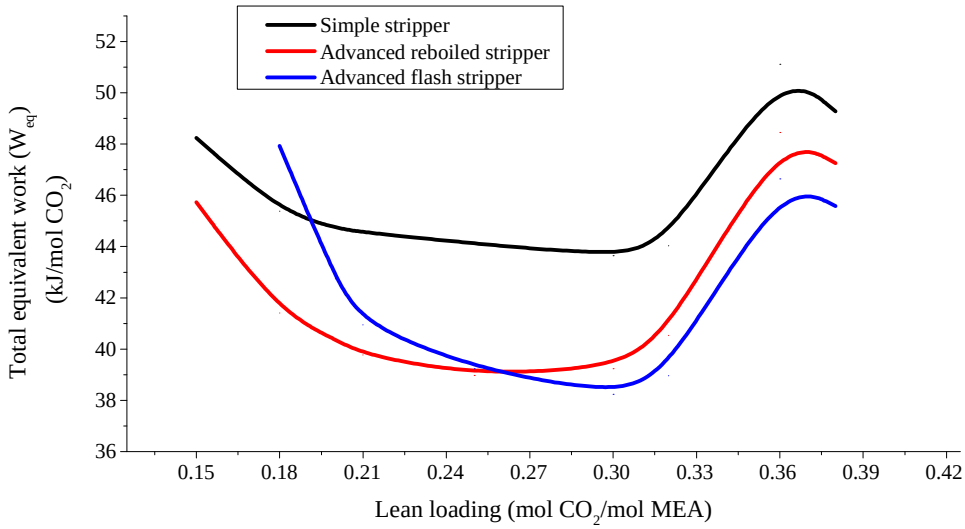

Figure 8-5. Comparison of the total equivalent work (Weq) of advanced configurations for a range of lean loading, CO_2 compression to 150 bar

At low lean loading, i.e. below 0.25, the performance of the advanced reboiled stripper is better than the advanced flash stripper. However, at higher lean loading, the trend reverses and the advanced flash stripper provides greater improvement, to the point that at the lean loading of 0.38, the improvement provided by the advanced flash stripper is almost double that of the advanced reboiled stripper.

One reason for this change might be correlated with the steam temperature. For the advanced reboiled stripper, the temperature of steam is identical to that of the simple stripper as both configurations employ the reboiler to provide the heat required for solvent regeneration with a 5 °C steam side approach temperature. However in the advanced flash stripper, the reboiler is replaced by a convective steam heater, by which the heat required for regeneration is provided by steam using a 5 °C LMTD. This difference resulted in different steam temperature used at each configuration. Figure 8-6 shows the temperature of steam used in the advanced reboiled and advanced flash strippers at optimum cases, and the relation to the

solvent temperature at the bottom of stripper column. As shown, at the lean loading of 0.25, the temperature of steam used at both advanced configurations is similar. At loading below 0.25, the steam temperature used at the advanced flash stripper is higher than that of the advanced reboiled stripper, whereas this trend reverses for lean loading higher than 0.25.

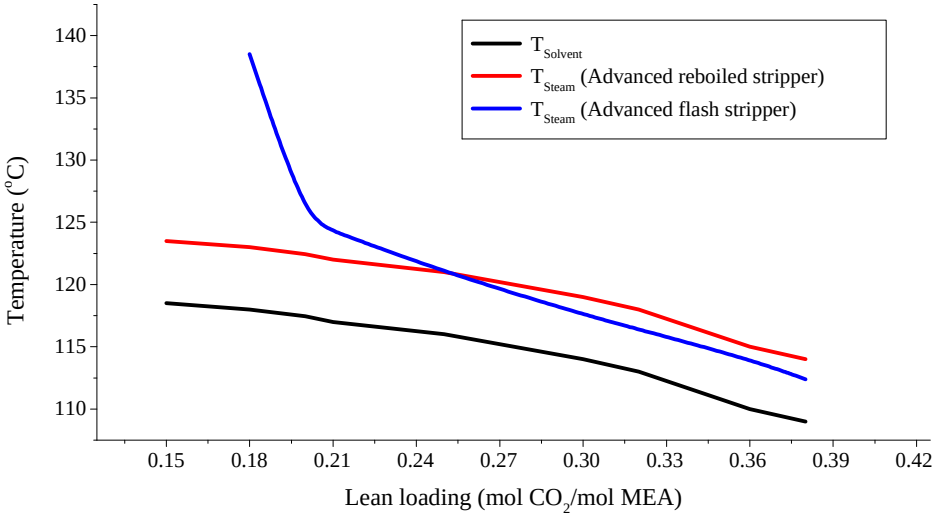

Figure 8-6. Comparison of steam and solvent temperatures for advanced configurations

8.4.2. Temperature Pinch

The stripper operation is frequently determined by a rich end pinch because of larger liquid to gas ratio at the top of the column relative to that at the bottom. In a simple stripper, when the pinch occurs at the rich end, the driving force at the lean end is excessively large with a loss of available work[4]. This condition is more pronounced at higher lean loading. In general, the stripping process is more reversible at lower lean loading since driving forces are to be relatively smaller at the lean end. Advanced reboiled and advanced flash stripper configurations were suggested to develop an equally distributed driving force through the column to reduce the energy required for regeneration and thus the total equivalent work.

To study the effectiveness of the advanced configurations on the stripper driving force, liquid and vapour temperature gradients through the stripper column at various lean loading were analysed and compared. The stripper column is comprised of 20 identical stages,

followed by a reboiler in the simple stripper and advanced reboiled stripper, or by a flash drum in the advanced flash stripper, as the stage 21. The temperature driving force is calculated by the difference between the temperature of the liquid stream leaving a stage (stage “n”) and the temperature of the vapour stream entering that stage, i.e. the temperature of the vapour stream leaving one stage below that stage (stage “n+1”).

Figures 8-7 to 8-9 show the temperature driving at each stage of the stripper packed column for simple, advanced reboiled and advanced flash stripper configurations at lean loading of 0.21, 0.25, and 0.30, respectively. For the simple stripper, the temperature driving force is more consistent at lean loading of 0.21 than that of 0.30. This confirms the stripping process in the simple stripper configuration is more reversible at low lean loading compared to higher lean loading. In this configuration, the pinch was observed at the rich end at various lean loading. As lean loading increases the area of pinch expands through the column height followed by extensively increasing temperature driving force at the lean end. For instance, the magnitude of the temperature driving force at stage 20 for lean loading of 0.30 is nearly three times higher than that of 0.21 causing excess energy requirement for solvent regeneration.

For the advanced reboiled stripper, regardless of lean loading, the column is pinched at the middle of the column where the second rich solvent feed enters. From this point, as the solvent flows downward the temperature driving force increases. Although in the advanced reboiled stripper, the magnitude of the temperature driving force at the lean end is similar to that of the simple stripper, the difference between the temperature driving force of the top and the bottom of the column is lesser than that of the simple stripper. The effect of the advanced reboiled stripper in terms of column driving force is shifting the pinch from the top of the column to the middle of the column.

As shown in Figures 8-7 to 8-9, the advanced flash stripper has the smallest temperature driving force at lean ends among the three configurations. This configuration shows a tendency to be also pinched at lean ends which is more evident at higher lean loading. For

instance, at 0.30 lean loading, the temperature driving force at the lean end is 0.6 °C, compared to 4.5 °C and 4.1 °C of the simple stripper and advanced reboiled stripper, respectively. Results suggest the effect of the advanced flash stripper on the column driving force is to form a pinch at the lean end, which contributes to improve the thermodynamic efficiency and lower the energy requirement for solvent regeneration. This finding is aligned with what was shown earlier that at 0.30 lean loading, the advanced flash stripper provides the highest improvement in terms of total equivalent work.

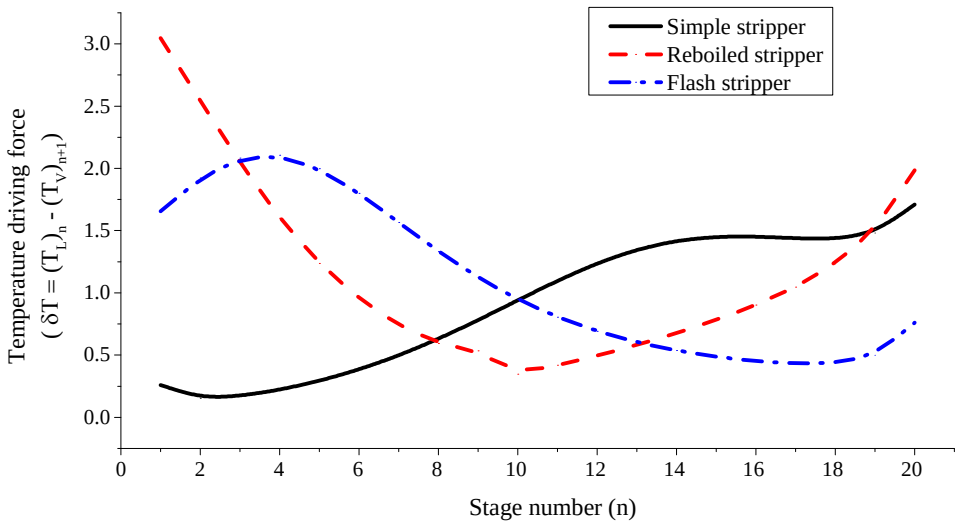

Figure 8-7. Temperature driving force at each stage for simple, advanced reboiled and advanced flash stripper at lean loading of 0.21 , (stripper packed column = 20 stages, stage 1 at the top of the column, stage 20 at the bottom of the column, ΔT= liquid temperature leaving stage (n) –vapour temperature leaving stage (n+1))

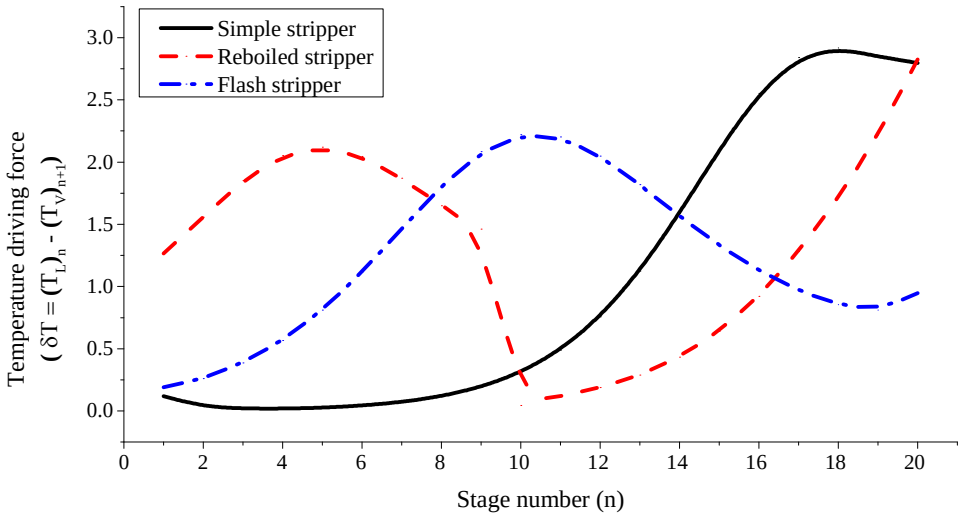

Figure 8-8. Temperature driving force at each stage for simple, advanced reboiled and advanced flash stripper at lean loading of 0.25, (stripper packed column = 20 stages, stage 1 at the top of the column, stage 20 at the bottom of the column, ΔT= liquid temperature leaving stage (n) –vapour temperature leaving stage (n+1))

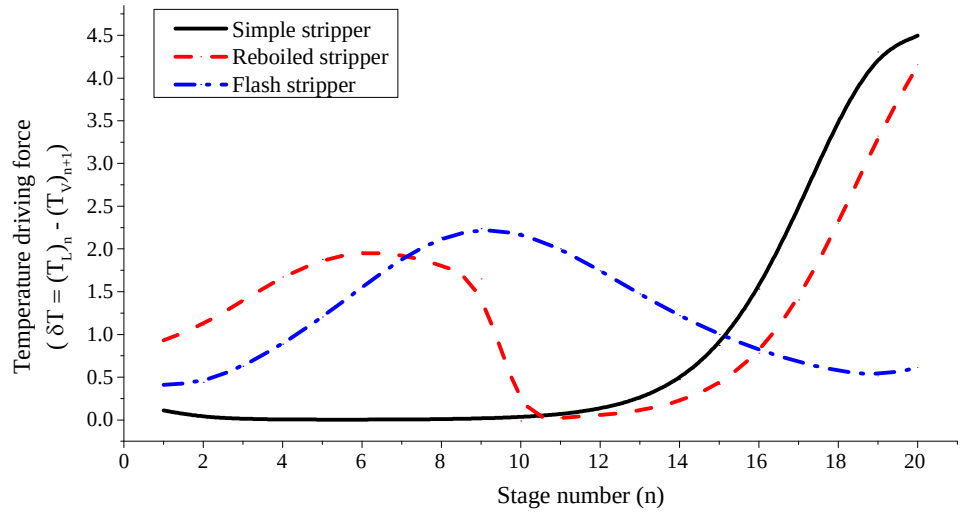

Figure 8-9. Liquid and vapour temperature driving forces at each stage for simple, advanced reboiled and advanced flash stripper at lean loading of 0.30, (stripper packed column = 20 stages, stage 1 at the top of the column, stage 20 at the bottom of the column, ΔT= liquid temperature leaving stage (n) – vapour temperature leaving stage (n+1))

8.4.3. Heat Recovery at Rich Bypass Heat Exchanger

In a simple stripper, the product vapour typically leaves the column containing 40-60 % water vapour (mole basis). This stream is cooled in a where the latent heat of the water

vapour is lost. In the advanced reboiled and flash stripper configurations, the latent heat of the water vapour is partially recovered by the cold rich bypass stream at the rich bypass heat exchanger contributing to improve the energy efficiency of the system. In fact, the rich bypass heat exchanger acts as a part of the overhead condenser where the cooling water is replaced by the cold rich bypass stream recovering the heat dissipated from the product vapour which would be otherwise wasted. Figure 8-10 shows the water vapour in the product vapour before and after the rich bypass heat exchanger of optimum cases of advanced reboiled and advanced flash strippers for a range of lean loading from 0.20 to 0.32. For comparison, the water vapour in the product vapour of the simple stripper before entering the overhead condenser is also shown.

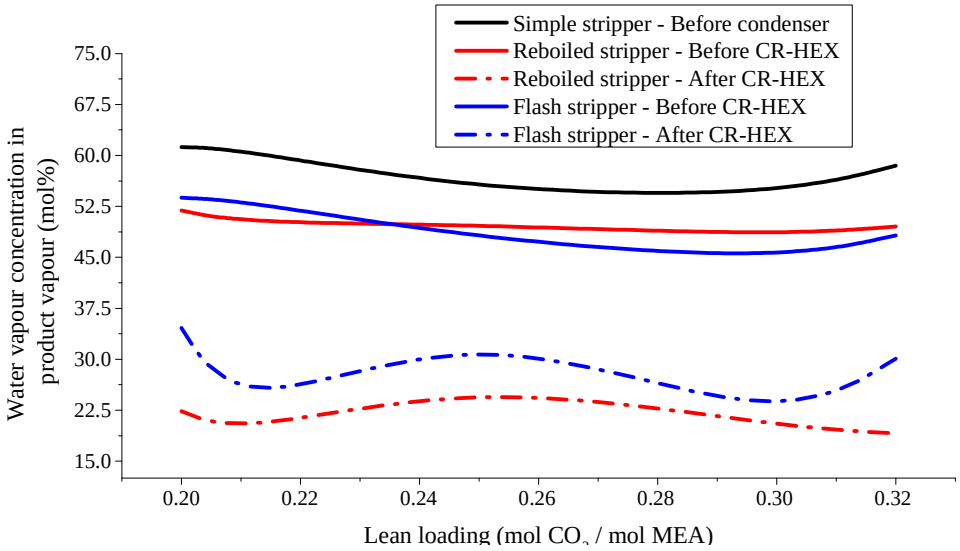

Figure 8-10. Water vapour concentration in the product vapour before and after cold rich heat exchanger (CR-HEX) of the optimum cases for simple, advanced reboiled and advanced flash strippers

The heat required for stripping is approximately the summation of three terms: the heat required to desorb the CO_2, the heat required to generate the water vapour at the top of the column, and the sensible heat required to increase the solvent temperature to the column temperature. According to Figure 8-10, in advanced configurations the water vapour content

in the product vapour is 9 to 18 % smaller than that of the simple stripper. This shows one of the positive contributions of advanced configurations on lowering the total heat requirement. In addition, the study showed the advanced stripper configurations contribute in lowering the plant total cooling water requirements. Table 8-6 summarises the reduction in the cooling water requirements (cooling water for the overhead condenser and the trim cooler) when using advanced reboiled and advanced flash strippers in relation to the simple stripper configuration.

The highest latent heat recovery in terms of the difference between the water vapour content before and after the rich bypass heat exchanger was observed at lean loading 0.25 for the advanced reboiled stripper and at 0.30 for the advanced flash stripper. These are the lean loading at which the corresponding advanced configurations offer the highest energy improvements in terms of total equivalent work. Furthermore, at lean loading 0.30 that the advanced flash stripper offers the highest energy savings, the water vapour content in the product vapour leaving the stripper column is the minimum amongst all optimum cases.

Table 8-6. Reduction in cooling water consumption in percentage when using advanced strippers in relation to the simple stripper configuration

Lean loading (mol CO_2/mol MEA)	**Advanced reboiled stripper**	**Advanced flash stripper**
0.18	19.2	3.8
0.20	23.1	15.4
0.21	30.4	26.8
0.25	17.4	17.4
0.30	20.0	20.0
0.32	16.7	23.3
0.36	1.6	4.8
0.38	3.2	6.3

The incremental capital cost to implement the advanced configurations should be small, so the energy saving should more than justify use of one of the advanced configurations. The reboiler or steam heater will cost less because it will have a reduced heat duty. The condenser is mostly replaced by the cold rich exchanger, which will have significantly less

heat duty than the condenser with the simple stripper. The cross exchanger will require two heat exchangers, but the total area will be about the same. The trim cooler will be larger. Additional piping and instrumentation will be required for the bypasses. Frailie (15) showed the purchase equipment cost of the advanced flash stripper with Piperazine (PZ) is smaller than the conventional stripper working with PZ and this is almost entirely due to the decrease in capital expenditure from using steam heater rather than reboiler.

The steam required for the advanced reboiled and advanced flash strippers will be extracted from the IP/LP cross over pipe at conditions similar to that of the simple stripper configuration, as both advanced configurations require steam at temperatures of 115-135 °C (with saturated pressures of 170-312 kPa) compared to 115-125 °C (with saturated pressure of 170-232 kPa) of the simple stripper configuration.

8.5. Conclusions & Remarks

The advanced reboiled and advanced flash stripper were evaluated with 7 m MEA to remove 90 % mole CO_2 from flue gases with 4 % CO_2, typical of a natural gas fired application, for a range of lean loading from 0.15 to 0.38. The energy efficiency improvement offered by the advanced configurations was evaluated and compared with that of a simple stripper configuration using the total equivalent work.

Simulation results confirmed both advanced configurations work equally well over the specified range of lean loading, except the advanced flash stripper fails to operate at lean loading below 0.18, as the solvent temperature at the steam heater outlet exceeds the solvent thermal degradation limit.

With lean loading from 0.21 to 0.32, the advanced reboiled stripper and flash stripper require an equivalent work of only 38 to 41 kJ/mol of CO_2 recovered, compared to 44-45 kJ/mol with the simple stripper. The regeneration heat duty was reduced 11 to 18 % to 136-148 kJ/mol of CO_2 recovered compared to 166-167 kJ/mol with the simple stripper. At lean loading of 0.30, the advanced flash stripper offers the highest reduction in the total

equivalent work of 12.4 %, and the highest reduction offered by the advanced reboiled stripper is 11.7 % at the lean loading of 0.25.

Simulations showed that the advanced flash stripper requires more equivalent work than the advanced reboiled stripper at lean loading less than 0.26 and more than the simple stripper at a lean loading less than 0.20, mainly due to the higher steam temperature required at those lean loading.

The variation of temperature driving force through the column showed that the advanced flash stripper tends to pinch at the lean end, opposed to the simple stripper which usually pinches at the rich end, contributing to enhance the thermodynamic efficiency of the stripping process and reducing the loss of work.

In both advanced reboiled and advanced flash stripper configurations, one contributor to improve the energy efficiency is less water vapour at the top of the column. In addition, both configurations contribute in lowering the plant cooling water requirement when compared with the plant with a simple stripper configuration.

8.6. List of References

(1) Freund, P.; Davison, J. *General Overview of costs for CCS*. Proceedings of the IPCC Workshop on CO_2 Capture and Storage, Regina Canada, Published by ECN, March **2003**, 79-94.

(2) Gottlicher G. *The Energetics of Carbon Dioxide Capture in Power Plants*. U.S. Department of Energy, National Energy Technology Laboratory, 2004.

(3) Page, S.C., Williamson, A.G., Mason, I.G., "Carbon capture and storage: fundamental thermodynamics and current technology. Energy Policy 2009 (37) 3314–3324.

(4) Oyenekan, B.A. *Modeling of strippers for CO_2 capture by aqueous amines*. PhD Dissertation, The University of Texas at Austin, 2007.

(5) Van Wagener, D.H. *Stripper Modeling for CO_2 Removal Using Monoethanolamine and Piperazine Solvents*. PhD Dissertation, The University of Texas at Austin, Austin, TX, 2011.

(6) Leites, I.L.; Sama, D.A.; Lior, N. The theory and practice of energy saving in the chemical industry: some methods for reducing thermodynamic irreversibility in chemical technology processes. *Energy* **2003**, 28, 55–97.

(7) Sama, D.A. *The use of the Second Law of thermodynamics in the design of heat exchangers, networks, and Processes*. Proceeding of the International Conference on Energy Systems and Ecology, ENSEC'93, **1993**, 1–24, Polish Ministry of National Education, Warsaw, Poland.

(8) Oyenekan, B.A.; Rochelle, G.T. Alternative stripper configurations for CO_2 capture by aqueous amines. *AIChE Journal* **2007**, 53 (12), 3144–3154.

(9) Jassim, M.S.; Rochelle, G.T. Innovative absorber/stripper configurations for CO_2 capture by aqueous monoethanolamine. *Ind. Eng. Chem. Res.* **2005**, 45 (8), 2465–2472.

(10) Karimi, M., Hillestad, M., & Svendsen, H. Capital costs and energy considerations of different alternative stripper configurations for post combustion CO_2 capture. *Chemical Engineering Research and Design* **2011** (89), 1229-1236.

(11) Lin, Y-J; Madan T.; Rochelle G.T. Regeneration with Rich Bypass of Aqueous Piperazine and Monoethanolamine for CO_2 Capture. *Ind. Eng. Chem. Res.* **2014**, 53, 4067-4074.

(12) Chen, E. *Pilot Plant Results for 5 m piperazine with the advanced flash stripper*. Presented at PCCC3, Regina Saskachewan, Sep 2015.

(13) Lin, Y-J.; Rochelle, G.T. Approaching a reversible stripping process for CO_2 capture. *Chemical Engineering Journal* **2016**, 283, 1033–1043.

(14) Lin Y-J.; Rochelle G.T. Optimization of Advanced Flash Stripper for CO_2 Capture using Piperazine. *Energy Procedia* **2014**, 63, 1504–1513.

(15) Frailie, P.T., *Modeling of Carbon Dioxide Absorption/Stripping by Aqueous Methyldiethanolamine/Piperazine*. PhD Dissertation, The University of Texas at Austin, 2014.

Chapter 9

Techno-Economic Analysis of Large Scale Post Combustion CO_2 Capture Systems for Various Flue Gas CO_2 Concentrations

This chapter evaluates the total cost of CO_2 capture as a function of flue gas CO_2 concentration. To do so, three different CO_2 capture processes were designed and their economics were evaluated to capture 90% CO_2 emitted from three different power plants with three levels of flue gas CO_2 concentrations. The three power plants are: a 650 MW_e natural gas fired combined cycle power plant with a flue gas concentration of 4 %, a 650 MW_e natural gas fired combined cycle power plant with exhaust gas recirculation (EGR) cycle with a flue gas CO_2 concentration of 6 %, and a 550 MW_e pulverised coal power plant with a flue gas CO_2 concentration of 13.5 %. For each plant, the specific regeneration and cooling duties and total capital expenditure (CAPEX) and operational expenditures (OPEX) were calculated. Accordingly, the total annual cost of each plant (TOTEX) was determined using the respective CAPEX and OPEX with taking into account an investment period of 20 years and an interest rate of 10 %. Finally, for each case the cost of CO_2 captured was estimated and compared.

9.1. Introduction

As mentioned earlier, post-combustion CO_2 capture (PCC) is the most near term solution to let the world continue to enjoy the benefits of using fossil fuels for electricity generation while significantly reducing the emissions associated with them. The condition of CO_2 sources will affect the cost of CO_2 capture (1). According to the IPCC special report (2), CO_2 volume, CO_2 concentration and partial pressure, integrated system aspects, and proximity to a suitable reservoir are the four important factors affecting the attractiveness of a particular CO_2 source to be integrated with a CO_2 capture process. As for various power generation

systems the flue gas CO_2 concentration varies with the fuel type and the design aspects of the plant, understanding the relative importance of this factor on the CO_2 capture cost is not only worthwhile when assessing the feasibility of incorporating a CO_2 capture plant to an existing plant but also it is beneficial to provide insight for future engineering and design of power generation plants. In future, it is expected to have three different types of fossil fuelled power plants, i.e. coal fired power plant, natural gas fired combined cycle power plant, and natural gas fired combined cycle power plant with exhaust gas recirculation cycle. The CO_2 concentration of atmospheric flue gases emitted from these plants ranges from 3 to 14 %, where the highest is related to coal fired plants and the lowest is related to the natural gas fired power plant. On the other hand, the flue gas CO_2 concentration is an important parameter when designing a chemical based absorption/desorption CO_2 capture plant. The size of the absorber column and the amount of circulating solvent are directly affected by the flue gas CO_2 concentration.

In this chapter the focus is on the CO_2 capture process using aqueous solution of 30 wt. % MEA as solvent which as mentioned before is relatively mature and suitable technology for atmospheric flue gases over the range of CO_2 concentrations mentioned above. In order to gain more insight to the CO_2 capture process with varying CO_2 concentrations, three different CO_2 capture processes were designed and simulated to capture 90% CO_2 of flue gases emitting from the following power generation plants:

- 650 MW_e natural gas fired combined cycle (NGCC) power plant (PCC-NGCC)
- 650 MW_e NGCC power plant using exhaust gas recirculation (EGR) cycle (PCC-NGCC+EGR)
- 550 MW_e subcritical pulverised coal power plant (PCC-COAL)

The simulations were performed in Aspen Plus® V8.4. For each case, the optimum lean solvent CO_2 loading was determined based on minimum specific regeneration energy requirement using minimum solvent flow rate (L_{min}). The economics of the CO_2 capture

process was optimised by designing the process with $1.2xL_{min}$ solvent flow rate to fulfil the optimisation of liquid to gas ratio in terms of plant economics to avoid using excessive amount of packing (5). . The total capital expenditure (CAPEX) and operational expenditures (OPEX) were estimated using Aspen Process Economic Analyser® to assess the economic performance of the CO_2 capture process from sources with different CO_2 concentrations. It should be noted here that this study only focuses on the CO_2 capture cost. CO_2 compression and CO_2 transport and storage costs were not included. Following sections provide the process description of each CO_2 capture process and the related techno-economical evaluations.

9.2. Process Description & Configuration

9.2.1. PCC-NGCC

The NGCC plant used in this configuration is the nominal 650 MW_e NGCC plant presented in the Chapter 6 of this thesis. The power plant is a multi-shaft combined cycle power plant comprising of two GE 7FA.05 gas turbines, two triple pressure level and single reheat type heat recovery steam generators (HRSG), and one condensing steam turbine. The net power plant output without PCC integration is 634 MW_e with a net thermal efficiency 57.8 % (LHV basis) when firing natural gas with compositions presented in Table 6-1 of Chapter 6 (3). The net power plant output with PCC integration is 552.8 MWe with a net plant efficiency of 50.1 % (LHV basis) when firing the same fuel. The heat required for the solvent regeneration of the CO_2 capture process was provided from the power plant water/steam cycle in form of steam extracted from the intermediate pressure (IP) and low pressure (LP) steam turbine crossover pipe. The methodology used to design the large-scale CO_2 capture process to remove 90% CO_2 from the power plant flue gases is as presented in Chapter 6. The NGCC flue gas compositions are provided in Table 9-1, and Figure 9-1 presents the schematic overview of the PCC-NGCC plant. The suggested PCC configuration comprises of two absorber columns and one stripper column. The optimum lean loading of 0.25 (mol CO_2/mol

MEA) was determined based on minimum specific regeneration energy requirement. The design specification of the large scale CO_2 capture process of the integrated PCC-NGCC plant is provided in Table 9-2, and Figure 9-2 presents the variation of specific regeneration energy requirement with lean loading for the CO_2 capture process of the PCC-NGCC plant.

Table 9-1. NGCC flue gas composition used for the PCC design

Components	**Mole fraction (%)**
CO_2	3.91
H_2O	8.43
N_2	74.39
O_2	12.37

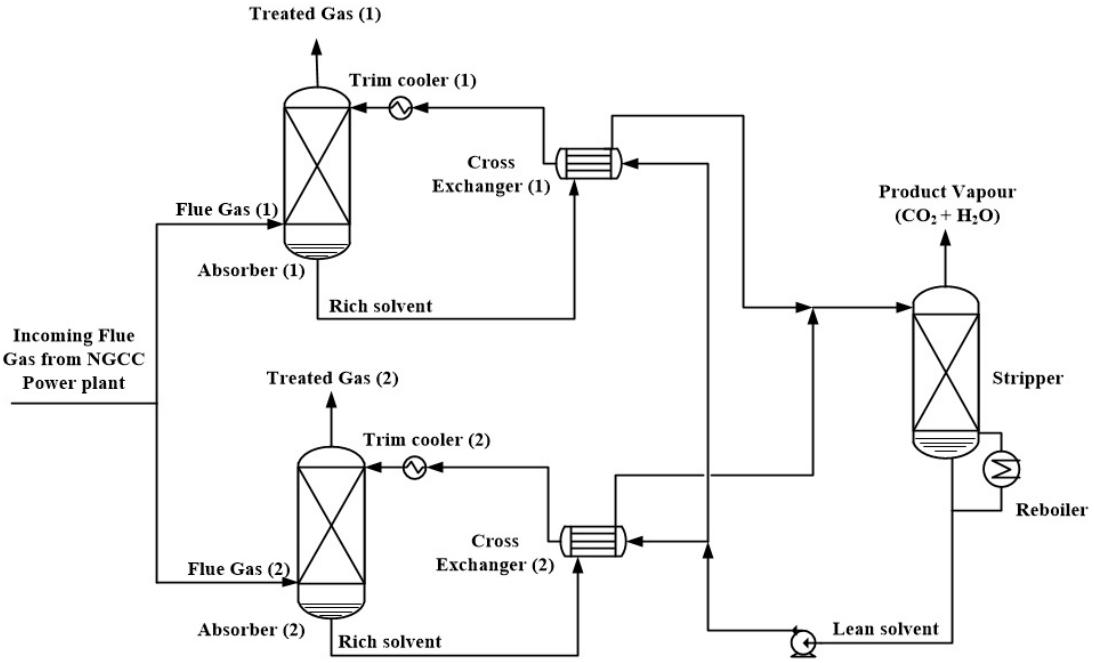

Figure 9-1. Schematic overview of the PCC unit for the use in the NGCC power plant

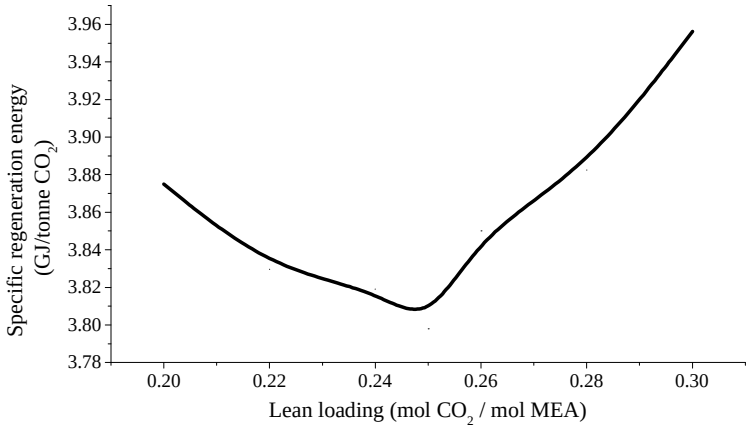

Figure 9-2. Variation of the total equivalent work with lean solvent CO2 loading for the PCC-NGCC integrated plant

Table 9-2. Process condition and design specifications of the PCC unit for NGCC application

Parameter	**Value**
Number of Absorber columns	2
Packing material	Sulzer Mellapak 250Y
Absorber column diameter (m)	15.6
Absorber column height (m)	11
Flue Gas at each absorber inlet	
Mass flow rate (tonne/h)	1866.8
Temperature (°C)	40
Pressure (kPa)	113.7
Solvent at each absorber inlet	
Mass flow rate (tonne/h)	2573.0
Temperature (°C)	40
Lean CO_2 loading (mol CO_2/mol MEA)	0.25
Liquid-to-gas ratio (L/G) (kg/kg)	1.38
Absorber column pressure (top stage) (kPa)	101.6
Number of Stripper columns	1
Packing material	Sulzer Mellapak 250Y
Stripper column diameter (m)	9.2
Stripper column height (m)	8
Stripper column pressure (top stage) (kPa)	180
Stripper condenser temperature (◦C)	35
Cross exchanger approach temperature (°C)	5
Reboiler energy requirement (MW)	239.1
Captured CO_2 mass flow rate (tonne/h)	207.198
Specific energy requirement (GJ/tonne CO_2)	4.15

9.2.2. PCC-NGCC+EGR

The NGCC+EGR power plant used in this concept also uses the same GE 7FA.05 gas turbines as that of the NGCC plant with the addition of an EGR cycle. In the NGCC plant with EGR, a portion of the gas turbine exhaust stream is recirculated back to the air inlet and the remainder enters to the CO_2 capture system after passing through the HRSG units. The gas turbine performance and the flue gas compositions were impacted due to the addition of the EGR cycle (3). In this study, the EGR rate of 35 % was considered (3), i.e. 35 % of the gas turbine exhaust gas was recycled back to the compression inlet. By applying the EGR cycle, the CO_2 composition in the flue gas increases from 3.9 % without EGR to 6.1 %, concurrently, the O_2 composition decreases from 8.3 % without EGR to 7.4 %. In addition, the flue gas flow rate fed to the CO_2 capture process was reduced by 35 % compared to that of the PCC-NGCC plant. The reduced flow rate of the flue gas and the higher concentration of the CO_2 in the flue gas reduce the energy requirement of the CO_2 capture process (3). The application of EGR also improves the net power output and plant thermal efficiency compared to the integrated plant without EGR (the previous case). For the PCC-NGCC+EGR, the net power plant output is 563.2 MW_e with a net thermal efficiency of 50.6 % when firing natural gas with compositions presented in Table 6-1 of Chapter 6 (3). By comparing the performance results with those of the NGCC-PCC plant, it is evident that the addition of EGR increases the thermal efficiency by 0.6 percentage points with an additional 10.4 MW_e power output. This is mainly due to the reduction in the steam requirements for the solvent regeneration, and partly the reduction in the flue gas flow rate entering the CO_2 capture process, i.e. 35 %. The flue gas composition of the NGCC+EGR plant fed to the CO_2 capture system is provided in Table 9-3. The heat required for the solvent regeneration process was provided by the power plant water/steam cycle similar to the previous case.

Figure 9-3 presents the schematic overview of the PCC-NGCC+EGR plant. The proposed configuration comprises of one absorber and one stripper column as shown in Figure 9-3. The optimum lean loading of 0.25 was determined based on minimum specific regeneration

energy requirement as presented in Figure 9-4. The design specifications of the CO_2 capture process for the PCC-NGCC+EGR integration are summarized in Table 9-4.

Table 9-3. NGCC+EGR flue gas composition used for the PCC design

Components	Mole fraction (%)
CO_2	6.07
H_2O	9.78
N_2	74.96
O_2	8.29

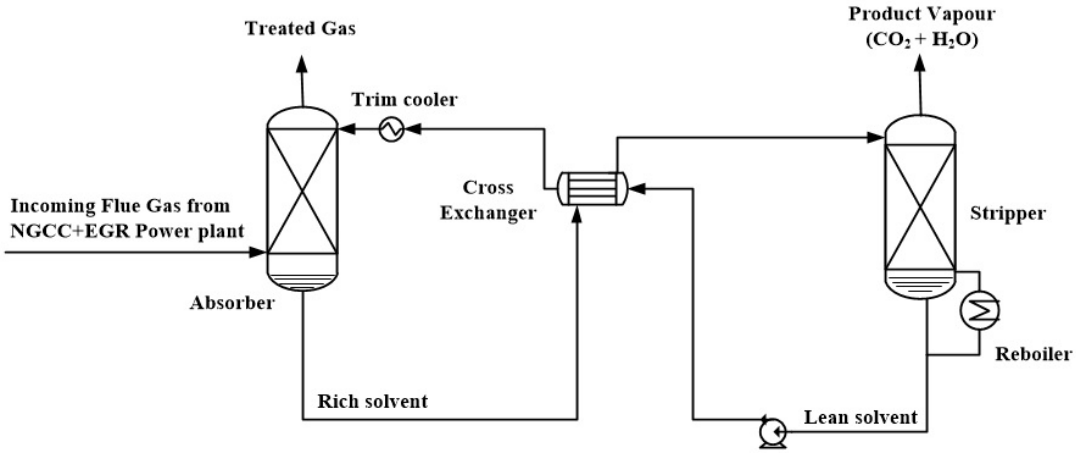

Figure 9-3. Schematic overview of the PCC unit for the use in the NGCC+EGR power plant

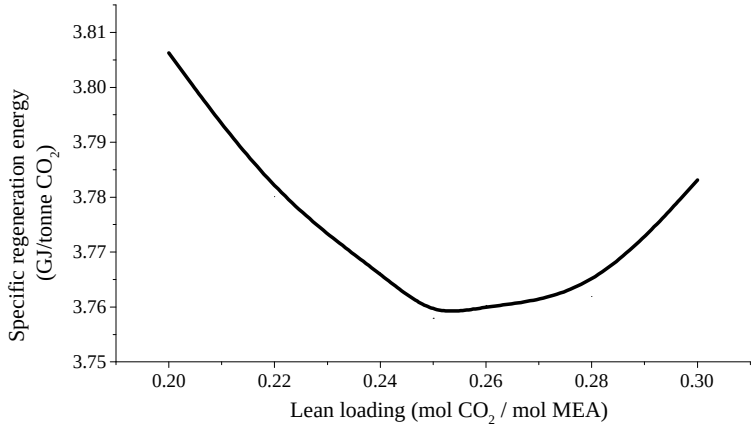

Figure 9-4. Variation of the total equivalent work with lean solvent CO_2 loading for the PCC-NGCC+EGR integrated plant

Table 9-4. Process condition and design specifications of the PCC unit for NGCC+EGR application

Parameter	**Value**
Number of Absorber columns	1
Packing material	Sulzer Mellapak 250Y
Absorber column diameter (m)	18.7
Absorber column height (m)	10
Flue Gas at absorber inlet	
Mass flow rate (tonne/hr)	2404.0
Temperature (°C)	40
Pressure (kPa)	113.7
Solvent at absorber inlet	
Mass flow rate (tonne/hr)	5016.5
Temperature (°C)	40
Lean CO_2 loading (mol CO_2/mol MEA)	0.25
Liquid-to-gas ratio (L/G) (kg/kg)	2.1
Absorber column pressure (top stage) (kPa)	101.6
Number of Stripper columns	1
Packing material	Sulzer Mellapak 250Y
Stripper column diameter (m)	9.1
Stripper column height (m)	9
Stripper column pressure (top stage) (kPa)	180
Stripper condenser temperature (°C)	35
Cross exchanger approach temperature (°C)	5
Reboiler energy requirement (MW)	235748
Captured CO_2 mass flow rate (tonne/hr)	208.9
Specific energy requirement (GJ/tonne CO_2)	4.06

9.2.3. PCC-COAL

The coal power plant studied in this section is a subcritical pulverised coal power plant which uses Illinois No. 6 coal as fuel as presented as the Case#10 in the 2010 report of the US Department of Energy (4). The power plant produces a net power output of 550 MW_e at a net plant efficiency of 36.8 % (HHV basis) without PCC integration. The net plant efficiency after the PCC integration is 26.2 % (HHV basis) to generate a net power of 500 MW_e when firing the same fuel. The rankine cycle is a single reheat subcritical steam generation cycle with 566 °C / 566 °C cycle conditions at 16.5 MPa. The flue gas compositions are provided in Table 9-5. The heat required for the solvent regeneration of the

CO_2 capture process was provided in the form of heat from the power plant water/steam cycle.

Figure 9-5 presents the schematic overview of the PCC-COAL plant. The simulated CO_2 capture process comprises of two absorber and one stripper columns. The optimum lean loading of 0.25 was determined based on the minimum specific regeneration energy requirement as presented in Figure 9-6. The design specifications of the CO_2 capture process for the PCC-COAL integrated plant were provided in Table 9-6.

Table 9-5. COAL flue gas composition used for the PCC design

Components	**Mole fraction (%)**
CO_2	13.50
H_2O	15.37
N_2	67.93
O_2	2.38

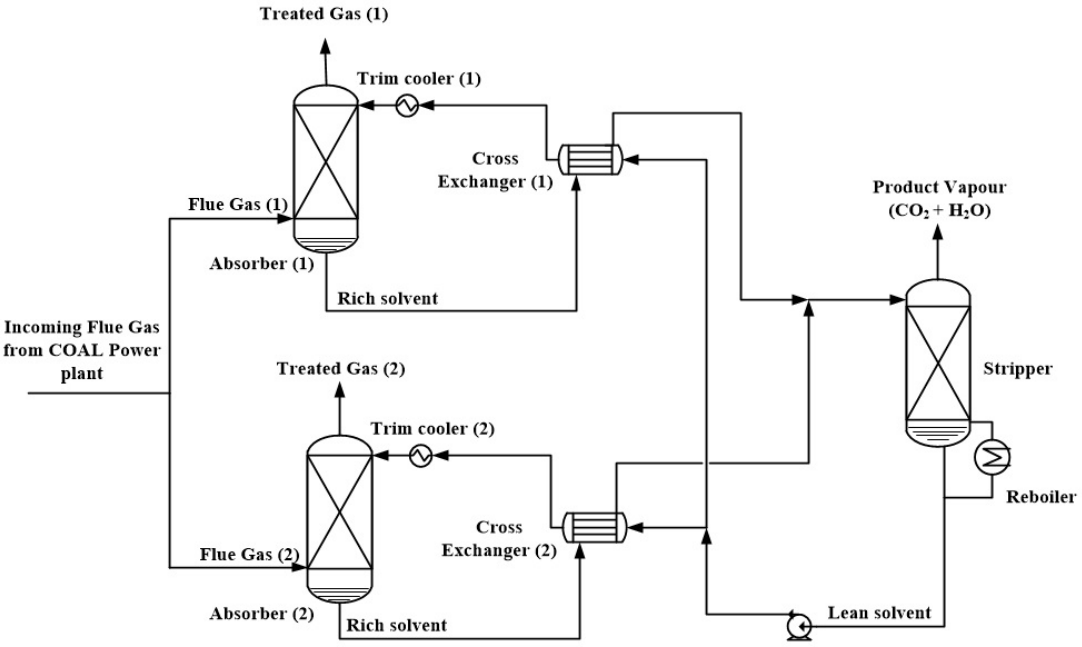

Figure 9-5. Schematic overview of the PCC unit for the use in the COAL power plant

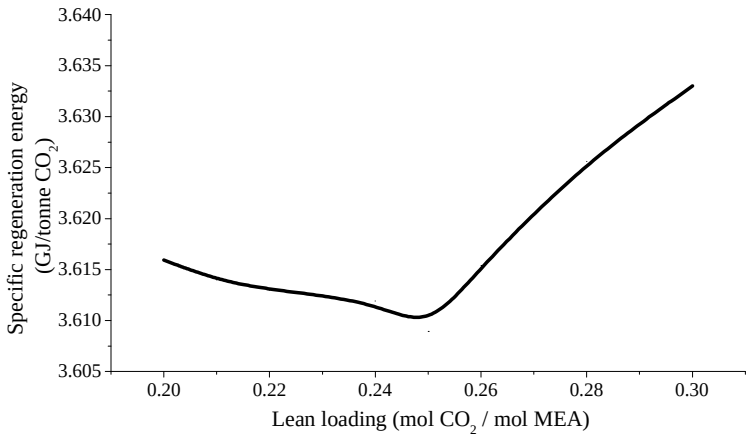

Figure 9-6. Variation of the total equivalent work with lean solvent CO_2 loading for the PCC-COAL integrated plant

Table 9-6. Process condition and design specifications of the PCC unit for the COAL power plant

Parameter	**Value**
Number of Absorber columns	2
Packing material	Sulzer Mellapak 250Y
Absorber column diameter (m)	16.4
Absorber column height (m)	9.2
Flue Gas at each absorber inlet	
Mass flow rate (tonne/hr)	1608.0
Temperature (°C)	40
Pressure (kPa)	113.7
Solvent at each absorber inlet	
Mass flow rate (tonne/hr)	5683.9
Temperature (°C)	40
Lean CO_2 loading (mol CO_2/mol MEA)	0.25
Liquid-to-gas ratio (L/G) (kg/kg)	3.53
Absorber column pressure (top stage) (kPa)	101.6
Number of Stripper columns	1
Packing material	Sulzer Mellapak 250Y
Stripper column diameter (m)	13.7
Stripper column height (m)	10
Stripper column pressure (top stage) (kPa)	180
Stripper condenser temperature (◦C)	35
Cross exchanger approach temperature (°C)	5
Reboiler energy requirement (MW)	542420
Captured CO_2 mass flow rate (tonne/hr)	494.0
Specific energy requirement (GJ/tonne CO_2)	3.95

9.3. Technical and Economical Evaluations

9-3.1. Technical Evaluations

The optimum design of the absorber and stripper columns based on energy performance analysis with 90 % CO_2 capture rate for three different flue gases are summarized in Table 9-2 to 9-4. The process design of each CO_2 capture plant with 90% CO_2 capture rate is based on 1.2 times the minimum solvent flow (L_{min}) rate to fulfil the optimisation of liquid to gas ratio in terms of plant economics to avoid using excessive amount of packing (5). For each case the minimum solvent flow rate was determined as described in Section 7.2 of Chapter 7 of this thesis. For each case, the absorber and stripper columns were sized based on $1.2xL_{min}$ solvent flow rate. Diameters were determined to provide a 75 % fractional approach to flooding, and heights were optimised to satisfy 90 % CO_2 removal rate. It is important to note here as mentioned earlier in chapter 6 of this thesis, the decision on the number of absorber and stripper column were made in line with what has currently been delivered by this technology. To date, the maximum diameter for an absorber column under operation is around 18.5 m (60 ft) as reported by Reddy et al. (6). The diameter of 19 m was therefore chosen as a criterion in determining the number of absorber and stripper columns to be used for each case.

Table 9-5 provides the total auxiliary energy consumption of each CO_2 capture plant along with the efficiency penalty associated with each integration based on fuel high heat value (HHV). The total auxiliary power consumption is as provided in the 2010 and 2013 reports published by the Department of Energy (3,4) as these data reflect more realistic values than those calculated by Aspen Process Economic Analyser®. The specific regeneration and cooling duties were calculated by dividing the stripper reboiler energy and plant cooling duties simulated in Aspen Plus® by the total amount of CO_2 captured, as presented in Figures 9-7 and 9-8, respectively. According to Table 9-7, the PCC-NGCC+EGR case is the least energy consuming option with the least impact on the power plant thermal efficiency whilst the PCC-COAL has the most negative impact on the power plant thermal efficiency with the

highest rate of auxiliary power consumption. On the other hand, as shown in Figure 9-7 the specific reboiler duty decreases exponentially with increasing the flue gas CO_2 concentration. The same trend is observed for the plant specific cooling duty requirement. As mentioned earlier, one major contributor to the high solvent regeneration energy requirement is the loss of latent heat available in the stripping steam leaving the stripper column as a part of product stream, i.e. mixture of CO_2 and vapour water. Although the water refluxes back to the stripper after being condensed at the condenser, its latent energy is lost. The simulation results showed that the amount of stripping steam leaving the stripper column increases at lower flue gas CO_2 concentrations. This also increases the cooling duty requirements at the stripper condenser as shown in Figure 9-8.

Although the total auxiliary power consumption of the PCC-COAL option is the highest, by comparing its specific regeneration energy and cooling duty requirements against the two other cases, as shown in Figures 9-7 and 9-8, it is clear that this option consumes less energy per unit of CO_2 captured. By comparing the PCC-NGCC+EGR case with the PCC-NGCC, it is evident that the NGCC+EGR case is a better option in all aspects of energy study: it requires lesser auxiliary power consumption and its specific regeneration energy requirement is lesser than that of the NGCC case. The impact of incorporating a CO_2 capture plant into a NGCC+EGR plant in terms of the power plant net efficiency is also lesser than that of the NGCC case. These findings encourage the application of exhaust gas recirculation for future NGCC power plants if stringent CO_2 reduction strategies are to be pursued.

Table 9-7. Auxiliary power consumptions and efficiency penalties of the three cases

Parameters	**PCC-NGCC**	**PCC-NGCC+EGR**	**PCC-COAL**
Auxiliary energy consumption (MW_e)	15.97	13.13	22.4
Power plant efficiency penalty (%-point)	6.6	6.1	10.6

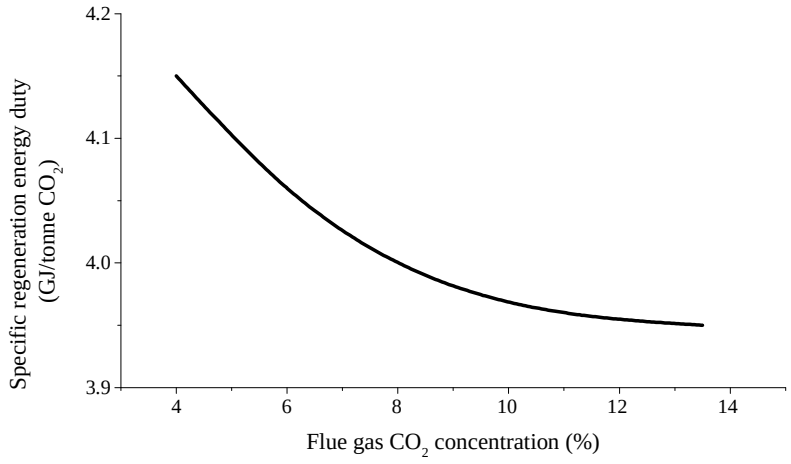

Figure 9-7. Variation of the specific regeneration energy requirement with flue gas CO_2 concentration

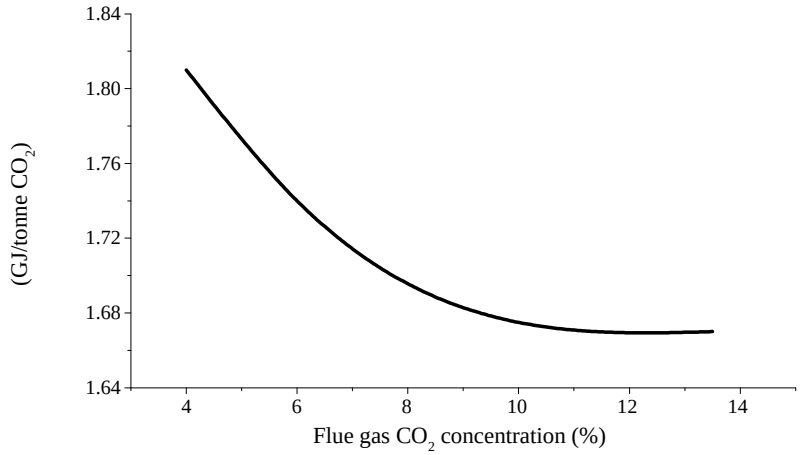

Figure 9-8. Variation of the plant specific cooling energy requirement with flue gas CO_2 concentration

Comparing the absorber packed height of the three cases, it is evident that the absorber height varies as a function of flue gas CO_2 concentration. For a given CO_2 capture rate, at higher CO_2 concentrations, as the liquid to gas ratio increases the required height of absorber to attain the desired 90 % CO_2 capture rate decreases. Table 9-8 shows the absorber height comparison. For the cases studied here, the absorber height for the NGCC application is approximately 10 % and 16 % more than that of the NGCC-EGR and COAL cases, respectively. This directly influences the plant CAPEX.

Table 9-8. The packed height of absorber to achieve 90% CO_2 capture rate using 1.2xL_{min} solvent flow

Parameters	PCC-NGCC	PCC-NGCC+EGR	PCC-COAL
Absorber packed height (m)	11.0	9.95	9.2

The height of stripper column was optimised to provide minimum regeneration energy requirement. As the lean solvent CO_2 loading is fixed at 0.25 in all three cases, the stripper height varies as a function of regeneration capacity which is the difference between the rich loading and lean loading as shown in Table 9-9.

Table 9-9. Stripper process and design parameters

Parameters	PCC-NGCC	PCC-NGCC+EGR	PCC-COAL
Stripper packed height (m)	8	9	10
Rich loading (mol CO_2/mol MEA)	0.414	0.420	0.428
Lean loading (mol CO_2/mol MEA)	0.250	0.250	0.250
Degree of regeneration (%)	39.6	40.5	41.6

9.3.2. Economic Evaluations

The capital cost (CAPEX) and the operational cost (OPEX) of each CO_2 capture plant were calculated using Aspen Process Economic Analyser ® V.8.4, using the UK costing template with default values. It is worth to mention the CAPEX and OPEX will be higher for an actual plant because of the other equipment (including spares) that must be installed based on a hazard and operability (HAZOP) study (7). Although using default values of the Aspen Process Economic Analyser® does not accurately reflect the economic evaluation of the plant, they properly indicate the effect of important design value, i.e. the variation of the flue gas CO_2 concentration, on the capital and operational cost of the CO_2 capture plant.

The operating costs are divided into fixed and variable operating costs. The fixed operating cost is related to the investment cost and includes plant maintenance, insurance and labour costs (1). The variable operating costs are a function of the total amount of CO_2 captured, and includes consumption of utilities: electricity, steam, water and MEA make up (1). The steam cost per ton of CO_2 captured was calculated for each case using the unit rate of steam

cost estimated by Aspen Process Economic Analyser® and the total amount of CO_2 captured by the plant. Similarly, the cost of total required cooling water is calculated for each case. Table 9-10 summarises the specific steam and cooling water costs for each plant, assuming the steam is provided by the power plant at 690 kPa pressure and 165 °C temperature, and the cooling water at 350 kPa pressure and 35 °C temperature

Table 9-10. Specific steam and cooling water cost for each case

Parameters	**PCC-NGCC**	**PCC-NGCC+EGR**	**PCC-COAL**
Steam cost (£/tonne CO_2)	3.6	3.52	3.42
Cooling water cost (£/tonne CO_2)	1.80	1.96	2.24

Similar to the trend previously observed for the plant specific regeneration energy requirement, the steam specific cost reduces as the flue gas CO_2 concentration increases. However, the cooling water specific cost shows a reverse trend. Although the specific stripper cooling duty decreases with increasing the flue gas CO_2 concentration, the plant total cooling water duty increases. This is due to the fact that the circulating solvent needs to be cooled down to 40 °C before entering the absorber column. Simulation results show that after regeneration, the lean solvent leaves the stripper column at 116 °C and after being partially cooled at the cross heat exchanger, its temperature reaches 49.4 °C, 53.2 °C, and 59.9 °C in PCC-NGCC, PCC-NGCC+EGR, and PCC-COAL, respectively. Provided the cross heat exchanger log mean temperature different (LMTD) is 5 °C for all three cases, the variable solvent temperature after the cross heat exchanger is reasonable. However, considering the relatively hotter circulating solvent at higher CO_2 concentration and the solvent higher flow rate at higher CO_2 concentration, it is meaningful to expect an increase in the plant cooling water requirement with increase in the flue gas CO_2 concentration. Table 9-11 summarises the specific cooling duty of each plant.

Table 9-11. Plant specific cooling duty and specific circulating solvent requirements

Parameters	**PCC-NGCC**	**PCC-NGCC+EGR**	**PCC-COAL**
Total plant specific cooling duty (GJ/tonne CO_2)	2.64	2.87	3.28

For each case, the total annual cost was calculated using the annualisation factor, i.e. AF, calculated as:

$$AF = \frac{i}{(1+i)^n} + i \quad (9\text{-}1)$$

Where, i is the interest rate and n is the total period of financing. For this study, a 10% interest rate and a financing period of 20 years were assumed. The annualized capital cost, i.e. AC, can be calculated using the annualisation factor as:

$$AC = \frac{CAPEX}{AF} \quad (9\text{-}2)$$

And the total annual cost (TOTEX) of the plant can be calculated using the equation:

$$AF = AC + OPEX \quad (9\text{-}3)$$

Table 9-8 summarizes the CAPEX, OPEX, and TOTEX values of each case. The total cost of CO_2 captured was calculated using the total annual cost assuming a 320-day operation in a year for each case and presented in Table 9-12. Figure 9-9 shows the variation of the CO_2 capture plant total annual cost with flue gas CO_2 concentration. From Figure 9-9 it is evident that capturing CO_2 from CO_2 flue gases at atmospheric pressure increases significantly as the flue gas CO_2 concentration lowers. Performed cost estimations show that the cost of capturing 90 % CO_2 from flue gases emitted by a NGCC power plant is approximately 8 %

more expensive than capturing CO_2 at the same rate from flue gases emitted from a COAL power plant, and approximately 5% more expensive than from a NGCC-EGR power plant.

Table 9-12. Summary of the plants total capital (CAPEX), operational (OPEX) and annual costs (TOTEX)

Parameters	**PCC-NGCC**	**PCC-NGCC+EGR**	**PCC-COAL**
CAPEX (M£)	40.13	26.57	43.94
OPEX (M£/year)	78.37	76.61	175.02
TOTEX (M£/year)	82.380	79.26	179.41
Cost of CO_2 captured (£/tonne CO_2)	51.77	49.41	48.00

The observed drop in the cost of CO_2 capture by increasing flue gas CO_2 concentration is clearly a motivation to select sources with high CO_2 concentrations provided all design specifications are equal. This fact encourages the efforts are being made to increase CO_2 concentrations in sources with relatively low CO_2 concentrations, such as the application of exhaust gas recirculation for natural gas fired power plants. According to economic calculations performed, a reduction in the capital cost of around 35 % was observed when increasing the flue gas CO_2 concentration from 4 %, i.e. typical of a NGCC plant, to 6 %, i.e. typical of a NGCC+EGR plant.

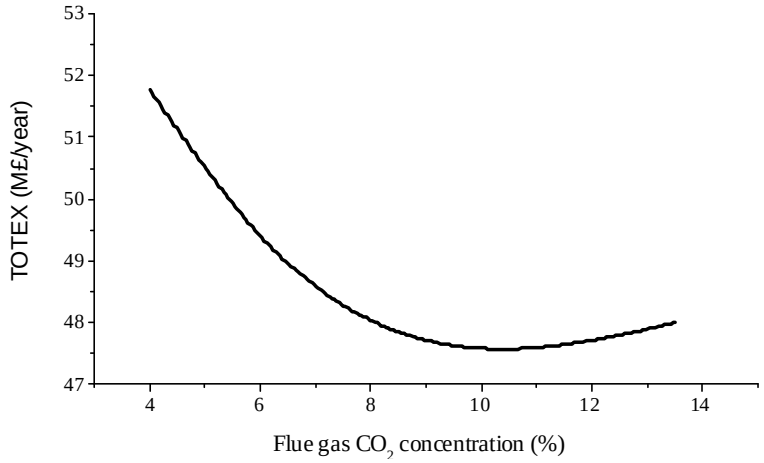

Figure 9-9. Variation of the plant total annual cost (TOTEX) in million pounds sterling (M£) with flue gas CO_2 concentration

9.4. Conclusions & Remarks

Process Simulation and economic estimations performed in this chapter clearly point out the effect of the flue gas CO_2 concentration on the design and cost of CO_2 capture processes when using 30 wt. % aqueous solution of MEA as solvent. Increasing atmospheric flue gas concentration reduces total annual cost of the CO_2 capture plant mainly due to lower specific energy/utility consumptions. The total annual cost reduced by approximately 8 % when moving from 4 % to 14 % flue gas CO_2 concentration, while a more moderate total annual cost decline was observed of nearly 5 % when moving from 4 % to 6 % flue gas CO_2 concentration. Although the specific energy requirement of solvent regeneration drops by increasing flue gas CO_2 concentration, the plant specific cooling requirements show an incremental trend with increasing flue gas CO_2 concentration. Performed studies have shown that the CO_2 capture specific regeneration energy requirement reduces significantly with increasing flue gas CO_2 concentration, encourage the application of exhaust gas recirculation in future NGCC power plants if stringent CO_2 reduction strategies are to be pursued. Furthermore, aaccording to economic calculations performed, a reduction in the capital cost of around 35 % was observed when increasing the flue gas CO_2 concentration from 4 %, i.e. typical of a NGCC plant, to 6 %, i.e. typical of a NGCC+EGR plant.

9.5. List of References

(1) Husebye, J.; Brunsvold, A. L.; Roussanaly, S.; Zhang, Z. Techno economic evaluation of amine based CO_2 capture: impact of CO_2 concentration and steam supply. *Energy Procedia* 2012, (23) 381 – 390.

(2) B. Metz, Intergovernmental Panel on Climate Change.Working Group III., IPCC special report on carbon dioxide capture and storage Cambridge University Press for the Intergovernmental Panel on Climate Change, 2005.

(3) National Energy Technology Laboratory. Current and Future Technologies for Natural Gas Combined Cycle (NGCC) Power Plants. DOE/NETL-341/061013, U.S. Department of Energy, Office of Fossil Energy, 2013.

(4) James Black, "Cost and performance baseline for fossil energy plants volume 1: bituminous coal and natural gas to electricity", Prepared by Research and Development Solutions, updated by Energy Sector Planning and Analysis (ESPA) for the U. S. Department of Energy, National Energy Technology Laboratory, (NETL), Morgantown, West Virginia, May, 2010.

(5) Perry, R.H.; Green, D.W. Perry's Chemical Engineers' Handbook. 8th edition", McGraw-Hill, New York, 2008.

(6) Reddy, S., Scherffius, J., Freguia, S., Fluor's Econamine FG PlusSM Technology: An Enhanced Amine-Based CO2 Capture Process. 2003. Second National Conference on Carbon Sequestration National Energy Technology Laboratory/Department of Energy, Alexandria, VA, May 5-8.

(7) E.O. Agbonghae, E.O.; Hughes, K.J.; Ingham, D,B,; Ma, l.; Pourkashanian, M. Optimal Process Design of Commercial-Scale Amine-Based CO2 Capture Plants. *Industrial & Engineering Chemistry Research* 2014, (53) 14815-14829.

Chapter 10

Conclusions & Recommendations

This chapter summarises the conclusions and remarks made of the research performed in this thesis, as well as suggestions and recommendations for future research that can be embarked upon by any interested researcher.

This thesis studied the design and operation of a post-combustion CO_2 capture for a 650 MW_e natural gas fired combined cycle (NGCC) power plant through modelling and simulation. The post combustion CO_2 capture is based on a chemical absorption/desorption process using an aqueous solution of 30 wt. % MEA as solvent, as this is the most mature technology for CO_2 capture from flue gases with relatively low CO_2 concentrations or partial pressures. The integrated process comprising of a natural gas fired combined cycle power plant, a CO_2 capture plant and a CO_2 compression unit were simulated and their energy performances were optimised. The modelling, simulations, and optimisations were performed in Aspen Plus® V8.4. The natural gas fired combined cycle power plant and the CO_2 compression unit were modelled based on a 2013 US Department of Energy report, while the MEA-based CO_2 capture plant was modelled using a rigorous rate-based modelling approach based on finite rates of mass and heat transfer between liquid and vapour. The CO_2 capture model was validated using experimental data reported from two different pilot plants: The UK Carbon Capture and Storage Research Centre/Pilot Scale Advanced Capture Technology (UKCCSRC/PACT) CO_2 capture plant located at Beighton, UK, and the MEA-based pilot plant at the University of Kaiserslautern, located in Kaiserslautern, Germany. The large-scale design of the CO_2 capture plant was performed using process design criteria recommended for large-scale absorber and stripper towers using the verified rate-based model.

The NGCC plant was simulated in Aspen Plus® V.8.4 at gas turbine full and part load operations. At each operational load, the CO_2 capture energy requirements, including the energy required for CO_2 compression, were determined. The study also investigates the performance of the NGCC plant during non-capture operation, especially the low pressure (LP) steam turbine; as at such conditions a considerable amount of steam will be available at the LP turbine inlet. In addition, issues requiring careful consideration for the NGCC plant in the case of non-capture operation were addressed. The study also measured the potential impact on the performance of the LP and intermediate pressure (IP) steam turbine sections.

As one of the challenging issues hindering the incorporation of post-combustion CO_2 capture plant into power generation systems is the process high energy requirement for solvent regeneration, this research focused on the effect of flow-sheet complexity on thermodynamic driving forces to improve the process energy performance via promoting thermodynamic irreversibility. The study included the benefits of using two configurations of absorber intercooling: in-and-out (simple) intercooling, and recycled (advanced) intercooling, for a range of lean loading. The benefits in terms of solvent absorption capacity and reduction in the circulating solvent flow rate were quantified and the plant energy improvements in terms of total equivalent work were also quantified. Also, this research explored the application of two advanced stripper configurations: the advanced reboiled and the advanced flash stripper. Both advanced configurations recover the stripping steam heat by means of a heat integration comprised of cold and warm rich solvent bypasses. The energy improvements in terms of total equivalent work offered by the two advanced configurations for natural gas fired applications for a range of lean loading were quantified.

The research also studied the relationship between the cost of CO_2 capture and the flue gas CO_2 concentration. Three different CO_2 capture processes were designed and their economics were evaluated to capture 90% CO_2 emitted from three different power plants with three levels of flue gas CO_2 concentrations. The three power plants are: a 650 MW_e natural gas fired combined cycle power plant with a flue gas concentration of 4 %, a 650

MW_e natural gas fired combined cycle power plant with exhaust gas recirculation (EGR) cycle with a flue gas CO_2 concentration of 6 %, and a 550 MW_e pulverised coal power plant with a flue gas CO_2 concentration of 13.5 %. For each plant, the specific regeneration and cooling duties and total capital expenditure (CAPEX) and operational expenditures (OPEX) were calculated. Accordingly, the total annual cost of each plant (TOTEX) was determined using the respective CAPEX and OPEX with taking into account an investment period of 20 years and an interest rate of 10 %. Finally, for each case the cost of CO_2 captured was estimated and compared.

10.1. UKCCSRC/PACT CO_2 Capture Plant Performance Evaluation and Optimisation

The rate-based model to simulate the CO_2 capture process using an aqueous solution of 30 wt. % MEA as solvent has been developed in Aspen Plus® V.8.4 and validated using results of 5 experimental studies carried out at the UKCCSRC/PACT pilot plant in Beighton, UK. The developed model was then used to assess the performance of the pilot plant in terms of energy consumption, and to propose new operating conditions to operate the pilot plant optimally in future. A number of performance parameters have been identified and varied for a given range of lean solvent CO_2 loading from 0.165 to 0.30 (mol CO_2/ mol MEA) to evaluate their effects on the plant energy performance. Two sets of operating conditions with two different packing materials were finally suggested to improve the pilot plant energy performance.

For the pilot plant to efficiently achieve 90 % CO_2 capture from flue gases with 5.5 % CO_2, typical of a natural gas fired applications, the following modifications were suggested:

- A more efficient cross heat exchanger has the potential to improve the stripper performance by providing the rich solvent with a temperature closer to its bubble point at the stripper inlet. Simulation results showed a nearly 5 % reduction in the specific regeneration energy requirement associated with the rich solvent being

heated up by further 13 °C when using a 5-°C LMTD cross heat exchanger instead of the current one with a 20 °C LMTD.

- Considerable energy savings can be achieved by increasing the lean loading level, provided that the absorber column is capable of operating at higher liquid rates, which is achievable for the case of the PACT pilot plant. Simulation results have shown that by solely increasing the lean loading from 0.165 to 0.23, with no other change of the pilot plant operating condition, the specific regeneration energy requirement was reduced by nearly 15 %. The additional cost associated with the 28 % increase in the solvent flow rate is insignificant compared to the energy gain realised in the regeneration process.

- The stripper operating pressure also has a significant effect on the regeneration energy performance. Simulation results showed that by increasing the stripper pressure from 125 to 180 kPa the specific regeneration energy requirement will reduced by 28 %. The optimum lean loading to realise this gain is at 0.21 with a 118.7 °C solvent temperature at the reboiler section, which is reasonably below the thermal degradation threshold of MEA solvents.

- An efficient and modern packing material can contribute to significantly improve the overall performance of the PACT pilot plant by providing higher mass transfer efficiency, lower pressure drop and more efficient liquid and gas distributions. Simulation results suggest replacing the existing packing material with higher performing structured packing, e.g. Sulzer Mellapak 250Y will result in a nearly 40 % reduction in the specific regeneration energy when compared with the plant existing conditions. The proposed operating condition with the Sulzer Mellapak 250Y structured packing outperformed the condition proposed with the IMTP25 random packing by nearly 15 %.

The main conclusions of this work should also hold for other plants of this type that employ 30 wt.% MEA solution as solvent.

10.1.1. Recommendations for Future Research

- The comprehensive baseline simulation study with 30 wt. % MEA conducted in this research needs to be verified using the UKCCSRC/PACT pilot plant to be used as a reference for future modelling verification.
- It is valuable to experimentally study the application of absorber intercooling using the UKCCSRC/PACT pilot plant with both IMTP25 random packing and Sulzer Mellapak 250Y structured packing.
- It is recommended to perform comprehensive experiment studies to develop reference data using other type of solvents: methyldiethanolamine (MDEA) and piperazine (PZ).

10.2. Process Design of Large-scale CO_2 Capture for Natural Gas Combined Cycle (NGCC) Power Plant Applications

Steady state simulation of a natural gas combined cycle power plant and post combustion CO_2 capture (PCC) unit were carried out in Aspen Plus V8.4. Simulations were made at full and part loads for two process options with and without CO_2 capture. The considered option to provide the heat for the solvent regeneration was the steam extraction at IP/LP crossover pipe for all cases. Part load cases were studied at gas turbine (GT) load of 90, 80, 70 and 60%. The results confirmed the performance viability of the NGCC-PCC plant at full and part loads down to the 60% load. By adjusting the solvent circulation rate to lower values, except for the GT 60% load, the CO_2 capture with 90% capture rate was achievable at part loads. The study of the absorber column hydraulics showed that in order to have a reliable operation at the 60% load, the minimum liquid load required in the absorber packed column led to an increase of 6% in the circulating solvent flow rate. A suggested solution to retain the CO_2 capture rate at 90% at this load is to increase the lean solvent CO_2 loading to 0.23 from its design value of 0.21.

Simulation results confirmed that there is sufficient steam available at the IP/LP crossover pipe to provide the steam required for the solvent regeneration at part loads up to 60% GT load. Moreover, the study of the IP/LP crossover pressure showed that the throttling loss related to the steam extraction is minimal as the pressure of the steam in the crossover pipe is close to that required in the reboiler. However, to reach a part load capability below the 60% GT load, a higher design pressure for the crossover pipe would be required. An analysis of net plant efficiency for the two process options revealed that at full load, the efficiency penalty associated with the CO_2 capture operation is 7.15% point at full load and will increase to 7.6% point at 60% GT load.

The study of the absorber column performance and the mass transfer efficiency revealed that at part loads, due to relatively lower load of gas and liquid in the column, the mass transfer efficiency slightly improves and leads to a slightly higher rich solvent CO_2 loading at the column discharge. This improvement however showed a negative effect on the stripper performance in terms of the specific energy required by the reboiler.

An evaluation was made to study the impact of non-capture operation on the LP steam turbine. the results showed that if the NGCC plant operates at full load while the PCC is off, the steam flow available at the LP turbine increases by 108%, which will result in an increase on the LP turbine inlet pressure from 337 to nearly 700 kPa. The increase on the LP inlet pressure will affect the IP turbine as well, leading to the turbine efficiency drop. To minimise the impact of non-capture operation, it was suggested to operate the power plant at a lower load with the net power output equivalent to that of the NGCC full load operation while fitted with the PCC unit. Specifically for this study, calculations showed that the suggested part load operation to minimise the impact of non-capture operation will be at the GT load of nearly 85%.

In addition to the IP and LP turbine performance, the non-capture operation will affect the condenser operating pressure due to the rise of the coolant temperature as a consequence of the increased steam flow, leading to a drop in the plant net power output. Moreover, to make

the plant capable of operating without capture, some provision must be considered in the steam turbine generator to handle the surplus electricity generation. These evaluations suggest that if an NGCC plant is designed to operate in a CO_2 capture integrated scheme, it is not beneficial to operate in a standalone mode, apart from inevitable situations such as CO_2 capture plant or CO_2 compression unit trip.

10.2.1. Recommendations for Future Research

- For large-scale MEA-based CO_2 capture plant that will serve commercial-scale natural gas fired power plants, complex thermal integration of these two processes can be advantageous in terms of plant overall thermal efficiency. For instance, one may evaluate the benefits of preheating the rich solvent via heat evaluable in the flue gas coming from the power plant. Full or partial integration of the power plant condenser as a heat source for the CO_2 capture plant for preheating purpose might be promising to explore.
- It is recommended to explore the design and operation of a large scale CO_2 capture process with the stripper column operating at vacuum pressure. The study may shed light to the possibility of integrating the power plant condenser to the stripper column as the heat source partially or fully eliminating the reboiler section of the stripper.
- The application of two strippers in series might be advantageous in terms of plant energy requirement. This should be done with taking into account the operational consideration at power plant part load operations.

10.3. Absorber Intercooling

Benefits of using two absorber intercooling configurations in the CO_2 capture unit using an aqueous solution of 30 wt. % MEA as solvent to remove 90 % CO_2 from natural gas fired flue gases for a range of lean loadings from 0.15 to 0.42 were studied. The effect of intercooling on the temperature bulge, liquid flow rate, liquid to gas (L/G) ratio, rich solvent

loading, and solvent absorption capacity were evaluated using the minimum solvent flow rate concept. Benefits of using absorber intercooling in terms of absorber packing area and overall energy requirement were quantified using 1.2 times the minimum solvent flow rate (L_{min}). The total equivalent work concept was used to evaluate the plant overall energy requirement.

In absorbers without intercooling with solvents with lean loading below 0.30, temperature bulges occurred near the top of the column and away from the equilibrium pinch at the rich-end of the column, suggesting the benefit of using absorber intercooling in terms of CO_2 mass transfer and solvent absorption capacity is insignificant. Minor differences in L_{min}/G ratios before and after using simple and advanced intercooling confirmed their minor benefits in this region. The plant overall energy study also showed minor gain in terms of total equivalent work which was associated with slightly increase in absorber total packing area when using simple or advanced intercooling.

At lean loading between 0.30 and 0.36, a remarkable increase in L_{min}/G, followed by a sharp reduction in rich solvent loading were observed in absorbers with no intercooling. At this range of this loading, the temperature bulge was positioned somewhere around the middle of the column. Applying simple and advanced absorber intercooling showed significant improvement on both L_{min}/G and rich loading. Studying the packing requirements and energy requirements confirmed the effectiveness of using absorber intercooling in this range. For lean loadings between 0.30 and 0.34, using simple and advanced absorber intercooling will reduce both absorber packing requirements and the plant overall energy requirements. For instance, using simple and advanced absorber intercooling at the lean loading of 0.34 benefited the process by reducing the absorber packing area by nearly 32.0 and 36.6 %, respectively, followed a reduction in the total equivalent work by 15.6 and 15.9 %, respectively.

At lean loading equal to and higher than 0.36, the use of absorber intercooling had positive effects on L_{min}/G and rich loading curves, resulting in significant reduction in the plant

overall energy requirement in terms of total equivalent work. However, these benefits are associated with the expense of requiring an excessive amount of packing in the absorber packed column.

These findings can be used as a guideline for future application of absorber intercooling for commercial scale natural gas fired flue gas applications (3-5 % mole CO_2 concentration) when using an aqueous solution of 30 wt. % MEA as solvent.

10.3.1. Recommendations for Future Research

- This research proved the benefits of using absorber intercooling as a means to improve the process when using aqueous solution of 30 wt. % MEA as solvent. Further research should continue to evaluate the benefits of both simple and advanced intercooling options with other solvents and process conditions.
- In this research, the solvent was cooled at an external cooler to the temperature the lean solvent initially entered the absorber column, i.e. 40 °C. Cooling the solvent to temperatures lower than that the solvent initially entered the absorber column may further improve the absorption performance and it may be a practical option when operating the CO_2 capture plant at locations where relatively cooler water or chilled water is freely available.
- The flue gas temperature also rises in the absorber column and has a limiting effect on the intercooling application. Future research in finding methods to reduce gas phase temperature in addition to solvent intercooling may provide additional benefits in terms of solvent absorption capacity.

10.4. Advanced Stripper Configurations

The advanced reboiled and advanced flash stripper were evaluated with 7 m (30 wt. %) MEA to remove 90 % mole CO_2 from flue gases with 4 % CO_2, typical of a natural gas fired application, for a range of lean loading from 0.15 to 0.38. The energy efficiency

improvement offered by the advanced configurations was evaluated and compared with that of a simple stripper configuration using the total equivalent work.

Simulation results confirmed both advanced configurations work equally well over the specified range of lean loading, except the advanced flash stripper fails to operate at lean loading below 0.18, as the solvent temperature at the steam heater outlet exceeds the solvent thermal degradation limit.

With lean loading from 0.21 to 0.32, the advanced reboiled stripper and flash stripper require an equivalent work of only 38 to 41 kJ/mol of CO_2 recovered, compared to 44-45 kJ/mol with the simple stripper. The regeneration heat duty was reduced 11 to 18 % to 136-148 kJ/mol of CO_2 recovered compared to 166-167 kJ/mol with the simple stripper. At lean loading of 0.30, the advanced flash stripper offers the highest reduction in the total equivalent work of 12.4 %, and the highest reduction offered by the advanced reboiled stripper is 11.7 % at the lean loading of 0.25.

Simulations showed that the advanced flash stripper requires more equivalent work than the advanced reboiled stripper at lean loading less than 0.26 and more than the simple stripper at a lean loading less than 0.20, mainly due to the higher steam temperature required at those lean loadings.

The variation of temperature driving force through the column showed that the advanced flash stripper tends to pinch at the lean end, opposed to the simple stripper which usually pinches at the rich end, contributing to enhance the thermodynamic efficiency of the stripping process and reducing the loss of work.

In both advanced reboiled and advanced flash stripper configurations, one contributor to improve the energy efficiency is less water vapour at the top of the column. In addition both configurations contribute in lowering the plant cooling water requirement when compared with the plant with a simple stripper configuration.

10.4.1. Recommendations for Future Research

- In this research the thermodynamic benefits of increasing stripper complexity using advanced reboiled and advanced flash stripper were quantified for a range of lean loading at the stripper pressure of 180 kPa. The thermodynamic benefits of these two complex configurations should be evaluated as function of stripper operating pressure as the pressure affects the solvent boiling point.
- The thermodynamic benefits of advanced stripper configurations for a wide range of lean loading when using aqueous solution of 30 wt. % MEA as solvent were evaluated. Further research should continue to evaluate the benefits of both advanced reboiled and advanced flash strippers with other solvents and process conditions.
- In this research, the cold-rich heat exchanger approach temperature was set to 20 °C; further research should continue to evaluate the benefits of lowering the approach temperature to 10 °C and 5 °C. A techno-economic evaluation may be useful to select a proper approach temperature.

10.5. Techno-Economic Analysis of Large Scale Post Combustion CO_2 Capture Systems for Various Flue Gas CO_2 Concentrations

Process Simulation and economic estimations performed in chapter 9 clearly point out the effect of the flue gas CO_2 concentration on the design and cost of CO_2 capture processes when using 30 wt. % aqueous solution of MEA as solvent. Increasing atmospheric flue gas concentration reduces total annual cost of the CO_2 capture plant mainly due to lower specific energy/utility consumptions. The total annual cost reduced by approximately 8 % when moving from 4 % to 14 % flue gas CO_2 concentration, while a more moderate total annual cost decline was observed by nearly 5 % when moving from 4 % to 6 % flue gas CO_2 concentration. Although the specific energy requirement of solvent regeneration drops by increasing flue gas CO_2 concentration, the plant specific cooling requirements show an

incremental trend with increasing flue gas CO_2 concentration. Performed studies have shown that the CO_2 capture specific regeneration energy requirement reduces exponentially with increasing flue gas CO_2 concentration encouraging the application of exhaust gas recirculation in future NGCC power plants if stringent CO_2 reduction strategies are to be pursued. Furthermore, according to economic calculations performed, a reduction in the capital cost of around 35 % was observed when increasing the flue gas CO_2 concentration from 4 %, i.e. typical of a NGCC plant, to 6 %, i.e. typical of a NGCC+EGR plant.

10.5.1. Recommendations for Future Research

The research showed the cost of CO_2 captured decreases significantly with the flue gas CO_2 concentration. According to the curve shown in Figure 9-9 of Chapter 9, there is an optimum flue gas CO_2 concentration, ranged from 8 % to 11 %, at which the cost of capturing CO_2 is a minimum. This finding ignited the idea of a new concept. The new concept suggests having a common PCC plant to serve a number of associated fossil-fuelled power generation plants, such as integrated coal and natural gas fired power plant (with or without exhaust gas recirculation cycle) or integrated coal and natural gas with exhaust gas recirculation power plant. My preliminary results show that the option of coal+natural gas with exhaust gas recirculation offers the best economics. Table 10-1 summarises of cost of capturing CO_2 for different type of power plants with the respective flue gas CO_2 concentrations.

Table 10-1. Summary of cost of CO_2 captured for different type of power plant

Parameters	**PCC-NGCC**	**PCC-NGCC+EGR**	**PCC-COAL**	**PCC-COAL +NGCC**	**PCC-COAL +NGCC+EGR**
Cost of CO_2 captured (£/tonne CO_2)	51.77	49.41	48.00	47.94	46.93
Flue gas CO_2 concentration (mole %)	3.91	6.07	13.50	7.23	8.98

Further research should continue to evaluate the benefits of integrated power generation systems on the total cost of CO_2 capture processes.